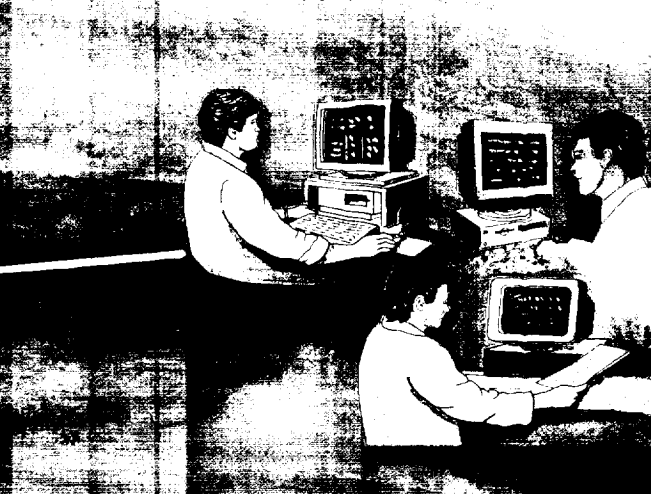




# RESEARCH & TECHNOLOGY REPORT

## JOHNSON SPACE FLIGHT CENTER



USER COMMUNITIES



*This is the SAMPEX Mission Operations Room (MOR). This represents the first operational use of the Transportable Payload Operations Control Center (TPOCC) to support the launch and operations of a GSFC spacecraft. All of the hardware and software required to support spacecraft health and safety monitoring have been entirely contained within the MOR starting with the SAMPEX mission (launched in July 1992). The TPOCC architecture represents a move from mainframe-based to workstation-based technology, and resulted in a significant increase in software reuse and expanded operational functionality.*

---

---

# **RESEARCH AND TECHNOLOGY**

**R&T REPORT**  
Goddard Space Flight Center



# FOREWORD

---

CHANGE IS THE HALLMARK of these times. On the international scene, changes have been startling! Change is certainly on the minds of our political leaders, and change is the strongest theme emanating from our Agency. These changes are a signal that we are heading on a new track as we look forward to the coming millennium. These winds of change will bring with them a need for a new vision. Americans have always benefited from seeing change as bringing with it opportunity—opportunity to re-examine, re-engineer, and review current practices. Invention is our strength; the nation depends upon it to retain our place in world leadership.

Goddard Space Flight Center is a shining example of adaptation to change, and the benefits afforded by opportunity. Earlier in my career, I saw GSFC as an engineer and manager; as recently appointed Director, I now have my turn at the helm, and I see opportunity as I view this great national asset with fresh—but experienced—eyes. New ideas, new goals, new ways of doing business, and new partners are clearly our calling.

The cutting edge at Goddard is revealed in the annual Research and Technology Report. The theme of this edition is Mission Operations and Data Systems, where some of the largest changes are taking place. We are shifting from centralized to distributed mission operations, and from human interactive operations to highly automated operations. We are taking advantage of commercial services and technologies wherever available to carry out our routine operations. What we retain is the leading-edge research and development—the new paths to efficiency, reliability, and simplicity. *Networking, multiuser tools, portability, autonomy, data compression, and World Wide Web* are the terms we find in increasing usage in the articles presented here.

The other mainstay of Goddard's activities, science, by its nature values skepticism and tends to resist change, just as space flight engineering recognizes risk and leans towards a conservative view. But, given the changes occurring all around us, investigators and engineers in both these coupled giants understand the need to usher in a new era. Goddard will work in partnership with other NASA Centers and government agencies, universities, and industry to introduce and utilize the technologies of the future. Examples of these partnerships are found throughout this Report, as articles address science and engineering research in cryogenics, low-power data systems, and new approaches to optics. In space science, such examples as the use of the South Pole as a viewing site, thin-foil technology to increase sensitivity, and data from an old Explorer mission reveal new opportunities for advances in science and technology. In the Earth system sciences, our work using global data sets, viewing boreal ecosystems, developing laser altimetry, and studying climatology herald the coming age of Mission to Planet Earth.

I am very proud to take my turn at the wheel of this magnificent enterprise that is the flagship of NASA's future in science and technology.



Joseph H. Rothenberg  
Director, Goddard Space Flight Center



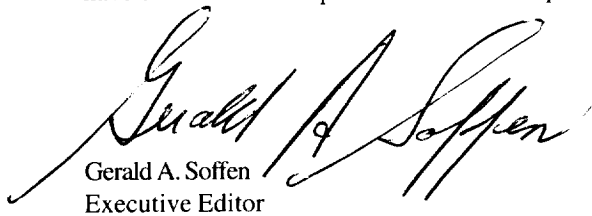
# PREFACE

---

**R**EADERS OF THIS MATERIAL will recognize the difficulty of condensing the work of thousands of people into fewer than a hundred articles while maintaining a strong representation of the accomplishments of this major national laboratory. As NASA redefines itself for the coming years, Goddard Space Flight Center's goal is to secure the strengths that we have developed, while repositioning ourselves for the future.

And what does the future hold? New competition from a developing world, new challenges for value by a demanding public, tougher restraints on resources, and, above all, a real sense of purpose. Our vision for the nation's future includes not only fiscal security, but also intellectual excitement and stimulation. The vitality of our people depends upon a robust and flexible economy related to progressive ideas and a willingness to take calculated risks.

In keeping with the spirit of this concept, we have sought to make a significant change in distribution of this document, most of which will be done on the World Wide Web. Reference copies will continue to be distributed to libraries and places of high usage, but most readers will use their computers to obtain the text and accompanying figures. NASA is strong in communications technology, and we would like to use this technology to distribute our message. Goddard's home page is the on-line gateway into the work of this Center; now, we will use the Web to communicate the results. We have entertained such possibilities over the past few years; now is the time to put it into practice!



Gerald A. Soffen  
Executive Editor



# CONTENTS

---

## MISSION OPERATIONS AND DATA SYSTEMS

### **Mission Planning and Operations**

---

<b>Heuristic Evolutionary Search in Space Communications Scheduling</b>	
<i>James Rash</i> .....	2
<b>Multiuser Multi-Interference Communication Analysis Tool</b>	
<i>Badri Younes and Ricardo Benn</i> .....	5
<b>Spacecraft Instrument Occultation and Visible-Target Prediction</b>	
<i>Chad Mendelsohn</i> .....	7
<b>Advanced Composition Explorer</b>	
<i>Carolyn Dent</i> .....	9
<b>Reusable Object Methodology to Reduce the Cost for Mission Operations</b>	
<i>Don Hei and Rhoda Shaller Hornstein</i> .....	11

### **TDRSS, Positioning Systems, and Orbit Determination**

---

<b>Performance Capabilities of the Tracking and Data Relay Satellite System for Low-Earth-Orbit Spacecraft</b>	
<i>Clarence Doll</i> .....	14
<b>NASA Autonomous Navigation Systems</b>	
<i>Cheryl Gramling</i> .....	17
<b>Portable TDRSS Communicator</b>	
<i>Arthur Jackson and Lou Koschmeder</i> .....	19
<b>Enhanced TDRSS User RF Test Set: Transportable TDRSS Ground Support Equipment</b>	
<i>John Badger and David Israel</i> .....	21
<b>Development of the GPS-Enhanced Orbit Determination Experiment</b>	
<i>Roger Hart and Stephen Leake</i> .....	24
<b>Ground System Software for Global Positioning System Attitude Determination</b>	
<i>Joseph Garrick</i> .....	26

# CONTENTS

---

## Ground System and Networks: Hardware

---

<b>NASCOM Internet Protocol Gateway: The Transition Begins</b>	
<i>Matthew Kirichok</i> .....	29
<b>New Communications Options for Small Satellites</b>	
<i>David Zillig and William Horne</i> .....	32
<b>Ground Network Advanced Receiver Prototype II: A Charge-Coupled Device Programmable Integrated Receiver</b>	
<i>David Zillig and Thomas Land</i> .....	35
<b>Evolving Charge-Coupled Device Signal Processing Technology</b>	
<i>David Zillig</i> .....	38
<b>Prototyping EDOS High-Rate Return-Link-Service Processing</b>	
<i>Alexander Krimchansky and Michael Lemon</i> .....	40
<b>Very Large-Scale Integration Return Link Processing Card for a Personal Computer</b>	
<i>Don Davis and Jonathan Harris</i> .....	42
<b>Satellite Telemetry and Return Link (STARLink)</b>	
<i>Greg Blaney</i> .....	44
<b>Parallel Integrated Frame Synchronizer Chip</b>	
<i>Don Davis, Parminder Ghuman, and Jeff Solomon</i> .....	46
<b>Frequency-Agile Fiber Optic Modem Tunes Two Decades</b>	
<i>Chi Le, Paul Casper, and Jim Shaughnessy</i> .....	48
<b>Ground Hardware Upgrades for Flight Software Development Utilizing VHDL/FPGA Technologies</b>	
<i>Steve McCarron, Rich Ambrose, and Ed Leventhal</i> .....	50

## Ground System and Networks: Software

---

<b>Cutting Costs Through Advanced Software and Systems Engineering Techniques: The Flight Dynamics Distributed System</b>	
<i>David Weidow</i> .....	53
<b>Generalized Support Software</b>	
<i>Michael Stark</i> .....	55

# CONTENTS

---

---

<b>Generic Inferential Executor: A Tool for Spacecraft Control Center Automation</b> <i>Jonathan Hartley</i> .....	57
<b>The User Interface and Executive</b> <i>Jeffrey Segal</i> .....	59
<b>Visualizing Spacecraft Ground System Data</b> <i>Gregory Shirah</i> .....	60
<b>How to Automate a Ground Tracking Station Using Commercial Off-the-Shelf Products</b> <i>Miles Smith and Peter Militch</i> .....	62
<b>IMACCS: An Operational, COTS-Based Ground Support System Proof-of-Concept Project</b> <i>Michael Bracken</i> .....	64
<b>Software Frame Synchronization for Spacecraft Telemetry</b> <i>Thomas Grubb and Steve Duran</i> .....	68
<b>Software Reed-Solomon Decoder for Space Telemetry Applications</b> <i>Steve Duran</i> .....	70
<b>Software Telemetry Processing on Low-Cost Workstations and Personal Computers</b> <i>Steve Duran and Thomas Grubb</i> .....	71

---

## Data Processing and Analysis

---

<b>End-to-End Ground-based Processing of Satellite Data</b> <i>Robert Cromp, Nicholas Short, Jr., and William Campbell</i> .....	73
<b>Real-Time Data Processing of Spacecraft and Instrument Telemetry</b> <i>Patrick Coronado and Nicholas Short, Jr.</i> .....	75
<b>The Beowulf Parallel Workstation Delivers New Capabilities for Earth and Space Sciences Applications</b> <i>John Dorband, Thomas Sterling, and Donald Becker</i> .....	78
<b>Signal Processing Workstation Simulation of the Landsat-7 X-Band Downlink</b> <i>Badri Younes, Armen Caroglanian, and Linda Harrel</i> .....	81
<b>Landsat-7 Raw Data Capture</b> <i>Clifford Brambora, Joy Henegar, and Robert Schweiss</i> .....	83
<b>EOSDIS Version 0 IMS Interconnects Existing Earth Science Data Systems</b> <i>Robin Pfister</i> .....	85

# CONTENTS

---

<b>GLOBE Visualization and Data Analysis</b> <i>Richard White</i> .....	88
<b>Model-Based Vector Quantization for Image Browse and Compression</b> <i>James Tilton</i> .....	91
<b>Satellite Image Content Extraction and Catalog Augmentation: An EOSDIS Data Mining Prototype</b> <i>Mike Moore</i> .....	93

## World Wide Web

---

<b>Latest Study Information? Call "Home"</b> <i>Bill Anselm</i> .....	96
<b>Distributing Flight Dynamics Products via the World Wide Web</b> <i>David Matusow and Mark Woodard</i> .....	98
<b>Exploiting World Wide Web Technology to Make Data Finding and Access Easier</b> <i>G. Jason Mathews and Syed Towheed</i> .....	101
<b>Hubble Space Telescope's Long-Term Trending System Uses the World Wide Web to Distribute Engineering Data</b> <i>Andrew Dougherty</i> .....	104

## FLIGHT PROJECTS

<b>EOS AM-1: Project Update</b> <i>Christopher Scolese, Steven Neeck, and Francesco Bordi</i> .....	110
<b>EnviroNET Satellite End-of-Life Disposal Computational Model</b> <i>Michael Lauriente</i> .....	112
<b>NASA Lessons-Learned Information System World Wide Web Interface</b> <i>Michael Lauriente</i> .....	114
<b>Advanced System Synthesis and Evaluation Tool</b> <i>John Oberright and Ronald Leung</i> .....	116
<b>Remote Manipulator System Control Using Fuzzy Logic</b> <i>Joe Mica</i> .....	118
<b>The Hemispherical Resonator Gyroscope</b> <i>Mark Jaster</i> .....	120

# CONTENTS

---

## SPACE SCIENCES

### **Solar System**

---

<b>New Science from Archived Data: Hawkeye Observations of High-Latitude Reconnection of Magnetic Fields</b>	
<i>Ramona Kessel</i> .....	126
<b>A Three-Dimensional Magnetofluid Simulation of Shear-Driven Turbulence: Application to Solar Wind Observations</b>	
<i>D. Aaron Roberts and Melvyn Goldstein</i> .....	129
<b>The Nonlinear Dynamics of the Magnetosphere and Space Weather Prediction</b>	
<i>Alex Klimas</i> .....	131
<b>Ulysses Radio and Plasma Wave Observations at High Southern Heliographic Latitudes</b>	
<i>Robert Stone</i> .....	133
<b>Measurements of Ammonia on Jupiter After SL9</b>	
<i>Theodor Kostiuk, Kelly Fast, and Timothy Livengood</i> .....	135

### **Cosmology and Astrophysics**

---

<b>Cosmic Microwave Background Radiation</b>	
<i>John Mather</i> .....	138
<b>Exploring the Limits of Astronomy from Earth</b>	
<i>Harvey Moseley</i> .....	141
<b>Thin-Foil Replicated Optics for X-ray Astronomy</b>	
<i>Peter Serlemitsos</i> .....	143
<b>CdZnTe Hard X-ray Semiconductor Detector Development</b>	
<i>Ann Parsons, Neil Gehrels, and Jack Tueller</i> .....	145
<b>The New Shape of the Galactic Bulge</b>	
<i>Eli Dwek</i> .....	147
<b>An Object-Oriented Multimission and Multispectral Astrophysics Data Catalog</b>	
<i>Cynthia Cheung</i> .....	150

# CONTENTS

---

## EARTH SYSTEM SCIENCE

### Water

---

#### Estimates of Sensible and Latent Heat Flux Over Global Oceans

*Joel Susskind and Ebby Anyamba* ..... 156

#### Diurnal Variations in Tropical Atmospheric Convection Over Oceanic Regions

*Chung-Hsiung Sui, William K.-M. Lau, and Xiaofan Li* ..... 158

#### Comparison of DAO and NMC Reanalyses with Satellite Data Over Tropical Ocean During 1987 and 1988

*Sandrine Bony, William K.-M. Lau, and Yogesh C. Sud* ..... 160

#### Improving and Evaluating Remotely-Sensed Snow/Microwave Algorithms and Snow Output from General Circulation Models

*James Foster* ..... 163

#### Monitoring Soil Conditions in the Northern Tibetan Plateau Using SSM/I Data

*Alfred T.C. Chang* ..... 165

#### Airborne Laser/GPS Mapping of Ice Sheet Topography for Monitoring Ice Sheet Mass Balance

*William Krabill* ..... 168

### Land

---

#### Precision Orbit Determination and Gravity Field Improvement Derived from TDRSS

*Andrew Marshall and Frank Lemoine* ..... 170

#### Boreal Ecosystem Atmosphere Study (BOREAS)

*Forrest Hall and Piers Sellers* ..... 173

#### Mapping Urban Sprawl from Space: Evaluating Land Use Change with Nighttime Views of the Earth

*Marc Imhoff* ..... 176

#### Nitrogenous Fertilizers: Global Data Sets of Consumption and Associated Trace-gas Emissions

*Elaine Matthews and Inez Fung* ..... 179

#### Remote Sensing of Recently Active Volcanoes in the Middle-Atlantic Region

*James Garvin* ..... 183

# CONTENTS

---

---

<b>Using Very Long Baseline Interferometry to Measure Contemporary Postglacial Rebound</b> <i>James Ryan</i> .....	186
<b>Shuttle Laser Altimeter: A Pathfinder for Space-Based Laser Altimetry and Lidar</b> <i>Jack Bufton</i> .....	189
<b>Has Climate Changed the Earth's Tilt?</b> <i>David Rubincam</i> .....	192

---

## Climatology

---

<b>Semiannual and Quasi-biennial Oscillations Generated by Gravity Waves in the Middle Atmosphere</b> <i>Hans Mayr, John Mengel, and Colin Hines</i> .....	195
<b>In-phase Quasi-biennial Oscillations of the Tropical Surface Temperature and Outgoing Longwave Radiation</b> <i>H. Lee Kyle</i> .....	198
<b>The Super Greenhouse Effect and Cloud Radiative Forcing in the Tropical Atmosphere</b> <i>Sandrine Bony, William K.-M Lau, and Y. C. Sud</i> .....	200

## ENGINEERING AND MATERIALS

---

### Spacecraft Subsystems

---

<b>Cost-Effectiveness of Advanced Solar Cells</b> <i>Edward Gaddy</i> .....	206
<b>Development of a Heat-Driven Pulse Pump</b> <i>Steve Benner</i> .....	207
<b>Boron Carbide as a High-Reflectance Coating for Extreme Ultraviolet Optics</b> <i>Gerry Blumenstock and Ritva Keski-Kuha</i> .....	209
<b>Spaceflight Fiber Optics in the X-ray Timing Explorer Spacecraft</b> <i>John Kolasinski</i> .....	211

# **CONTENTS**

---

## **Cryogenic Developments and Applications**

---

<b>Low-Cost Cryocoolers for High-Temperature Superconductor Filters</b> <i>Stephen Castles</i> .....	214
<b>Cryogenic Gas Replenishment System for Long-Duration Balloons</b> <i>Steven Raqué</i> .....	216

## **New Tools and Capabilities**

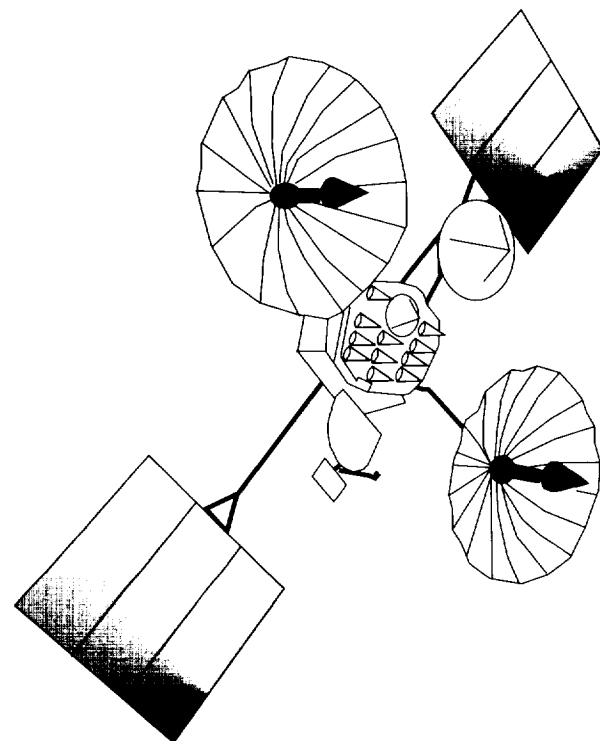
---

<b>The Detector Development Laboratory</b> <i>Brent Mott</i> .....	218
<b>An Improved Lightning Detection and Ranging System</b> <i>John Gerlach</i> .....	222
<b>The Essential Services Node: A Low-Power Data System on a Chip</b> <i>Robert Caffrey</i> .....	224
<b>Acronyms</b> .....	227
<b>Author Index</b> .....	235

---

---

***MISSION  
OPERATIONS AND  
DATA SYSTEMS***

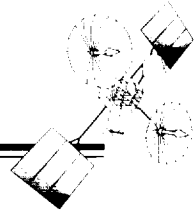


## Spacecraft Data

### Ground Data Systems

## Ground Data Visualizations

*In the near future spacecraft ground/space systems will become more autonomous resulting in less reliance on standing flight operations teams. When spacecraft anomalies arise which require human attention, engineers will be called in to correct the problems. Ground data visualizations systems will be instrumental in helping these engineers diagnose problems by enabling them to quickly and accurately comprehend the large amounts of data and information in the ground and space systems.*



---

# MISSION OPERATIONS AND DATA SYSTEMS

IT IS A PLEASURE and an honor to have the 1995 edition of the Goddard Space Flight Center *Research and Technology Report* focus on Mission Operations and Data Systems.

Throughout its history, the Mission Operations and Data Systems Directorate has played a major role in the success of GSFC's operational missions. It has provided the infrastructure for an end-to-end system of enormous complexity. At one end of this infrastructure is the unmanned, Earth-orbiting scientific satellite; at the other are the communities of scientists and other users served by GSFC. The front and back covers of this report represent the major components of the current end-to-end system.

Over the last several years, much has changed in the way that the Mission Operations and Data Systems Directorate provides its services and systems to GSFC. These changes are both technological and managerial in nature, and this state of constant change will continue into the future. Although the challenges for the Mission Operations and Data Systems Directorate are great, they are being met head-on with aggressive and innovative technical programs, and with the development and application of creative management solutions that will successfully carry the organization into the 21st century.

Discussion of technical advances, found in the articles in this section, demonstrates that there is now more emphasis on:

- the reuse of operational system components between missions to bring down development costs, while maintaining effective and efficient high-performance systems;
- the utilization of commercial-off-the-shelf and government-off-the-shelf tools and application packages to develop lower-cost operational systems with minimal development time;

- the transition from centralized to modular work-station-based distributed system architectures; and
- the growing use of automation in all aspects of the end-to-end system infrastructure.

From a management perspective, the changes for Missions Operations and Data Systems are also significant. This year marks the arrival of Dr. Arthur Fuchs as the new Director of GSFC's Mission Operations and Data Systems Directorate. Under his direction, the Mission Operations and Data Systems Directorate will be re-engineered to respond better to the challenges of the future and to the agency-wide changes relating to mission operations.

The 35 papers in this section of the *Research and Technology Report* are fine examples of an outstanding research and development program. The papers are organized into groups addressing Mission Planning and Operations; TDRSS, Positioning Systems and Orbit Determination; Ground Systems and Networks—Hardware; Ground Systems and Networks—Software; Data Processing and Analysis; and the World Wide Web. These contributions reveal an active and comprehensive research and development program that spans the full spectrum of the end-to-end system responsibilities of the Mission Operations and Data Systems Directorate. This program is making significant contributions to the success of the Mission Operations and Data Systems Directorate in maintaining its leadership role of providing state-of-the-art development and operational services for GSFC missions during this era of change.

*Walt Truszkowski*

**MISSION PLANNING AND OPERATIONS****HEURISTIC EVOLUTIONARY SEARCH IN  
SPACE COMMUNICATIONS SCHEDULING**

**G**ENETIC ALGORITHMS belong to a class of probabilistic search strategies that have been developed for searching large solution spaces to converge on optimum solutions in reasonable time. We have developed a prototype computer program by applying a genetic algorithm variant to the problem of scheduling user spacecraft communications events in the context of NASA's Tracking and Data Relay Satellite System (TDRSS).

Nontrivial scheduling problems typically have a solution space so large that finding near-optimal solutions is a practical impossibility for algorithms that do not exploit statistical or probabilistic search strategies. Nonstatistical, deterministic search algorithms typically explore only the solutions along some (branched) path through the solution space. The found solution may or may not be good enough to satisfy the requirements of the application, and merely increasing the run time does not always ensure improvement. Further, deterministic search algorithms cannot in general avoid getting caught near a "local minimum" (i.e., a solution that is better than all others in some region of the solution space, while not as good as solutions in other regions). Thus arises the motivation to use various nondeterministic (probabilistic) strategies for searching large solution spaces.

Scheduling TDRSS resources to provide communications services for user spacecraft entails a very large solution space. A "point" in the solution space is a complete schedule that satisfies some subset of the requests for user spacecraft communications events. A schedule consists of a set of user spacecraft communications events, each of which consists of one or more "services." A service is represented as the assignment of a TDRSS resource (a specific antenna on a specific TDRSS) to a specific user spacecraft during some specific time interval.

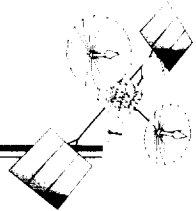
The size of the solution space for the TDRSS scheduling problem is a function of the number of assignable TDRSS resources, the number of communications events requested by user spacecraft, the number of services per request, the amount of flexibility in the duration and start time of the services, the amount of flexibility in the assignment of TDRSS resources to the services, and the granularity of the scheduling time line (e.g., services may be scheduled on 5-second break points). For a typical 1-week scheduling scenario, assuming 3500 user requests, two

services per event, event start time flexibility of 600 seconds, service start time flexibility of 300 seconds (for all except the first service in an event), service duration flexibility of 300 seconds, three allowable resources to support a service, and a granularity of 5 seconds, the solution space would include in excess of  $10^{900}$  "points" or potential schedules that might be evaluated by a search algorithm. Depending on the specific rules and constraints for the TDRSS scheduling problem, the vast majority of the points in the solution space would not represent viable solutions; but beyond merely avoiding wasting time considering nonviable solutions, the search algorithm must be able to efficiently locate good ones.

The Heuristic Evolutionary Search (HES) algorithm, specifically designed to attack the TDRSS scheduling problem, uses a genetic-algorithm-inspired approach to probabilistically explore the solution space. As is characteristic of genetic algorithms, HES avoids the trap of local minima by using random processes that continually consider solutions not necessarily "near" the currently best solutions. Further, heuristics embedded in the algorithm embody temporal logic, TDRSS domain constraints, and rules to ensure a controlled exploration process that minimizes consideration of nonviable solutions.

HES differs somewhat from canonical genetic algorithms by representing members of the population of organisms (i.e., solutions) using variable-length data structures instead of fixed-length strings, which, although feasible, were considered to be a somewhat less natural and more cumbersome representation for this problem domain. In common with other members of the class of reproductive population search algorithms, HES encompasses the biological evolution concepts of fitness, selection, reproduction (via mutation and mating), and iterative replacement of members of the population by fitter organisms. The evolutionary search process is aimed ultimately towards convergence on an optimum organism—a member of the population that, as a solution to the problem, cannot be improved upon.

In HES, the data structure representing a solution (a schedule) is a variable-length, time-ordered list of communications events, each of which satisfies one user request. An event is itself represented by a data structure—a list of resource assignments corresponding to the services in the event. An event has a specific start time and



is an instance of a prototype event predefined by the user. A prototype event prescribes various pieces of information, such as data rates for secondary resources required for the services in the event, a list of TDRSS resources allowed to support the user, and service duration and start time flexibilities. The HES coding scheme encompasses all possible solutions in the search space for the TDRSS scheduling problem.

A random process creates the initial population of solutions, conditioned only by the requirement that each solution be viable (i.e., satisfies at least some of the user requests and is free of TDRSS constraint violations and resource conflicts). Random initialization of the population is important to avoid systematic bias in favor of any particular region of the search space: any possible solution may be selected for inclusion in the initial population. After creation and evaluation (scoring) of the initial population, the evolutionary search process repeats the following steps until some termination condition (a run-time limit or a convergence criterion) is satisfied:

- select a subset of the population to engage in reproduction;
- generate new members of the population from members of the reproduction set using various methods of reproduction;
- calculate a fitness score for each member of the population; and
- replace some members of the population with some of the new members, based on fitness scores.

Each repetition of the four steps results in a new generation. The number of generations necessary to achieve convergence varies depending on the details of the scheduling scenario and on the specific fitness function used to perform schedule evaluation. HES incorporates a variety of fitness functions as required by the application domain. As implemented in HES, a fitness function returns a value of 1.0 for a perfect schedule or a greater value for an imperfect schedule. The fitness score for the best member of the population can be thought of as a function of the generation number during execution of the program. Convergence is achieved when the slope of the graph of the fitness score falls below some prescribed value.

The asymptote of the graph (approached as the slope approaches zero) is expected to be a value greater than 1.0, because the best possible schedule is not, in general, expected to be “perfect.” For a truly rich solution space such as the TDRSS scheduling problem, the slope of the graph would not be expected to become zero for a large number of generations.

Reproduction in typical genetic algorithms is accomplished by the processes of mutation and crossover, both inspired by the corresponding biological processes. In mutation, an offspring results from cloning a member of the reproduction set and then altering the clone by randomly choosing one of its attributes and altering its value. In crossover, two offspring result from “mating” two members of the reproduction set, where the offspring are the same as the parents, except that portions of their attributes are exchanged.

In addition to using a variable length list of time-tagged data (events) instead of a fixed-length string of bits to represent a problem solution, HES differs in two key ways from canonical genetic algorithms: (a) during the reproduction step, HES does not employ completely random mutations of organisms, but instead uses heuristics to limit alterations to those that produce viable mutants; and (b) in the reproductive process of cross-over, after performing the exchange of “genetic” material, HES uses heuristics to modify the offspring to ensure viability. The choices that led to these characteristics are rationalized by considerations of performance: there is a large cost in creating and evaluating an organism, entailing a needless waste whenever a nonviable organism is created and installed in the population.

Genetic algorithm implementations characteristically have adjustable execution parameters that affect performance (i.e., the nominal population size and the rates at which mutations and crossovers are allowed to occur). HES has similar parameters.

In HES, however, there are multiple mutation rate parameters, not just one. Mutations are allowed to occur simultaneously in multiple attributes of a solution (schedule). That is, each generation includes new organisms, (i.e., clones of existing members of the population), each containing a variation in the value of just one of the following attributes: event start time, service start time,

## MISSION OPERATIONS AND DATA SYSTEMS

---

service duration, TDRS assigned to the user spacecraft, and TDRS antenna assigned to a service. Also, each generation includes new solutions, and each is the clone of an old solution in the current population but with an event deleted or with an event added (where the added event satisfies a user request that was unsatisfied in the old solution). Each of these individual mutations has a corresponding adjustable rate parameter.

Together with the crossover rate parameter and the nominal population size parameter, the mutation rate parameters determine the performance of the HES prototype. All of the parameters are set prior to the start of execution. By observation, varying the values of the parameters can produce a large effect on performance. Thus, determination of the optimum parameter values is itself an important part of solving the overall problem.

The difficulty of manually trying to find an optimum combination of so many parameters having such a complex, but unknown, relationship to each other will quickly become apparent to anyone who makes the attempt. However, this parameter optimization problem can itself be attacked by a genetic algorithm approach—a metalevel genetic algorithm. Part of the HES prototype package

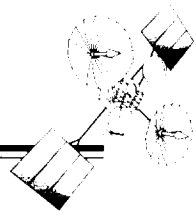
includes such a parameter optimization capability, which is useful not only in maximizing efficiency for each different fitness function, but also in restoring performance following any significant change in the implementation.

In testing against other available scheduling algorithms, HES has longer run times but produces better solutions, so experience to date with the HES prototype is promising. Future work with HES would include enhancing the mutation and crossover operators and experimenting with alternative solution representations.

Contact: James Rash (Code 522.3)  
301-286-5246  
Internet: James.L.Rash.1@gsfc.nasa.gov

Sponsor: Office of Space Communications

*Mr. Rash holds an M.A. in Mathematics from the University of Texas at Austin. He has worked at GSFC since 1985 and is a mathematician in the Software and Automation Systems Branch. He is responsible for development of artificial intelligence applications and has been guest editor for numerous journal special issues devoted to space applications of artificial intelligence.*



## THE MULTIUSER MULTI-INTERFERENCE COMMUNICATION ANALYSIS TOOL

THE MULTIUSER, multi-interference communication analysis tool (MUMICAT) aids satellite systems engineers with the process of satellite system design. They must know how to design efficient systems, what they will cost, how they will perform, and what potential problems might arise. The process of evaluating these systems through the use of software and making modifications based on the results are cheaper and faster, and allow for extensive modifications during the design phases of a project rather than trying to make changes after deployment.

MUMICAT is a unified tool for analyzing arbitrary communication and interference scenarios. With MUMICAT, satellite systems engineers are able to design their own networks consisting of any combination of orbital bodies (the Earth, Sun, Moon, etc.), ground stations or ground station networks, and satellites or satellite constellations. They may analyze parameters such as space-space, space-ground, or ground-space interference, solar interference, blockage and multipath, and atmospherics. Users configure effective isotropic radiated power, antenna pattern, frequency band, polarization, pointing direction, location (orbit), and operating schedule for each source or group of sources. Radio frequency communications systems are either a single hop or an arbitrary multihop relay network. Engineers can perform communication scenario analyses, such as determining what will happen during launches, antenna switches, tumbling, and emergency situations. The program can also calculate statistical parameters such as interference intervals, view periods, look angles, and bit error rates. Output is in the form of time lines, contour plots, interference probability density functions (PDFs), or histograms.

MUMICAT is more flexible than conventional software programs that are designed for a specific analysis and must be rewritten for each possible scenario. It is an object-oriented, C++ program, designed specifically for satellite communication analysis, and is flexible enough to analyze a wide variety of scenarios without program modification. MUMICAT achieves this flexibility through the use of the MUMICAT programming language, which the user writes and the core C++ program interprets. It has an extensive library of predefined functions; users may also write their own functions. The potential for errors is reduced because each scenario is developed through this specialized language, not by hard-coding the core C++ program.

MUMICAT simulations model the operation and performance of simulated elements called "sources." A source can be a planet, a satellite, the Sun, a ground station, an atmosphere, a group of ground stations, a group of satellites, or a custom source defined by the user. Sources can communicate, emit interference, block electromagnetic signals, orbit other bodies, or perform any function defined by the user. Users configure the system by defining operational parameters for the sources. These parameters can be constants or rules. For example, a satellite's solar panels can be set to track the Sun while the satellite is not in the Earth's shadow.

Multiple sources can be configured simultaneously using source constellations. A source template is used to define the operation of the sources in the constellation. For example, a source constellation can consist of 30 relay satellites communicating with each other. Another example could be 100 interferers in a trend line that are corrupting a desired link.

The operation of each source is controlled by dependent variables. Any dependent variable can be a function of any other variable(s) within the simulation. Dependent variables can be functions of variables at the present time or at a previous time. Examples of dependent variables include location, orientation, transmit power, in-view flags, and all other parameters that describe the operation of each source.

MUMICAT contains an extensive library of predefined expressions that can be specified for each dependent variable. These expressions include functions, binary operators, and nested parentheses. The binary operators include addition, subtraction, division, multiplication, and other operators for real numbers. There is also a set of binary operators for vector-dependent variables. These include addition, subtraction, dot product, and cross product.

Conditional expressions can be used to modify the behavior of a dependent variable for any specified condition. In the solar panel example described above, the dependent variable "solar panel angle" has two possible equations. When the Sun is in view of the satellite, the solar panel angle equation tracks the Sun. When the satellite is in the Earth's shadow, the solar panel angle is set to zero.

## MISSION OPERATIONS AND DATA SYSTEMS

Dependent variables can track information stored in a data file. The data file contains a list of values and times so the dependent variable can change its value as a function of time. For example, if the user wants a satellite to follow a predefined flight path, the location-dependent variable can be tied to a data file containing the flight path as a function of time.

Any dependent variable can be tied to any type of output. Output types include timelines, histograms, PDFs, common data formats, and contour plots. During the simulation, appropriate statistics are compiled for the dependent variable. Summary graphs of the dependent variables tied to the output can then be plotted.

The figure represents an example of a satellite relay network configuration. The Earth is set to orbit the Sun, the Moon will orbit the Earth, Relay Sat1 will orbit the Moon, and Relay Sat2 will orbit the Earth. The axis of Relay Sat2 will point to the center of the Earth. GStation1 is located at a specified latitude and longitude on the Moon. Its transmitter is connected to the receiver of Relay Sat1. Relay Sat1, in turn, communicates with Relay Sat2, which, in turn, communicates with GStation 2. Solar interference, Earth blockage and multipath, lunar blockage and multipath, and all communications parameters are calculated for every time point in the simulation.

Development of MUMICAT would not have been possible without the expert work of Jeff Freedman and Ted Berman, Communications Link Analysis Simulation Systems (CLASS) Project Analysts for Stanford Telecommunications, Inc.

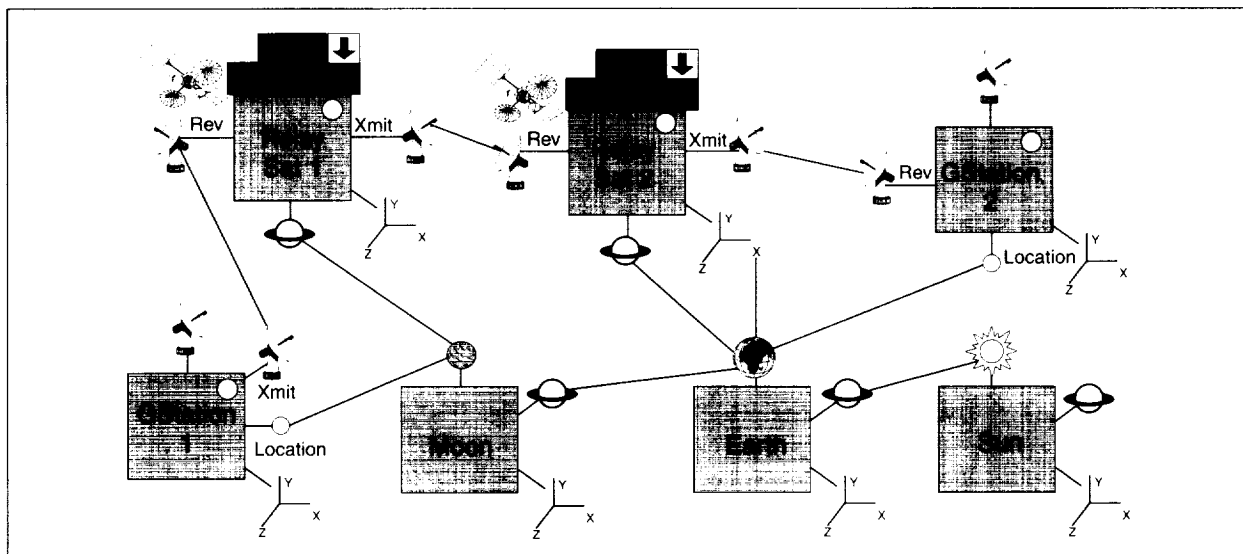
Contact: Badri Younes (Code 531.1)  
301-286-5089

Ricardo Benn (Code 531.1)  
301-286-8869

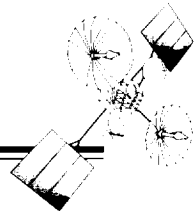
Sponsor: Office of Space Communications

*Mr. Younes completed 2 years of scientific studies (Math and Physics) at the University of Grenoble, France, in 1980. He received his B.S.E.E. and M.S.E.E. from the Catholic University of America (CUA) in 1984 and 1988, respectively. He is presently working on his Ph.D. dissertation at CUA. Mr. Younes joined NASA in 1990 to work on the Second TDRSS Ground Terminal (STGT) Project, where he later became the hardware systems manager. Mr. Younes is currently the CLASS Project Manager.*

*Mr. Benn received a B.S.E.E. from the University of Maryland, College Park, in 1994 and is currently pursuing his M.S.E.E. in Communications at the University of Maryland, College Park. In 1989, he joined the RF Analysis Section of the Networks Division at GSFC. Mr. Benn is currently the CLASS Deputy Project Manager.*



*Example configuration of a satellite relay network designed with MUMICAT.*

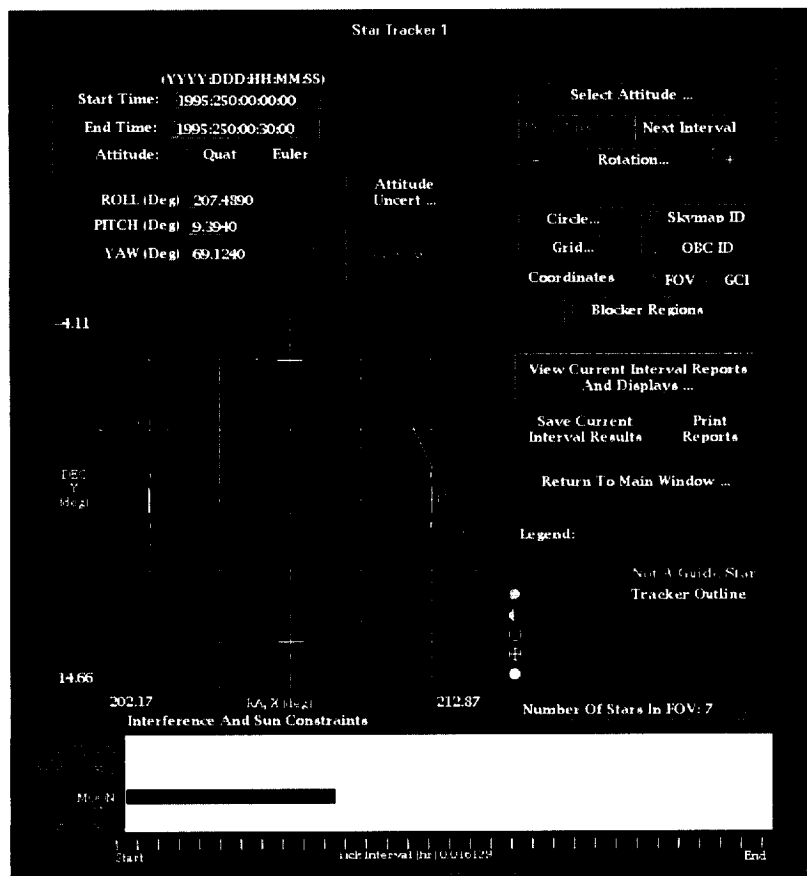


## SPACECRAFT INSTRUMENT OCCULTATION AND VISIBLE-TARGET PREDICTION

**K**EY TO SPACECRAFT maneuver planning and attitude determination is the answer to the question, "When will a target be within a spacecraft attitude sensor's or scientific instrument's field of view (FOV), and when will that instrument have its FOV occulted by another body?" In the past, determining the answers to these questions has been a labor-intensive and time-consuming effort for personnel in the Flight Dynamics Division (FDD.) The need for this information during spacecraft maneuver planning and attitude determination has driven the effort to develop a software utility to predict these events. Early attempts resulted in a simple, mainframe-based system that focused on determining guide stars for spacecraft star trackers. The output consisted of a crude, hard copy plot of stars within a tracker's FOV during a requested time and attitude. The user had few computational options, and the software was not readily

reconfigurable from mission to mission. Although this system provided important information, its functionality was still too limited for any practical and cost-effective use over a wide variety of spacecraft missions. Since there was need for increased functionality, operational environments were changing, and there was a push to move ground support software from mainframe platforms to UNIX workstations; the FDD launched a new effort to satisfy these requirements.

The new Guide Star Occultation Prediction Utility (GSOC) shown below, retains its predecessor's name but is a very different system. Although a primary focus is still the selection of guide stars for spacecraft star trackers, the new utility is capable of modeling and predicting events for other attitude sensors (namely Sun and Earth sensors) and up to six scientific instru-



*The new Guide Star Occultation Prediction Utility.*

## MISSION OPERATIONS AND DATA SYSTEMS

---

ments. It has greatly enhanced graphical display capabilities and improved performance. It is general enough to support an unlimited variety of missions and is designed to run in both the Flight Dynamics Facility (FDF) and the Mission Operations Center (MOC) environments. Detailed, color displays of sensor FOVs, combined with faster-than-real-time performance and the ability to interactively manipulate numerous parameters, allows the user to see almost instantaneous results while modifying a spacecraft's attitude. Tabular displays for each sensor/instrument type—containing such information as interference period start and stop times, target-present indicators, constraint violation indicators, identification of interfering bodies, spacecraft attitude, and target angles—can be viewed interactively on pop-up windows or sent to a file or printer. FOV displays include timeline plots of various events that may occur during a processing interval. As shown in the figure, GSOC reads star catalogues and a Solar/Lunar/Planetary file for positions of celestial bodies. It can either read a spacecraft ephemeris file or use an internal, analytical propagator to determine spacecraft position. Spacecraft attitude is computed by reading a target attitude file or by direct user input (i.e., namelist, text entry field, or attitude manipulation widgets). The system is designed to run in both interactive and automatic modes and executes on a Hewlett-Packard Series 700 UNIX workstation, using an X Windows and OSF Motif user interface.

Because GSOC is a planning, verification, and analysis tool, a typical operational scenario might include running

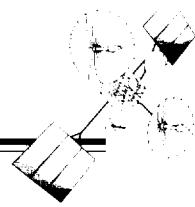
the utility daily in the MOC. Planned target attitudes would be input and available guide stars would be checked for good candidates. GSOC would also be run in the FDF to plan calibration maneuvers and verify the spacecraft's onboard computer performance. It may also be used to find proposed targets for gyroscope calibration and to examine star fields associated with targets when a spacecraft experiences difficulty.

The development of the GSOC utility is part of the FDD's ongoing efforts to enhance operational systems used for spacecraft attitude determination support. These efforts involve moving away from large, mainframe-based systems to smaller, faster, graphics-oriented systems running on workstation platforms, to provide better real-time monitoring and enhanced visualization of spacecraft attitude data.

Contact: Chad Mendelsohn (Code 552.1)  
301-286-4259

Sponsor: Office of Space Communications

*Mr. Mendelsohn is a software systems engineer and manages the development of flight dynamics systems in the FDD Software Engineering Branch. He was the GSOC System Development Project Manager and one of the software development engineers. Mr. Mendelsohn holds a B.S. in Physics and Mathematics from Northern Michigan University and has worked at GSFC for the past 10 years.*



## ADVANCED COMPOSITION EXPLORER

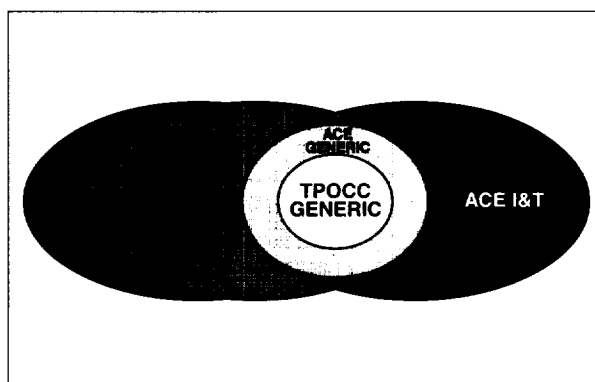
**A** NEW APPROACH for developing ground data systems is being pioneered in support of the Advanced Composition Explorer (ACE) program. The major innovation being applied to ACE is using a common hardware/software baseline for the ACE Integrated Mission Operations Center (IMOC), the ACE spacecraft Integration and Test Operations Control Center (ITOCC), and the ACE Science Center (ASC). The ITOCC will serve as the primary system for commanding and controlling the ACE spacecraft during integration and test prior to launch. The ACE IMOC will serve as the center of real-time and off-line operations after the ACE spacecraft is launched. The ASC will serve as the focal point for ACE science operations, for both command generation and data processing. The use of a common system approach will accrue several benefits to the ACE project in the areas of testing, training, and transition to operations. This approach will also provide several building blocks that can be used for future missions.

Traditionally, these three systems would be built under separate development efforts and would share no common system heritage. However, the ACE ground system development team has defined a core set of capabilities that these three systems will share. This common set of capabilities will be implemented as the baseline system named ACE Generic. These core capabilities include

- external communications to provide communication with the ground network and the spacecraft;
- telemetry processing for receipt and decommutation of spacecraft telemetry;
- Systems Test and Operations Language (STOL) to generate system and spacecraft commands;
- STOL syntax checker for off-line validation of STOL procedure syntax;
- command processing to generate and transmit commands;
- command graphical user interface (GUI) to provide a menu-based interface for building spacecraft commands;
- events processing to generate and log spacecraft and ground system events;

- real-time display of selected telemetry parameters;
- generation of the ACE command and telemetry database;
- memory dump/compare of spacecraft memory dumps to a ground reference image;
- Generic Spacecraft Automated Analysis to create expert systems to monitor selected telemetry parameters; and
- Instrument Ground Support Equipment (IGSE) communications for transmission of spacecraft telemetry to the IGSE via serial lines.

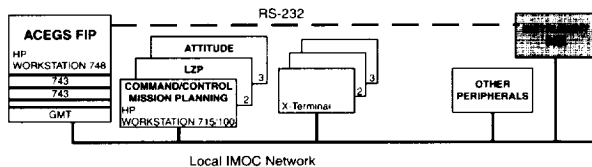
ACE Generic will form the core of the ITOCC, IMOC, and ASC. ACE Generic itself is based upon the Transportable Payload Operations Control Center (TPOCC) architecture. TPOCC provides a generic set of control center functions for telemetry processing and communications. ACE Generic will configure TPOCC to support ACE and to provide command and other ACE-unique functions. In turn, the ITOCC, IMOC, and ASC will add capabilities to provide full system functionality. The ITOCC will add software that allows it to interface with spacecraft-unique integration and test ground support equipment. The IMOC will add software to provide mission planning, attitude determination, data trending, and level-zero processing functions. The ASC will build upon the IMOC capabilities and add software to perform instrument-unique telemetry processing and science data browsing functions. The interrelationships of the software components are shown in the first figure.



*ACE software architecture.*

## MISSION OPERATIONS AND DATA SYSTEMS

The IMOC, ITOCC and ASC will also share a common hardware architecture, consisting of a networked "string" of Hewlett-Packard (HP) workstations and X terminals. One of the HP workstations handles communications with the outside world, and serves as the front-end processor for spacecraft telemetry receipt and spacecraft command. This front-end workstation also acts as the telemetry server for the other workstations in the string. The other HP workstations host software that provides other control center functions, such as real-time display, mission planning, attitude determination, and trending. The second figure shows the mission operations room configuration for the IMOC. The ITOCC and ASC will use similar configurations.



*IMOC MOR configuration.*

This common system approach will provide several benefits to the ACE Project. First, the ACE Generic implementation approach will allow a more efficient process for testing basic system capabilities. Testing the ACE Generic will occur prior to integration with other capabilities. This testing will allow detection and correction of discrepancies of core capabilities early in the development process. Tests in the spacecraft integration and test environment, using the ACE ITOCC, will uncover any incompatibility problems between the spacecraft and ACE Generic. These problems can then be corrected well in advance of the delivery of the launch system.

Second, the common system approach will provide enhanced training opportunities for operations personnel. ACE Generic releases were provided to the flight operations team (FOT) and ASC personnel 2 years prior to launch. This gave the FOT and the scientist early opportunities to familiarize themselves with basic system interface and core capabilities. The FOT and ASC personnel will also participate in receiving spacecraft data flows from the spacecraft integration and test facility. These data flows are facilitated by the implementation of the shared front-end processor between the ITOCC, IMOC, and ASC.

Finally, the common system approach will ease the transition from the spacecraft integration and test environment into the operational environment. Traditionally, a significant effort is required to convert the command and telemetry database and STOL procedures from the integration and test system to the operational system. Since ACE Generic provides a common format for the project database and STOL procedures, no conversion will be necessary. Another major effort would have been to develop the interface for the IGSE to receive telemetry during launch and early orbit. Since the ITOCC and IMOC will have identical IGSE interfaces, this will require minimal effort for ACE.

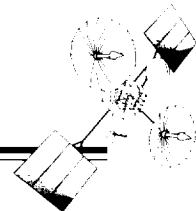
This approach will provide several building blocks for future ground data systems. ACE Generic will serve as a general tool that can be tailored for other missions, with several ACE Generic capabilities candidates for reuse, including

- the ACE front-end processor providing a general capability for receiving and distributing telemetry using the Internet Protocol;
- the IGSE interface, providing a general capability for telemetry distribution over serial lines;
- the command GUI, providing on-line support for building commands; and
- the STOL syntax checker, providing a method for validating STOL procedure syntax in non-real-time.

Contact: Carolyn Dent (Code 511)  
301-286-6801

Sponsor: Office of Space Communications

*Ms. Dent is the Implementation Manager for the ACE mission. She manages all ACE ground data system development activities. She has worked at GSFC for 10 years and previously provided support for the Upper Atmosphere Research Satellite mission and the Hubble Space Telescope first servicing mission. She holds an M.S. in Systems Management with a specialty in space operations.*



## REUSABLE OBJECT METHODOLOGY TO REDUCE THE COST FOR MISSION OPERATIONS

A NEW PARADIGM for planning and providing mission operations services was developed and extended during 1995. In contrast with today's space mission operations infrastructures, this paradigm emphasizes systems that are simple, generalized, resilient, cost-effective, designed to accommodate change easily, and responsive to anticipating, meeting, and exceeding customer needs. It is the intent of our continuing effort to realize these characteristics by directly and aggressively attacking the development (and hence operations and maintenance) of one-of-a-kind, start-from-scratch systems for similar mission operations functions. We believe that this path provides the most promising potential for achieving substantive reductions in cost and complexity. The methodology we are using fosters early collaboration and coordination among seemingly diverse mission elements, such as those for mission platform, communications and tracking networks, and science payloads. The research project in progress is the work of NASA's COST LESS team for Mission Operations.

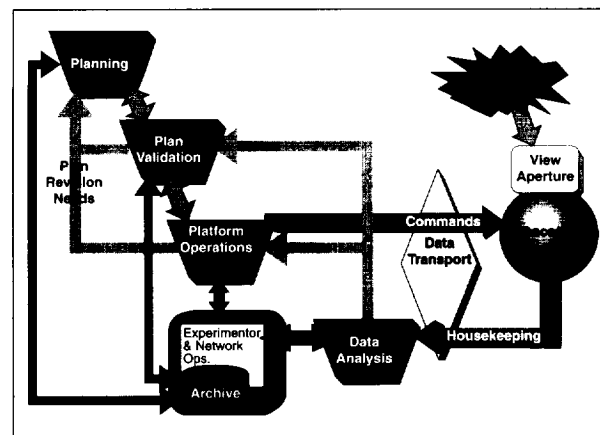
In the traditional view, collaboration among these elements is accomplished through agreements and procedures between the elements at the system interface level, without necessarily examining the systems as a whole. It is our assertion that similar functions are performed within these elements. By not acknowledging these similarities, science, mission, and network segmentation has been preserved, as evidenced by the evolution of separate infrastructures for each of the supporting elements or organizations. These infrastructures are often characterized as complex, specialized, fragile, costly, not designed for change, and not always responsive to customer needs.

The COST LESS team's recurring theme is to reverse the trend of engineering special (unique) solutions for similar problems by focusing on discovering similarities, rather than on preserving differences, and insisting on reducing complexity, rather than on accommodating complexity with ever-more-elaborate management and integration techniques. This dual emphasis evolved from the findings of a predecessor blue team that evaluated the mission operations infrastructure. The blue team found that (1) the numerous and seemingly diverse systems used in mission operations can be represented by only two functional categories, namely, information handling and resource management and control; and (2) "faster, better, cheaper" is more appropriately portrayed as realistic,

credible, responsive, simpler, and smaller. Additionally, the predecessor blue team recognized that focusing on similarities, rather than on differences, expands the solution set for achieving economies of scale, while creating opportunities for reducing complexity of the existing operations infrastructures within the program, science, and tracking networks communities.

Many different modeling perspectives are available to define the space mission operations problem domain. It is our assertion that how the problem is modeled has a lot to do with the uniqueness or commonality of the solution and to whether similar elements are identified within and across missions. It also has a bearing on how many and how effectively off-the-shelf elements are used in the final design.

The data flow model, as illustrated in the first figure, is useful at the highest level to show basic interactions among elements. To adequately describe a system with this methodology, however, many levels of data flow representations are required. The data flow diagrams typically become complicated very quickly as one moves to lower levels of the model's representation. More significantly, the data flow model is designed to identify and emphasize uniqueness of functionality and does not facilitate identification of similarities among similar functions.



*Example of data flow model figure.*

Object-oriented modeling methodologies, on the other hand, typically do enable identification of common elements. However, many object-oriented approaches are just as complicated and detailed as their predecessor data-flow

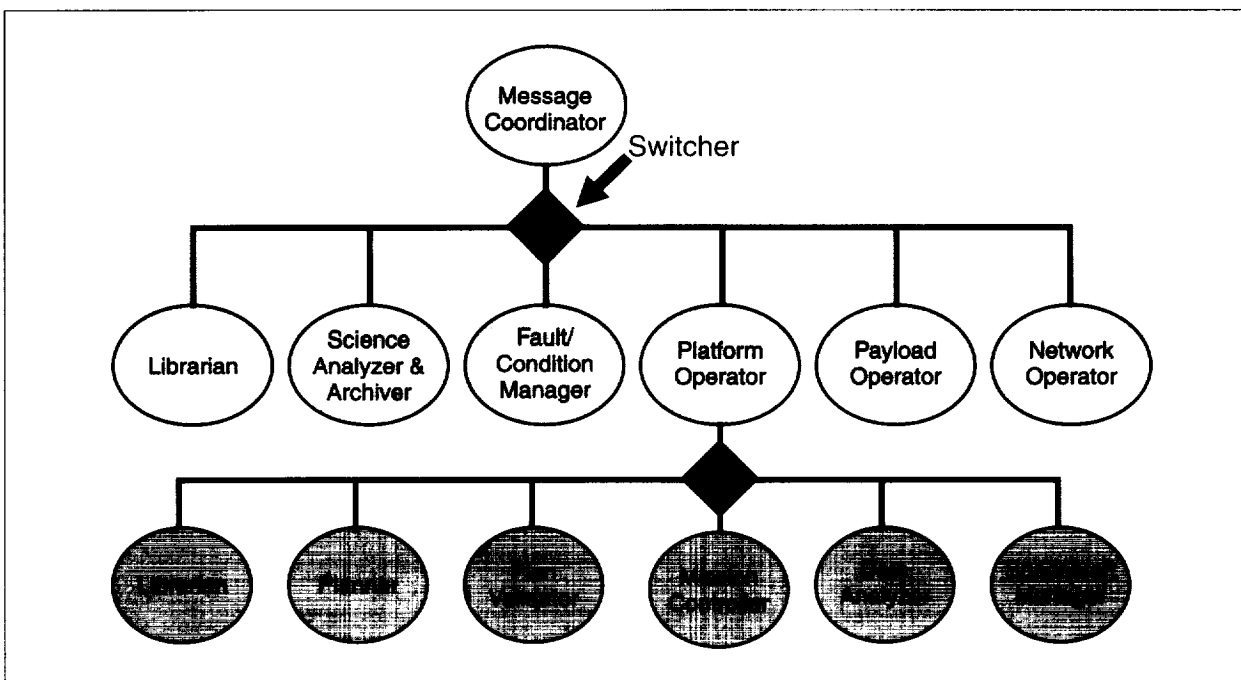
methodologies. Further, due to the complexity of the modeling approach and associated tools, object-oriented models often are neither understood nor used as effectively as they could be used. The reusable object approach that we will describe is proposed because it is simple at all levels of the analysis, and we think it is easy to use. It emphasizes simplicity of elements and interactions among elements within the model. It is object-based rather than strictly object-oriented, since we do not include object-oriented concepts such as polymorphism and inheritance to achieve object reuse. Rather, we emphasize object independence.

We have a reusable object perspective that emphasizes simplicity and reusability. The methodology is called the reUsable Object Technology (UOT). The methodology first emphasizes object usability by creating simple, well-structured standard objects that are easy to implement, test, and maintain. The methodology emphasizes reusability by organizing these objects within libraries for easy identification and access. UOT was first applied to a prototype Distributed Application Monitor Tool (DAMT) in 1991. Since then, other applications have been put to use nationally and internationally. Information on

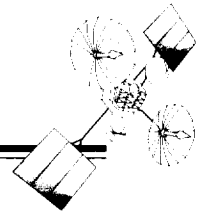
reusable object technology is distributed via the World Wide Web (<http://192.86.20.180>) and through more traditional means, such as presentations and articles.

The reusable object model perspective makes use of beneficial characteristics found in traditional modeling representations, including hierarchical structure and implementation independence. With UOT, however, these characteristics are an integral part of the methodology and complement the unique characteristics of UOT.

The hierarchical structure of UOT, as illustrated in the second figure, allows complex systems to be represented in a straightforward fashion. This allows easy identification of similar objects which can be reused elsewhere. It also allows for easy handling of aggregations of objects. The UOT is aimed at being implementation-independent. That is, the function being performed by an object could be accomplished manually, by an automated computational process, by a specialized instrument, or in any other appropriate manner. Being implementation-independent enables us to specify the mission first, view various trade-offs in design along the way, and prove feasibility properties of the mission specification prior to worrying



*Example object diagram.*



about details specific to implementation. Additionally, it provides a convenient mechanism to ensure that the mission documentation is maintained throughout the mission life cycle.

The UOT also has several characteristics which provide advantages over traditional methodologies, including emphasis on reuse, flexibility and scalability, simplicity of element representation, and independence of objects.

Our UOT was developed with an awareness of prevalent object-oriented methodologies, but stresses reducing complexity, emphasizing reusability and enhanced architectural flexibility. Emphasis on reuse is a feature of most object-based approaches, and UOT is no exception. This characteristic is a departure and improvement from previous methodologies, which emphasized uniqueness. The UOT model also provides flexibility to use the same components in alternative architectures. Components can function within small and large systems and operate in alternative configurations. Perhaps one of the most important characteristics of UOT is its emphasis on simplicity and its use of standard analysis and implementation approaches to assure simplicity. The UOT also achieves a measure of complexity hiding by emphasizing control relationships among its hierarchical representation of objects in the analysis approach.

We want to acknowledge Donald Sawyer of the National Space Science Data Center (NSSDC) at NASA GSFC for bringing the seeds of the UOT to the team's attention, and for having the vision and fortitude to pursue

development of both the standard formatted data unit technology and the NSSDC workbench.

Contact: Don Hei (Code 401)  
301-286-9440  
Internet: [djhei@gsfccost.gsfc.nasa.gov](mailto:djhei@gsfccost.gsfc.nasa.gov)

Rhoda Shaller Hornstein (NASA HQ)  
202-358-4805

Sponsor: Office of Space Communications

*Dr. Hei has been with GSFC since 1969. He is currently colocated with the Advanced Mission Integration Office from the Flight Mission Support Office. He received his Ph.D. in Plasma Physics from the University of Maine in 1976, and is currently working with GSFC's advanced mission analysis group and the agency's COSTLESS team.*

*Ms. Hornstein has been with NASA for approximately 27 years. She is currently the Manager, Integrated Policy and Planning in NASA's Office of Space Communications. She is also leading a cross-cutting team of government, industry, and academia, charged with reducing the cost of success for NASA's space mission operations. Throughout her career, Ms. Hornstein has relentlessly pursued initiatives to produce successfully integrated human/computer systems for responsive and efficient operations over the long term. Ms. Hornstein has received numerous awards, including NASA's Exceptional Service Medal, the Human Flight Awareness Silver Snoopy, and the Cooperative External Achievement Honor Award.*

### ***TDRSS, POSITIONING SYSTEMS, AND ORBIT DETERMINATION***

### **PERFORMANCE CAPABILITIES OF THE TRACKING AND DATA RELAY SATELLITE SYSTEM FOR LOW-EARTH-ORBIT SPACECRAFT**

THE TRACKING and Data Relay Satellite System (TDRSS) is a geosynchronous relay satellite network that currently consists of six geosynchronous spacecraft and the White Sands Complex (WSC) located at White Sands, NM. Three TDRSSs (TDRS-East, TDRS-West, and TDRS-Stored, located at 41°, 174°, and 46°W longitude, respectively) actively support tracking of TDRS-user spacecraft. Of the three remaining TDRSSs, one (located at 275°W longitude) is used only for spacecraft communications, while the others (located at 150° and 139°W longitude), are being reserved for future use. The Bilateral Ranging Transponder System (BRTS) is an integral part of TDRSS, providing range and Doppler measurements for determination of each TDRS orbit. TDRSS can provide 85 to 100 percent coverage, depending on the low-Earth-orbit (LEO) spacecraft altitude.

The performance capabilities of the TDRSS have been demonstrated by the Flight Dynamics Support Branch through the generation of high-accuracy orbit determination solutions for the Ocean Topography Experiment (TOPEX/Poseidon) and Landsat-4 spacecraft. In order to generate high-accuracy orbit solutions for TDRS users, high-accuracy orbit solutions for each TDRS must also be established. The demonstrated ability to obtain high-accuracy orbit solutions for TOPEX/Poseidon, Landsat-4, and the TDRS spacecraft has been due to enhanced mathematical modeling, tracking distributions, and advanced computational techniques.

One of the fundamental efforts in the field of astrodynamics has been the continuing improvement of geophysical and environmental modeling within a generic computational system to support high-accuracy ephemeris generation. The generic computational system at GSFC that supports high-accuracy orbit determination is the Goddard Trajectory Determination System (GTDS). GTDS is a batch-weighted, least-squares algorithm that estimates sets of orbital states, force, environmental modeling parameters, and measurement-related parameters that minimize the squared difference between observed and calculated values of selected tracking measurements such as those obtained for TDRSS and BRTS. It should be emphasized that improvements in mathematical modeling frequently require enhancements to the computational techniques of GTDS.

Through the effective use of improved mathematical modeling and the computational techniques used for the determination and evaluation of range biases and transponder delays within the TDRSS, precision orbit ephemerides for each TDRS have been obtained to support the precision orbit determination effort for the TOPEX/Poseidon and Landsat-4 spacecraft. These improvements in the quality and accuracy of the TDRS ephemerides have resulted from the effective use of simultaneous solutions for TOPEX/Poseidon and TDRS-East and TDRS-West, or for Landsat-4 and TDRS-East and TDRS-West, using the tracking data from both TDRSS and BRTS to support the generation of precision ephemerides. An assessment of the TDRS's ephemerides have been made within the Flight Dynamics Support Branch, indicating that these ephemerides are at the 5 to 15 m level of accuracy.

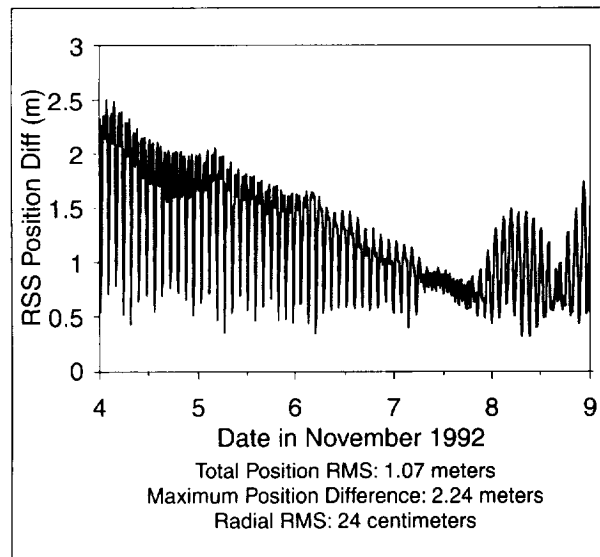
The computational procedure for simultaneous solutions for the TOPEX/Poseidon, TDRS-East, and TDRS-West have been used to generate different levels of precision ephemerides for the TDRS-East and TDRS-West. This simultaneous solution process has been used to determine and evaluate the multiple levels of precision ephemerides that have been obtained for use in the TOPEX/Poseidon standalone solution, which is the precision orbit ephemerides for that specific tracking data interval. We established the simultaneous solution process to determine precision orbits for the TDRSS and for TDRS users through determination and evaluation of range biases, transponder delays for the user spacecraft, TDRS spacecraft, and BRTS sites. Through the effective use of simultaneous solution processes, precision orbits for TDRS-East and TDRS-West—with an uncertainty of 5 to 15 m—were used as the TDRS ephemerides in the precision orbit solutions for TOPEX/Poseidon.

Through the use of the precision orbits generated for the TDRS-East and TDRS-West, improved geophysical and environmental modeling, improved computational techniques, and enhanced spacecraft modeling, TOPEX/Poseidon precision orbit ephemerides were generated and evaluated. An assessment of the accuracy of the TOPEX/Poseidon precision ephemerides generated by the GTDS batch least-squares process was performed by through the comparison and evaluation of these precision

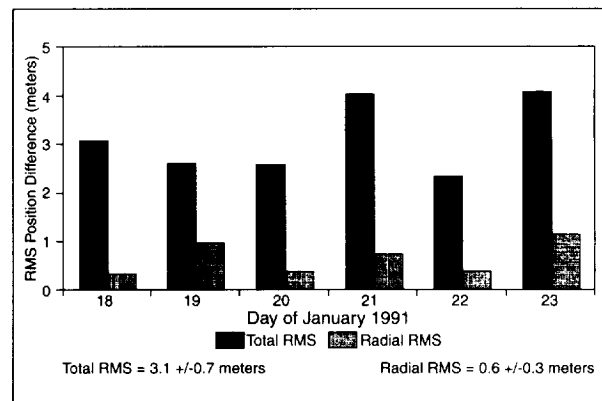


ephemerides with the precision orbit ephemerides generated by using laser and Doppler Orbitography and Radiopositioning Integrated by Satellite (DORIS) tracking measurements. The precision orbit ephemerides for the TOPEX/Poseidon mission science data include a maximum 13 cm ( $1\sigma$ ) radial position error requirement. The radial uncertainty in the precision orbit ephemeris generated by the Space Geodesy Branch for this particular tracking interval is 5 to 6 cm.

The comparison of the TOPEX/Poseidon precision ephemeris generated by the Flight Dynamics Branch with the precision orbit ephemerides obtained by the Space Geodesy Branch shows a total position root-mean-square (rms) of 1.07 m and a radial rms of 24 cm for the total data arc from November 4, 1992, through November 9, 1992, as shown in the first figure. The 24-cm difference in the radial direction between the Flight Dynamics Branch TOPEX/Poseidon precision orbit ephemeris using TDRSS data and the Space Geodesy Branch precision orbit ephemerides using laser and DORIS data is a measure of the accuracy of the TDRSS data and its performance capabilities. The Flight Dynamics Branch expects the 24-cm value to continue to decrease as improvements in mathematical modeling and computational techniques are made within GTDS.



The computational procedures for simultaneous solutions that were used for the TOPEX/Poseidon, TDRS-East, and TDRS-West have also been used to generate the precision orbit ephemerides for the Landsat-4, TDRS-East, and TDRS-West using the improvements in the mathematical modeling, tracking distributions, and computational techniques. Through the use of the computational enhancements that had been established for the TOPEX/Poseidon solutions, precision orbit ephemerides have been generated and evaluated for the Landsat-4, TDRS-East, and TDRS-West. Through the simultaneous solution process, precision orbit ephemerides for TDRS-East and TDRS-West have been obtained that have uncertainty between 5 m and 15 m. Since an accuracy assessment of the Landsat-4 solutions cannot be established similar to the TOPEX/Poseidon technique, the technique of overlap consistency was used. Due to an enhanced tracking data distribution for TDRS users, seven 34-hour data arcs for Landsat-4 were generated, with each solution containing ten hours of data with the previous solution (i.e., overlap interval of 10 hours), beginning at 0 hours UTC of each day from January 17 to January 23, 1991. The total rms and radial rms values of the six Landsat-4 overlap comparisons are summarized in the second figure. The total position overlap differences, the mean and sample standard deviation of the rms distribution is  $5.3 \pm 1.4$  meters. For the radial position overlap differences, the mean and sample standard deviation of the rms distribution is  $0.6 \pm 0.3$  meters.



## MISSION OPERATIONS AND DATA SYSTEMS

---

The analysis which has been performed by the Flight Dynamics Branch using the TDRSS data and BRTS data for precision orbit determination for TOPEX/Poseidon, Landsat-4, TDRS-East, and TDRS-West clearly indicates that the centimeter-level of uncertainty in the radial direction can be met using these data to support future NASA altimetry missions. The primary reason for the differences between the TOPEX/Poseidon precision orbit ephemerides generated by the Space Geodesy Branch and the TOPEX/Poseidon precision orbits obtained by the Flight Dynamics Branch using the TDRSS data are the differences in geophysical and environmental modeling that exist within the individual orbit determination systems.

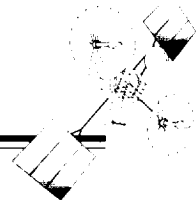
Existing mathematical models that have not been included in GTDS for generation of precision ephemerides are the ocean tides, Earth radiation pressure, and spacecraft macro models for the TOPEX/Poseidon, Landsat-4, and the TDRSSs.

These results clearly demonstrate that the existing TDRSS data have overall performance capabilities to support precision orbit determination for LEO missions for a spectrum of altitudes (i.e., 600 km and higher). The support of a NASA altimetry mission which would have a requirement of a few centimeters in the radial direction for precision orbit determination could be supported with TDRSS and within the Flight Dynamics Branch using GTDS along with improvements in the mathematical modeling, tracking data distributions, and computational techniques.

Contact: Clarence Doll (Code 553.2)  
301-286-6037

Sponsor: Office of Space Communications

*Mr. Doll is an astrodynamist within the Flight Dynamics Division of GSFC's Mission Operations and Data Systems Directorate. Mr. Doll manages the research and development of mathematical and computational techniques that support the field of astrodynamics within the Flight Dynamics Design.*



## NASA AUTONOMOUS NAVIGATION SYSTEMS

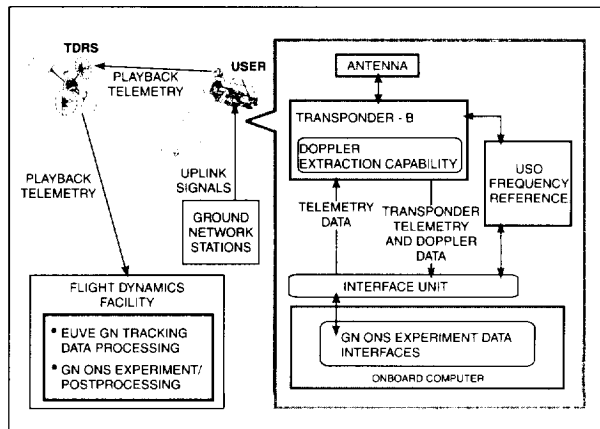
**A**UTONOMOUS ONBOARD navigation products are available to NASA user spacecraft in real time via the Tracking and Data Relay Satellite System (TDRSS) Onboard Navigation System (TONS). The Flight Dynamics Division has developed this capability by using communication equipment already available on the user spacecraft to measure the Doppler shift due to the relative motion between the user and the TDRS spacecraft of an S-band forward link carrier signal. The experiment on the Extreme Ultraviolet Explorer (EUVE) mission in 1992 flew a Motorola second-generation TDRSS user transponder and an ultrastable oscillator, successfully flight-demonstrating TONS for autonomous navigation by extracting Doppler data onboard, and processing the data on the ground in a flight emulation system that included flight navigation software. The success of the TONS experiment is being applied operationally to Earth Observing System AM-1, flying an improved TONS as the prime navigation system.

This past year, as a follow-on to the TONS experiment, Doppler data from ground station communication signals were passively extracted onboard EUVE and similarly processed on the ground to demonstrate an autonomous onboard navigation system (ONS) capability for ground station-only users, as shown in figure. Results of the ONS flight demonstration showed that real-time user position accuracy of 150m can be obtained with two 5-minute communication contacts per day. Improved performance can be realized by increasing the number of daily contacts. Alternatively, many future NASA users whose missions do not require the high-accuracy performance demonstrated in the past, will realize the benefits of a simplified approach to autonomous navigation in ground operations cost savings and in spacecraft implementation and test costs. In addition, the algorithms can be tailored to meet specific user needs.

Extending the use of ONS to small satellites requires that the user transponder or command receiver measure the Doppler shift in a communication signal uplinked from a ground station. Measuring Doppler on the received carrier can be a by-product of a digital receiver using a numerically controlled oscillator (NCO); accumulating the carrier tracking loop NCO offset provides an effective measure of the Doppler effect on the carrier. The receiver must be able to accept and use a very stable oscillator as its frequency reference to provide viable

measurements for navigation. The Doppler observations can then be processed in navigation flight software in real time or as needed by the spacecraft, providing definitive and predicted navigation products that include position, velocity, frequency, and time maintenance. The real-time navigation solutions are used in the attitude control system, science telemetry annotation, ground track prediction, and autonomous signal acquisition. The required navigation flight software could be included in the onboard computer. However, significant reductions in risks and costs associated with redeveloping the software and integrating the system for each user of ONS would be realized by incorporating the navigation flight software into the transponder or command receiver. The compactness of the ONS (since it is software based) has minimal impact on a user spacecraft power, weight, and volume attributes. For missions not requiring precision navigation solutions to the 10 cm level, ONS is a cost-effective alternative to Global Positioning System (GPS) techniques, from both fiscal and physical perspectives. Unlike ONS, GPS requires additional hardware (GPS receiver/processor and L-band antennas) in addition to the normal satellite complement of communication equipment.

When the navigation products are received on the ground via the downlinked telemetry, ONS performance can be monitored periodically (e.g., once per month) in an automated ground support system available from the Flight Dynamics Division. The ONS ground support system is a workstation-based portable quality assurance and performance monitoring tools set that can be hosted in any user-selected environment, or within Flight Dynamics itself.



Ground station ONS (GONS) experiment configuration.

## MISSION OPERATIONS AND DATA SYSTEMS

---

Cost reductions obtained from ONS are realized in the following areas:

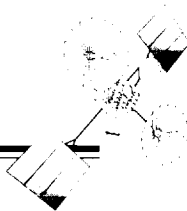
- special tracking services—other than contacts needed for communication—are eliminated, since ONS relies on the communication uplink carrier for its passive data collection;
- ONS provides a definitive navigation solution, thereby eliminating the need for routine ground-based orbit determination and associated operations support for uplinking ephemeris data to the spacecraft;
- the ONS solution can be directly propagated (without further processing of either the raw data or the navigation solutions) either onboard or on the ground to support science planning or communication scheduling;
- the navigation information can be downlinked in the telemetry, simplifying interfaces between elements of the ground support system ordinarily required to pass definitive and predicted ephemerides from ground-based orbit determination;
- the navigation solutions can be sent directly to scientists and to the ground terminal, and used to autonomously generate acquisition and ground track data;
- station scheduling information could be generated autonomously from ONS navigation solutions since the data is fresh and available onboard, eliminating the need for ground generation of such data;
- errors in the attitude control system due to propagation of an uploaded ephemeris are reduced, since definitive data are available onboard, thereby providing more robust attitude control;
- ONS navigation solutions also provide a means for autonomous ground track prediction onboard, eliminating the need for *post facto* determination on the ground; and
- placing the ONS flight software in the command receiver significantly reduces life cycle costs by eliminating the need to redevelop, integrate, and test all or parts of the software for each mission. The ONS flight software can be tested during the command receiver acceptance test phase, eliminating the need for the additional interface testing that would be required if the flight software resided in a user's onboard computer.

ONS has been proven to meet future navigation requirements with no additional hardware needed on the spacecraft, and is capable of high accuracy performance. As a software-based function, a Doppler extractor can be integrated into alternative command receivers or transponders with no hardware impact. Integrating proven flight software with the communications receiver reduces the risk associated with redeveloping the ONS flight software to serve each new mission. As a consolidated box, ONS in the receiver provides a synchronized implementation which is vital to quality tracking measurements and the resultant navigation solution. Because of all these features, ONS provides an elegant solution for satellite autonomous navigation.

Contact: Cheryl Gramling (Code 553)  
301-286-8002  
Internet: Cheryl.Gramling@gsfc.nasa.gov

Sponsor: Office of Space Communications

*Ms. Gramling is an aerospace engineer in the Flight Dynamics Support Branch developing advanced technologies for spacecraft autonomous navigation systems. Ms. Gramling earned a B.S. in Aerospace Engineering from the University of Maryland, and has been at GSFC for 12 years.*

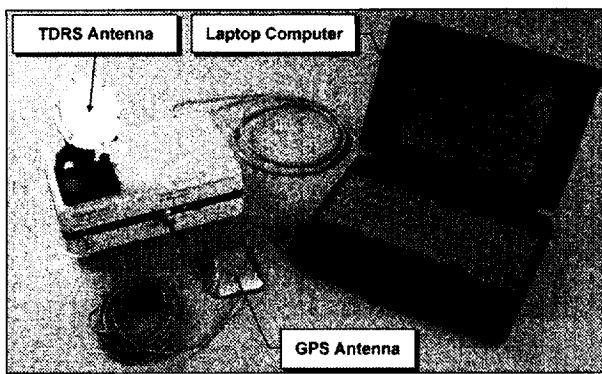


## PORTABLE TDRSS COMMUNICATOR

THE PORTABLE TRACKING and Data Relay Satellite System (TDRSS) Communicator (PORTCOM) Project is a follow-on to the Global Learning and Observation to Benefit the Environment (GLOBE) Project. GSFC's Systems Engineering Office was tasked as lead for the GLOBE activity to design, build, integrate, and test 10 low-powered, battery-operated transmitters and 10 commercially powered receivers. Each transmitter and receiver is supported by a laptop computer using commercial and project-specific software. These units were fabricated to be used in the field by school children (K-12) to collect environmental data and to communicate with the National Oceanic and Atmospheric Administration (NOAA) in Boulder, CO, via TDRSS and associated communication facilities at GSFC.

Each spread-spectrum transmitter (shown in the first figure) contains a global positioning system (GPS) receiver and antenna (for local position and TDRS pointing information), a 1 W power amplifier, a 3-in-diameter patch antenna with 6.8 dBi of gain, and an interface to a laptop computer for data entry, message formatting (which includes GPS position information), rate one-half convolutional encoding via a microprocessor, and associated control functions. The transmitter weighs less than 5 pounds including the battery, which itself weighs a little over 2 pounds.

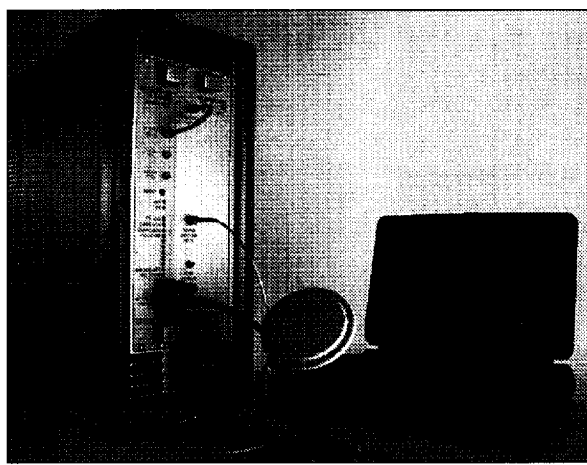
A single transmitter has been modified to handle digital voice communications and increase the data rate from 4.8 kbps to 19.2 kbps (38.4 ksps rate one-half coded) or 38.4 kbps uncoded, by replacing the stock processor with one that was pin-compatible, and a crystal for higher clock-rate capability.



Portable transmitter.

Each spread-spectrum receiver (shown in the second figure) uses state-of-the-art technology, including a charged coupled device (CCD) correlator, digital signal processing (DSP), and a Viterbi decoder, which effectively makes these digital receivers. The CCD correlator is pseudo-random noise (PN) code programmable, and performs PN code match filtering and parallel processing for rapid acquisition. The DSP performs all acquisition and tracking processing and uses feed-forward processing, which is amenable to implementation via application-specific integrated circuits. The Viterbi decoder is contained on a chip that is an off-the-shelf product of Stanford Telecom (STel). The receiver also uses a 3-in-diameter patch antenna with a gain of 6.5 dBi in conjunction with a low-noise amplifier to yield an antenna-gain-to-system-noise-temperature ratio of -20 dBi/K. The receiver has an RS-232 interface to an IBM-compatible laptop or other compatible computer for display of NOAA data and control functions.

A successful demonstration of the transmitter and receiver capability was performed on May 9, 1995, at NASA Headquarters (HQ). Image and text data files were transmitted from the roof to the White Sands Complex (WSC) via TDRS East, where they were relayed to the Packet Processor (PACOR) at GSFC via the NASA Communications Network (NASCOM). The error-free data were reformatted for return to NASA HQ via NASCOM, WSC, and TDRS East. The Associate Administrators of the Office of Space Communications personnel were able to view transmission and reception of a color image file and view it shortly after it was received.



Portable receiver.

## MISSION OPERATIONS AND DATA SYSTEMS

---

Two transmitters and associated laptop computers were successfully used at McMurdo, Antarctica, for determining future site location of a communication system to work with the TDRSS. NOAA has purchased a PORTCOM transmitter and laptop computer from GSFC for testing as part of their ocean buoy program to be used with TDRSS. NOAA will be working with the System Engineering Office at GSFC and STel in Reston, VA, during their test phase to see if any changes are necessary to incorporate the transmitter into the existing buoy design. Full-scale application would be from 70 to 100 units. Future consideration is being given to incorporation of a receiver.

Successful end-to-end testing of the modified transmitter and receiver was accomplished between Reston, VA, and GSFC via TDRS East using TDRSS S-band single access (SSA) service, WSC, NASCOM, and PACOR in mid-August 1995. During this test period, 19.2 kbps data (38.4 kbps rate one-half encoded) were transmitted and received error-free with over 4 dB of margin in clear-weather conditions. Voice transmission and reception were very clear and crisp. This activity concluded the proof of concept associated with modifying the existing design. The TDRSS SSA service was used to avoid making a phased-array patch antenna to close the link using the multiple access (MA) system. We are now developing an MA demand access proof of concept using the digital portion of the PORTCOM receivers to interface to the output of the MA beamformer at WSC, so that users can be supported continuously without requiring advanced scheduling.

The technology that is being used in the PORTCOM activity is applicable to many areas, such as replacement for the bilateration ranging transponder system transponders; communication equipment for use in balloon missions; transponders or separate transmitters/re-

ceivers in ground, sea, and air applications; and space-craft with flight-qualified components.

The authors wish to acknowledge the outstanding support provided by Mr. Dan Urban and his team in the various phases of designing, building and testing of the transmitters, receivers and related software; and that provided by Mr. Steve Duran from GSFC Mission Operations and Systems Development Division, for his superb contribution of packet processing software in the reception of data at PACOR, and for software he developed for the forward-link data transfer to WSC.

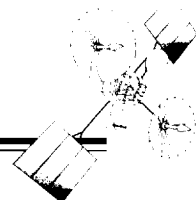
Contact: Arthur Jackson (Code 504 )  
301-286-9058

Lou Koschmeder (STel)  
703-438-7919

Sponsor: Office of Space Communications

*Mr. Jackson is the Space Network Systems Manager in the Systems Engineering Office. Mr. Jackson earned his B.S.E.E. in 1967 and his M.S.E.E. in 1968 from the University of Miami in Coral Gables, Florida. Mr. Jackson has completed over 30 credit hours at George Washington University in a doctoral program. He is responsible for top-level systems requirements and specifications, total end-to-end system design, interface definitions, and preparation of all technical specifications leading to systems procurement.*

*Mr. Koschmeder is the Director of Information Processing for Stanford Telecom, Inc. He has a B.S.E.E. in 1959 from the University of Maryland. Prior to his retirement from GSFC, he served as the Chief of the Information Processing Division in the Mission Operations and Data Systems Directorate.*



## ENHANCED TDRSS USER RF TEST SET: TRANSPORTABLE TDRSS GROUND SUPPORT EQUIPMENT

THE RADIO FREQUENCY (RF) Systems Section has developed a low-cost, state-of-the-art Tracking and Data Relay Satellite System (TDRSS) User RF Test Set (TURFTS), offering enhanced TDRSS and Ground Network (GN) communications-testing capabilities to NASA missions at a fraction of the cost of earlier hardware. TURFTS emulates the forward link (F/L) TDRSS signals, receives and demodulates return link (R/L) signals from the user spacecraft, and provides the necessary characterization and testing of overall communications system performance.

During the past year, TURFTS hardware and software have been upgraded to support a variety of spacecraft projects, providing enhancements to meet their unique requirements. Some of these new requirements included providing

- uplink and downlink modifications to test transponder GN modes of operation;
- a capability for deinterleaving R/L signals (plus a data interleaver capability to produce simulated data streams for test); and
- the ability to vary the transmitter frequency at a rate of 4000 updates per second to generate a precision orbital Doppler profile for simulating signal dynamics in the Space Network (SN) and GN modes, and testing customers using the TDRSS Onboard Navigation System (TONS).

The TURFTS design incorporates many new technologies that have greatly reduced the space requirements of the test set. TURFTS is packaged in one 24" W x 78" H x 30" D enclosure, which houses a spectrum analyzer, a digital oscilloscope, a time interval counter, a system controller, an RF distribution unit (RFDU), and a signal processing unit (SPU). The system controller consists of a PC executing National Instruments' LabView graphical user interface to control TURFTS and its supporting commercial test equipment. The RFDU is a custom-designed RF chassis providing the RF interface between the user transponder and the TURFTS system. The SPU is a chassis housing custom-designed analog and digital modules providing frequency synthesis, intermediate frequency (IF), and base-band functions. The TURFTS transmitter provides a direct sequence spread-spectrum signal required

for the TDRSS modes of operation, and also provides a phase-modulated signal required for the GN mode to support preintegration testing of user transponders and final spacecraft-level testing.

Currently, the TURFTS system can be configured and controlled remotely via a bidirectional RS232 serial data port; plans call for adding software to include a TCP/IP remote interface. The remote control capability of TURFTS offers spacecraft project engineers the ability to integrate the TURFTS system into a spacecraft test bed under the control of a central computer. Using simple commands, the central computer can then control complex transponder test sequences, with the capability of configuring the signal paths, operating modes, and power levels, and adjusting and monitoring all essential communications parameters.

Transportability has been a very important consideration in the design of the TURFTS enclosure, which has packaging options allowing easy shipment and setup at the launch site or other remote locations. The TURFTS remote control capability allows RF system engineers to monitor and control the system from their office or home for more efficient and timely problem resolution.

The TURFTS was upgraded to incorporate a phase modulator module that contains the necessary circuitry to provide the GN uplink transmit signal. The TURFTS phase-modulates the S-band carrier with a subcarrier that is provided by the satellite checkout station. When phase-modulation is not selected, TURFTS also has the capabilities of quadrature phase-shift keying or binary phase-shift keying the RF signal to be transmitted. The data simulator is another one of TURFTS unique features, providing pseudo-random-noise (PN) data patterns, rate one-half and one-third encoding, convolutional interleaving (Q-channel only), and NRZ-L NRZ-M, NRZ-S or binary-phase L, M, or S data formats at user-specified data rates between 100 bps and 300 Kbps for the I-channel and between 100 bps and 3 Mbps for the Q-channel. In addition to generating all 85 NASA/TDRSS PN codes, TURFTS also generates the 85 National Space Development Agency of Japan codes and 85 European Space Agency codes for the forward- and return-links for future use in testing multinational communications hardware.

## MISSION OPERATIONS AND DATA SYSTEMS

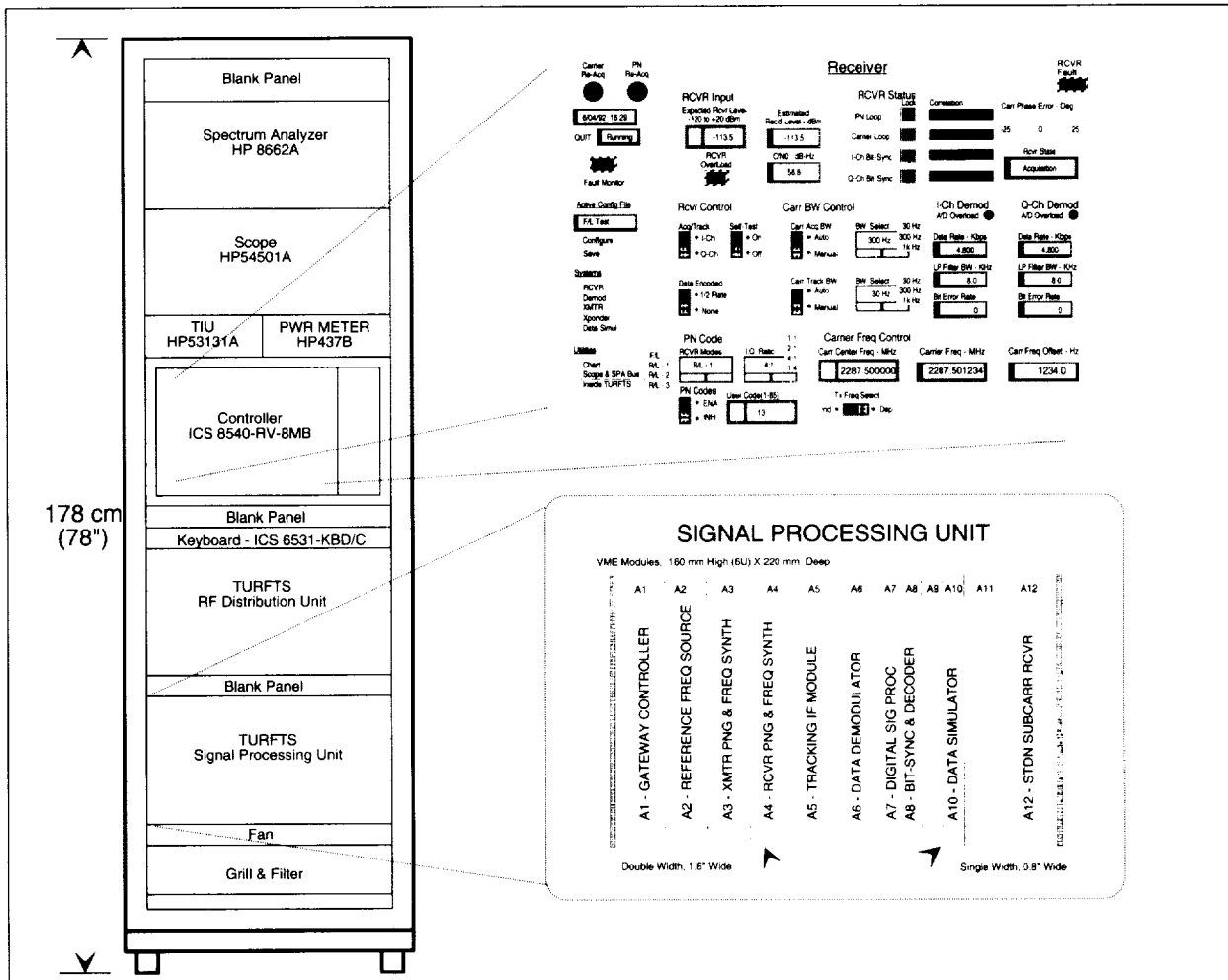
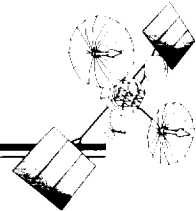


Diagram of the TDRSS User Radio Frequency test set.

The TURFTS receiver is based on a DSP design and contains a bit synchronizer and capabilities for deinterleaving, rate one-half or one-third Viterbi decoding, and multiple data/symbol formats. A Q-channel and I-channel bit-sync input has also been provided, which enables the user to bypass the receiver function of the TURFTS system by directly injecting the I-channel/Q-channel demodulated data streams.

Verification of the TURFTS RF communications links are made possible in the self-test mode by utilizing a frequency translator and identical PN coders in the transmitter and receiver. The TURFTS receiver can acquire its transmitter signal using PN codes for the forward and return-link modes. This configuration allows verification of the TURFTS RF links and components to assist in isolating problems during troubleshooting.



The TURFTS Operations and Maintenance Manual is currently distributed electronically in portable document format, via the Internet. In the near future, users will be able to electronically download current TURFTS specifications, customer support instructions, diagnostic suggestions, test procedures, and system software updates.

The Wallops Flight Facility Long Duration Balloon Project was the first to take advantage of the TURFTS system. The TURFTS system was used to support balloon flight tests at Lynn Lake, Canada, in 1993 and 1994. The TURFTS design was then modified to provide Compton Gamma Ray Observatory (CGRO) science data reception capabilities (both single and multiple access), and the TDRSS multiple access (MA) beamformer equipment calibration signal generation capabilities for the fast-track CGRO remote terminal system (GRTS) installation in Australia to close the TDRSS zone-of-exclusion. Remote control capabilities were also incorporated to interface to the Operations Monitor and Control System to allow the TURFTS in Australia to be controlled via a Sun workstation located in White Sands, NM. The TURFTS' receivers in GRTS have been providing greater than 99 percent of the scheduled data from CGRO. During 1995, the TURFTS design was enhanced, and units were built to support integration and test of GSFC's Earth Observing System AM, Tropical Rainfall Measuring Mission and Landsat-7 projects.

The TURFTS design supports a wide range of operational modes, modulation types, and data rates while remaining compact, flexible, maintainable, and reliable. In addition, the improvements and diversity realized in the

current TURFTS design—and those planned for the future—will have far-reaching implications, setting new standards for serving the communications testing needs of the NASA community.

The authors would like to acknowledge the essential contributions made by Frank McCluer and Carlos Taveras of the RF Systems Section, and Steven Leslie, Hollys Allen, Bruce Friend, Mae Blevins, Thomas Winter and Rosemary Feeney of ATSC.

Contact: John Badger (Code 531.2)  
301-286-4675

David Israel (Code 531.2)  
301-286-5294

Sponsors: Office of Space Communications

*Mr. Badger is a senior electronics designer in the RF Systems Section of the Network Engineering Branch. He is Project Manager and Design Team Leader for the development of the TURFTS system. Mr. Badger has 35 years of experience in electronic circuit and system design of communications and tracking systems for NASA's Ground and Space Networks.*

*Mr. Israel is a senior electronics engineer in the RF Systems section of the Network Engineering Branch. He earned a B.S.E.E. from Johns Hopkins University in 1989 and an M.S.E.E. from George Washington University in 1995. His TURFTS responsibilities include receiver design, operator interface software development, and customer applications support.*

## DEVELOPMENT OF THE GPS-ENHANCED ORBIT DETERMINATION EXPERIMENT

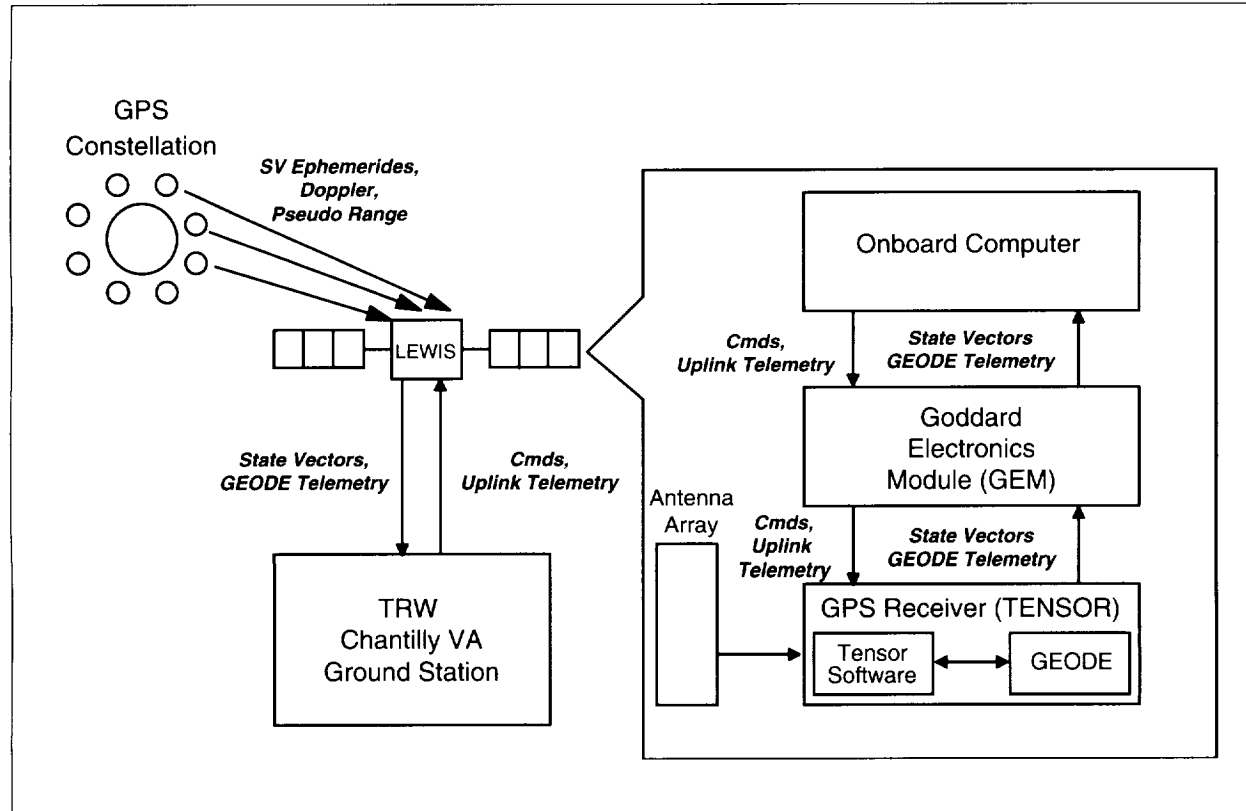
**N**ASA'S SMALL SATELLITE Technology Initiative (SSTI) program, including the Lewis and Clark satellites currently under construction, provides platforms for demonstration of emerging science and engineering technologies. As one of the technology demonstrations, the SSTI/Lewis spacecraft will carry redundant Space Systems/Loral Tensor Global Positioning System (GPS) receivers for orbit, attitude, and time determination in the GPS Attitude Determination Flyer (GADFLY) experiment. Spacecraft attitude derived from the experiment is purely experimental, but Tensor-determined state vectors and timing will be made available to the spacecraft systems. Single-point solutions generated by coarse-acquisition code receivers are not expected to meet the 150 m,  $3\sigma$  real-time position requirement of the Hyperspectral Imager (HSI) due to signal degradation affecting nonmilitary users; additional processing is necessary to achieve this goal. The Tensor incorporates a Kalman filter, which is specified to meet the HSI requirements. However, excess central processing unit and memory capacity of the Tensor offered the opportunity to incorporate improved filtering software directly into the receiver to produce vectors with even higher accuracy. Flight Dynamics Division (FDD) analysts and programmers at GSFC have teamed with the Guidance and Control Branch to develop filtering algorithms for enhanced orbit determination to be integrated into the Tensor. In addition to providing improved real-time positions for the HSI instrument, the filter provides strong dynamic coupling between spacecraft position and velocity, which is lacking in point solutions. This is particularly important when state vectors are to be used for ephemeris prediction. The improved dynamics allow the receiver to continue to generate accurate states during signal outages or degraded coverage, as the filter propagates the state without measurements. Science planning and scheduling will also benefit from the enhanced solutions.

Development of the GPS-Enhanced Orbit Determination Experiment (GEODE) has benefited from such considerations, and is continuing toward a high degree of software modularity for enhanced reusability. To meet more accurate onboard orbit requirements and to reduce operations costs for Tracking and Data Relay Satellite System (TDRSS) user spacecraft, the FDD developed an autonomous navigation system that passively obtains onboard

tracking from the nominally scheduled communications uplink signal. The TDRSS Onboard Navigation System (TONS) coordinates the transponder and flight computer to acquire tracking data and to compute orbit solutions. This creates a navigation system that is inherent to existing spacecraft systems, one that imposes few or no additional hardware or power requirements. TONS implements an extended Kalman filter with high-fidelity force and statistical models to sequentially process Doppler observations output by the transponder-carrier tracking loop; it is capable of producing solutions at the level of the GPS precise-positioning service. GEODE will use applicable experience from TONS software and a 1-year flight demonstration conducted on the Extreme Ultraviolet Explorer spacecraft to substantially shorten the development schedule of less than 1 year and meet Lewis milestones.

While TONS uses integrated Doppler observations for input to the filter, the Tensor provides pseudo-range, carrier phase, and Doppler data. However, the filter structure and spacecraft dynamics are not dependent on data type, and the intent is to modify the TONS filter to accept the GPS observations and reuse much of the flight software developed for the Earth Observing System AM-1 satellite, scheduled for launch in 1998. Key algorithms to be developed for GEODE include measurement models for the GPS observables and a routine for satellite selection. Extraction of the GPS broadcast data message is done by the Tensor, and the basic GPS constellation position and timing information will be available to the GEODE software in memory.

The Tensor procured for GADFLY is an off-the-shelf position, attitude, and time determination system. As shown in the block diagram in the figure, GEODE software will be added to the Tensor after delivery to GSFC, and will run as a process in addition to the standard Tensor functions, producing a second position/velocity solution. Analysts and software developers will work closely to generate specifications, define code changes, and evaluate updated code using an evolving prototype approach. Code development will take place on a Sun and an RS6000-based workstation. Another RS6000 workstation will be used to emulate the Tensor (which uses a compatible RAD6000 processor) to gain experience in downloading code, and to evaluate timing and code size before the Tensor delivery.



*SSTI/Lewis configuration showing Tensor and embedded GODE software.*

Following launch in July 1996, the spacecraft state, covariances, and other parameters sufficient for complete performance evaluation will be downlinked in telemetry. Raw observations from the Tensor will be postprocessed in combination with data from a network of ground-based GPS receivers to produce high-accuracy solutions that can be used as a baseline for comparison. Orbits derived from S-band tracking may also be used to provide an independent check of GODE solutions.

Contact: Roger Hart (Code 553.2)  
301- 286-8729

Stephen Leake (Code 712.1)  
301- 286-6023

Sponsor: Office of Space Communications

*Mr. Hart has been an aerospace engineer in the Trajectory Section of the Flight Dynamics Support branch at the GSFC for 6 years, working in development of sequential orbit determination techniques and autonomous spacecraft navigation. He received his B.A. in Physics in 1986, and an M.S. in Mechanical Engineering in 1989 from Utah State University.*

*Mr. Leake has been an attitude controller in the Control System Software and Simulation Section of the Guidance and Control Branch at GSFC since January 1995. Before that, he worked on robotics for GSFC. His specialty is embedded systems software. He received his B.S. in Physics in 1980 from Rensselaer Polytechnic, and an M.S. in Physics in 1982 from the University of Maryland.*

## GROUND SYSTEM SOFTWARE FOR GLOBAL POSITIONING SYSTEM ATTITUDE DETERMINATION

THE FLIGHT DYNAMICS DIVISION (FDD) is advancing the state of the art in determining spacecraft attitude using the latest in attitude sensor hardware. The latest example is the use of global positioning system (GPS) antennas for attitude determination. This technology is gaining popularity mainly because of its low cost and weight, and its theoretical capability to provide attitude accuracy in the tenths of degrees. The FDD is responsible for using this technology to produce models and algorithms for ground support systems to support future missions. The models and algorithms developed deal not only with attitude determination, which itself has special application for GPS data, but also with calibration of the attitude sensor and prediction of GPS visibility.

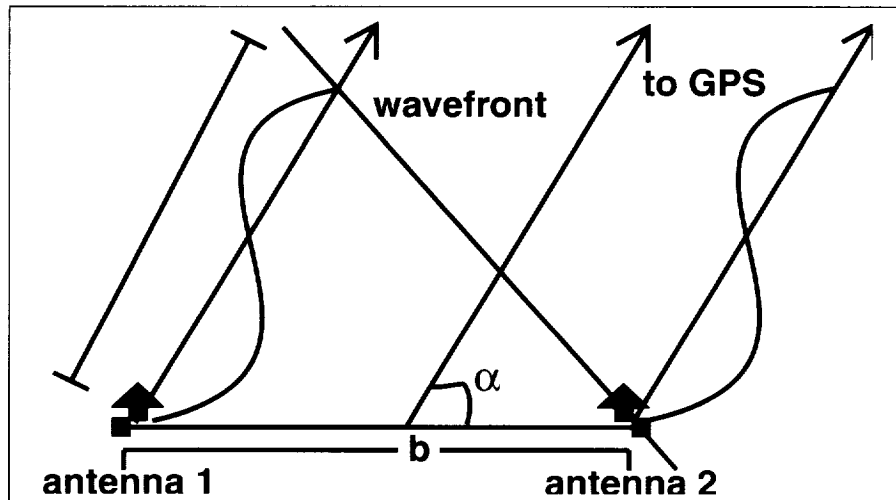
The GPS sensor is actually two antennas that act in tandem to form a baseline, as shown in the first figure. From this baseline, a phase difference between signals received at the antennas is computed, which can be transformed into an angle, according to the equation:

$$\cos \alpha = (n+k\phi) (\lambda/b)$$

where  $\alpha$  is the angular measurement,  $n$  is the integer ambiguity,  $k$  is a conversion scale factor,  $\phi$  is the decimal phase difference,  $\lambda$  is the wavelength of the GPS signal, and  $b$  is the baseline length. The phase difference is given by the quantity in the first set of parentheses.

With another baseline, the two angular measurements can be converted into a line-of-sight vector to the visible GPS satellite. Several components add to the uncertainty of the measurement, such as the integer ambiguity ( $n$ ). The phase difference ( $\phi$ ) produces only the decimal part; the integer part must be determined by another means. Several methods have been suggested to specify the integer part, and FDD is looking into these. The other components are noise, a time bias in the electronics, and any misalignment of the antennas. All these make it necessary to employ an estimation process that best fits the mission's conditions and configuration to meet attitude requirements.

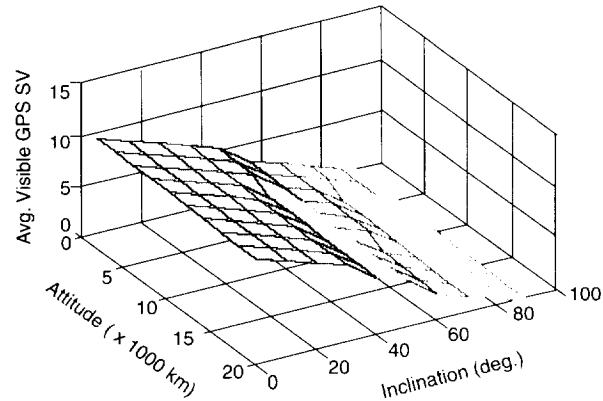
FDD's first effort was to produce an estimation simulator to help investigate the modeling and algorithms that would be needed not only for attitude determination, but also for calibration purposes. The simulator was developed as an analysis tool in Microsoft FORTRAN on an IBM-compatible PC. The simulator models both the user spacecraft and the GPS constellation, and includes dynamics to represent a realistic spacecraft attitude history. The GPS sensor modeling outputs phase difference, taking into account such things as the integer ambiguity, Gaussian noise addition, biases, misalignments to each antenna, and resolution of the least significant bit in the telemetry word. The output from the two baselines is then used as input to an estimation process, which first applies



*Relationship between the phase difference and computed angle.*

the integer ambiguity correction to the phase; several methods have been investigated for this purpose. The routine then converts the output to a line-of-sight unit vector. The unit vector is then paired with a GPS line-of-sight reference vector, that is, where the GPS should be at that time in the geocentric inertial coordinate system. This observation/reference pairing of data is then fed into the estimator, of which there are two in our simulator's case. An extended Kalman filter and a single frame estimator (known as QUEST) were implemented to evaluate fine and coarse attitude determination capabilities. The Kalman filter has shown that if the phase center is well known, in the absence of multipath it is possible to achieve better than one-half a degree resolution per axis for a one-meter baseline length. QUEST demonstrated a resolution capability to within two degrees. Both these methods have opened up new considerations, such as observability and geometric dilution of precision, the subset of GPS satellites at any one time that will yield the best measurement data. The results of investigating modeling using this simulator have produced specifications that are currently being implemented in FDD's ground support system for future missions.

Investigations of observability, geometric considerations, and selection processes were done using a prediction utility also developed on the PC in Microsoft FORTRAN. The utility has no attitude considerations, but simply employs line-of-sight with a user-supplied mask angle, and takes into account occultation by the Earth. Through menu-driven input, the user can configure the spacecraft's orbit and the alignment of the GPS sensors. This allows for a variety of case setups, determined by the requirements of a particular mission. The utility results in the output of two data sets. The first simply records at each time step whether each GPS satellite in the 24-GPS-satellite constellation is visible, and the total number that are visible. The second data set reports the input configuration and gives a detailed statistical analysis of the simulation. For each GPS satellite, the statistics include the percentage of time visible, the total number of observations (i.e., the visibility of a GPS at each time step), and the minimum and maximum length of time visible. A density report for the entire constellation is given in terms of how many times a total number of GPS satellites were visible at any given step. The second figure plots the output from the prediction utility to show what a typical average number of GPS observations per step



*Average GPS observations for various altitudes and inclinations.*

would be for varying inclinations and altitudes. In this setup, the GPS antennas on the user spacecraft are pointing anti-Earth (i.e., towards the zenith).

Besides being able to use the output to configure the estimation simulator and provide information on the observability of the GPS constellation, the utility provides a quick simulation for the development and investigation of observability and selection algorithms.

An invaluable tool used by FDD to determine the expected in-flight attitude accuracy is the Attitude Determination Error Analysis System (ADEAS). This is a general purpose, linear error analysis tool that allows the user to compute an error budget based on different configurations and combinations of attitude sensors. ADEAS can estimate the accuracy using either a sequential filter (a Kalman filter), or a batch-weighted, least-squares method. ADEAS' strength lies in its flexibility. It was designed to handle most existing and anticipated attitude sensors, and is easily updated to provide modeling for any new attitude sensors, such as the GPS sensors. The system takes into account errors typically found with any system (e.g., measurement noise, sensor misalignments, gyro drifts, etc.), and allows the user to specify the type and magnitude of each of these errors. The error sources can also be solved as part of the system state, or just used as input to the modeling, as a "consider parameter." The GPS attitude sensor modeling in ADEAS is similar to that for traditional attitude sensors, such as star cameras, but the measurement for GPS-based modeling is the decimal

## MISSION OPERATIONS AND DATA SYSTEMS

---

phase difference. Because ADEAS is concerned not with the actual attitude errors but only with the uncertainty (the covariances), the integer ambiguity need not be determined. The modeling for the GPS attitude sensors is an extension of the well-known equation that relates phase differences to direction cosines. The addition to this equation, GPS data adds parameters to account for misalignment of the baseline, noises and biases applied to the phase difference, and the location of the antennas, which determines the phase center.

Each of these tools has a separate but important purpose in understanding and developing new modeling and algorithms, not only for GPS, but also for any future technology advancement in attitude sensors. The FDD is always on the leading edge for developing new processing techniques for attitude determination and calibration. Advanced applications for GPS attitude determination and

calibration will be realized with the launch of the Spartan mission in late 1995, and the launch of the Transition Region and Coronal Explorer mission in 1998. Both missions are flying GPS attitude sensor experiments to collect realistic data and to evaluate the performance of a GPS-configured attitude system to compare its utility to existing attitude sensor technology.

Contact: Joseph Garrick (Code 553.1)  
301-286-5474

Sponsor: Office of Space Communications

*Mr. Garrick has been an aerospace engineer for the FDD for the past 8 years. He received his B.S. in Mathematics from the University of Missouri and his M.S. in Electrical Engineering from the Johns Hopkins University.*

## GROUND SYSTEM AND NETWORKS: HARDWARE

### NASCOM INTERNET PROTOCOL GATEWAY: THE TRANSITION BEGINS

WITH THE ADVENT OF THE Earth Observing System (EOS), a part of the Mission to Planet Earth, the NASA Communication (NASCOM) Division has been tasked to implement a high-speed data communications network. This network is designed to use commercial, off-the-shelf (COTS) data communication products and industry-standard communication protocols to help reduce development costs. This network had originally been designated as the EOS Communication (Ecom) network, but has since been expanded as the EOS Data Information System Backbone Network (EBnet). Within this network there are systems that communicate with the current NASCOM Institutional network that cannot interface to the EBnet using COTS products and industry-standard protocols. The NASCOM Division has developed a frame encapsulator/decapsulator (FED) device to provide this interface between an industry-standard-protocol-based network and the NASCOM Institutional communication network.

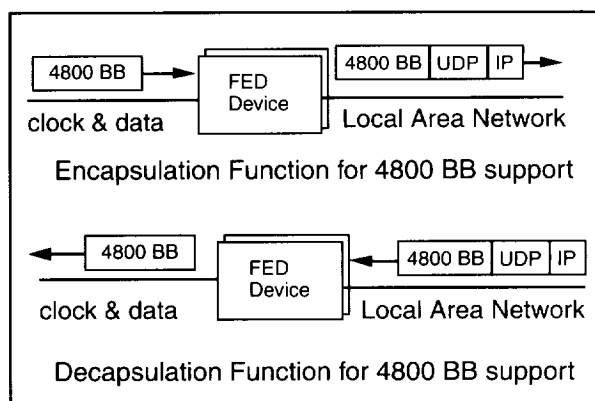
The purpose of the FED is to encapsulate 4800-bit blocks (BBs) received over a serial line, and then send them to the proper end-systems within Internet Protocol (IP) packets, using a local area network (LAN). The FED is also designed to decapsulate 4800-BBs from within IP packets and transmit them over the proper serial line. The FED has been designed to provide this encapsulation/decapsulation function not only for 4800-BBs but for Consultative Committee for Space Data Systems (CCSDS) data as well. A Simple Network Management Protocol (SNMP) interface has been included with the FED to allow configuration and monitoring of the device. This interface allows a COTS network management system to remotely configure and monitor the FED.

The objective of the FED design was to maximize the use of COTS software and hardware by re-using currently available operational software. To support the serial interface of the FED, software was adapted from the serial interface driver developed by the serial interface vendor. Software from SNMP Research, Inc. was used to implement and support the SNMP interface with the FED and Management Information Base II table. Most of the design for the FED came from a prototype effort called the Communications Address Processor (CAP). The main function of the CAP was to provide a gateway service between the Advanced Orbiting Systems Testbed internal LAN and the Internet. The FED's local operator interface

screens were designed around those used for the Tracking Data System (TDS). The TDS provides a text-based menu system for an operator to manage the system. The design used to provide a primary and secondary FED with automatic switchover capability came from the operational Message Switching System, which provides message switching for the operational NASCOM institutional communication network.

The FED device makes use of a Sun SPARC-based workstation and a Performance Technology Inc. 4-port, high-speed RS-422 serial Sbus interface card. It also uses a UconX Corp. protocol toolkit to provide the required software drivers to interface with the serial Sbus card. The SNMP interface was provided by SNMP Research, Inc. This COTS software package provided an SNMP agent for the FED and other command line utilities to use for testing and development purposes. The standard ANSI C programming language was used to integrate all of these COTS pieces in addition to providing the encapsulation/decapsulation functionality.

The FED device performs encapsulation of 4800-BB received from one of four high-speed serial interfaces within an User Datagram Protocol (UDP)/IP datagram, and sends this datagram to those end-systems that have been configured in the FED to receive the 4800-BB based on the destination code within the 4800-BB, as shown in the first figure.

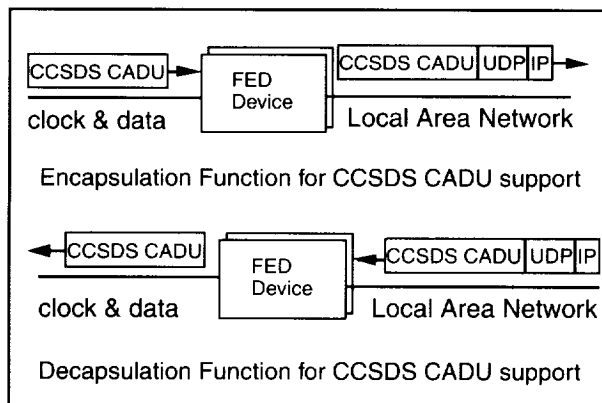


4800 BB FED service.

The FED can also be configured to receive CCSDS Channel Access Data Units (CADUs) from any of the serial

## MISSION OPERATIONS AND DATA SYSTEMS

lines, and send the CADUs encapsulated within UDP/IP datagrams based on the serial port on which the CADU was received, as shown in the second figure. The FED is capable of encapsulating either 4800-BB or CCSDS CADUs, but not simultaneously. The FED is also capable of decapsulating 4800-BBs from within UDP/IP datagrams. The FED was designed based on the assumption that all encapsulated data received from the UDP/IP datagram interface are to be sent out a single serial interface. When the FED is configured to encapsulate/decapsulate CCSDS data, the user data portion of an UDP/IP datagram is sent out via this single serial interface.



### CCSDS CADU FED service.

To support the availability and mean-time-to-restore service that is required of the FED within EBnet, the FED is configured in a redundant manner. Two complete FED hardware devices are configured to provide a primary operational device and a secondary hot-spare device. In this configuration, the system is capable of automatically switching from the primary device to the secondary when a fatal error is detected. To be able to detect that a primary device has failed, the primary and secondary FED devices communicate with each other across a LAN using heartbeat messages.

As described earlier, the FED is configured and monitored by use of the SNMP. The FED contains an SNMP agent that is responsible for processing all SNMP requests.

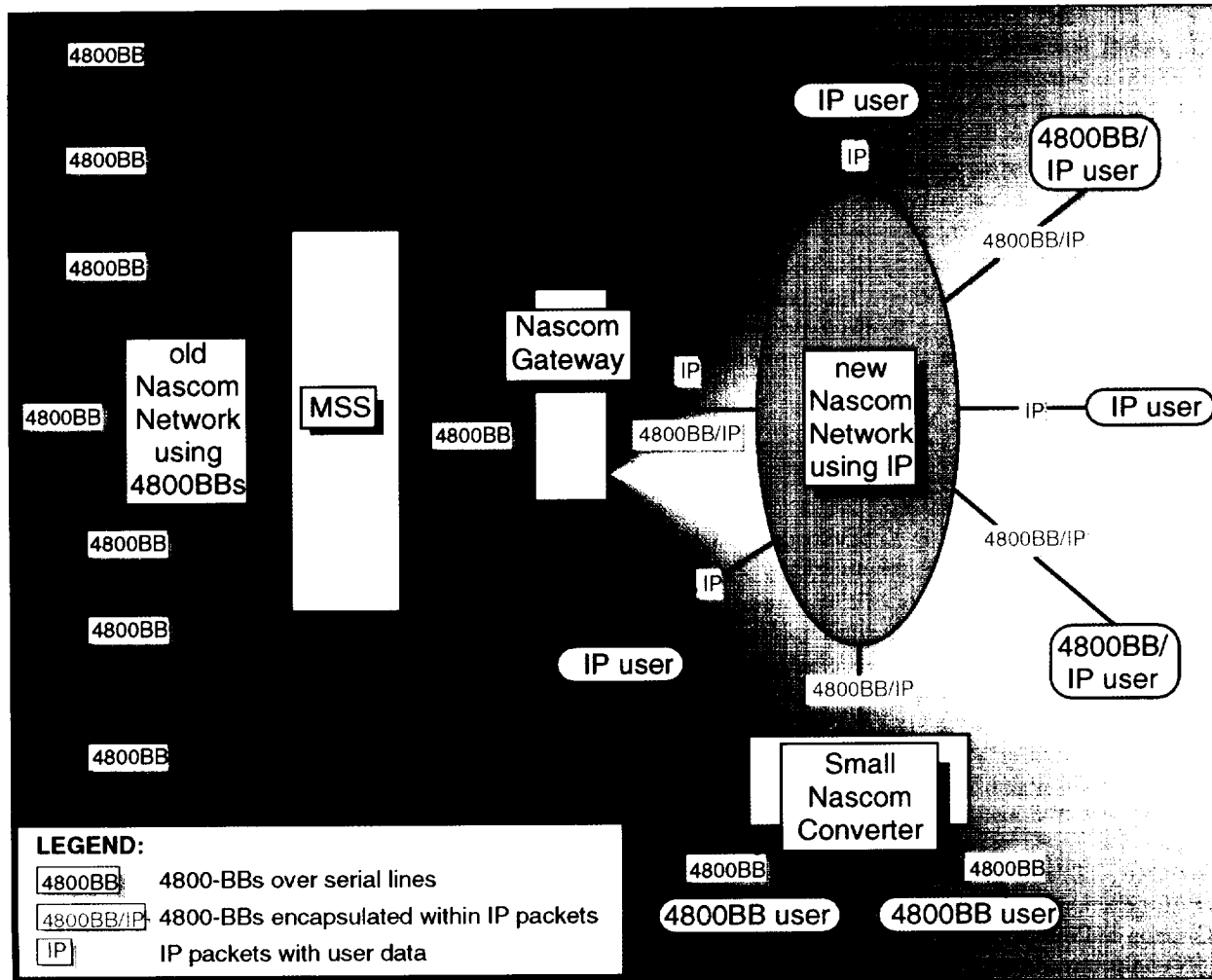
In addition, the FED has a local operator interface in which text-style menu-driven choices are presented to a local operator to allow configuration and monitoring of the FED. This interface will only be used if the remote network management system is unavailable and for maintenance check-outs.

The FED has been built to meet requirements for the EOS program. The NASCOM Division plans to use this FED device to assist in the transition from 4800-BBs to an IP network. Plans are underway to add additional capabilities and functions to the FED device. Work has started to increase the serial line rates from 512 Kbps to a T1 (1.544 Mbps) rate. In addition, the capability of encapsulating 4800-BBs within TCP/IP packets is also being examined. This new device will be the NASCOM Gateway, and will be used to provide a path between the old NASCOM network of transferring 4800-BBs to the new NASCOM network of transferring IP packets. To help users in their transition to the new NASCOM network, the NASCOM Gateway will also have the capability of blocking/deblocking user's data that is received within IP packets, or sent from users on the old NASCOM network, as shown in the third figure. It is our goal and intention to add the functionality of receiving raw serial data and blocking (or just encapsulating) these data within IP packets, in addition to decapsulating or deblocking and sending raw serial data to the NASCOM Gateway.

Contact: Matthew Kirichok (Code 541.3)  
301-286-3435

Sponsor: Office of Mission to Planet Earth

*Mr. Kirichok, an electronics engineer with the Advanced Development Section, holds a B.S. in Electrical/Computer Engineering from Northeastern University, Boston, MA. He also holds an M.S. in Computer Engineering from Johns Hopkins University, Baltimore, MD. His professional interests include computer network design, computer systems, computer security, and communication systems. Mr. Kirichok has been working in the Systems Engineering Branch of the NASCOM Division for the past 5 years.*



NASCOM IP transition.

### NEW COMMUNICATIONS OPTIONS FOR SMALL SATELLITES

**T**o expand the benefits and the use of the global Tracking and Data Relay Satellite System (TDRSS) communications infrastructure, GSFC is now embarking on a technology initiative to bring new operations concepts and life cycle cost savings to the growing small-satellite community. In the past, small spacecraft had problems using the global TDRSS communications network due to the relatively high weight and power consumption of existing TDRSS-compatible user transponder hardware. In addition, the signal attenuation caused by the distance to geosynchronous orbit and the operational complexity and cost of scheduling TDRSS service has made TDRSS too difficult to use efficiently.

New hardware and a flexible operations concept for small spacecraft will greatly increase communications coverage and lower the costs of using TDRSS. These benefits will derive from advances in TDRSS user transponder and phased-array antenna technology, and a new, unscheduled demand access service being introduced in the Space Network (SN), which will allow users to share the TDRSS forward link on a first-come, first-served basis.

The small-satellite community currently has problems using the SN because the receiver power consumption of second- and third-generation TDRSS user transponders is too high for the limited capacity of small-satellite power systems. The GSFC Network Engineering and Microwave Technology Branches are collaborating to develop a fourth-generation transponder, to achieve power consumption and weights comparable to the Ground Network (GN)-only transponders currently being flown by the Small Explorer project. The transponder is designed to interface with other small-satellite subsystems via a standard interface. The fourth-generation transponder will be an S-band transponder capable of working with TDRSS or ground terminals. This will allow mixed mode operation, where a project can use TDRSS for command, house-keeping telemetry, and tracking, and dump high-rate science data (at 2 to 3 Mbps) to a ground station, using the same S-band omnidirectional antenna in either mode.

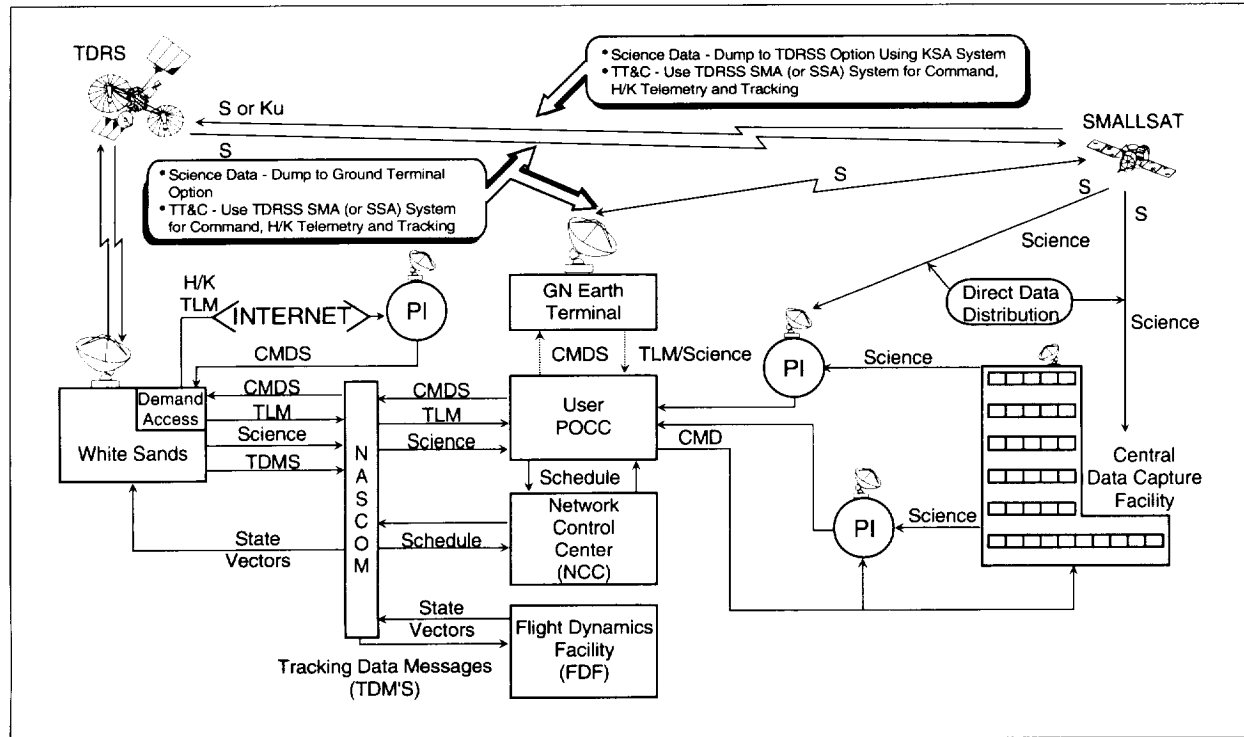
For users seeking the advantages of a total TDRSS solution, the fourth-generation transponder will provide an optional Ku-band signal source, which, together with an external Ku-Band high-power amplifier and phased-array antenna, will allow a small satellite to dump 2 to 3

Mbps of science data to TDRSS with roughly the same transmission power consumption as needed for transmission to the ground, as shown in the figure.

The use of Ku-band and the TDRSS Ku-band single-access service provides additional gain to allow the small-satellite user to overcome the path attenuation to geosynchronous orbit with only a small, body-mounted antenna. The Branches, with support from the NASA Lewis Research Center, are collaborating to develop a Ku-band phased array. The array will electronically steer up to 30° from boresight, providing ample contact time with TDRSS—far greater than would be available from a ground station. It will be small (dimensions not greater than 12" x 12" x 6") and will attach to the side of the spacecraft. This innovative operations concept will lead to cost savings in pre-launch testing, launch and early orbit support, spacecraft control and monitoring, and data transport. When available in 1999, the Ku-band phased array, coupled with the fourth-generation TDRSS user transponder, will eliminate dependence on ground stations, and provide flexible and low-cost SN-only mission operations. Studies in FY 96 will examine the implications of migrating the Ku-band service to Ka-band to take advantage of potentially smaller hardware or higher data rate capability that will result from the new Ka-band service to be provided by TDRS H, I, and J at the turn of the century.

Integration and test of the new spacecraft hardware will be facilitated by modern, low-cost radio frequency (RF) test equipment. This test equipment, known as the TDRSS User RF Test Set (TURFTS), employs a user-friendly design and emulates both TDRSS and GN modes of operation to fully characterize spacecraft communications system performance. TURFTS units have been or are being built for Earth Observing System AM, Tropical Rainfall Measuring Mission, Landsat-7, MSFC, Compatibility Test Vans, the RF Simulation Operation Center, and the Long Duration Balloon Project. Units are also returning data from the Compton Gamma Ray Observatory (CGRO) via the GRO Remote Terminal System in Australia on an around-the-clock basis. To support the new operations concept, TURFTS will be upgraded for K-band support capability.

Scheduling TDRSS access has been a concern that is now being addressed. Users of TDRSS theoretically have



The TDRSS User RF Test Set employs a user-friendly design and emulates both TDRSS and GN modes of operation to fully characterize spacecraft communications system performance.

continuous, global access to their spacecraft but, in practice, must share the limited system resources by scheduling contact time, generally two weeks in advance of the service. The TDRSS multiple access (MA) system, which is capable of supporting multiple return-link users by allowing them to share the single MA forward link, is scheduled (for the most part) in the same fashion as the single-access system. This scheduling process is perceived by low-budget, fast-track, small-satellite projects to add unwarranted cost and complexity to the use of the SN. A new demand access service to be incorporated in the MA system will greatly improve the TDRSS MA service by providing first-come, first-served access to the forward link (over short intervals, to provide high availability to many users) and will provide continuous return link service. This will eliminate scheduling MA service for users, thereby making flexible operations concepts possible, lowering mission operations costs, and allowing receipt of random return transmissions and service requests directly from the spacecraft when desired.

These operations concepts are more than just plans and theory. A government/industry team from GSFC successfully demonstrated demand access user service using TDRSS on January 20, 1995. The CGRO and Earth Radiation Budget Satellite (ERBS) Payload Operation Control Centers successfully sent forward link commands to their spacecraft via TDRS-3 and the White Sands Ground Terminal. ERBS had three, and CGRO had eight command services over two orbits with no advance scheduling by the Network Control Center. Both spacecraft had continuous return link service throughout the demonstration.

The demand access service promises to more effectively tap the power of the global SN to provide exciting new possibilities for telescience and for operations concepts that are more flexible and offer significant opportunities for reducing the cost of mission operations, especially for small-satellite systems.

## MISSION OPERATIONS AND DATA SYSTEMS

---

Contact: David Zillig (Code 531.2)  
301- 286-8003

William Horne (STel)  
703- 438-8148

Sponsor: Office of Space Communications

*Mr. Zillig is Head of the RF Systems Section in the Network Engineering Branch at GSFC. He manages several tasks in future technology and systems development for the Office of Space Communications Advanced Technology Program. Mr. Zillig earned a B.S.E.E. from the*

*Pennsylvania State University and has been involved in developing communications and tracking systems for NASA GN and SN for 29 years.*

*Mr. Horne is an engineering specialist at Stanford Telecommunications, Inc. After earning his B.S.E.E. from Lehigh University and his M.S.E.E. from Princeton University, Mr. Horne supported satellite communications engineering and spectrum management activities for NASA, including the GSFC TDRSS program. He has also been assisting GSFC with the development of demand access service.*

## GROUND NETWORK ADVANCED RECEIVER PROTOTYPE II: A CHARGE-COUPLED DEVICE PROGRAMMABLE INTEGRATED RECEIVER

FOR THE PAST 4 years, the Network Engineering Branch has sponsored the development of evolutionary, multifunctional, software-programmable, integrated receivers in anticipation of future space and ground system requirements for a high degree of communications flexibility, automation compatibility, and power and size reduction. In the past year, this initiative has led to expanding the operational application of the second-generation Ground Network (GN) Advanced Receiver Prototype (GARP). We have also designed and developed a third-generation receiver, the GARP II, that will provide flexible communications support for multiple modulation formats, spread and nonspread signals, and tone ranging of user spacecraft with 1-m accuracy. Highly configurable through software changes, these charge-coupled device (CCD) programmable integrated receivers allow integration of both GN and Space Network (SN) modes of operation in the same electronics system, and have been specifically designed for effective and cost-saving automation of most operational and maintenance functions. A key feature of these receivers is an architecture that optimally leverages the use of new CCD technology against a powerful, high-speed multiprocessor arrangement to provide flexible, multimodal, multimission support over a broad continuum of data rates that presently spans the range from 1 Kbps to 1.8 Mbps; support is planned for data rates to 10 Mbps and beyond.

The CCD technology employed (and developed under NASA's sponsorship) is MIT Lincoln Laboratory's programmable analog correlator chip, the 2ATC CCD, which serves as the receiver's pseudo-random-noise (PN)-code matched filter for spread spectrum applications, and as an intermediate frequency (IF)-matched filter for nonspread applications. By nature a quasi-analog device, the CCD correlator chip performs signal correlation in the analog domain at digital domain-equivalent rates exceeding 10 billion multiply-accumulate instructions per second when clocked at the maximum rate of 40 MHz—all while consuming less than 1 W. Within a signal processing environment, the computational capacity of the CCD may be used to great advantage, adding tremendous signal processing capacity to receiver architectures specifically designed to exploit its strengths.

The complete IF-to-baseband data receiver is composed of three cards: the IF module, the CCD module, and the digital signal-processing (DSP) module, as shown in the

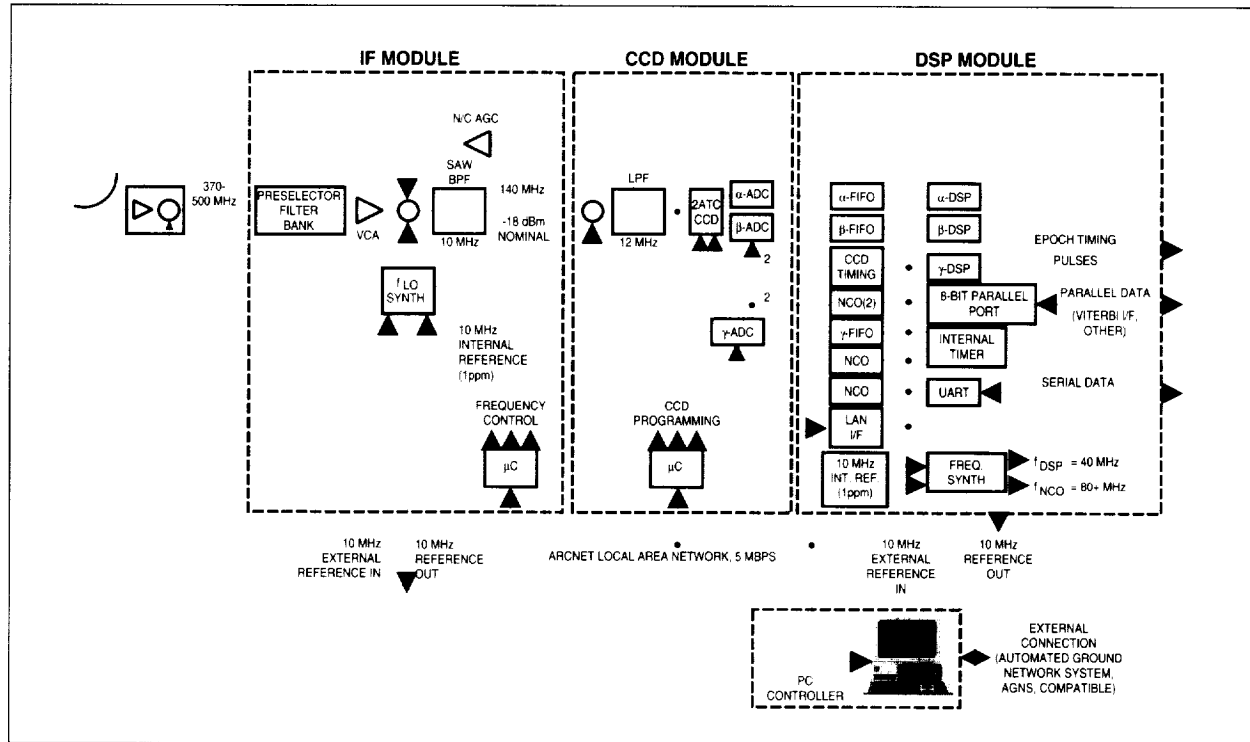
block diagram in the figure. The form factor of each of these modules conforms to a standard 220 mm, 6U VME card. In addition, electrical power compatibility with the VME standard has been preserved, making possible the use of a commercially available VME chassis. Communications and control connectivity between each of the modules and a local PC controller is achieved using a 5 Mbps industrial ARCNET local area network (LAN) standard.

The IF module accepts a radio frequency (RF) input in the range of 370 to 500 MHz (selected for application both at NASA's White Sands and GN ground stations), and at an input power level between -75 and -15 dBm. It down-converts to a 10 MHz band, centered about the fixed IF of 140 MHz, and at a user-programmable output power from 0 to -20 dBm. The RF input frequency is selectable in 100 KHz steps over the entire 130 MHz input frequency range, and is remotely programmable via the ARCNET LAN interface. Additionally, the IF output level is also remotely programmable via the LAN, and provides noncoherent automatic gain control to within 1 dB of the programmed setting.

The 140 MHz gain-controlled output signal from the IF module is then sent to the CCD module, where it is conditioned and preprocessed prior to being sent to the CCD chip. Part of this signal preprocessing includes application of a unique discrete-time linear down-conversion and reconstruction technique based on signal aliasing, which is used to track the received carrier signal dynamics. For PN-spread signals, the resultant IF waveform is sent to the CCD correlator for removal of the PN code (despread) prior to digitization; for nonspread signals, the CCD correlator is used simultaneously for both IF demodulation and partial- or whole-symbol demodulation. The output of the CCD correlator is then sampled, digitized to 8-bit resolution, and passed onto the DSP module, where the samples are then processed to acquire and track the received signal.

Signal processing within the GARP resides in a multi-processor array of three Motorola DSP96002 dual-port, 32-bit floating point DSPs connected in a master-slave wye topology. This topology will support concurrent processing of up to three embedded signals on three signal paths, with each processor assigned to one signal path. In this master-slave arrangement, input sample timing and

## MISSION OPERATIONS AND DATA SYSTEMS



The GARP II receiver configuration can support high resolution spacecraft ranging with the addition of a simple exciter system.

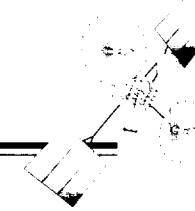
control is done through the master processor; together, these three processors execute all of the algorithms necessary to acquire, track, and demodulate the received signal(s). With the recent addition of an add-on Viterbi decoder board, additional support for convolutionally encoded signals has been added.

During the past year, program activity has been focused on two objectives: refining and expanding receiver mission applicability through challenging technical demonstrations, and the development of hardware and software architecture and algorithms that would support high-resolution tone ranging of user spacecraft for orbit determination.

Technical demonstrations in past years have testified to the advantages of the programmable CCD-based receiver technology. In the 2-year period between December 1992 and December 1994, this receiver technology had been

successfully demonstrated to support PN-spread binary phase-shift keying (BPSK) modulated signals, space shuttle SN communication at 288 Ksps, shuttle analog FM support, 192 Kbps shuttle launch support, and for subcarrier-modulated signals.

In 1995, four new and distinct receiver modes of operation were developed, covering a broad range of signal structures, modulation types, and data rates. In testimony to the advantages of software programmable receiver technology, two of these operational modes were developed, tested, and fielded within 1 month. Mission support in 1995 included Titan-Centaur launch support via the Tracking and Data Relay System Satellite (TDRSS) from the White Sands Complex (WSC), using a 128 Kbps, rate one-half convolutionally encoded, BPSK signal; space shuttle Inertial Upper Stage launch support via TDRSS from the WSC, using a 64 Kbps, rate one-half convolutionally encoded, near-BPSK signal on a 1 MHz



subcarrier; and support from the Greenbelt test bed for the Solar Anomalous Magnetospheric Particle Explorer, a small Explorer-class satellite requiring support for a 900 Kbps (1.8 Msps), rate one-half convolutionally encoded, phase-modulated signal. The receiver was also readied to provide Total Ozone Mapping Spectrometer launch support via TDRSS from WSC, using a 1.123 Kbps, rate one-half convolutionally encoded BPSK signal on a subcarrier.

A second focus in 1995 was architectural refinement and algorithm development to support high-resolution tone ranging of user satellites for range and orbit determination. With the addition of a subsystem composed of a baseband range tone exciter and an S-band upconverter, this capability will be added to the GARP II system in 1996. The baseband range tone exciter has two outputs: a composite two-tone analog signal made up of one 500 KHz major tone and one minor tone in the frequency range 4 to 100 KHz that is used to modulate a commercial S-band upconverter, and a resampled version of the baseband composite signal which is passed to one path of the DSP module. By resampling the two-tone baseband stimulus and sampling the received return signal from the target spacecraft, a phase difference estimate between the transmitted and received signals can be calculated, thereby allowing estimates of spacecraft range through the TDRS communication link. To resolve ambiguities in range determination by the received signal phase differential, the algorithm requires sequentially stepping the minor tone signal over its frequency range. In simulation, the algorithm currently under development will provide an accurate range estimate in less than 10 seconds and at a resolution below 1 m. With this accuracy requirement, the GARP II system could provide improved TDRS orbit determination services from WSC facilities, where current TDRS tone ranging accuracies are accompanied by 50 m (root mean square) uncertainties.

Over the 4 years that NASA has sponsored the development of multifunctional, software-programmable integrated receivers, it has been demonstrated that it is possible, utilizing state-of-the-art signal processing technologies—such as DSPs and CCDs—to develop powerful and flexible receiver architectures that are suited to a wide variety of NASA, military, and commercial applications, and that can effectively address future requirements for faster, smaller, less expensive, and more reliable systems.

This work was done with the support of Stanford Telecommunications' Advanced Hardware Development Laboratory, which is currently developing the GARP II.

Contact: David Zillig (Code 531.2)  
301- 286-8003

Thomas Land (STel)  
703- 438-8097

Sponsor: Office of Space Communications

*Mr. Zillig is Head of the RF Systems Section in the Network Engineering Branch at GSFC. He manages several tasks in future technology and systems development for the Office of Space Communications Advanced Technology Program. Mr. Zillig earned a B.S.E.E. from the Pennsylvania State University and has been involved in developing communications and tracking systems for NASA Ground and Space Networks for 29 years.*

*Mr. Land is a project manager with Stanford Telecommunications, Inc. (STel) Advanced Hardware Development Laboratory, which is currently developing the GARP II. He earned a B.S.E.E., a B.S. in Computer Science, and a B.A. in Biology from Washington University in St. Louis. Mr. Land has supported GSFC prototyping and hardware evaluation projects for 7 years.*

### EVOLVING CHARGE-COUPLED DEVICE SIGNAL-PROCESSING TECHNOLOGY

THE DEVELOPMENT AT MIT/Lincoln Laboratory (MIT/LL) of programmable charge-coupled device (CCD) correlator technology for use in advanced signal-processing receiver applications has been supported by the GSFC Network Engineering Branch over the last decade under the sponsorship of the Office of Space Communications Advanced Systems Program.

The CCD correlator is a complementary metal-oxide semiconductor (CMOS) integrated circuit operating as a time-discrete tapped delay line with no amplitude quantization. The incoming signal is sampled at the CCD input, and the analog voltage is converted to charge. This charge is then transferred from one end of the CCD to the other by a string of CMOS capacitors, each serving as a distinct stage in a shift register; the charge transfer rate is controlled by an external clock. The charge at each capacitor may be externally accessed at each clock cycle, generating the tapping operation of a tapped delay line.

The current analog ternary correlator (2ATC) chip has 512 stages, 256 of which are tapped. The digital tap weights are externally controlled and updated in real time. This CCD correlator therefore can be used to implement a pseudo-random noise (PN)-matched filter (PNMF) that can provide parallel capability to a degree effectively equal to the number of stages. This PNMF flexibility, coupled with high-level parallel processing capability, makes the CCD correlator approach extremely powerful for Tracking and Data Relay Satellite System (TDRSS) spread-spectrum applications, and especially for rapid acquisition of PN-coded signals.

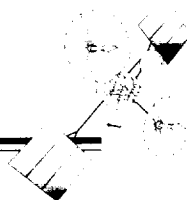
The Network Engineering Branch has supported the use of MIT/LL-developed CCD correlator chips by Stanford Telecommunications, Inc. in developing signal-processing technology in several different receiver designs for a wide variety of different applications. These chips were used to

- demonstrate a two-card receiver implementation of a Demand Access demodulator capable of inexpensively expanding customer capacity at the White Sands Complex to service users of a new demand access service in the TDRSS multiple access system;

- introduce TDRSS communications to the NASA long-duration ballooning and remotely-piloted aircraft science communities in a balloon-flight-qualified receiver design in a TDRSS user transponder;
- demonstrate a portable TDRSS communications receiver, capable of being used in automated, remote data collection platforms on land or sea. The National Oceanic and Atmospheric Administration (NOAA) has expressed interest in using TDRSS for communications with its network of ocean buoys; and
- demonstrate in laboratory and field work an advanced integrated receiver design, capable of supporting numerous NASA Ground Network (GN) and Space Network (SN) modes of operation. Within the past year, it supported shuttle GN and SN operational modes; TDRSS mode (direct-to-ground) to a low-cost ground terminal (Extreme Ultraviolet Explorer to LEO-D); expendable launch vehicle support through the SN in non-TDRSS modes (Titan Centaur and TDRS inertial upper stage), and Solar, Anomalous, and Magnetospheric Particle Explorer support in a low-cost ground terminal configuration.

In addition to the work being done by Stanford Telecommunications, Inc., Motorola, funded through the Air Force Rome Laboratory, is using a 2ATC chip on loan from GSFC in a brassboard upgrade to their Combat Survivor Evader Locator handheld radio. Other Department of Defense agencies have an interest in this technology for use in universal modems and handheld, low-probability-of-intercept radio applications.

A new effort by GSFC and MIT/LL will produce a prototype low-power chip (ATC-LP), which will slash the power by an order of magnitude, and incorporate an on-chip analog/digital (A/D) converter for more compact and convenient receiver technology. The ATC-LP will eliminate most of the static power consumed in the 2ATC, about three-quarters of which is used by the more than 500 tap amplifiers that buffer signals tapped from CCD delay lines within the correlators. Recent advances in CCD technology allow the tap amplifiers to be replaced with



charge replicators that nondestructively image the charge packets in the delay lines without bias currents; as a result, they consume no power.

In most receivers the analog outputs are digitized prior to further processing, and the required external A/Ds are an additional power load for the receiver. The replacement of output amplifiers and off-chip A/Ds by on-chip A/Ds is now feasible. MIT/LL has demonstrated a charge-domain 9-bit A/D that consumes only about 10 mW of static power. An A/D of this type will be incorporated in the ATC-LP along with charge replication taps. This usage will decrease the static power requirement to some 15 mW for the combined correlator/converter. Dynamic power will be approximately 2.5 mW/MHz, so that, at the projected maximum clock rate of 40 MHz, the ATC-LP is expected to consume only 115 mW total power. Sample quantities of the ATC-LP will be available in September 1996.

The impact of this technology is expected to spread beyond NASA and other government applications. MIT owns and continues to generate patents as a result of their

work in CCD signal processing technology. These patents are being licensed by the MIT Technology Licensing Office for commercial use, which is stimulating corporate strategic business investment. Additional patents that should become available as a result of NASA's investment in low-power correlator development will further stimulate investment and accelerate the technology's impact on the burgeoning commercial field of spread-spectrum communications.

Contact: David Zillig (Code 531.2)  
(301) 286-8003

Sponsor: Office of Space Communications

*Mr. Zillig is Head of the RF Systems Section in the Network Engineering Branch at GSFC. He manages several tasks in future technology and systems development for the Office of Space Communications Advanced Technology Program. Mr. Zillig earned a B.S.E.E. from the Pennsylvania State University and has been involved in developing communications and tracking systems for NASA GN and SN for 29 years.*

### PROTOTYPING EDOS HIGH-RATE RETURN-LINK-SERVICE PROCESSING

AS PART OF THE EFFORT to explore the feasibility of using general-purpose computers to meet key functional and performance requirements for the Earth Observing System Data and Operations System (EDOS), a prototype parallel service processor (PSP) was developed and tested on a Digital Equipment Corporation (DEC) Alpha 7000 computer. Results to date indicate that an operational version of the prototype may be able to perform the Consultative Committee for Space Data Systems (CCSDS) path service at the rates specified for EDOS if it is hosted on a platform with the appropriate hardware features, i.e., multiple central processing units (CPUs), the appropriate input/output (I/O) interfaces, and a very-high-speed system bus.

The reason for developing the prototype was to exploit the potential of symmetric multiprocessing (SMP) on general-purpose computers. It was thought that building a parallel service processor based on SMP technology would close the gap between current operational capabilities and future requirements. For example, traditional service processors, which process incoming data sequentially, support throughput rates of less than 20 Mbps; but the requirement for EDOS is to support throughput rates in excess of 150 Mbps, an increase in excess of sevenfold.

The advantage of SMP technology is that it allows the software developer to build true parallelism into a single computer program, resulting in an application process that executes as multiple threads of execution on multiple CPUs. When the workload of a single process is balanced over multiple CPUs, the execution time may be reduced by a factor of the number of CPUs executing in parallel.

Most sequential service processing algorithms perform three "copies:" the first, input, copies data from external media to computer memory; the second is an in-memory copy of reassembled packet data to another part of computer memory; the third, output, copies the data to external media. Throughput is limited by the sum of the times taken to perform the copies. One way to increase throughput is to redesign the algorithm as a pipeline that performs the three copies in parallel as it reassembles packets within incoming blocks of telemetry data. Throughput is then limited only by the time taken by the longest of the three copies.

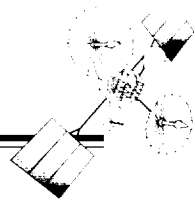
Personnel assigned to the Systems Engineering and Analysis Support EDOS Prototyping task designed, coded, and tested a pipelined PSP based on GSFC's Advanced Orbiting Systems Testbed Service Processor. The work was accomplished using a pair of DEC Alpha 7000 Model 610 computers connected by a fiber data distributed interface (FDDI). The Alpha that hosted PSP was equipped with three 200-MHz CPUs.

The PSP was coded as five tasks: READ, SORT, COPY, VERIFY, and WRITE. The five tasks executed in parallel within a single executable image. The READ and WRITE tasks communicated with the external media via TCP/IP to input blocks of virtual channel data units and output blocks of demultiplexed packets, while the SORT task constructed a list of pointers to packets in the input buffer; the COPY task accessed the list of pointers to copy packets to an output buffer. The VERIFY task was stubbed for this initial capability. Prior to testing, PSP was instrumented to obtain throughput rates and thread diagnostics.

To facilitate the collection of performance data, PSP was run in three modes: MEMORY mode, in which I/O was simulated and packets were copied only once from input to output buffers in computer memory; INPUT mode, in which output was simulated and blocks of frames were copied via FDDI into buffers in computer memory as packets were simultaneously copied from input to output buffers in computer memory; and OUTPUT mode, in which input was simulated as packets were copied from input to output buffers in computer memory and blocks of packets were simultaneously output via FDDI. Because of hardware limitations (only one FDDI ring), it was not possible for PSP to perform three simultaneous copies.

Testing revealed that PSP's copy rate—the rate at which packets could be copied from incoming frames to outgoing blocks—varied as a function of the load placed on the DEC Alpha system bus. All copy operations performed by CPUs and the I/O processor (IOP) required access to physical memory, which in turn required access to the system bus.

During PSP testing, when two copies took place simultaneously, copy rates slowed, suggesting that simultaneous access to the system bus by multiple CPUs and the IOP resulted in contention for the system bus. For example, in



MEMORY mode, the COPY task supported an input data rate of 221 Mbps for 221-byte packets, well above the EDOS requirement. However, in INPUT mode, test measurements indicated that the COPY task supported an input data rate of only 165 Mbps. Similarly, in OUTPUT mode, the input data rate supported by the COPY task was only 148 Mbps.

Current test results may not be representative, because computers that were later selected for EDOS development, such as the Silicon Graphics, Inc. Challenge, are equipped with system buses with two to three times the bandwidth of the system bus on the DEC Alpha. Also, TCP/IP requires several memory accesses to move data to and from memory owned by an application process. Lighter-weight protocols, for example the High Performance Parallel Interface framing protocol, make considerably less use of the system bus. Therefore, further testing on a computer with more appropriate hardware features will be necessary to determine if the system bus is a factor that will seriously limit throughput rates in an operational environment.

PSP prototyping has shown that the speed of key hardware components and the number of times the software accesses physical memory are the limiting factors when performing

CCSDS path service processing on general-purpose computers. If PSP source code is enhanced to perform in the EDOS operational environment, it may have the potential to perform at the required 150 Mbps.

Contact: Alexander Krimchansky (Code 510.2)  
301-286-2072

Michael Lemon (CSC)  
301-794-2436

Sponsor: Office of Space Communications

*Mr. Krimchansky is an EDOS hardware systems engineer. He has been at GSFC since 1983 as a hardware design engineer. Mr. Krimchansky holds a B.E.E.E. from City College of New York and an M.S.E.E. from John Hopkins School of Engineering.*

*Mr. Lemon is a computer scientist at CSC. He obtained an M.S. in Mathematics from Western Washington University. Mr. Lemon has 10 years experience in the GSFC environment.*

### VERY LARGE-SCALE INTEGRATION RETURN LINK PROCESSING CARD FOR A PERSONAL COMPUTER

THE WIDE USE OF STANDARD telemetry protocols based on the Consultative Committee for Space Data Systems (CCSDS) protocols in current and future space science missions has created a large demand for low-cost ground CCSDS processing systems. Some NASA missions using CCSDS telemetry include Small Explorer, Earth Observing System (EOS), Space Station, X-ray Timing Explorer, Tropical Rainfall Measuring Mission, and Mid-Sized Explorer Satellite (MIDEX). For each mission ground telemetry systems are typically used in a variety of applications, including spacecraft development facilities, mission control centers, science data processing sites, tracking stations, launch support equipment, and compatibility test systems. The future deployment of EOS spacecraft, designed to allow direct broadcast of data to science users, will further increase demand for such systems.

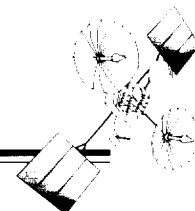
To meet these and future needs of NASA's telemetry data systems, a low-cost, high-performance return-link processor card for use in personal computers has been developed. This card can process standard satellite telemetry formats—including CCSDS protocols—at real-time rates up to 150 Mbps. The very-large-scale (VLSI) Return Link Processor Card performs all CCSDS return link processing functions and data sorting and routing. The key components of the system are based on two state-of-the-art, commercial, integrated VLSI circuit, complementary metal-oxide semiconductor (CMOS), application-specific integrated circuit (ASICs): the Parallel Integrated Frame Synchronizer Chip (PIFS) and the Reed-Solomon Error Correction Chip (RSEC). These key components perform frame synchronization, bit transition density decoding, cyclic redundancy check (CRC) error checking, Reed-Solomon decoding, virtual channel sorting/filtering, packet extraction and data distribution. The chips were developed by the Microelectronic Systems Branch at GSFC, and are available commercially through an ongoing technology transfer program. The chips are highly configurable to allow processing of different data formats, and can be controlled through a standard memory-mapped microprocessor interface technology. Because these ASICs are based on CMOS commercial foundry processes, a very low replication cost can be achieved.

The interface between the VLSI Return Link Processing Card and the host personal computer is realized through

the use of the Peripheral Components Interface (PCI) bus. This local bus is a processor-independent bridge between the central processing unit (CPU) and high-speed input/output. The PCI bus is a rapidly emerging industry standard that provides high performance (> 1 Gbps maximum transfer rate), low cost, and broad industry support. The PCI bus was developed by Intel, and is currently available in systems from IBM, Apple, Motorola, DEC, Compaq, and many other PC and workstation manufacturers. Recently, Sun announced that it will use the PCI bus in the future. The VLSI Return Link Processor Card has been carefully designed to take full advantage of the PCI bus bandwidth, so it can route data from any of up to 8000 sources to over 16,000 destinations at full PCI burst rate. This feature allows the card to act as a data server distributing the incoming processed data to various devices as necessary. For example, real-time spacecraft health and safety data could be routed to a mission operations workstation over Ethernet while a fully processed data set could be dumped to a disk system via a small computer systems interface (SCSI) bus. In addition, selected instrument data could be routed to an asynchronous transfer mode (ATM) network interface card to allow distant science data users the ability to work with the full set of data in real time.

The features described above offer several advantages for the VLSI Return Link Processor Card. First, the high bandwidth permits the rapid transfer of data through the system for high-rate data distribution (>150 Mbps) to network interfaces. The broad support that PCI enjoys throughout the industry means that multiple systems are available to host the VLSI Return Link Processor Card. In addition, there are a multitude of plug-in expansion cards available and, due to economies of scale, they are very reasonably priced. For example, more than three vendors currently offer 155 Mbps ATM interface cards for less than \$1,000 apiece. This is about one-fifth the cost of current VME-based platforms. These prices should continue to fall, thereby making the approach described here even more viable and cost-effective.

The VLSI Return Link Processing Card allows telemetry data processing in a single, low-cost desktop box. By utilizing commercial standards, state-of-the-art commercial CMOS VLSI ASIC technology, and flexible hardware acceleration of telemetry protocol processing, the VLSI Return Link Processing Card achieves a breakthrough in price/performance characteristics.



Further development is underway to target parallel radio frequency digital signal processing and science data processing. These development areas will utilize a similar architecture and innovative design methodology, and promise similar improvements over current implementations.

Contact: Don Davis (Code 521.1)  
301-286-5823

Jonathan Harris (RMS Technologies)  
301-286-4751

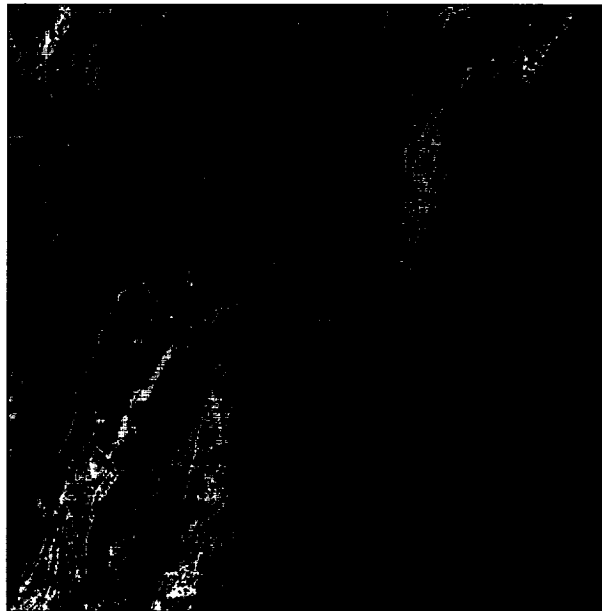
Sponsor: Office of Space Communications

*Mr. Davis is the technical lead for the development of next generation VLSI telemetry systems in the Micro-electronic Systems Branch. He received his B.S. in Electrical Engineering from the University of Maryland. Mr. Davis has worked at GSFC since 1988, during which time he has been involved in the design and implementation of several real-time hardware components and systems used for telemetry data processing.*

*Mr. Harris has worked at GSFC for 6 years. He received a B.S.E.E. from the University of Maryland. Mr. Harris has been involved in the design and implementation of a variety of real-time telemetry processing components, including a VLSI level zero processing system.*

### SATELLITE TELEMETRY AND RETURN LINK (STARLINK)

THE SATELLITE Telemetry and Return Link (STARLink) is a real-time airborne science and disaster assessment system on NASA's high-altitude ER-2 aircraft. One of its main mission objectives is to provide real-time, digitized image, voice, and video data for scientists and engineers performing Earth resource, stratospheric, and tropospheric research. Another major objective is to provide image data for primary disaster relief coordinators. For example, STARLink will give a fire chief infrared image data to determine hot spots, as shown in the first figure. Federal emergency managers will receive timely information to assess earthquakes, hurricanes, and floods. With existing disaster management resources, it can be hours after landing before data can be provided to appropriate disaster control agencies. Through STARLink, data can be transmitted instantaneously. This real-time data transfer and display also provides telepresence and telescience capabilities to maximize the data value from science missions.

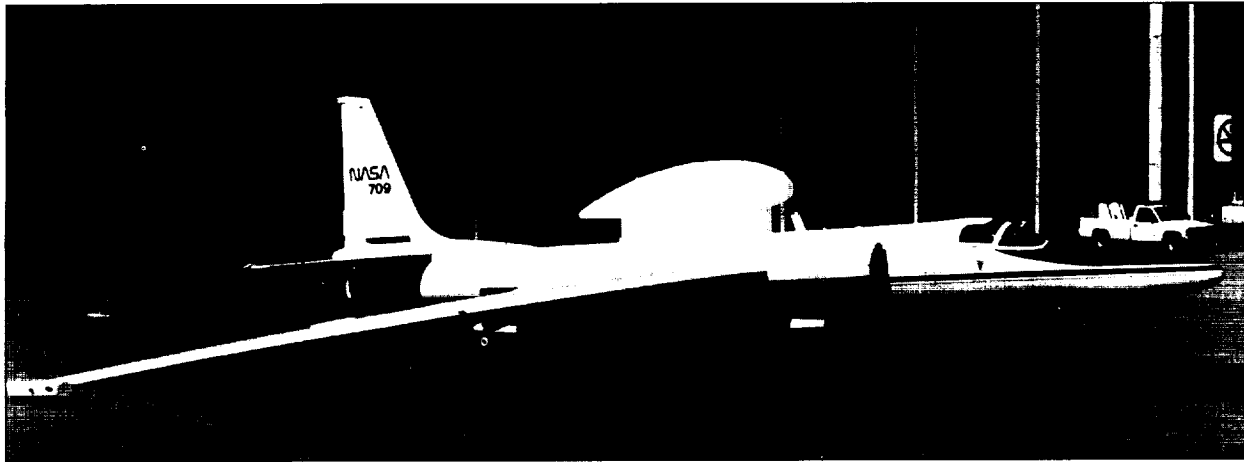


*Multiple burn scars and a bright red active fire are depicted near Ft. Hunter Liggett, CA. The detailed remote sensing imagery was relayed in real time from a NASA ER-2 research aircraft via a TDRS satellite using NASA's new STARLink system. Flames are seen as the yellow ring surrounding the 75-acre fire. Image resolution is 25 m (81 ft) and is composed of infrared bands in the 11-, 2.2-, and 1.6-micron regions.*

As its name suggests, STARLink uses an innovative approach to communicate with the ground. An advanced wideband data link system on the ER-2 relays the signal via the NASA Tracking and Data Relay Satellite System (TDRSS) to the White Sands Complex (WSC) ground station for distribution to users. The emphasis is on providing full duplex data between the on-board experiments and ground facilities to allow real-time processing and command of experiments and observations. The system will reduce the need for scientists and technicians to be stationed at central control facilities by allowing them to remotely support, control, or adjust their in-flight instruments. The audio link will support the pilot during emergency missions or allow the chief scientist to communicate with the pilot to redirect a science mission once the aircraft is airborne. Continuous TDRSS coverage for all these missions will normally be 4 to 6 hours, but could be up to 8 hours during extended missions. This coverage must be sustained over the entire 5000-km range of the ER-2.

The STARLink Project is being managed by the High Altitude Mission Branch of NASA's Ames Research Center (ARC). The Mission Operations and Data Systems Directorate at GSFC was asked by NASA Headquarters to support the project with communications analysis, interface definition, scheduling system development, simulation, testing, and other mission requirements for the TDRSS space and ground segments of the end-to-end link. GSFC developed the scheduling and control system that allows ARC to schedule TDRSS support through the Network Control Center at GSFC. The NASA Communications Division at GSFC also contributed the statistical multiplexer (STATMUX) equipment to the ground station element at ARC. Although the STARLink signal structure does not conform completely with the requested standard TDRSS return-service mode, GSFC developed design recommendations to implement STARLink support with no modification to existing TDRSS ground equipment at WSC.

The STARLink architecture is made up of three major elements: the Airborne Element, the TDRSS/Space Network Element, and the Ground Station/Control Center Element at ARC. The Airborne Element (as shown in the second figure) consists of a data recorder, which is used as a temporary buffer and storage for digital data channels from on-board experiments. The recorder



*Almost 17-ft-long, 401-lb STARLink antenna pod is mounted on a NASA Lockheed ER-2. The airborne element consists of a data recorder, which is used as a temporary buffer and storage for digital data channels from on-board experiments.*

interfaces with a modem, which multiplexes and demultiplexes various channels; modulates the aggregate return link I and Q channels, with capacities of 137 Mbps each; and demodulates the forward link channel, with a 200 Kbps capacity. The return link signal is converted to the TDRSS Ku-band frequency, amplified by a 400 W traveling wave tube amplifier, and transmitted to the satellite via a 30-in steerable parabolic antenna. After relay through the TDRSS spacecraft, the return channels are received and demodulated at the WSC ground terminal, where newly installed STARLink-unique equipment demultiplexes the channels and reduces the total data throughput to 48 Mbps (the maximum capacity of the current STATMUX). The data is relayed by satellite from the WSC to ARC via an existing domestic satellite. The Ground Station Element at ARC allows investigators to use telephone modems, Internet, or a private on-site local area network to access their data. This data distribution center will also coordinate all command link activity to send information back to the aircraft through NASA Communications Network circuits and TDRSS.

As of this writing, STARLink was scheduled to be fully operational in late 1995 and has already successfully completed its first flight. The ER-2 departed at noon on

July 31, 1995, and flew a 105-minute mission from ARC to Salinas, CA, and back to ARC. The aircraft flew at altitudes up to 68,000 ft, approaching the maximum mission altitude of 70,000 ft. As part of its first flight, the ER-2 scanned a small brushfire located near Fort Hunter Liggett, CA. Other detailed imagery originated from a Daedulus Thematic Mapper Simulator and a video imaging system carried aloft in the payload bays. The multispectral imagery will be used to fine-tune STARLink's ability to provide real-time, highly detailed data to firefighters. STARLink data can be accessed through the Internet via World Wide Web at <http://hawkeye.arc.nasa.gov>.

Contact: Greg Blaney (Code 532.1)  
301-286-7920

Sponsor: Office of Space Communications

*Mr. Blaney is the Network Director at GSFC for the STARLink mission. He received a Professional Aeronautics degree from the Embry-Riddle Aeronautics University. Mr. Blaney has been at GSFC for 12 years where he works in the Networks Division performing customer integration and operations management.*

### PARALLEL INTEGRATED FRAME SYNCHRONIZER CHIP

**I**N AN ERA OF CONDUCTING “better, cheaper, faster” missions, NASA must find ways to reduce the cost of acquiring and processing spacecraft data, while increasing the flexibility and performance of these data processing systems. One of the major functional tasks of any ground system is to provide frame synchronization of incoming telemetry data. This involves the delineation of framed data structures using specific data patterns to mark frame boundaries based on sophisticated search algorithms to ensure correct synchronization of data transmitted across an inherently unstable space-to-ground link. In recent years, a set of standard protocols developed by the Consultative Committee for Space Data Systems (CCSDS) has seen wide-scale adoption by NASA and its international partners. These protocols offer the potential for significant cost savings by allowing the use of standard building blocks for telemetry processing across multiple missions. In addition, with the advent of the Earth Observing System, which is a series of low-Earth-orbiting spacecraft to monitor the Earth’s environment, demand for cost-effective CCSDS protocol processing systems is expected to increase dramatically because of the high level of interest and large user base for this project.

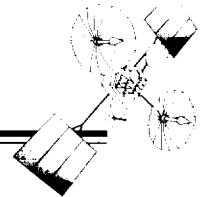
The ability of very-large-scale integration (VLSI), application-specific integrated circuit (ASIC) technology to enable substantially smaller, cheaper, and more capable computing systems is widely recognized. To date, the rapid growth in commercial ASIC fabrication densities has far outpaced the application of this technology to telemetry systems. As part of an effort to apply these advanced “system-in-a-chip” ASIC technologies to telemetry systems, GSFC has developed a high-performance parallel integrated frame synchronizer (PIFS) chip. The development of the PIFS chip for use in return link processing applications will enable low-cost, high-performance solutions to NASA’s telemetry processing needs for the foreseeable future. By combining commercial CMOS ASIC technology with an innovative parallel processing algorithm, the complex task of frame synchronization can be performed for all known data formats using a single chip for the core processing.

The PIFS chip was designed to trivialize the task of performing frame synchronization for any type of telemetry data, including CCSDS and weather satellite protocols. It is a single-chip solution for frame synchronization. Some of its features include

- true and inverted 64 bit sync marker correlation with programmable error tolerances;
- programmable frame length;
- programmable frame marker pattern;
- programmable search-check-lock-flywheel acquisition strategy;
- bit slip detection;
- optional flexible timecode annotation;
- optional frame quality annotation;
- cyclic redundancy check (CRC) error detection;
- bit transition density decoding;
- cumulative accounting registers for data quality monitoring;
- differential decoding (NRZ-L, NRZ-M and NRZ-S); and
- correlation and processing of all known weather satellite formats.

The PIFS chip processes real-time weather satellite formats at rates over 50 Mbps, and all other data formats (including CCSDS) in real-time at rates over 400 Mbps. The PIFS chip can achieve this performance through the use of parallel algorithms to perform its major functions. This is different from previous generation VLSI frame synchronizer chips, which used serial processing algorithms. While parallel approaches to improve performance are not new, they require significantly more logic than serial approaches, and were not cost-effective until recent advances in VLSI chip technology greatly lowered the cost and size of implementing complex logic functions.

The PIFS chip is controlled by a set of internal registers that are configured through a standard microprocessor interface prior to operation. The registers allow the chip to be reconfigured to meet the needs of many different space missions. During operation, data enters the chip via one of two paths. For very high-rate data, the serial data is first externally converted to 8-bit wide parallel data and



then input to the chip. For data rates below 50 Mbps, serial data are input directly, and converted to a parallel stream internally. As the data are accepted by the chip, they are stored in an internal first-in, first-out memory. This feature allows the PIFS internal logic to operate from a separate master clock that is not coupled to the data clock. This feature, combined with the data flow architecture of the chip, provides a latency through the chip of 37 master clock cycles (for a 50 MHz master clock, this works out to be 0.74  $\mu$ sec), independent of input data rate. As the data pass through the chip, correlations are performed, the synchronization mark locations are calculated, and the data are aligned to the frame boundaries. In addition, the frames can be bit-transition-density-decoded, CRC error detection can be performed, and the frames can be time-tagged.

While all of this processing is happening, the PIFS chip is keeping track of the cumulative quality of the data and other processing parameters. These parameters include

- number of frames processed;
- number of search, check, lock and flywheel frames;
- number of sync marker errors;
- number of slip errors;
- number of forward, reverse, true and inverted frames; and
- number of CRC errors.

This cumulative quality information is available via the microprocessor interface and can be read at any time.

The PIFS chip is only one example of a new generation of return link processing elements that will help lower the cost and increase the performance of NASA's future data systems. A Reed-Solomon chip VLSI ASIC has already been developed and deployed, and other aspects

of return link processing utilizing VLSI technology packet processing, digital signal processing, and science data processing are currently under development that promise similar improvements over current implementations.

Contact: Don Davis (Code 521.1)  
301-286-5823

Parminder Ghuman (Code 521.1)  
301-286-5365

Jeff Solomon (RMS Technologies)  
301-286-5330

Sponsor: Office of Space Operations

*Mr. Davis is the technical lead for the development of next generation VLSI telemetry systems in the Technology Applications Section of the Microelectronics Systems Branch. He received his B.S. in Electrical Engineering from the University of Maryland. Mr. Davis has worked at GSFC since 1988, during which time he has been involved in the design and implementation of several real-time hardware components and systems used for telemetry data processing.*

*Mr. Ghuman, an electrical engineer, has worked at GSFC since 1991. Mr. Ghuman holds a B.S.E.E. from the North Carolina Agricultural and Technical State University and an M.S. in Electrical Engineering from George Washington University. Mr. Ghuman has worked extensively in the area of VLSI design for high-performance telemetry systems.*

*Mr. Solomon has worked at GSFC for 3 years. During this time, he has been involved in the design of two VLSI ASICs for the real-time processing of telemetry data. Mr. Solomon did his undergraduate studies at Duke University, where he received a B.S. in Electrical Engineering and Computer Science in 1992. In September of 1995, Mr. Solomon began graduate studies at Stanford University towards completion of a Ph.D. in Computer Engineering.*

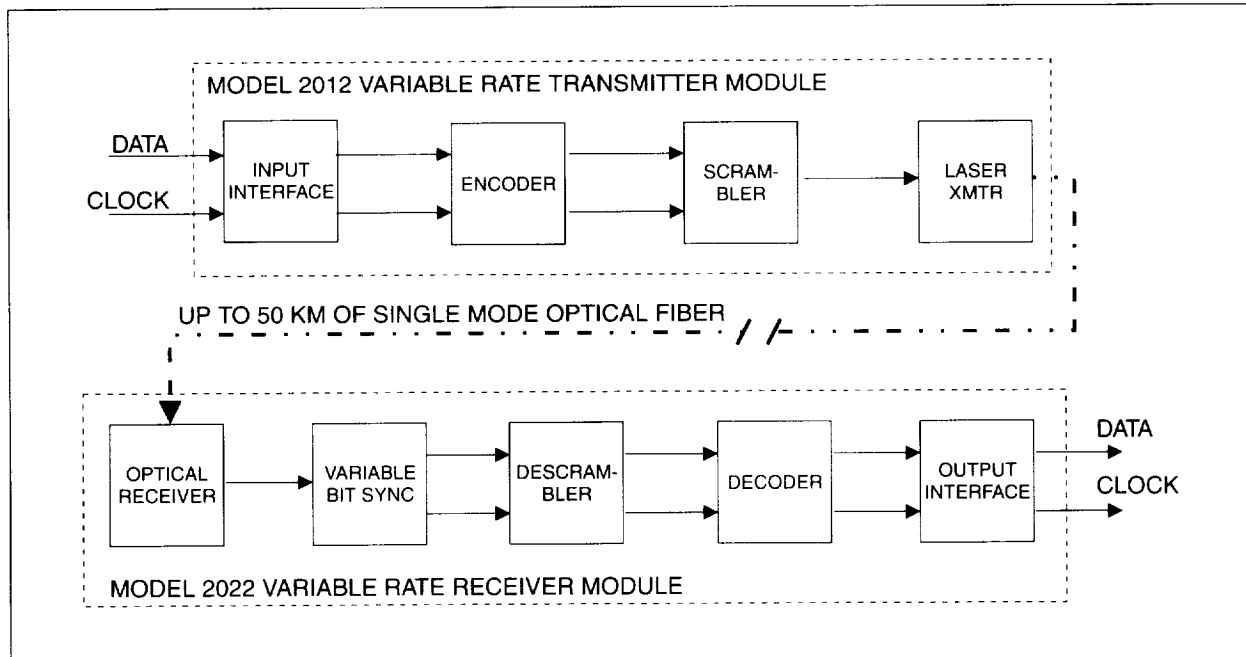
## FREQUENCY-AGILE FIBER OPTIC MODEM TUNES TWO DECADES

IN 1992, GSFC's NASA Communications (NASCOM) procured a system of high-speed, fixed-rate fiber optic transceiver (FOT) equipment for operational requirements at the White Sands Complex (WSC) to support the Tracking and Data Relay Satellite System (TDRSS) program. Any fixed rate FOT, such as those used at WSC, requires individually "tuned" clock and data recovery units, but acquiring a separate FOT for each separate clock rate is both expensive and problematic. The use of fixed-rate FOTs can be costly, since an FOT and spare are needed for each of the different data rates. In addition, the use of these fixed-rate FOTs could create a potential security problem, as each rate must be known in advance in order to procure a FOT for each discrete data rate. Thus, specific frequencies must be provided to vendors and others prior to a mission to procure the appropriate FOTs.

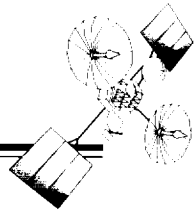
A high-speed, frequency-agile FOT has been developed to replace the fixed-rate transmission equipment used at WSC. The new variable-rate FOT offers considerable advantages over the fixed-rate FOTs in current use. A particularly attractive feature of the variable-rate FOT is its ability to function without operator intervention. Through the use of this transceiver, any digital data

transfer rate from 10 to 300 MBps can be transferred via fiber optic (FO) media from point-to-point or point-to-multipoint by simply changing the connection at the input port. The appropriate rate will then be precisely reproduced at the output at a bit error rate of  $10^{-13}$  or better.

The transceiver clock recovery circuit is the critical element in this unit. In an effort to improve the clock recovery process in the complex systems required to accommodate a continuum of data rates over a wide range, Broadband Communications Products, Inc. developed a variable-rate clock recovery method, referred to as variable-bit synchronization (VBS) technology. In VBS technology, the clock recovery circuit reconstitutes the clock from the composite (clock and data) FO light signal, and reclocks the data to provide clock and data at the receiver output. This process enables variable-rate, non-return-to-zero (NRZ) data and clock to be transmitted and recovered over a communications channel within a wide broadband frequency range of approximately 2 decades (100:1). The block diagram of the transmit/receive link is shown in the first figure. The primary function performed by the transmitter is accomplished by the encoder, which inserts one overhead bit for every eight data bits. This overhead is



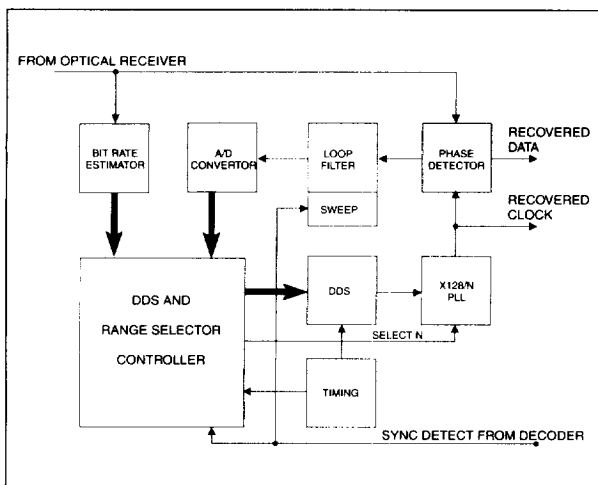
*BCP variable rate high speed synchronous optical link.*



used to prevent subsequent scrambler lockup, and it removes all constraints on the input data pattern. The serial data stream of the laser transmitter is thus nine-eighth times the actual input rate.

The optical receiver performs an optical-to-electronic conversion of the incoming optical signal, and outputs a serial electrical signal to the VBS. The VBS has the task of automatically acquiring the bit rate frequency, recovering a synchronous clock, and regenerating the data. The decoder processes these two signals, strips off the overhead bit, frame-locks to it, and reconstructs the original NRZ serial data stream. The decoder also performs an eight-ninths reduction in clock frequency to return to the original clock rate. The presence of the overhead bit and the frame synchronizer provides the benefit of continuous in-service error detection.

The VBS is the key to the bit-rate transparency of this synchronous link. The second figure illustrates the major functions of the VBS. The bit rate estimator provides an estimate of the actual incoming optical data rate. This estimate is used by the Direct Digital Synthesizer (DDS) Controller to achieve macro frequency acquisition. The Controller sets up the DDS (as multiplied by the X128/N loop) to within 3 percent of the correct frequency. The DDS is then swept into exact frequency and phase lock by the vernier sweep circuit. The acquisition process, including the transmitter, typically occurs in about two seconds.



Model 2022 Variable Bit Sync block diagram.

While the greatest present and future benefit of the variable-rate FOT may be the reduction in acquisition and maintenance and operation costs, the new FOT also provides improvements in efficiency and reliability.

This work was done by the NASCOM Division, GSFC via a Computer Sciences Corporation contract with Broadband Communications Products, Inc.

Contact: Chi Le (Code 541.1)  
301-286-3442

Paul Casper (BCP)  
407-984-3671

Jim Shaughnessy (CSC)  
301-794-2884

Sponsor: Office of Space Communications

*Mr. Le is the Technical Officer for the Interbuilding Communications Link Upgrade project, which was implemented at GSFC, and for the Data Block Emulator and the Reverse Engineering of the Code 541 Voice Distribution System keyset instruments. Mr. Lee received his B.S. in Electrical Engineering from the University of Maryland, and his M.S. in Communications from George Washington.*

*Mr. Casper has over 22 years of experience in fiber optic communications. After 15 years as president of BCP, Inc., which he cofounded, he became Vice President, R&D. Many of the product innovations from BCP were engineered by Mr. Casper, and he was the circuit designer/developer of this particular high speed frequency agile modem. Paul holds both a B.S. and M.S. in Electrical Engineering from the University of Florida.*

*Mr. Shaughnessy has a B.S. and M.S. in Electrical Engineering and 41 years of experience in Telecommunications Systems. He is a Senior Consulting Engineer for CSC, for the SEAS contract and provides system engineering consulting for CSC and to the NASCOM Division at GSFC. He has been responsible for several Fiber Optic Communication System projects such as the Inter-Facility Link, (IFL) at the White Sands Complex. He currently manages the development of the Frequency Agile Fiber Optic Modem for NASCOM.*

### GROUND HARDWARE UPGRADES FOR FLIGHT SOFTWARE DEVELOPMENT UTILIZING VHDL/FPGA TECHNOLOGIES

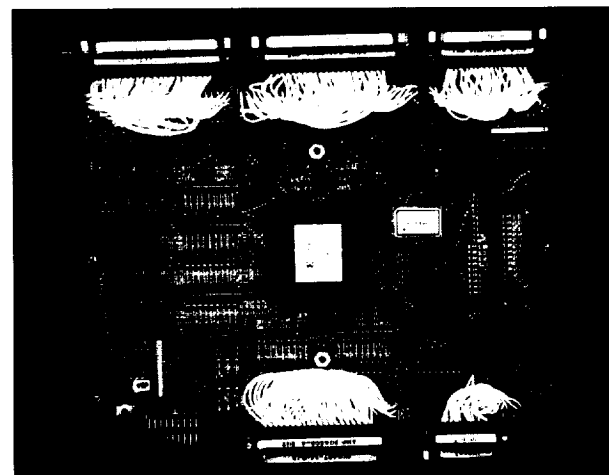
THE HUBBLE SPACE TELESCOPE, the Compton Gamma Ray Observatory (CGRO), and the Extreme Ultraviolet Explorer are types of multimission modular spacecraft that use the standard interface (STINT) for the on-board computer (OBC) in the command and data handling (C&DH) system. The OBC for a multimission modular spacecraft is often referred to as the NASA Standard Spacecraft Computer-1 (NSSC-1). The function of the STINT is to provide the necessary interfaces for the exchange of information among the core memory, the central unit, the remote interface unit (RIU), and the premodulation processor in the C&DH system. The OBC performs a variety of tasks during the life of the spacecraft. These tasks require the following capabilities:

- memory loading under software or hardware control;
- control of the OBC by ground command;
- distribution of stored commands;
- telemetry format control by the OBC;
- acquisition of data for OBC use;
- OBC access to all transmitted telemetry data;
- exchange of data between the OBC and the RIU; and
- memory readout under software or hardware control.

The STINT performance requirements necessary to achieve the listed capabilities are contained in GSFC document S-700-52, Rev. A, *Standard Telemetry and Command Components Standard Interface for Computer Requirements Document*. The NSSC-1 performance requirements are contained in GSFC document S-714-20, Rev. A, *NASA Standard Spacecraft Computer (NSSC-1) Design and Performance Specification*.

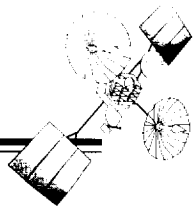
The STINT and NSSC-1 (both no longer produced) were implemented using discrete transistor-transistor logic (TTL) technology and custom metallized multigate array (CMMA) technology, respectively. Functionally, these technologies are sound; however they require much circuit board "real-estate" and power. These factors decrease reliability, and increase manufacturing and maintenance costs.

Under a contract, a single-string field-programmable gate array (FPGA) STINT (shown in the first figure) was developed, which uses a leading-edge technology Xilinx chip to hold the design. It is packaged in a case with a footprint identical to that of the original TTL version, which enables it to be stacked on the NSSC-1 for use in a C&DH simulator rack. The FPGA STINT is fully compliant with the GSFC document S-700-52, Rev. A, which makes it an ideal spare part for checking out flight modules. The pinout of all connectors and input/output characteristics are identical, so existing integration and test procedures can be used to verify electrical integrity when transferring the unit from system to system. Unlike the TTL version, the FPGA STINT has only one circuit card, significantly increasing reliability. Additionally, the FPGA STINT passes all worst-case timing requirements by synchronizing the design to a 10 MHz clock and performing digital timing analysis on the design. The most attractive feature of the FPGA STINT is the cost. The technology used to design and manufacture this unit—while increasing the performance—has reduced the expense to a small fraction of the cost required to produce the TTL version of the STINT.



STINT FPGA design.

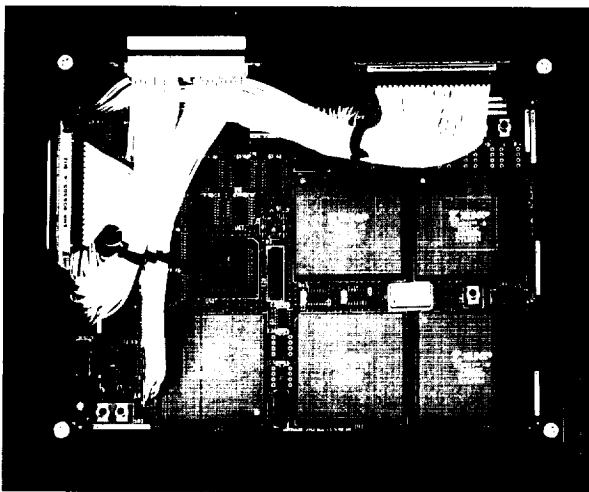
Under another contract, a single-string FPGA NSSC-1—also utilizing Xilinx-chip technology to hold the design—was developed. As with the FPGA STINT, the FPGA NSSC-1 is packaged in a case with a footprint identical to that of the original design so that it also can be stacked in



a C&DH simulator rack. The FPGA NSSC-1 is fully compliant with the GSFC document S-714-20, Rev. A.

The contents of the FPGA on the FPGA STINT circuit board were designed by using traditional schematic capture techniques. In contrast, the contents of the FPGAs on the FPGA NSSC-1 circuit board were designed by using a very-high-speed integrated circuit hardware description language (VHDL) methodology, in conjunction with a logic synthesis process. This type of design flow incorporates textual VHDL code, which describes the behavior of the NSSC-1 at a register transfer level, combined with computer-aided engineering tools that compile the code into a digital logic representation. Simulation of the design at various stages was accomplished through back annotation features so that logical and timing errors were caught and corrected. A traditional schematic capture approach was then used to generate an overall circuit board schematic. A VHDL design methodology provides several benefits over schematic-capture-based approaches, including easier portability to other vendor's FPGAs with very little or no change in code; the ability to readily determine the source of problematic signals (i.e., text is easier to read than graphical schematics); and the ability to design at a higher level of abstraction.

The FPGA NSSC-1 (shown in the second figure) is contained on a single circuit card. The circuit board also contains a 64K x 18 static random access memory chip



NSSC-1 FPGA design.

(SRAM). The SRAM chip, at a small fraction of core-memory cost, replaces the CMMA NSSC-1 core-memory module. Since the STINT shares this memory with the NSSC-1, a memory/STINT interface connector is provided on the FPGA NSSC-1 board. The FPGA NSSC-1 uses an identical connector to interface with the primary STINT signals, making integration into a current C&DH simulator rack very straightforward. The FPGA NSSC-1 may then serve as a replacement part, or be used to develop flight software to be executed on existing NSSC-1 units currently functioning in space environments.

The FPGA STINT was rigidly exercised through open-frame testing using the Fairchild STINT tester following the procedure in the Fairchild STINT testing document. Due to the programmability of the Xilinx gate array, any modifications required during open-frame testing were implemented quickly. The circuit card was then re-enclosed in its case and integrated into the CGRO software development rack, which simulates a single-string C&DH system with a VAX Interface Unit.

Spacecraft test operation language (STOL) programs were written to test the unit. The function of these programs is to load and dump all 16 banks of memory to check for data errors, and then to turn on and operate all required application processors in the NSSC-1 while continuously monitoring the RIU telemetry. The FPGA STINT functioned flawlessly the first time power was applied in the CGRO rack. After integration, the FPGA STINT was further tested using the CGRO flight software patch development program. Again, the FPGA STINT performed perfectly. A copy of the real time events listing is available for review.

The FPGA NSSC-1 unit was submitted in place of the CMMA NSSC-1 unit in the CGRO rack, and the same STOL programs were used to test it in conjunction with a copy of the latest version of CGRO flight software. The FPGA NSSC-1 acceptance test lasted one week. It performed perfectly, with no differences found in comparison with the CMMA NSSC-1 running the same software. The FPGA versions of the STINT and NSSC-1 are scheduled for integration into the HST Extended Software Test and Integration Facility, where they will undergo the final acceptance test.

## MISSION OPERATIONS AND DATA SYSTEMS

---

The remaining components of the HST Extended Software Test and Integration Facility—including an RIU—are scheduled for later development using the same FPGA Xilinx-chip technology.

Contact: Steve McCarron (Code 512)  
301-286-9716

Rich Ambrose (Omitron, Inc.)  
301-474-1700

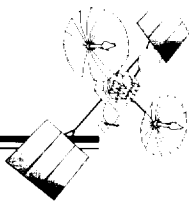
Ed Leventhal (Omitron, Inc.)  
301-474-1700

Sponsor: Office of Space Communications

*Mr. McCarron works in the Flight Software Systems Branch of the Mission Operations and Systems Development Division of GSFC, where he is currently managing the effort to develop a second string for the HST Extended Software Test and Integration Facility. He received an M.S. in Management Science from the Johns Hopkins University.*

*Mr. Ambrose is Director of Electrical Engineering at Omitron, Inc. in Greenbelt, MD. He earned a B.S. in Computer Engineering and is currently a Ph.D. candidate at Kennedy Western University.*

*Mr. Leventhal received a B.S.E.E. from Carnegie Mellon University and is currently pursuing an M.S.E.E. from the Johns Hopkins University. He is an electrical design engineer at Omitron, Inc.*



## **CUTTING COSTS THROUGH ADVANCED SOFTWARE AND SYSTEMS ENGINEERING TECHNIQUES: THE FLIGHT DYNAMICS DISTRIBUTED SYSTEM**

**R**EDUCED BUDGETS, REDUCED staffing, and an agency-wide directive to accomplish NASA's mission in ways that are "faster, better, and cheaper" have inspired all NASA organizations to seek significant increases in efficiencies within their organizations. In recent years, the Flight Dynamics Division (FDD) of the Mission Operations and Data Systems Directorate has decreased by half the support costs associated with the development of the flight dynamics elements of ground systems. To go beyond the savings achievable through more conventional approaches, and to fully embrace NASA's "faster, better, and cheaper" directive, the FDD is developing a new flight dynamics support architecture within which to develop and operate flight dynamics ground systems.

The Flight Dynamics Distributed System (FDDS) is designed to integrate new and reused software from a variety of sources, and to be portable to and operable from a range of platforms and facilities. The FDDS approach employs advanced systems engineering technologies—including the application of object-oriented concepts, open system standards, and distributed processing concepts—to implement flight dynamics functions and to provide a framework within which those functions can be assembled and operated.

The FDD employs a number of approaches to implement flight dynamics functions to address the specific needs of the customer. These approaches consist of the development of custom software, the use of legacy software systems, and the use of commercial off-the-shelf (COTS) products. Each of these approaches results in the configuration of application programs which are subsequently integrated within a flight dynamics system.

The approach to custom software development within the FDDS is encapsulated in the development and implementation of the Generalized Support Software (GSS) and User Interface Executive (UIX) environments; these tools are discussed in detail in separate articles elsewhere in this volume. The use of custom software solutions within the FDD is complemented by the use of legacy software systems and/or COTS products when appropriate. Legacy software systems may be used in their entirety, i.e., as stand-alone executables, or may be modified to support the specific needs of the mission. Similarly, COTS

products may be utilized as stand-alone executables or, when available in application program interface form from the vendor, may be used to complement the existing class library of custom software components in the GSS to achieve a custom software solution.

A flight dynamics system consists of the various custom, legacy, and/or COTS application programs that satisfy the needs of the customer relative to the data being generated and processed by these programs, all hosted within a workstation environment. The FDDS framework provides the "glue" which supports the integration of the various application programs and data within this system. This framework is described at various levels within FDDS. These levels consist of application program execution control, data management, communications, and interfacing between the FDDS environment and non-FDDS environments. Within each level of this framework, approaches and standards have been defined, which, through compliance by the components of the flight dynamics systems, support the integration, of these systems.

Application program execution control includes initiation and termination of program execution, sequencing of programs, and scripting of program execution within a sequence. The UIX Session Manager offers an implementation of these functions within FDDS and provides a single point from which to control application program execution within a flight dynamics system. The Session Manager provides a standard look and feel to the system from the user's perspective, which is independent of the platform(s) upon which the application programs that comprise the system reside and the application programs themselves. The FDD is pursuing the incorporation of scheduling systems to control the execution of application programs and the use of agents to support automated operations of flight dynamics systems.

The data management component of the FDDS integration framework defines the standards associated with the storage and retrieval of data within the FDDS distributed environment. These standards include the use of distributed file systems and platform-independent data representations. The FDD is currently investigating the use of databases and database integration schemes within the data management architecture to further support the management of data within a distributed environment.

## MISSION OPERATIONS AND DATA SYSTEMS

---

Communication standards define the manner in which application programs communicate with each other. These standards currently consist of socket-based approaches to interprocess communications. The FDD is currently evaluating—via a number of prototype efforts—the use of remote procedure calls and the Common Object Request Broker Architecture for applicability within FDDS.

The external interface component of the FDDS integration framework addresses the issues associated with adapting the FDDS environment to non-FDDS environments. This adaptation is necessary to support interfaces with systems external to the flight dynamics system (e.g., reliance on a non-FDDS data server for spacecraft telemetry), supporting the installation of flight dynamics systems at the customer site (e.g., within the larger ground data system located within the mission operations control center), or supporting the inclusion of legacy or COTS application programs within a flight dynamics system. This adaptation can occur at several levels, including the data and functional levels, and is accomplished through the use of “wrappers,” which provide the translation between the standards used in the FDDS and non-FDDS environments. Wrappers can be additions to a flight dynamics system (e.g., pre- and post-processors which

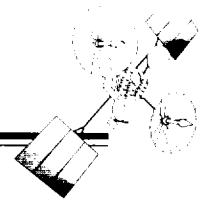
accomplish this translation), or replacements for components within application programs (e.g., a new driver for GSS-based application programs to support execution within a flight/flight software executive controlled environment versus execution in a ground/user controlled environment). The FDD is currently evaluating the use of Common Object Request Broker Architecture in this area as well.

The combination of the approaches being used within the FDD to implement functionality and to provide a framework within which flight dynamics systems are integrated are allowing the FDD to seriously address the challenge of accomplishing its mission in a way that is “faster, better, and cheaper.”

Contact: David Weidow (Code 552)  
301-286-5711

Sponsor: Office of Space Communications

*Mr. Weidow is Head of the Institutional Software Section of the Flight Dynamics Division. Mr. Weidow earned a B.S. in Astronomy from the Pennsylvania State University in 1984, and has been an employee of GSFC since then.*



## GENERALIZED SUPPORT SOFTWARE

THE GENERALIZED SUPPORT Software (GSS) project has developed a set of reusable, reconfigurable software components for use within the Flight Dynamics Distributed System (FDDS). These components are specified using a standardized, object-oriented notation, and are implemented using a generalized, object-oriented design approach. The GSS approach enables rapid development of components and rapid configuration of systems to support missions. The first GSS-based system to support a mission is a real-time attitude-estimation system, built to support the Tropical Rainfall Measuring Mission. Later releases of GSS will add functionality for the orbit and mission planning domains. The expectation is that the Flight Dynamics Division's (FDD) software development costs will be reduced by a factor of two, and that development time will also be shortened.

The specifications for GSS are being produced by a Domain Analysis Working Group. Domain analysis is the specification of models for a family of software systems rather than for a single system. In GSS, this implies modeling the same activity (e.g., attitude estimation) for multiple missions, and identifying models that are shared between activities (e.g., orbit propagation is done in orbit, attitude, and maneuver planning systems). Domain analysis allows the FDD to reduce the amount of software to be maintained, and to provide the same functions as current systems by eliminating redundant models.

The basic component of an object-oriented specification is a "class." Classes specify both the mathematical algorithms and the stored data for a given type of object being modeled. Classes act as templates both for physical objects, such as sensors, and more abstract objects, such as orbit dynamics models or estimation algorithms.

The object-oriented approach to domain analysis has two major benefits. First, object-oriented approaches place classes into a hierarchy of "superclasses" and "subclasses." Writing algorithms to depend on the more general superclasses, rather than specific models, is a powerful tool for generalizing systems. For example, sensor models are organized in a hierarchy with a sensor superclass and individual subclasses for each type of attitude sensor. State estimation algorithms (such as Kalman filters) are written in terms of the superclass. This allows the estimation algorithm to be configured with a different set of sensors

for each mission without rewriting any code, and allows the addition of new sensor subclasses without rewriting either the more general sensor class or the estimation algorithms.

The second benefit of the object-oriented approach is that the notation defined for the specification maps closely to object-oriented programming languages such as Ada and C++. This makes it possible to develop a design concept where the configuration of systems can be done with virtually no coding. The GSS design concepts support system configuration by selection of what components are to be linked together and through run-time tables.

The implementation concepts for GSS provide a generalized system design that determines how components are implemented from class specifications and how these components fit into the FDDS architecture. These concepts have been fully developed for Ada 83, and have been prototyped for C++ and Ada 95. The general design concept, however, is the same for each language.

Each class in the generalized specifications is implemented with two components (packages in Ada, classes in C++). The first is a component that directly implements the mathematical specification for a class. The second is a component that provides an interface between the implementation component and the FDDS User Interface and Executive (UIX, described elsewhere in this volume). This interface component provides the mechanism for the run-time configuration of objects and their interrelationships, for passing parameters between the UIX and the application, and for error handling.

Separating the essential mathematical models from the scaffolding needed to bind them to a particular system architecture is one of the major innovations of the GSS project. This separation was motivated by the difficulty in understanding the design of some of the first Ada systems developed in the FDD. The GSS uses Ada private types to define the data and operations associated with a class, and dynamically allocates variables of these types to represent objects. The corresponding C++ implementation concepts use the C++ class construct to implement both the interface and implementation modules.

In addition to making the design easier to understand, separating implementation and interface components

## MISSION OPERATIONS AND DATA SYSTEMS

---

allows the former to be reused outside the context of FDDS. In this case, the mathematical modeling remains the same, but the system architecture in which these models are used may be completely different. The FDDS applications run on UNIX workstations in a networked, open-systems environment. The FDD is currently investigating the use of the GSS implementation components as part of orbit-determination flight software.

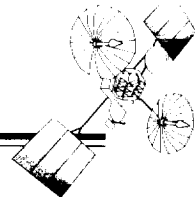
The standardization of the specification notation and the creation of a generalized design has enabled the development of a code generator tool. This tool reads an input file that is written in a language that maps to the specifications, and then generates the entire interface component and a large part of the implementation. This tool generates 10 lines of output for every line of input, leaving only the mathematical functions themselves to be

coded. For a typical component, the generated code is approximately 75 percent of the total code needed. This has reduced GSS development costs by approximately 30 percent from the usual cost for a system of this size.

Contact: Michael Stark (Code 552)  
301-286-5048

Sponsor: Office of Space Communications

*Mr. Stark specifies, develops, and manages generalized software for orbit, attitude, and maneuver planning applications in the Advanced Technology Section. He holds a B.A. in Mathematics and Economics from Oberlin College, and an M.S. in Computer Science from the Johns Hopkins University. Mr. Stark has 14 years of experience at GSFC.*



## GENERIC INFERENTIAL EXECUTOR: A TOOL FOR SPACECRAFT CONTROL CENTER AUTOMATION

THE INCREASING NEED to dramatically reduce the cost of mission operations has opened the door to automation technologies that have been generally available, but not yet applied to spacecraft control centers. Expert system technology, in the form of the Generic Spacecraft Analyst Assistant (GenSAA) and its predecessors, has been available and in use at GSFC for several years for spacecraft monitoring and diagnosis. This expert system technology can also be readily applied to automation of spacecraft control center activities, allowing the Flight Operations Team (FOT) to do more with constant (or decreasing) resources.

Most spacecraft-ground contacts, or passes, are routine activities, during which the FOT oversees the dumping of tables and science data and loading the onboard of stored commands. The process is well-understood and repetitive, and is therefore an ideal candidate for automation. An ideal application is automation of multispacecraft control centers, where operation of mature spacecraft may be largely automated, thereby allowing most attention to be focused on newly launched satellites. This approach is low risk because the FOT is immediately available if the automation system detects an anomalous condition. This technology can also be used to provide so-called "lights out" automation, where evening and night shifts have only a skeleton staff or no staffing at all.

The Generic Inferential Executor, or Genie, is a tool that allows easy construction of pass automation applications. Graphical workbench software, running on a UNIX workstation, allows the user to build pass script templates to encode the tasks necessary to mimic FOT interactions with the spacecraft during a pass. These templates are then configured by a mission planner with data specific to a particular pass. The script is loaded into the Genie runtime software during prepass preparations, and then executed. Animated graphical displays on a workstation show progress during the pass. If an anomalous condition occurs, the FOT can be notified; otherwise, tasks are fully automated.

The runtime Genie software was derived from GenSAA. GenSAA is a tool for building highly graphical expert systems to monitor spacecraft. It allows the FOT to construct expert systems on a UNIX workstation with a graphical interface by selecting mission data to be monitored and writing expert system rules that infer

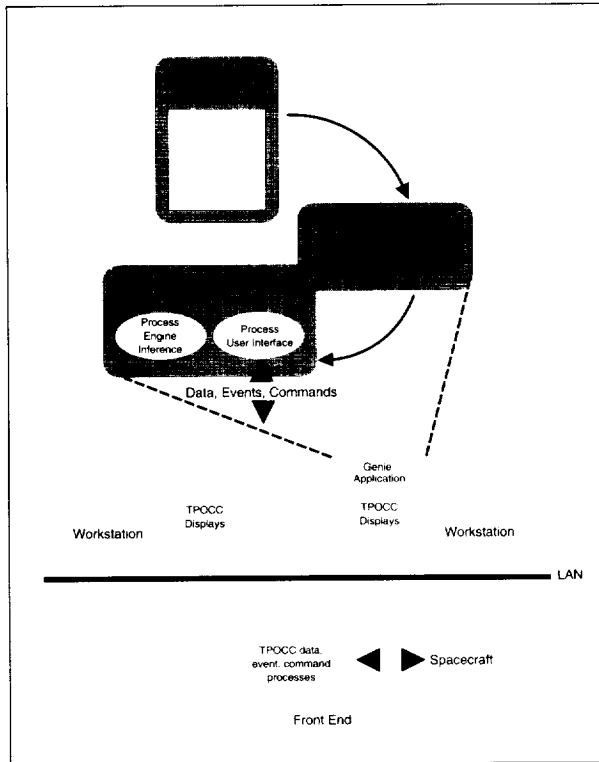
conditions not available as raw telemetry values. During runtime execution, the incoming telemetry causes execution of expert system rules and, together with the inferred data, drive the graphical display. The expert system inference engine in GenSAA is the C Language Integrated Production System (CLIPS), which was developed by NASA's Johnson Space Center.

Development of the Genie software required three separate efforts: (1) minor modifications were made to GenSAA software, adding interfaces to receive events from, and to send commands to, the control center software; (2) a graphical pass script builder was implemented; and (3) a script executor was coded in CLIPS rules. GenSAA and Genie both interoperate with spacecraft control center software based on the Transportable Payload Operations Control Center (TPOCC), a library of reusable software that has provided significant savings in developing control centers for GSFC missions. TPOCC allows external software applications to be integrated, and to send or receive data. GenSAA had already developed the interface to receive telemetry data from the spacecraft through TPOCC. For Genie, we added a similar interface to receive events from the control center that indicate the occurrence of some action such as activation of a procedure, an error condition, configuration changes, or communication status. We also added an interface to TPOCC to allow Genie to send commands to the spacecraft, typically by invoking a procedure running on the control center's command language interpreter.

We developed a stand-alone software application, called the Graphical Pass Script Builder, which allows an FOT member to graphically construct a picture of actions required for a spacecraft pass. The elements of a pass are required and optional tasks, decisions, and splits and joins for concurrent processing. The graphical pass script resembles a computer flow chart. Each element of the script can be "opened up" to provide details on exactly what is occurring. The actions desired in a task are specified in a combination of CLIPS expert system rules and control center command procedures. During runtime execution the graphical script is animated, with changing colors and updating alphanumeric displays to show status of the pass. Because the tasks are defined by expert system rules, the full inferential power of the expert system is available to make decisions about what should occur next in the script. This allows the scripts to embody

## MISSION OPERATIONS AND DATA SYSTEMS

complex logic, if that is required for a particular automation application. A block diagram of the system is shown in the figure.



*Pass automation applications, built with the Graphical Pass Script Builder, are executed by the GenSAA/Genie runtime system, which "plugs" into the Transportable Payload Operations Control Center software through network socket connections.*

The execution of the script itself is guided by another set of CLIPS expert system rules. These rules form what is called the script executor. Prior to executing a Genie application, the graphical pass script is converted into computer-readable form and loaded into the runtime system. The script executor performs actions as defined by the pass script, while keeping track of current time,

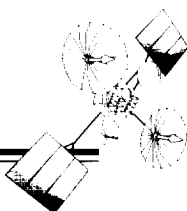
status of the script, and which tasks are active or waiting. Each task consists of a set of preconditions which must hold for the task to begin execution, a set of actions to be completed, and a set of results which must be obtained for successful execution. To effectively mimic the FOT, execution of tasks in parallel is necessary. For example, to save time, the FOT may dump data from the spacecraft while uploading other data to the spacecraft. The script executor keeps track of this simultaneous execution of multiple tasks. The script executor can run a script in one of three different modes: shadow, advisory, or controlled automation. Shadow mode allows testing the Genie application by allowing it to receive data but not send commands. Advisory mode requires an operator acknowledgment prior to releasing each individual command. Controlled automation mode is fully automated, with Genie initiating tasks at the pace defined in the pass script, with no human involvement.

The first Genie application that was developed automates passes of the Solar, Anomalous, and Magnetospheric Particle Explorer (SAMPEX) spacecraft. Over 40 passes have been completed with the live spacecraft in shadow, advisory, and controlled automation mode. These automated passes with SAMPEX, while performed as a proof of concept, give every indication that control center automation is feasible with today's tools. Applications for new missions should be relatively easy to build once routine spacecraft operation is established and understood. Our near-term goal is to apply this technology aggressively to existing and future GSFC missions, including the Earth Observing System, to reduce operations costs.

Contact: Jonathan Hartley (Code 520)  
301-286-6663

Sponsor: Office of Space Access and Technology

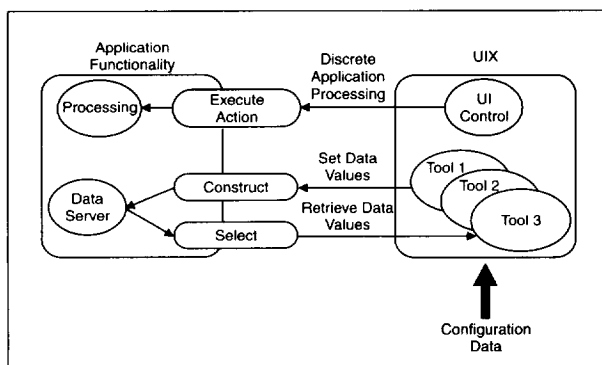
*Mr. Hartley is Associate Chief of the Data Systems Technology Division. He has a B.A. in Physics from the University of Maryland, Baltimore County, and a Master's degree in Computer Science from the University of Virginia. He joined GSFC in 1986.*



## THE USER INTERFACE AND EXECUTIVE

THE FLIGHT DYNAMICS DIVISION (FDD) at GSFC has developed an advanced, reusable, graphical user interface (GUI), known as the User Interface and Executive (UIX), to reduce development costs, development time, and operations costs. The UIX is a configurable GUI based on open systems standards (e.g., POSIX, X Windows, and Motif). It can be tailored to meet the user interface requirements for a specific application without source code modifications or the need to relink the application. This approach is a radical change to user interface development efforts, which typically use GUI builders for the same purpose. When the changing needs of the user and the application development community require it, the UIX is reconfigured through files rather than by changing source code. This concept allows the UIX to provide a standard GUI across all applications and platforms within the FDD.

Using an object-oriented design and implementation, the UIX logically separates the user interface component from application functionality. The object-oriented encapsulation of the application program allows the application and user interface to be treated as distinct entities, with a small and rigidly defined set of interfaces between them. These interactions include selection of data from the application, update of data within the application, and processing of execution directives. This relationship is illustrated in the figure.



*UIX Model.*

To implement this model, a behavior model was established to define interactions between the user interface and the application functionality. The behavior model describes how and when actions and data can be exchanged between the user interface and the application program.

The *how* is defined by the rigidly defined set of interfaces described above. The *when* is defined by a state-transition model within the application; the application program is described by a set of states and the transitions between the defined states. Whenever the application is in a stable state, control is passed to the user interface. In UIX terms, this is considered a "decision point." At this point, the user can perform any one of the defined actions based on information provided by the application visualization tools that support application-specific data. The figure illustrates the relationship of the configuration data and the UIX.

The UIX configuration interface provides the mechanism to choose a display type and associate the data presented, their positions on the display, any associated informational text (e.g., display titles, footers, and descriptive text), and other parameters relevant to the type of display (such as limits for range checks, and the locking of data entry fields). The UIX allows each type of display to be fully interactive and supports two-way exchange of information between the user and the application program. The characteristics of the display types were established after careful study of the needs of the flight dynamics application user community.

The flexibility offered by the UIX model allows the FDD to support new development efforts as well as legacy software that has been ported from the mainframe environment into its new, distributed computing environment. The UIX was first released in May 1995, and is currently supporting four newly-developed applications, including real-time and non-real-time attitude determination systems, and one ported application. The first upgrade to the UIX took place in September 1995; the next major release is due April 1, 1996.

Contact: Jeffrey Segal (Code 552)  
301-286-5316

Sponsor: Office of Space Communications

*Mr. Segal researches, develops, manages, and analyzes the flight dynamics computer graphics systems and other mission support software in the Advanced Technology Section at GSFC. He holds a B.S. in Math/Computer Science from Virginia Commonwealth University, and an M.S. in Engineering Management from George Washington University. Mr. Segal has 5 years of experience at GSFC.*

## **VISUALIZING SPACECRAFT GROUND SYSTEM DATA**

THE AUTOMATION Technology Section has been investigating the application of three-dimensional (3D) visualization technologies to the mission operations domain. Obvious sources of data to attempt to visualize this domain are spacecraft ground data systems. Such data sources contain enormous amounts of information about the state of spacecraft. By better understanding the data in these ground systems, operators can do their jobs more efficiently and effectively.

Classical scientific visualization techniques rely on relationships between points close to each other in 3D space. Using these relationships, isosurfaces are created that represent regions where particular variables are constant, such as temperature or pressure. In a spacecraft ground data system there can be many (e.g., 10,000) disjointed data elements that prohibit the use of isosurfaces. The data contained in these data servers consist of vectors (e.g., direction from the spacecraft to the Sun), scalar values (e.g., spacecraft altitude), discrete states (e.g., tape recorder is either ON or OFF), etc. Many of these values have limit information associated with them. The limits are typically green, yellow, and red, representing nominal, warning, and alert conditions, respectively. Using this information about the makeup of the data, we developed several techniques to visualize these disjointed data without using isosurfaces.

This work was originally motivated by the "CyberSpace" project at NASA's Jet Propulsion Laboratory (JPL). We created a rapid prototype of the concepts identified by the CyberSpace project and then extended these concepts. Multispace (shown in the first figure) is an attempt to monitor many data points from multiple spacecraft at once. The y-axis is broken down by spacecraft, the x-axis by subsystem, and the z-axis is the normalized value of each parameter. Each region on the bottom plane (xy) then may contain many different parameters. This technique will allow users to simultaneously monitor several spacecraft by subsystem.

The Ribbon Space prototype (shown in the second figure) displays multiple, independent, normalized data points in a 3D cube. Both current and past data points are displayed. The user can interactively change the time-axis interval, the current-value plane, and the threshold plane. This visualization is capable of showing both scalar and discrete data.

Cube Space (shown in the third figure) displays limit status (green, yellow, or red) of many different parameters at once. Each small cube within the bounding cube represents one parameter in the ground system. Given a 20 x 20 x 20 cube, we can monitor 8000 different parameters for limit violations simultaneously. The spatial representation of data can be partitioned using many different schemes, such as by subsystem, criticality, refresh rate, etc.

Since vectors are a distinct physically based type of data in spacecraft ground systems, we developed a simple tool for visualizing and monitoring 3D vector-based satellite telemetry data. This prototype, called Vector Space (shown in the fourth figure), allows user to view multiple vectors (e.g., antenna boresight, sun-angle, and star tracker vectors) projected onto a 3D grid. Vector Space also accurately depicts a satellite's attitude relative to the Earth and Sun.

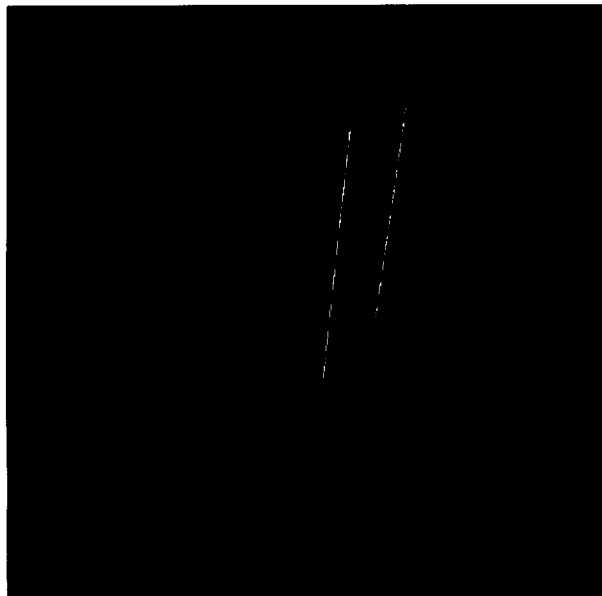
We are currently working on a prototype of a Data Carousel. This prototype consists of many plates arranged in a 3D carousel of data that the user can quickly flip through to examine details (including trend information) about any parameter in a ground system.

Targeted users for the visualization technologies described here are GSFC's mission operations teams. Other projects also looking at improving mission operations are enthusiastic about the work that we are doing and are considering incorporating our concepts. The techniques discussed here are widely applicable. Most databases consist of data that can not be represented using isosurfaces; by creating techniques for visualizing these databases, we can improve data monitoring across vast domains.

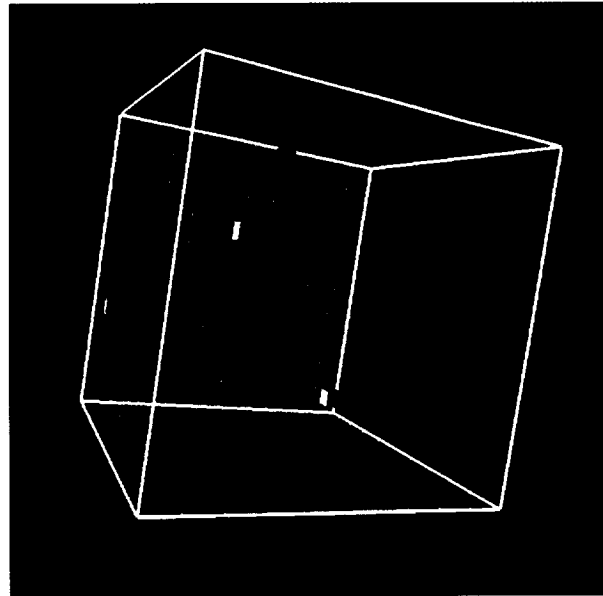
For more information on spacecraft ground system data visualization, please visit the project's World Wide Web home page at <http://groucho.gsfc.nasa.gov/eve/VR.html>.

Contact: Gregory Shirah (Code 522.3)  
301-286-7903  
Internet: [greg.shirah@gsfc.nasa.gov](mailto:greg.shirah@gsfc.nasa.gov)

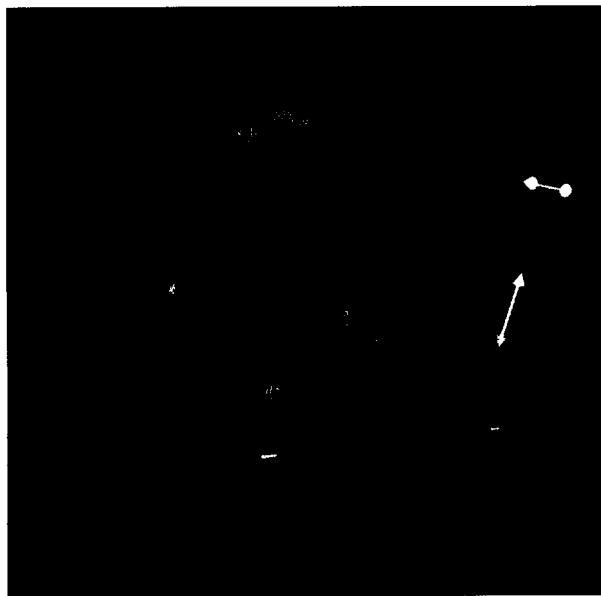
Sponsor: Office of Space Communications



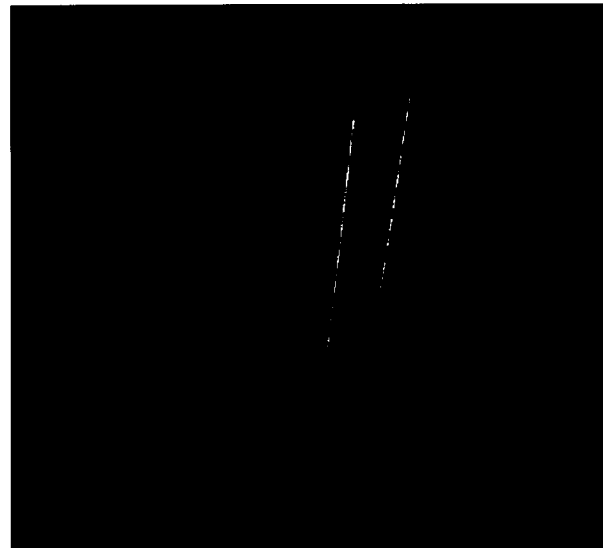
*Multispace.*



*Cube space.*



*Ribbon space.*



*Vector space.*

*Mr. Shirah works with expert systems and computer graphics in the Automation Technology Section. He received a B.S. in Mathematics and Computer Science*

*from the University of Georgia, and an M.S. in Computer Science from the George Washington University.*

### HOW TO AUTOMATE A GROUND TRACKING STATION USING COMMERCIAL OFF-THE-SHELF PRODUCTS

**T**O REDUCE LIFE-CYCLE costs and increase flexibility, the GSFC Networks Division is automating its Ground Tracking Stations in Florida and Bermuda through the Automated Ground Network System (AGNS) project. Key to the project's success is the capability provided by modern operating systems, networks, and applications software to easily implement interprocess communications. Although no single "shrink-wrapped" commercial product exists to automate the stations, the AGNS project minimized custom software development by seamlessly integrating a variety of commercial off-the-shelf products, each optimized for solving one part of the overall task.

The AGNS project used a commercial Supervisory Control and Data Acquisition product, the Tate Integrated Systems TIS4000™, to implement remote, geographically-independent monitoring and control of station equipment, as shown in the first figure. Commercial industrial control systems like the TIS4000™ must meet high standards of safety and reliability, as they are often used to control critical manufacturing plant processes. Such products are ideally suited to NASA's operational needs, and offer great functionality at very low cost.

Although the TIS4000™ software provides an excellent solution for monitor and control of station equipment, it did not provide an adequate interface to view test equipment displays for troubleshooting. The AGNS

project installed programmable test switches to allow an operator to graphically select test points using the TIS4000™ software, and direct the selected test signals to the test equipment. The project used LabVIEW™, a product of National Instruments Corporation, to monitor and control the test equipment, and to view the test equipment displays.

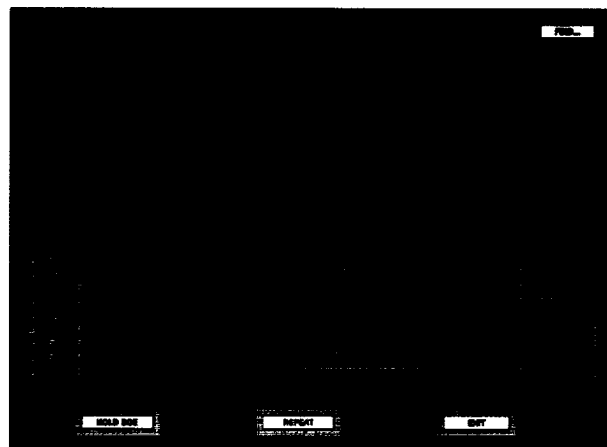
Providing remote monitor and control "hooks" into station equipment is only the first step toward automation. Configuring a station with only the TIS4000™ software would still require an operator to go through several lower-layer screens to manually configure all parameters. Also, the TIS4000™ software does not interface with a station's operations schedule. Therefore, the project team provided a higher layer of intelligence in the AGNS, called the Pass Management Program (PMP). The PMP, which is shown in the second figure, uses two commercial database products from Oracle Corporation: Oracle™, and its companion graphical Structured Query Language front-end, SQL\*Forms™.

These products provide capabilities for

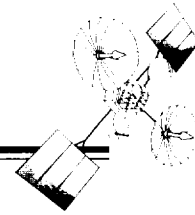
- ingesting, interpreting, and managing all operations schedules;
- storing all site operations procedures, equipment parameters, and other configuration information in a master "sequence-of-events" dictionary;



AGNS Monitor and Control Subsystem (MCS) using Tate TIS4000™.



AGNS Pass Management Program (PMP) using Oracle™.



- extracting all procedures from the master “sequence-of-events” dictionary necessary to support each scheduled activity, and specifying a desired time for each procedure to be executed based on the current schedule;
- extracting the currently available set of equipment from an equipment status database, comparing it with the standard set of equipment required to support currently scheduled events, allocating the equipment resources, and presenting operators with alternative equipment choices if default items are not available;
- extracting all configuration information required to set-up the selected equipment;
- presenting all of the selected procedures to an operator for authorization to proceed on an item-by-item basis, and then initiating these procedures, once authorized, to pass information extracted from database tables to the TIS4000™ software, which configures and tests the equipment and software. An operator can authorize any event at any time, elect to ignore or repeat events if necessary, and can authorize as many events simultaneously as desired; and
- receiving status back from the TIS4000™ software and logging it in tables for subsequent analysis and reporting.

Since every item of information needed to conduct station operations is stored in Oracle™ tables, operators can add, delete, or modify sequence definitions, equipment items, configuration information, and other data necessary to conduct routine operations without the support of programmers. Since Oracle™ is accessible over the network, this can be performed from a central configuration management facility or locally at each site. Management reports can be generated from any authorized location in the network and can be based on database joins across all sites. Since all equipment status, operations procedures, site actions, and equipment responses are recorded by Oracle™, these databases provide a reference library for continuous improvement analysis.

The procedures in the master “sequence-of-events” can be chained together in parent-child relationships. This means that once an operator is satisfied that a subset of the procedures works correctly, these procedures can be linked and activated by a single mouse click. Ultimately, it is conceivable that an operator will make one mouse click to configure the entire station and run the entire mission support. In the meantime, however, the PMP provides a useful transition tool.

The commercial products used by the AGNS project enabled a team of only eight people to implement this automation project in 2 years. These products provide far more detailed, accurate information and greater flexibility than has ever been available to the stations.

Contact: Miles Smith (Code 531.3)  
301-286-5748  
Internet: Miles.T.Smith.1@gsfc.nasa.gov

Peter Militch (ATSC)  
301-805-3338  
Internet: Peter.N.Militch.1@gsfc.nasa.gov

Sponsor: Office of Space Communications

*Mr. Smith is an electrical engineer in the Baseband and Control Systems Section of the Network Engineering Branch. He is the NASA Project Manager for the AGNS project. Mr. Smith has a B.S.E.E. from Arizona State University, and an M.S.E.E. from George Washington University. Mr. Smith has been working at GSFC for 6 years in the areas of telemetry systems, tracking and control systems, and automation.*

*Mr. Militch is an electrical engineer with AlliedSignal Technical Services Corporation (ATSC). He was the ATSC Project Manager for the AGNS project. Mr. Militch has a Bachelor of Technology degree from South Australia Institute of Technology, and an M.S.E.E. from the Johns Hopkins University. Mr. Militch has been supporting GSFC in Ground Network efforts for the past 12 years, and he worked at the Orroral Tracking Station at Canberra, Australia, for 5 years.*

### IMACCS: AN OPERATIONAL, COTS-BASED GROUND SUPPORT SYSTEM PROOF-OF-CONCEPT PROJECT

THE INCREASING AVAILABILITY, low cost, and automation potential of commercial off-the-shelf (COTS) hardware and software designed for spaceflight ground support make these products attractive prospects to help reduce the cost of ground systems and flight operations. However, the use of such tools, especially for scientific missions with complex operational profiles, is made problematical by their relative immaturity, in that they have not been validated by extensive operational use. The Integrated Monitoring, Analysis, and Control COTS System (IMACCS) is a proof-of-concept demonstration of the ability of COTS products to meet the ground system needs of an existing mission at GSFC.

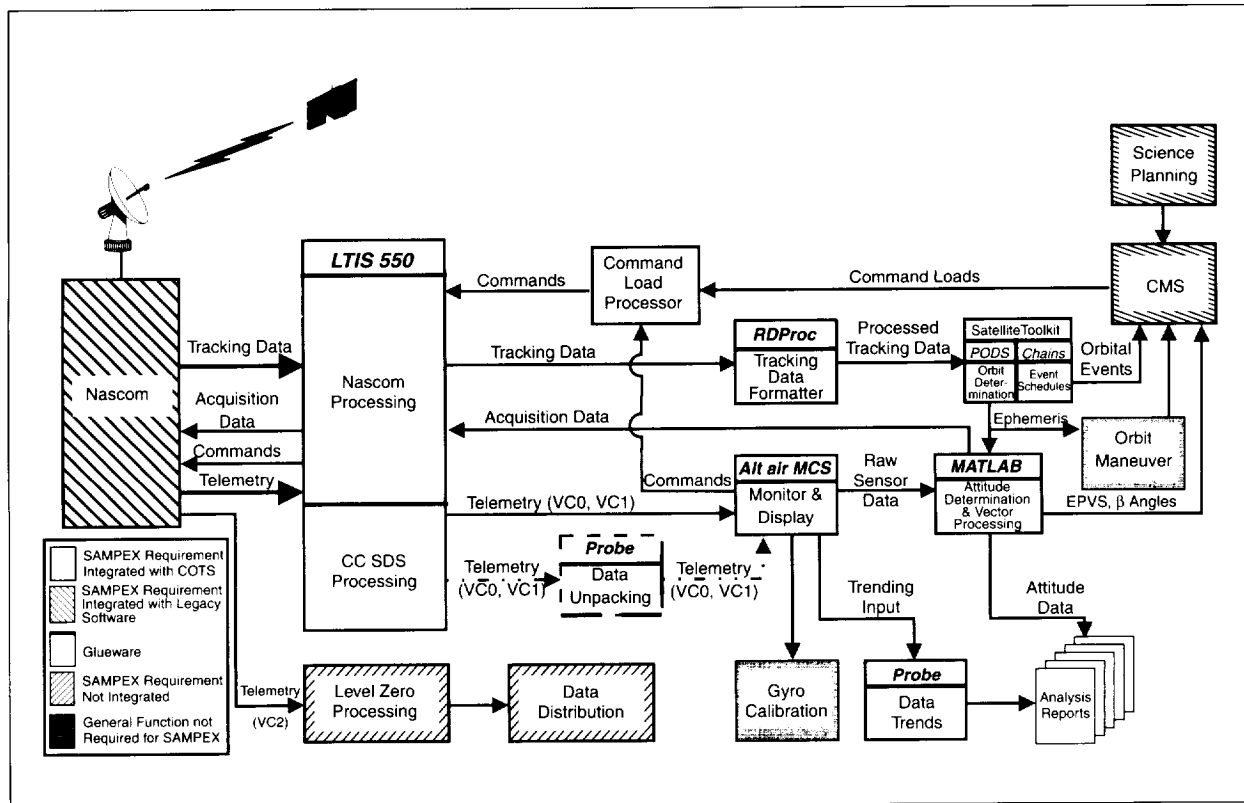
To make the project more credible, an existing spacecraft was targeted. The spacecraft for this demonstration is the Solar, Anomalous, and Magnetospheric Particle Explorer (SAMPEX), which is the first Small Explorer (SMEX) satellite. This satellite is in a low-Earth orbit (altitude 800 km), with a payload of four scientific instruments. The mission is approaching the end of its prescribed science mission life, and thus is an excellent candidate for this type of demonstration.

The major objectives of this demonstration were to

- compare IMACCS' performance to existing SAMPEX ground system performance;
- compare IMACCS' functions to existing SAMPEX ground system functions;
- compare IMACCS' user interface to existing SAMPEX ground system user interface;
- evaluate the ease and feasibility of integrating COTS products;
- determine the lines of code that had to be developed in order to integrate the various products;
- determine whether IMACCS could be operated by a single analyst or be unattended overnight; and
- determine the cost of developing and operating IMACCS compared to the existing SAMPEX ground system.

By evaluating IMACCS against these objectives using live telemetry and tracking data, the extent of its operational viability could be determined. The reader should note that evaluating specific COTS products is not included in the list of objectives. Tools chosen for IMACCS were representative in their capabilities, and were chosen from among available products based on a variety of criteria. In some cases, the choice was made based on the willingness of the vendor to make demonstration licenses available. In other cases, there was some familiarity with the product within the Mission Operations and Data Systems Directorate. The primary focus for this investigation was integration feasibility, not the choice of an optimum tool set. However, we did evaluate the current maturity and applicability of COTS products in IMACCS for use in the NASA operational environment.

To acquire COTS products, individual vendors were contacted. In most cases, vendors provided demonstration copies of their products for the planned 90-day integration period. All COTS products were hosted on RISC-based workstations (Hewlett-Packard and Sun processors) under UNIX, configured as a local area network (LAN). The system architecture for IMACCS (shown in the figure) consists of a loosely coupled set of functions that start with the communications front-end processor, the Loral Test and Information Systems (LTIS) Series 550. The front end receives telemetry (Consultative Committee for Space Data Systems (CCSDS) packet telemetry) from the SAMPEX spacecraft, and tracking data from the ground stations through the NASA Communications (NASCOM) ground network. Similarly, the front end transmits command data using the Command Load Processor (CLP) to the SAMPEX spacecraft through NASCOM via the ground stations, and transmits station acquisition data (Improved Inter-Range Vectors (IIRVs)) to the ground stations. In addition to receiving data, the front end also decommutes and converts the data to engineering units for other ground elements. The Altair Mission Control System (MCS) monitors spacecraft health and status. MathWorks Inc.'s MatLab provides a toolset to compute spacecraft attitude, and BBN Inc.'s Probe analyzes and reports data trends using these data. Tracking data are also collected by the front end. The Storm Integration Precision Orbit Determination System (PODS), Analytical Graphics Inc.'s Chains, and Computer



Typical ground system with IMACCS components.

Science Corporation (CSC) Inc.'s RDProc tools use these data to determine spacecraft orbit.

In addition to these COTS products, IMACCS interfaced to the existing Command Management System (CMS) using file transfer protocol (ftp) through an Ethernet LAN. CMS performs the command load generation function for SAMPEX. It is questionable whether any COTS products could readily reproduce this largely SAMPEX-specific mission planning function. The CLP, developed as "glueware," converted SAMPEX command strings into proper CCSDS, NASCOM, and mission-specific formats for transmission. For IMACCS, glueware is defined as software developed using a high-level programming language. Since we were reproducing a SAMPEX ground system, we needed to transmit commands that SAMPEX could understand.

Level-zero processing, science data distribution, and science planning were not implemented in the prototype, but are part of the currently operating SAMPEX ground system. Orbit maneuver planning and gyroscope calibration are functions typically found in a ground system, but were not required for SAMPEX. However, COTS products are available that perform these functions. CSC Navigator performs orbit maneuver planning, and MathWorks MatLab performs gyroscope calibration.

The next major effort involved integrating the various pieces by defining the interfaces and developing the necessary glueware to implement them. Glueware was developed to convert commands and command loads to a form suitable for transmission by the front end (the CLP), to enable the MCS to receive telemetry data from the LTIS 550. In addition to glueware, the Practical Extraction and

## MISSION OPERATIONS AND DATA SYSTEMS

---

Report Language was used to create code that enabled the LTIS 550 to extract telemetry parameters from telemetry.

Successful integration was defined as complete end-to-end throughput, with telemetry received and processed and commands generated. At the end of the 90-day period, IMACCS could read and display all telemetry and tracking data, process these data into attitude and orbit solutions, trend the data, display orbital events, and perform station acquisition data computation. However, the command capability was not complete. To allow for SAMPEX-specific command formats, a mission-specific reformatting process was needed. Therefore, custom glueware had to be written (the CLP). The command capability became operational on the 95th day.

Several significant obstacles were encountered in the configuration, installation, and integration effort, including

- difficulty in performing the installation without direct assistance from the vendor;
- difficulty in getting products to interface with one another as initially expected or advertised;
- difficulty in getting the product to work as advertised;
- expiring licenses;
- hardware failures;
- difficulty in getting demonstration versions of a COTS product to do all the functions needed; and
- software bugs.

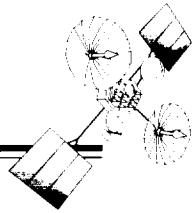
In general, most of the COTS vendors were eager to collaborate, and were generous with demonstration licenses and technical support. The products varied in maturity, but all were found capable of supporting this application. Documentation was uniformly difficult to use, and, since vendors were geographically distributed, communications were somewhat hampered, although electronic mail helped overcome this difficulty.

We found that COTS products offer trade-offs in flexibility and configuration ease. Experience proved that the easier a product was to install and use, the less flexible the product tended to be, and vice versa. As system integrators, we need to remember that these COTS products are very complex, requiring a significant integration effort. Some of the products were somewhat unreliable because it was difficult to determine why a particular problem kept occurring. Other products were awkward to use and did not process data directly, as we would have liked. This necessitated development of additional glueware. However, even though these products were developed independently of each other, interfaces could be developed to produce an integrated system.

Another important lesson to remember when using COTS products is that licenses expire. This was particularly evident for the prototype, since demonstration versions of the products were used, but must be considered for any development and long-term use effort.

One very important part of the process that was skipped for this exercise, and which must not be underestimated, is the product selection process. It is extremely important to evaluate each product thoroughly in order to make an informed choice. This is usually achieved through telephone discussions with vendors, vendor demonstrations, or hands-on evaluations to obtain a thorough understanding of the real operational requirements of the target system.

IMACCS has been an overwhelming success. As a result of trying this approach for SAMPEX, we have a clearer understanding of what is involved in building systems using COTS. In addition, we are more knowledgeable about the products selected—their capabilities and shortcomings—and their suitability for satellite ground operations support. In many cases, we were significantly impressed with the capabilities that the product provided, and learned that many products exist that offer the excellent prospects for automating operations for future missions. In addition, through our evaluation, we were able to determine that currently-available COTS products can be satisfactorily integrated with products developed by GSFC.



Much was learned about the process of collecting and integrating the COTS products and about the COTS products themselves during this project. These products provide an unprecedented capability to build a ground system faster, easier, and cheaper than by using more traditional development approaches. The COTS approach has been substantially established for future GFSC missions, with projects taking a hard look at using this approach.

We wish to acknowledge the support and/or efforts of the IMACCS development team composed of individuals from CSC, GSFC, Loral Aerosys, Altair Aerospace, and RMS, Inc. In addition, we wish to acknowledge the

vendors that provided demonstration copies of their products. Special recognition goes to the Renaissance project manager, Gary Meyers, for his dedication in promoting and supporting the effort of IMACCS.

Contact: Michael Bracken (Code 522)  
301-286-7896

Sponsor: Office of Space Communications

*Mr. Bracken is a computer engineer and has been with GSFC for 9 years. Recent professional activities include work in reuse repositories, systems engineering and ground data system architectures, and COTS and systems integration.*

## SOFTWARE FRAME SYNCHRONIZATION FOR SPACECRAFT TELEMETRY

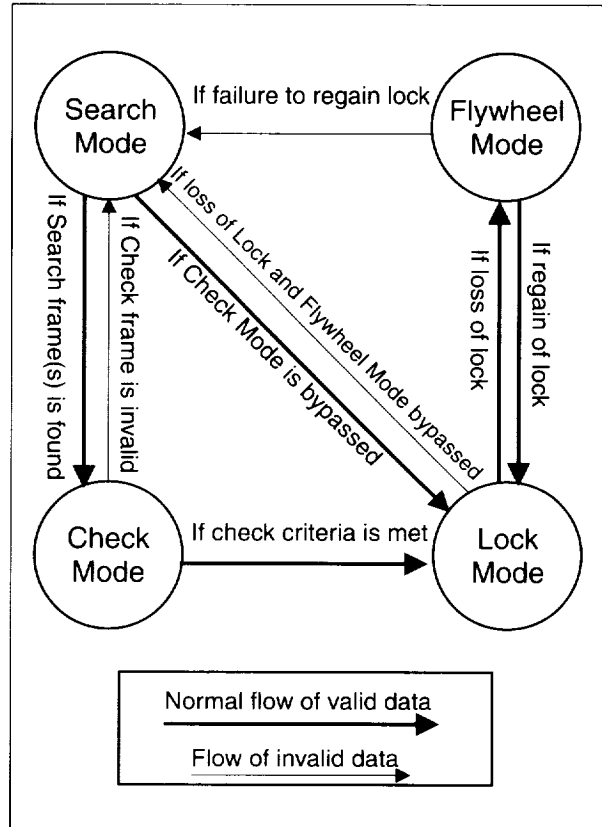
FRAME SYNCHRONIZATION is the process of extracting blocks of data (frames) from raw data telemetry streams by searching for a specific bit pattern that identifies the frames. For performance reasons, such telemetry processing functions have traditionally been performed in custom hardware. However, with the advent of faster and less-expensive computers, software frame synchronization has become a practical approach, and has led to the development of generic frame synchronization software that provides a low-cost and easily extensible alternative to hardware frame synchronization. This software may be run as a separate application, or be used as a software library in existing software. This software provides acceptable performance on low-cost desktop UNIX workstations and portable laptop computers.

The frame synchronization process employs a set of strategies that ensure that false acquisition of data is minimized. These strategies are embodied in a state machine containing four states, or “modes of operation,” which set the rules for the synchronization process. The four modes of operation for frame synchronization are: Search, Check, Lock, and Flywheel, as shown in the figure. Search Mode can be re-entered from any of the other three modes. Upon acquisition of signal, loss of signal, or software reset, the algorithm defaults to Search Mode.

Search Mode is conducted starting with the first byte of data received. Shifting via bitwise operators is used to conduct a bit-by-bit search. After each shift, the value contained in the register is compared against a previously generated look-up table, based on the chosen frame synchronization pattern. The use of a look-up table provides many benefits, including increased speed, programmable error thresholds, and detection of inverted frame synchronization patterns.

Check, Lock, and Flywheel are not bit-by-bit search operations. These operations look for the synchronization pattern at the expected end of the previous frame window. The size of this window can be set by the user, and can range from  $\pm n$  bits to allow detection of frames that have slipped from the expected frame position by  $\pm n$  bits.

The primary mode of frame synchronization is called Lock Mode. In order to get into Lock Mode, the Search and Check criteria must first be passed. Entering Lock gives

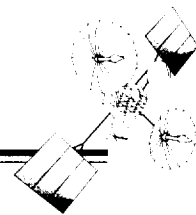


Frame Synchronizer State diagram.

an indication that data are good, and that the frame synchronizer should remain in Lock Mode unless the error tolerance is exceeded. If the error tolerance is exceeded, the operation will “drop lock,” indicating a loss of signal, and will cause the system to enter Flywheel Mode.

Flywheel Mode allows a momentary dropout or a noise hit directly on the synchronization pattern. If the synchronization pattern is unrecognizable, the software will jump to the next frame in hopes of reestablishing Lock Mode. If Flywheel frames continue to exceed error tolerance and Lock cannot be regained, the frame synchronizer then re-enters Search Mode.

Once the frame synchronization pattern is matched, a frame is byte-aligned. Byte alignment is the process of shifting a frame’s bits to ensure the first bit of a frame starts in bit 0 of a byte. The shifting is performed bitwise across the entire frame (including the frame synchronization pattern)



32 or 64 bits at a time, depending on the computer's maximum register length.

Finally, frame synchronization must output the found and aligned frames. Frames can be output starting at any mode: Search, Check, Lock, or Flywheel.

The frame synchronization software has been developed as a library of routines developers may integrate directly into telemetry software. It has also been integrated into an application which provides input/output options, frame synchronization, and software Reed-Solomon error correction. The frame synchronization software was written to be flexible in order to handle multiple missions. It provides two levels of flexibility. First, the routines are written to allow the input/output routines to be codified by the developer/integrator. Second, most aspects of the frame synchronization software—such as the frame synchronization pattern, the length of the frame, and the error tolerance—are defined at run-time upon initialization. The frame synchronization software handles all buffering of data for frames which may “bridge” two data buffers. The raw data buffers may vary in size from buffer to buffer, the only restrictions being that a buffer may not be less than the size of a frame, and may not be greater than some maximum specified when initializing the software.

The frame synchronization routine runs at up to 50 Mbps on an SGI Challenge L with a 150 MHz processor, and up to 30 Mbps on a 70 MHz Sun SPARC 5. These numbers include reading the raw data from disk and writing the aligned frames to disk.

Software frame synchronization provides many benefits. System costs are reduced by reusing software and by using commercial hardware to run the software. Also, maintenance costs are reduced, since in an “all software” solution, only standard vendor maintenance is required for the commercial hardware; no custom card maintenance is necessary. It therefore makes sense to choose a software

implementation for telemetry processing functions whenever performance requirements allow. The actual performance threshold will increase each year due to advances in commercial processor technology, and not due to the constant and costly hardware redesign that usually takes place in order to increase performance. Clearly, this new approach offers many possibilities for future, low-cost, ground system applications.

Contact: Thomas Grubb (Code 514)  
301-286-8594  
Internet: Thomas.G.Grubb.1@gsfc.nasa.gov

Steve Duran (Code 514)  
301-286-9262  
Internet: Steve.G.Duran.1@gsfc.nasa.gov

Sponsor: Office of Space Communications

*Mr. Grubb is a computer engineer currently working on the Landsat-7 mission. Mr. Grubb earned an M.S. in Computer Science from Johns Hopkins University. He has been at GSFC for 7 years, where he works in the Data Processing Systems Branch. Previously, he developed software for Upper Atmosphere Research Satellite, the International Solar/Terrestrial Project, the Cosmic Background Explorer Satellite, and other projects.*

*Mr. Duran received a B.S. in computer engineering from the University of New Mexico in Albuquerque in 1994. He is currently working towards an M.S. in Electrical Engineering, with an emphasis in Signal Processing, at the Johns Hopkins University in Baltimore, MD. Mr. Duran works full time at GSFC in the Data Processing Systems Branch, developing and building prototypes of the latest in telemetry processing software applications. His interests include neural networks, image processing, pattern recognition, error control coding, and space telemetry processing.*

### SOFTWARE REED-SOLOMON DECODER FOR SPACE TELEMETRY APPLICATIONS

**R**EED-SOLOMON ERROR correction coding is a vital part of the space communications link, since without a robust method of error correction, a significant percentage of satellite telemetry data would be useless. Until recently, Reed-Solomon decoders for ground data systems have always been implemented in hardware, primarily because custom hardware provided the most cost-effective implementation. Also, a hardware implementation was necessary to perform the time-consuming calculations required for the Reed-Solomon decoding algorithm. Within the last few years, with low-cost, high-performance computers becoming available, a software implementation has become the most cost-effective implementation for medium-to low-telemetry data rates. Software implementation of a Reed-Solomon decoder has many advantages over hardware implementation. The main advantage is cost; once the code has been developed, debugged and tested, there are no additional manufacturing costs. Scalability is also an advantage, since, as computers get faster, the decoder inherently gets faster, without the need for redesign. Also important is maintainability; the software decoder does not have parts that can wear out.

The software Reed-Solomon decoder developed in the Data Processing Systems Branch is fully compliant with the standards set forth by the Consultative Committee for Space Data Standards (CCSDS). The decoder can also decode non-CCSDS compliant codes, with only a change in its configuration parameters. This is a desirable feature, since decoding different codes in hardware often requires a different hardware design for each code. The software decoder was written in ANSI C for portability. The decoding algorithms were written to provide the most efficient implementation possible. The decoder has been tested on many platforms and

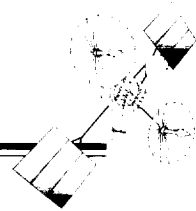
operating systems, and is currently available as a software library module.

The software Reed-Solomon decoder has been used for a number of projects, either as part of a custom application, or as a library routine integrated with a user's application. It was an important part of the software telemetry processing system used for the Portable Tracking and Data Relay Satellite System Communicator (formerly known as the Global Learning Observations to Benefit the Environment) project. The decoder for this project ran on both a Sun workstation running UNIX, and on a laptop PC running DOS. The software Reed-Solomon decoder was easily integrated with the Test Systems Branch's Programmable Telemetry Processor, which runs on a PC using OS/2-Warp. It has also been chosen to perform the frame header Reed-Solomon decoding for Landsat-7, running on an SGI machine using IRIX.

Contact: Steve Duran (Code 514.2)  
301-286-9262  
Internet: Steve.G.Duran.1@gsfc.nasa.gov

Sponsor: Office of Space Communications

*Mr. Duran received a B.S. in computer engineering from the University of New Mexico in Albuquerque in 1994. He is currently working towards an M.S. in Electrical Engineering, with an emphasis in Signal Processing, at the Johns Hopkins University in Baltimore, MD. Mr. Duran works full time at GSFC in the Data Processing Systems Branch, developing and building prototypes of the latest in telemetry processing software applications. His interests include neural networks, image processing, pattern recognition, error control coding, and space telemetry processing.*



## SOFTWARE TELEMETRY PROCESSING ON LOW-COST WORKSTATIONS AND PERSONAL COMPUTERS

OVER THE PAST YEAR, satellite telemetry processing software has been developed for use as a low-cost alternative to traditional hardware approaches. The software approach is perfect for low-to-medium-data-rate missions since, in the past, low-to-medium-data-rate missions had to absorb the high cost of the high-data rate hardware, the only implementation then available. Now, the only hardware needed is a commercial-off-the-shelf (COTS) low-end workstation or PC and a COTS serial input/output (I/O) card. Together, these components comprise the I/O system, the data processing system, and the status/control system. There are two primary forms of data I/O. The first is a programmable, high-speed serial card, and the second is through a network (either Ethernet or FDDI), using TCP/IP sockets for data transport. The data processing and status/control systems are built upon a number of software building blocks.

For I/O, the serial card can capture binary data or NASA Communications (NASCOM) block-formatted data, write the data to disk to back up the raw data, and then send the data to other processing routines for further processing using network-standard TCP/IP sockets. This allows processing to be distributed among remote machines on the network in addition to the local machine. Data from a file or a network connection can also be transmitted from the serial card, either as binary data or as NASCOM blocks.

The main components of the data processing system are the frame synchronizer (FS) and the Reed-Solomon Decoder (RSD; described elsewhere in this volume). Both units have traditionally been hardware components, but in this system they are both implemented in software. Both the FS and RSD are available as software libraries, allowing a user to easily develop a system using the telemetry processing functions. Both units are capable of processing data following the space data standard format as set forth in the Consultative Committee for Space Data Standards (CCSDS) Blue Books. In addition, both modules can also process non-CCSDS type data, with little or no modification to the core software libraries.

The status/control system provides the user with control over the system through configuration files. It also supports a simple level of process automation, allowing the system to run partially autonomously, thereby eliminating the need for a human operator 24 hours a day. Cumulative

statistics are maintained by each processing unit, are reported in real-time to the main control screen, and are logged to a file.

The current system and parts of it have been used for a number of projects. The entire system was used for the Portable Tracking and Data Relay Satellite System Communicator (formerly known as the Global Learning Observations to Benefit the Environment) project. This project allows students and/or scientists to transmit and receive data anywhere in the world via NASA's Tracking and Data Relay Satellite System. The telemetry processing software runs on low-cost workstations at GSFC and on laptop PCs in remote locations. Another system was configured to capture and process real-time Extreme Ultraviolet Explorer data. A standalone frame synchronizer application is being used for the Advanced Composition Explorer ground data system, described elsewhere in this volume.

Clearly, a software telemetry processing system has many advantages over the traditional hardware approach for lower-data-rate missions. It is economical, easily maintainable, and flexible. Also, users can continue to use the workstation or PC for other work, even during data flow activities.

Contact: Steve Duran (Code 514.2)  
301-286-9262  
Internet: Steve.G.Duran.1@gsfc.nasa.gov

Thomas Grubb (Code 514.3)  
301-286-8594  
Internet: Thomas.G.Grubb.1@gsfc.nasa.gov

Sponsor: Office of Space Communications

*Mr. Duran received a B.S. in computer engineering from the University of New Mexico in Albuquerque in 1994. He is currently working towards an M.S. in Electrical Engineering, with an emphasis in Signal Processing, at the Johns Hopkins University in Baltimore, MD. Mr. Duran works full time at GSFC in the Data Processing Systems Branch, developing and building prototypes of the latest in telemetry processing software applications. His interests include neural networks, image processing, pattern recognition, error control coding, and space telemetry processing.*

## MISSION OPERATIONS AND DATA SYSTEMS

---

*Mr. Grubb is a computer engineer currently working on the Landsat-7 mission. Mr. Grubb earned an M.S. in Computer Science from Johns Hopkins University. He has been at GSFC for 7 years, where he works in the Data Processing*

*Systems Branch. Previously, he developed software for the Upper Atmosphere Research Satellite, the International Solar/Terrestrial Project, the Cosmic Background Explorer Satellite, and other projects.*

## DATA PROCESSING AND ANALYSIS

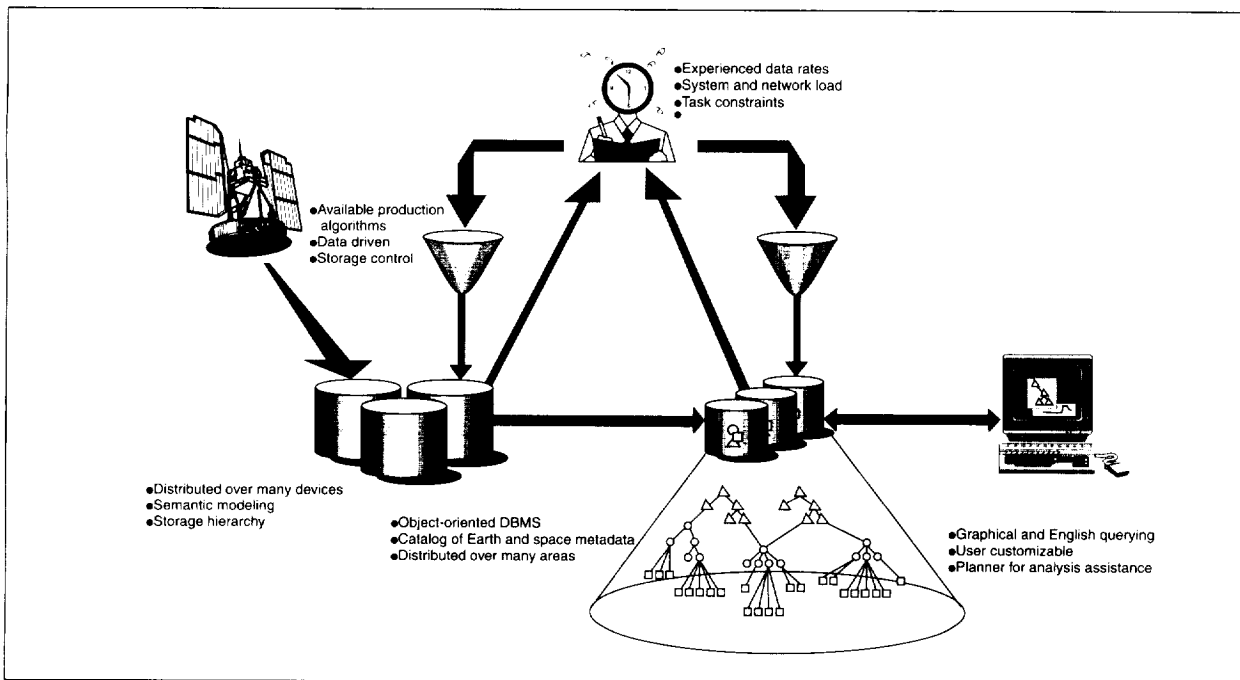
### END-TO-END GROUND-BASED PROCESSING OF SATELLITE DATA

**I**N THE LATE 1990's, NASA will launch a series of satellites to study the Earth as a dynamic system. The information system required to manage data from these satellites will be one of the world's largest, requiring an ingest, storage, and distribution capacity far in excess of any data holdings known today. The enormous size of the data holdings and the complexity of the information system pose several challenges to computer scientists, who must apply advanced techniques from software engineering, artificial intelligence, computer graphics, and signal processing if there is to be any practical chance of success.

For a number of years, researchers in the Information Sciences and Technology Branch have strived to build a fully automated computer system that enables unsophisticated users to access up-to-date satellite imagery. For the first time ever, in 1995 the Branch completed an end-to-end implementation of an Intelligent Information Fusion System (IIFS), which automatically acquires and archives direct broadcast Advanced Very High Resolution Radiometer data from NOAA-9 and NOAA-14 satellites, permitting general users to access these data using a variety of search criteria.

As a prototype system, the IIFS serves as a testbed for computer scientists to learn about the complexities of designing robust scientific information management systems. To enable easy search of large data holdings, the IIFS uses novel methods for extracting image content from the data, specialized data structures for storing data acquired from all over the world, and object-oriented representations to express the complex interrelationships pervasive throughout the scientific domains. These advanced techniques are transparent to the users, yet allow for fast and easy access to data to meet users' needs.

As shown in the figure, the IIFS modules are used to perform two functions: archiving and retrieving. When new data arrives, a unique ID is assigned to each meaningful granule (in most instances, this is a scene or "snapshot" from an instrument). This ID permits the planner to communicate additional metadata about a scene as it becomes available asynchronously. Meanwhile, the object database instantiates a new entity, and fills in its structure with basic information such as spatial location and platform/sensor/channel—information that is readily available from header files associated with the data. Depending on the type of data, scientific data requirements,



*The Intelligent Information Fusion System components.*

## MISSION OPERATIONS AND DATA SYSTEMS

---

popularity of the data set and related products, and available resources, the planner may spawn a number of processes to derive additional information from the data, such as performing special calibrations or running standard analyses (e.g., land use/land cover percentages, cloud type). The object database is updated as this additional information becomes available or demand for particular products increases.

In the retrieval role, the object database communicates what it knows to the user interface module so that the user can always query the system about available holdings. Thus, when the object database learns of a new platform and its instruments, all future user interface connections automatically display the availability of that data type. The satisfaction of a user's query may be done directly by the object database, as in the case of "Which Landsat Thematic Mapper scenes exist for May 1995 that include the Chesapeake Bay?" Other queries, however, cause the object database to invoke the planner module, as in a request for a vegetation index for some study area at a specific time. The object database, after locating an appropriate complete scene containing the user's region, would need to invoke the planner to have a vegetation index algorithm performed on the specific study area. Satisfaction of such a request may require multiple steps by the planner: allocate a machine for the task, isolate the region, compute the algorithm, place the resulting file in an appropriate location so that the user interface can retrieve it, and inform the object database of the status and availability of the result. The object database can then relay the result to the user interface, where the file can then be retrieved and displayed automatically. Thus, the IIFS runs in both a data- and demand-driven mode.

In the near future, an on-line tutorial on remote sensing will be made available in the hope that interested people in general—not just scientists—can use the system to acquire data and, in return, furnish photo-interpretations that the IIFS can use to hone its classification skills.

A number of users from both the scientific and educational communities will evaluate the IIFS. The feedback garnered from these sessions will permit examination of the effectiveness of the user interface, the overall system response time, and the applicability of the data holdings.

Contact: Robert Crompt (Code 935)  
301-286-4351

Nicholas Short, Jr. (Code 935)  
301-286-6604

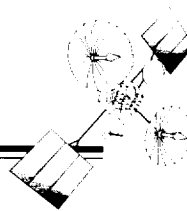
William Campbell (Code 935)  
301-286-8785

Sponsor: Office of Space Access and Technology

*Dr. Crompt is Principal Investigator on the Office of Space Access and Technology-sponsored Archive and Retrieval for Mission to Planet Earth project. He received a Ph.D. in Computer Science, concentrating in artificial intelligence, from Arizona State University in 1988. For the 7 years he has been at GSFC, he has developed numerous systems to help scientists and users more easily find data which fits their needs.*

*Mr. Short is Co-Principal Investigator to the Archive and Retrieval activity for the Mission to Planet Earth project. He received an M.E. in Computer Science from the University of Pennsylvania in 1989, and has been at GSFC for 8 years. His main interests are in the use of intelligent planning and scheduling agents for efficiently managing large data rates and volumes.*

*Mr. Campbell is Head of the Information Sciences and Technology Branch, and serves as Principal Investigator on an Earth Observing System Data and Information System (EOSDIS) NASA Research Announcement (NRA) related to this work. He holds an M.S. in Physical Geography from Southern Illinois University and is pursuing advanced studies in oenology. He has been at GSFC since 1978.*

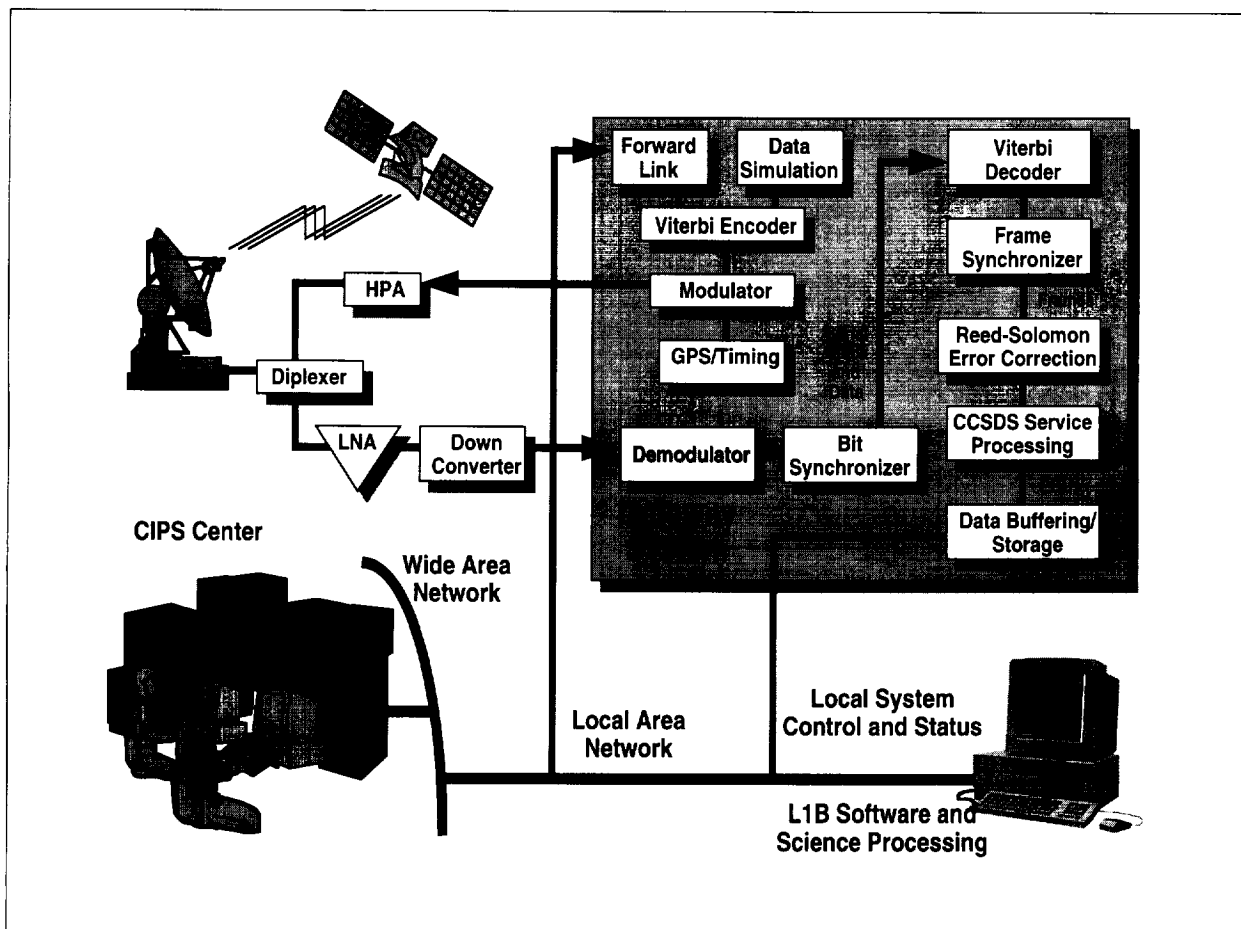


## REAL-TIME DATA PROCESSING OF SPACECRAFT AND INSTRUMENT TELEMETRY

OVER THE LAST 2 YEARS, spacecraft mission operations, telemetry processing, archiving, and distribution have all become, operationally, very closely related due to a reduction in mission size, near real-time data availability requirements, and increasing sophistication of the spacecraft. More than ever, these requirements are bringing the scientist back into the loop, allowing greater flexibility and control in scientific observation.

In order to address these demands, the Microelectronics and Systems Branch and the Information Science and Technology Branch have integrated two technologies: the Macintosh Telemetry and Command System (MacTAC) and Constraint-Based Intelligent Planners and Schedulers (CIPS). The combination of these two technologies provides an exceptionally efficient soft- and hard-resource

management mechanism. What makes this possible are the highly programmable MacTAC very large-scale integration (VLSI) chips that handle frame synchronization, Reed-Solomon error correction, packet processing (such as for Consultative Committee for Space Data Systems (CCSDS) format), and a forward-link chip for high-speed data transfer to hard disk, as shown in the first figure. All these functions can be tailored for any mission data encoding and packetization in near real-time by CIPS. The implementation of CIPS depends on particular science requirements. If the science data products are well-defined in the form of a simple data flow diagram, then a scheduler that minimizes resources according to a set of user-defined deadlines is used. If the products are not well-defined, then a planner/scheduler can be used to dynamically create the data flow graphs to



*Integrated MacTAC/CIPS.*

## MISSION OPERATIONS AND DATA SYSTEMS

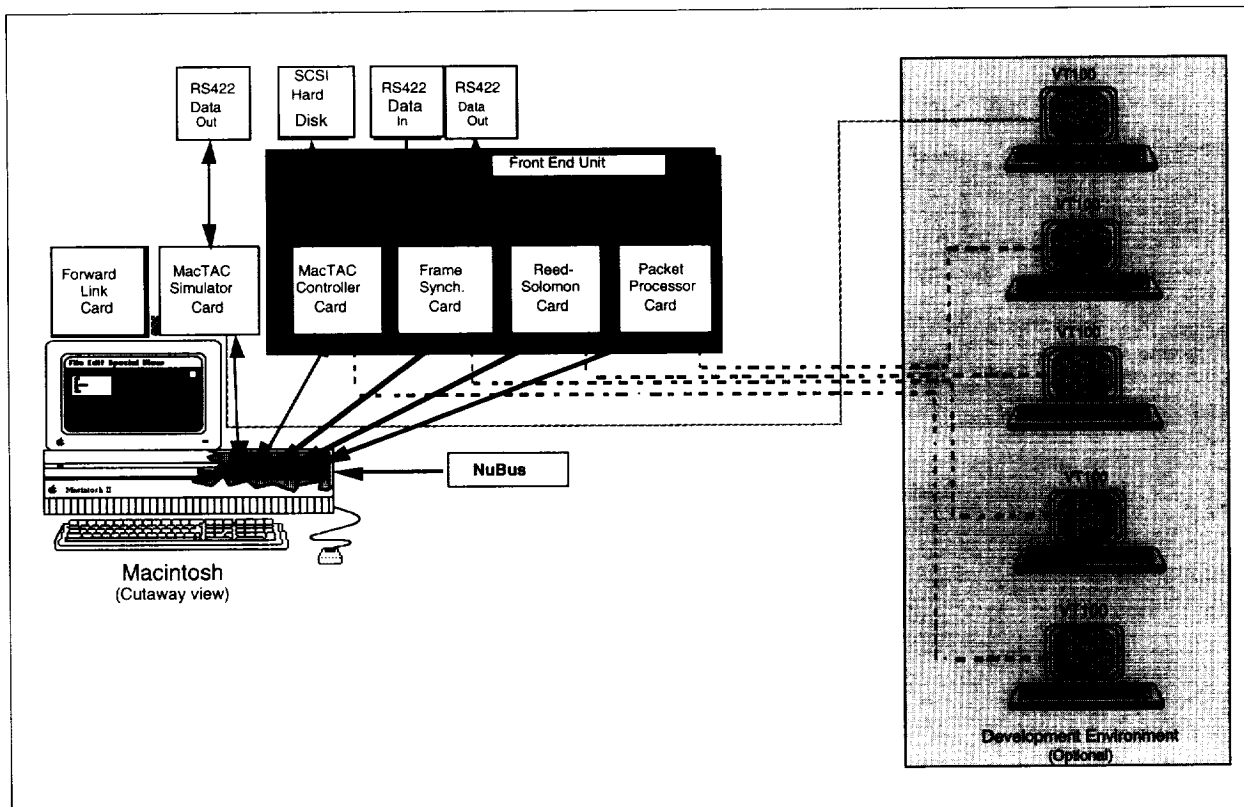
meet particular deadlines and resource requirements. If the data products are still being formulated, then a planner can be used to send data flow graphs to a visual programming environment called Khoros, wherein the scientists can test and modify the algorithms.

MacTAC is being used as an inexpensive solution based on VLSI component technology. Using the CCSDS international standard for space telecommunication, MacTAC can process Reed-Solomon encoded frames at roughly 13 Mbps. After the frame synchronizer accepts CCSDS frames in the form of RS422 data, it changes the incoming serial stream into a parallel output stream. In a full system, the Reed-Solomon error detection and correction cards work much the same way as a CD player, by correcting errors found in the data stream. The frames can be passed to the packet processor card for extracting packets stored in the frames. Software then handles the reordering of the packets into a usable stream, which can be sent to an image processing system for science data processing, as

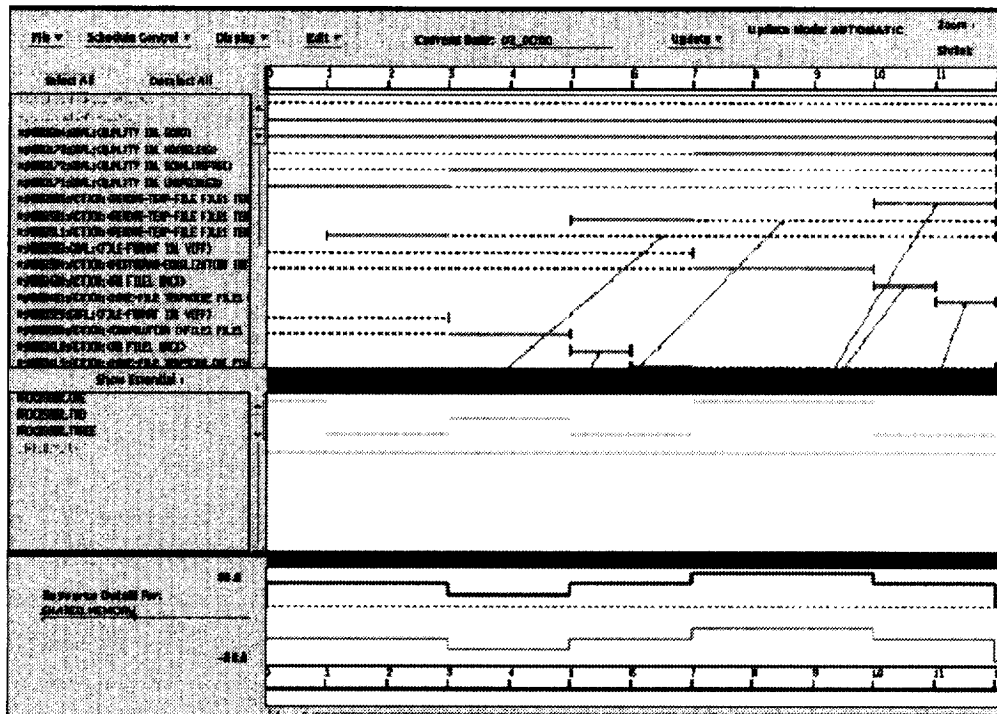
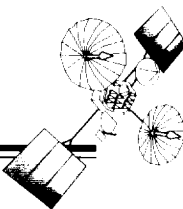
shown in the second figure.

Since the MacTAC ingest system will provide higher data volumes from higher data rates, efficient management of computational resources and numerous events will become an issue if operators are going to manage real-time data. In particular, many existing product generation tasks will be coordinated to keep both the operators and the computers from being overwhelmed. Hence, CIPS is being used to manage all events (both internal and external) to remove many of the logistical burdens on the operators, and to ensure that adequate computer resources can be applied to data production and monitoring.

Currently, we are integrating the Honeywell Task and Resource Scheduler (HTRS) as shown in the third figure. HTRS is an application of the Kronos scheduling engine that was designed to be adaptive and dynamic; it has been successfully applied to domains such as space shuttle mission scheduling, demand flow manufacturing, and avi-



MacTAC Ingest System.



*Honeywell Task and Resource Scheduler*

onics communications scheduling. It has handled scheduling problems involving 20,000 tasks and 140,000 constraints, with interactive response times for schedule modification on the order of a few seconds on a SPARC10 workstation.

In addition to providing a direct real-time science interface to the instrument, CIPS and MacTAC ingest, in parallel, all state-of-health telemetry from both the sensor and spacecraft. CIPS then autonomously monitors power levels, spacecraft attitude, thermal levels, and communications, making sure that all systems are operating nominally. In the case of emergencies or malfunctions, CIPS and MacTAC are able to provide a solution and/or visually show the operator—in flow diagram form—the problem and possible system reconfiguration solutions, since CIPS is able access several databases containing spacecraft and sensor specifications and design parameters.

The integration of these two powerful systems has enabled very efficient monitoring and troubleshooting.

capabilities for both instruments and spacecraft in real-time, given complete information on the systems in question.

Contact: Patrick Coronado (Code 935)  
301-286-9323  
Internet: cwifs@suzieq.gsfc.nasa.gov

Nicholas Short, Jr. (Code 935)  
301-286-6604  
Internet: short@danville.gsfc.nasa.gov

Sponsor: Office of Mission to Planet Earth

*Mr. Coronado is the Ground Systems Manager of the Sea-viewing Wide Field of View Sensor (SeaWiFS) project. He is a senior engineer responsible for the design and implementation of nine NASA remote sensing ground systems worldwide.*

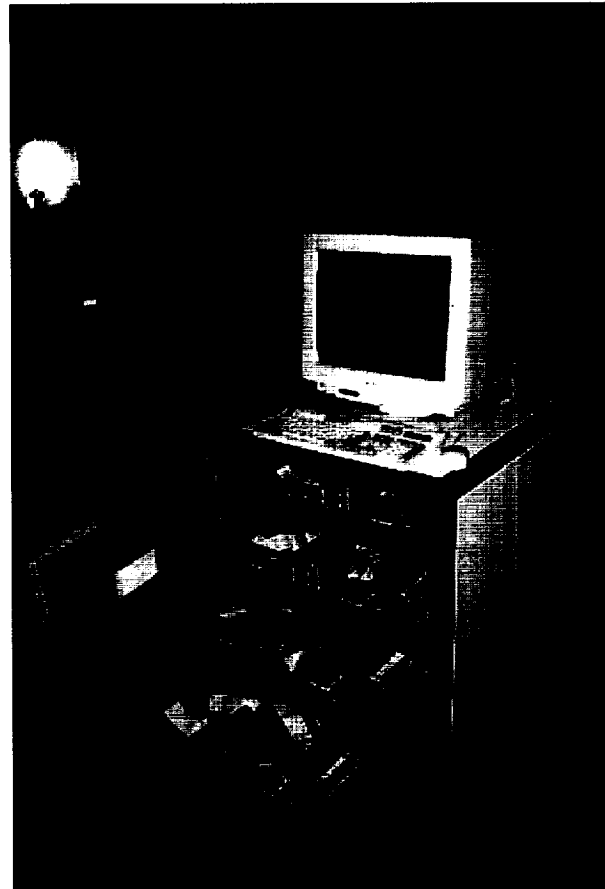
*Mr. Short is the Senior Developer of artificially intelligent systems, including CIPS. He also heads the development of MacTAC and spacecraft planning and scheduling.*

### THE BEOWULF PARALLEL WORKSTATION DELIVERS NEW CAPABILITIES FOR EARTH AND SPACE SCIENCES APPLICATIONS

THE COMPUTATIONAL requirements of applications in the Earth and space sciences (ESS) stress the performance capabilities of high-performance computers, from the largest supercomputers to desktop workstations used for scientific visualization. The NASA High-Performance Computing and Communications (HPCC) program and its ESS project at GSFC are directly involved in advancing the state-of-the-art at both ends of the spectrum in support of NASA mission-driven computing demands. A significant contribution by this program is being made in the area of scientific workstations. The exploitation of parallelism and commodity computing subsystems is yielding a tool for scientific exploration that greatly extends the capabilities of single-user workstations at a cost no greater than that of conventional systems in use today.

The Beowulf Parallel Workstation project was organized to respond to the requirements of the NASA HPCC ESS project for a GOPS (1 billion operations per second) workstation by integrating readily available hardware and software subsystems, available largely from the ranks of commodity-level PCs. With this approach, Beowulf (shown in the figure) has demonstrated capabilities between 4 and 10 times greater than those available with conventional high-end scientific workstations, but at lower cost.

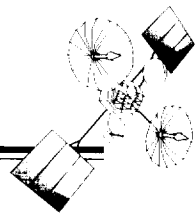
The development of a new generation of scientific workstations is a product of the advances in commodity computing capabilities and the emergence of sophisticated and open operating systems for PC-class microprocessors. Personal computers now incorporate microprocessor, memory, and communications technologies that rival those found in scientific workstations, such that high-end PCs now outperform low-end workstations at a fraction of the cost. This is due largely to economy of scale, as 10 to 100 times more PCs are manufactured annually than workstations. At the same time, a version of the widely used UNIX operating system, Linux, has been developed by a worldwide consortium of computer scientists for the dominant microprocessor architecture family (Intel x86). Linux is available with full source code at no cost via the Internet. As all workstations employ some version of UNIX, and Linux is fully compliant with community-established UNIX standards, a workstation-grade software environment is now available for PC-based systems. The final component that is helping to realize



*The Beowulf Parallel Workstation.*

new capabilities in scientific workstations is parallelism, the balanced integration of multiple subsystems to multiply their respective qualities in a mutually supporting environment.

Large science applications for scientific workstations (such as those found in the ESS community) exhibit workload characteristics that can significantly benefit from the Beowulf model. In particular, these problems often involve very large data sets that are repeatedly examined, visualized, and manipulated. These data sets are too large to fit into main memory, and often too large to fit within the capacity of the disks commonly found on conventional workstations. Often, remote, shared file servers are employed through a shared local area network, resulting in long latency and response times to the user and



contention for resources by all users of the system. Beowulf dramatically alters the operating point of this aspect of mass storage computing by taking advantage of the availability of low-cost commodity disks to provide more than 10 times the disk capacity ordinarily supplied, to stage the large data sets being studied directly on the scientific workstation.

Mass storage capacity would be of limited value if suitable scaling of bandwidth to access main memory was not implemented. Since the mechanical speed of the disk is the principal factor constraining performance, commodity processors can be employed in parallel to deliver many times the disk-to-memory throughput found on conventional workstations. Beowulf addresses this by providing a processor subsystem for each disk. The prototype incorporates 16 Intel 80486/DX-4 processors (100 MHz clock) subsystems and 16 520-MB IDE disk drives. Similarly, the Beowulf demonstration system uses Intel Pentium processors (100 MHz clock) and 1.2 GB IDE disk drives, for a total of almost 20 GB of secondary storage.

While parallelism is successfully used to address increased capacity and performance, additional problems arise as a result; the separate subsystems must be able to interact in a coordinated manner as a single aggregate system, which requires adequate internal communications bandwidth. In the case of the Beowulf commodity-based architecture model, such interconnection must be achieved by means of commodity networking. The most cost-effective industry standard is Ethernet, which provides a peak 10 Mbps (million bits per second) throughput. Experiments conducted by the Beowulf project have shown that sustained throughput of 1 MB per second can be achieved. Additional tests have demonstrated average file transfer rates of 18 MB per second when performing separate local file transfers on all 16 processor-disk pairs simultaneously. However, as the file transfers are nonlocal (i.e., between processors), the apparent file transfer rate would be severely constrained by inadequate internal network bandwidth. Beowulf addresses this challenge in three ways, each exploiting readily available commodity networking subsystems.

The Beowulf project has devised a method for exploiting multiple Ethernet networks to increase the internal interprocessor bandwidth over that available from a single

Ethernet network. The project has developed "channel bonding" enhancements to the operating system, and demonstrated scaled communication throughput by successfully harnessing two and three networks together. This required changes to the Linux operating system kernel, but has resulted in a technology that delivers significant increase in sustainable throughput over a single Ethernet channel, while remaining completely transparent to the applications programmer. Experiments have demonstrated that a sustained throughput of 2.5 MB per second can be realized using three parallel Ethernet channels, although this is sensitive to message packet size.

The second approach to the global file transfer problem exploits new technology. The Beowulf demonstration system incorporates "Fast Ethernet" technology, only now emerging on the commodity market. While somewhat more expensive than its predecessor, Fast Ethernet has a peak capacity of 100 Mbps, 10 times that of basic Ethernet. Tests have demonstrated point-to-point sustained throughput of 4.5 MB per second. Using the channel bonding techniques, two Fast Ethernets operating in parallel provide sufficient internal interconnect bandwidth to support the maximum parallel disk access traffic that can be generated by the ensemble of Beowulf disks. This is an important contribution of the Beowulf project, and software developed to achieve this is already being adopted by other organizations.

A third approach to addressing the challenge of achieving high internal interconnect bandwidth is being studied by the Beowulf project. It exploits opportunities in network topologies permitted within the constraints of available subsystems. It has been shown that, by network segmentation using off-the-shelf active switches, throughput of dual channels can be increased by a factor of four across the system. This is the range of improvement required to remove the network as the bottleneck for file transfers under most operational circumstances using 10 Mbps Ethernet. An important side-effect of this work, if successful, is in the area of packaging. A Beowulf parallel workstation could be assembled in less than one quarter of the volume of the current prototype system through the use of laptop PC subsystems. However, these use new, high-density PCMCIA Ethernet control cards, which are not yet available for Fast Ethernet. Being able to multiply the effective operational bandwidth of basic Ethernet would allow these potentially highly compact

## MISSION OPERATIONS AND DATA SYSTEMS

---

Beowulf systems to meet internal communications needs in support of global file transfer rates.

While much of the workload for a scientific workstation is at the job stream level, with many independent tasks being performed simultaneously, some applications require the full capability of the workstation. Beowulf therefore must be able to exploit parallel computing resources as such. Message passing libraries—including PVM and MPI—have been successfully ported to Beowulf. Also, the Condor distributed scheduling package has been ported to Beowulf, and is now operational. These provide the logical framework for programming and managing parallel scientific applications to take advantage of the full power of the parallel resources incorporated in Beowulf.

For example, ESS parallel codes using message-passing techniques for synchronization and data transfers have been ported to Beowulf. Among these are a gravitational N-body simulation application using a “tree code,” and a computational fluid dynamics program for astrophysics applications, using a fixed regular grid Euler solver. Both application programs demonstrated good scaling characteristics and were shown to be performance-competitive with the Intel Paragon and TMC CM-5, which are of comparable size. Additional applications in visualization, data management, and data assimilation are being developed. As a consequence, Beowulf is now being considered as a platform for NASA applications beyond the HPCC program. This high-performance, low-cost approach is also being evaluated as the basis for terabyte-scale mass storage servers.

Contact: John Dorband (Code 934)  
301-286-9419

Thomas Sterling (USRA)  
301-286-2757

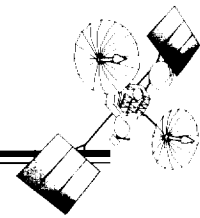
Donald Becker (USRA)  
301-286-0882

Sponsor: Office of Aeronautics

*Dr. Dorband received his Ph.D. in Computer Science in 1985 from the Pennsylvania State University. He did his thesis work under a grant from NASA to apply SIMD computation to image processing of astronomical images on the Goodyear Massively Parallel Processor (MPP). Since then, he has directed the MPP research effort at GSFC. This includes collaborations with the University of Maryland and Microelectronics Center of North Carolina to develop SIMD processor chips ranging from 64 to 128 processors per chip, and development of the efficient implementations of image rotation/registration, neural networks, adaptively refined unstructured grid CFD, gravitational N-body tree codes, and many other algorithms for parallel computers. Current efforts include the understanding and formulation of an architecture-independent programming style, paradigm, and language.*

*Dr. Sterling is a senior scientist and Branch Head of the Scalable Systems Technology Branch at the Center of Excellence in Space Data and Information Sciences (CESDIS) housed at GSFC. Dr. Sterling earned his Ph.D. in Electrical Engineering from the Massachusetts Institute of Technology. Dr. Sterling has been at CESDIS for 3 years working with the High Performance Computing Branch working on parallel system architecture, hardware, and software, with emphasis on issues of efficiency, scalability, and programming.*

*Mr. Becker is a staff scientist with the USRA Center of Excellence in Space Data and Information Sciences. He received his B.S. in Electrical Engineering from the Massachusetts Institution of Technology in 1987 and was on the research staff at Harris Corporation and the IDA Supercomputing Research Center prior to joining USRA in 1994. Mr. Becker has earned a worldwide reputation as one of the principal designers of networking software for the Linux operating system and is the principal scientist in system software for the Beowulf Parallel Workstation project as part of the NASA HPCC program.*



## SIGNAL PROCESSING WORKSTATION SIMULATION OF THE LANDSAT-7 X-BAND DOWNLINK

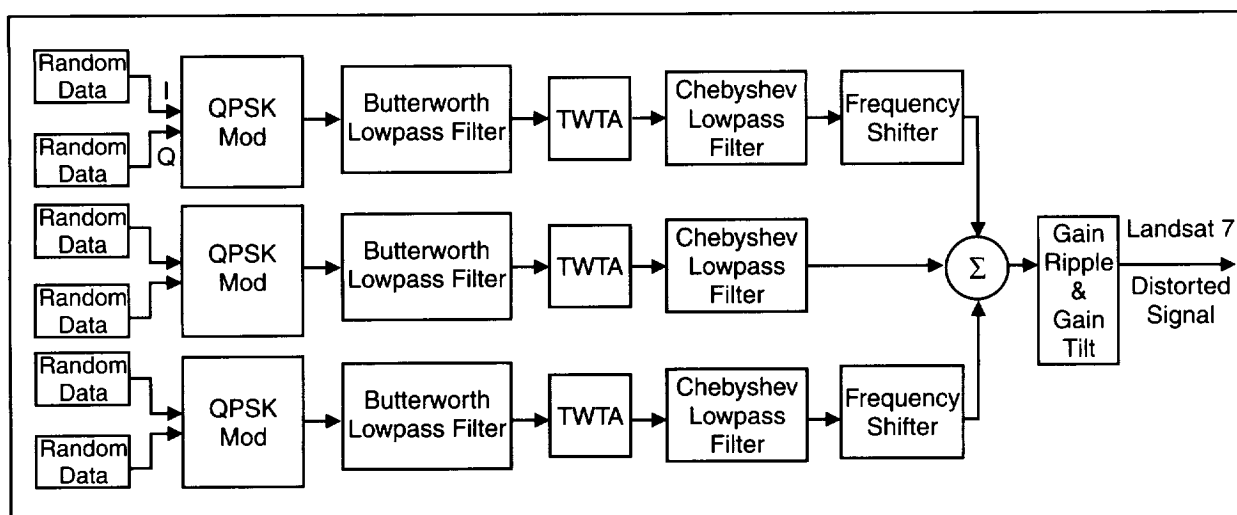
THE COMMUNICATIONS LINK Analysis and Simulation System (CLASS) project is made up of a group of dedicated and highly skilled communications and software engineers who provide systems analysis and support services for space missions and NASA's space and ground networks. CLASS recently added the Signal Processing Workstation (SPW) analysis tool to the existing suite of tools that assess the communications performance of NASA missions.

SPW is a time domain simulator that can be used to simulate, test, and analyze communication and digital signal processing systems. It is a state-of-the-art design and analysis tool that is gaining widespread acceptance and popularity as advances in computer memory and processing speed make time domain simulations feasible even for large systems. SPW contains a graphical block diagram editor and extensive block libraries that enable system designers and analysts to quickly construct a system model and assess its performance in terms of bit error rate (BER), signal acquisition and tracking, etc. In addition to measuring system performance, any signal at any point in the system can be measured in the time or frequency domain, or in a scatter plot, eye diagram, or histogram format. Simulations with SPW can provide significant cost and time savings when compared to building expensive engineering test models.

CLASS personnel recently used SPW to model the Landsat-7 X-band downlink. The first figure shows the current Landsat-7 design model, which consists of three identical 150 Mbps quadrature phase shift key (QPSK) channels separated by 130 MHz. All three channels are distorted with gain imbalance and phase imbalance in the QPSK modulator, rise and fall times in the second-order lowpass Butterworth filter, and amplitude modulation (AM)/AM and AM/Phase Modulation in the traveling wave tube amplifier. All three channels are filtered with either a 4-pole Chebychev Type 1 filter or a 6-pole elliptic filter. For simplicity, only the Chebychev filters are shown in the figure. The combined channel is distorted by a gain ripple and gain tilt filter.

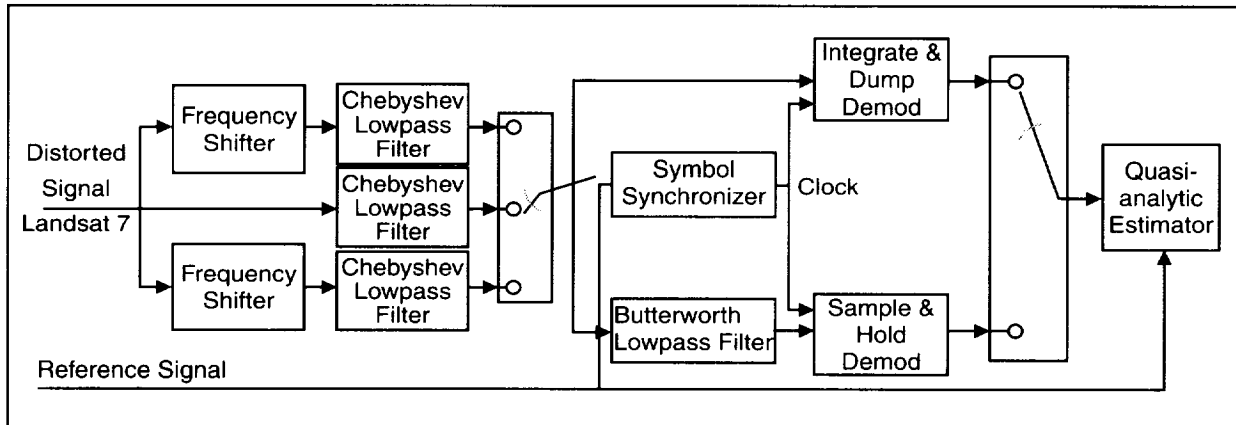
As shown in the second figure, the ground station separates the three received channels and filters them with the same filters as in the Landsat-7 model. The receiver selects one of the channels and detects the signal with either an integrate-and-dump detector, or a Butterworth filter followed by a sample-and-hold filter. The simulation assumes ideal symbol synchronization, ideal carrier tracking, and zero receiver losses, although the model could be modified to account for symbol synchronization, carrier tracking errors, and receiver losses.

The BER is estimated in the presence of interference from the other two channels, as well as hardware distortions.



Landsat-7 X-band direct downlink channel model.

## MISSION OPERATIONS AND DATA SYSTEMS



Ground Station channel model.

The BER could have been estimated using a pure Monte Carlo simulation, which involves modeling the system and the noise and counting errors to determine the BER. This can be very time consuming since a large number of bits must be generated to evaluate very low BER performance. Instead, the analysis was performed using a quasi-analytic approach, since a quasi-analytic simulation is much faster than a Monte Carlo simulation. The quasi-analytic approach involves simulating the system without noise added, measuring the received signal, and calculating the effects of the noise. A BER curve as a function of Bit Energy/Noise Density ( $E_b/N_0$ ) is obtained in only 10 minutes with the quasi-analytic method, rather than nearly 24 hours required with the Monte Carlo method.

The CLASS group required less than 2 months to model the Landsat-7 downlink (including all hardware distortions), and to perform the simulations. CLASS analysts determined the degradation due to interference and hardware distortions will be about 2 decibels. As part of the remaining work on this task, CLASS analysts will assess methods of mitigating the interference and distortions with equalizers in the ground station receiver. Changes to the system design can be quickly and easily assessed because SPW provides a friendly graphical user interface, and each run can be simulated in such a short time. The results will be used by the Landsat Project as a basis for evaluating proposals for the ground station elements.

Contact: Badri Younes (Code 531.1)  
301-286-5089

Armen Caroglanian (Code 531.2)  
301-286-4340

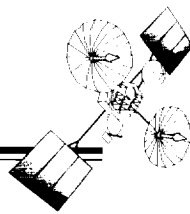
Linda Harrel (STel)  
301-464-8900

Sponsor: Landsat Project

*Mr. Younes completed 2 years of scientific studies (Math and Physics) at the University of Grenoble, France in 1980. He received his B.S.E.E. and M.S.E.E. from The Catholic University of America in 1984 and 1988, respectively. Mr. Younes joined NASA in 1990 to work on the STGT project, where he later became the hardware systems manager. Mr. Younes is currently the CLASS Project Manager.*

*Mr. Caroglanian received his B.S.E.E. and M.S.E.E. from the University of Maryland, College Park, in 1985 and 1989, respectively. In 1985, he joined the RF Systems Section of the Networks Division at GSFC. Mr. Caroglanian is responsible for development of the RF Systems Section's antenna design and analysis modeling tools. He is currently the LGS Project Manager.*

*Ms. Harrell received an M.S.E.E. in Communications from the George Washington University in 1990, and is currently employed by Stanford Telecommunications, Inc. Her experience includes receiver hardware system design, modeling, simulation, test, frequency interference, and vulnerability analysis. Ms. Harrell has been supporting the CLASS and Space Network System Engineering projects for more than 5 years.*



## LANDSAT-7 RAW DATA CAPTURE

THE LANDSAT-7 satellite will be launched in mid-1998 to provide a global, seasonal archive of land images for a multitude of scientific, commercial, and defense purposes. The satellite will transmit the image data directly to a receiving antenna at the Earth Resources Observation System Data Center (EDC) located in Sioux Falls, SD. At EDC, the incoming data will be recorded and processed to produce high-resolution images of the Earth's surface using a system composed of highly advanced technologies.

The Landsat-7 satellite will move around the Earth in a polar orbit. This orbital configuration results in the satellite being able to acquire images of any area on the surface of the Earth. A compromise associated with this orbit is that the satellite will only be in view of the receiving antenna at EDC six times a day, with a maximum contact duration of 14 minutes for each of the six passes.

During each of the passes over EDC, the satellite will transmit the image data to the receiving antenna, where it will be routed through specialized equipment and then to the Landsat-7 processing system. Typically, all data are transmitted from the satellite to the EDC using four channels (two for transmitting the satellite's current view, and two for transmitting what the satellite recorded while it was out of range of EDC). Each channel is a separate path for the data to get from the satellite to the ground. Data sent on each of the channels are transmitted at a rate of 75 million bits per second. On the ground, all data are recorded for later processing of the image.

Traditionally, data from orbiting satellites are recorded using expensive, maintenance-intensive, high-speed tape drives. These tape drives can cost anywhere from \$100,000 to \$300,000 for each unit, and the tapes can cost more than \$100 each. The process of transferring data to and from any magnetic tape media can induce errors in the data. Most errors can be corrected through the use of complex error-correction algorithms, but if the tape is dirty or damaged, or if the tape drive is in need of maintenance, the data may be lost forever. Additionally, the magnetic heads that read the data from the tape must be kept clean, and require periodic replacement at a cost of approximately \$25,000 per head.

The system being developed by NASA for Landsat-7 will take advantage of state-of-the-art technology to record the image data. Just as the home PC has a hard disk drive to

store data, the Landsat-7 processing system will make use of a series of disk drives housed in a single rack-mounted assembly. The Landsat-7 data will be stored on eight disk drives in a parallel arrangement, which allows the data to be distributed, or striped, across all eight disk drives simultaneously. A ninth disk drive is used to store the results of a mathematical summation of the data stored on the eight drives. In the event of a failure on one of the eight disk drives, the system uses the data stored on the ninth drive to recreate the data that was stored on the malfunctioning drive. This capability increases the robustness of the system greatly and contributes to error-free data recording. This data capture technology is referred to as a redundant array of inexpensive devices (RAID) system. The system is maintenance-free, and can be purchased for approximately \$40,000. If one of the nine disk drives develops a problem, the replacement drive can be "hot swapped" without removing power from the unit. The cost for the replacement drive is substantially lower (~\$2000) than the corresponding magnetic head assembly for a high-speed tape drive. The results of the data processing are stored on a second RAID disk, which is used to stage the data prior to transferring it to a large data archive located at EDC, where users from around the world can access the image data. Once all of the recorded source data has been processed and its corresponding image data staged on the second RAID, the original unprocessed data is deleted from the first RAID to make room for the next pass.

The Landsat-7 processing system also takes advantage of another recent innovation in data recording technology. A digital linear tape drive is connected to the system to provide an archive function. These tape drives are low-cost units (\$6000), and can record the entire volume of data from a pass onto a single compact tape cartridge. The unit can record the data at approximately one-seventh the Landsat-7 data transfer rate, so it takes longer to transfer the data to the archive tape than it takes to record the data on the RAID. This step is necessary so that raw image data can be archived for up to 60 days to allow users to reprocess an image of the Earth at a later date. The processing system will record the data from a pass and begin processing the data as soon as the pass is complete. Since the data are stored on the RAID disks as a large data file, the data can be processed in ways that are normally difficult when data are recorded on tape. Programs written to process the millions of bits of information can access large

## MISSION OPERATIONS AND DATA SYSTEMS

---

pieces of the image data without having to wait for a tape to be rewound or moved forward to a particular position to get the required data. Unlike a tape drive, the RAID system allows the programs to read and write data simultaneously. Additionally, the errors that can be associated with the recovery of recorded data from a tape-based system are eliminated. The significant advantages associated with storing data on disk drives result in a dramatic increase in the processing throughput of the system, and allow the LPS to perform its data processing in time to prepare for the next transmission of data from the satellite.

These processes will occur every day throughout the life of the satellite, and will result in high-resolution images being made available to the scientific world with reduced error rates, improved efficiency, and with greatly reduced operational costs.

Contact: Clifford Brambora (Code 514.3)  
301-286-7001

Joy Henegar (Code 514.1)  
301-286-8415

Robert Schweiss (Code 514.3)  
301-286-1223

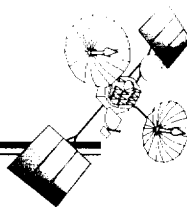
Sponsor: Office of Mission to Planet Earth

*Mr. Brambora is Hardware Manager for the Landsat-7 Processing System. Mr. Brambora earned a B.S.E.E. in Electrical Engineering from the New York Institute*

*of Technology in 1987. Mr. Brambora has been at GSFC for 5 years, where he has worked for the last year in the Data Processing Support Branch developing data processing systems. Prior to his work on the Landsat-7 project, Mr. Brambora was the Hardware Manager for the Spacelab Data Processing Facility at GSFC.*

*Ms. Henegar is the Project Manager for the Landsat-7 Processing System. She earned a B.S. in Computer Science from the University of Maryland, and an M.S. in Computer Science from the Johns Hopkins University. Ms. Henegar has been at GSFC for 8 years where she has worked for the Mission Operations and System Development Division, developing data processing systems. Prior to her work on the Landsat-7 project, she managed the software development of data processing systems supporting the Upper Atmosphere Research Satellite, the International Solar-Terrestrial Physics Program, the X-ray Timing Explorer satellite, and the Small Explorer program. Prior to joining NASA, Ms. Henegar spent 3 years with the National Weather Service.*

*Mr. Schweiss is the System Engineering Manager for the Landsat-7 Processing System. He earned a B.S. in Computer Science from the University of Maryland, and is nearing the completion of his masters degree from the George Washington University. Mr. Schweiss has been at GSFC for 5 years and has worked on the Landsat-7 project since January 1995. Prior to his work on Landsat-7, he was a software manager for the Spacelab Data Processing Facility.*



## EOSDIS VERSION 0 IMS INTERCONNECTS EXISTING EARTH SCIENCE DATA SYSTEMS

**S**CIENTISTS CAN SEARCH and access Earth science data held at archives across the U.S. through the Earth Observing System Data and Information System (EOSDIS), which is designed as a distributed system to support archiving and distribution of data stored at multiple sites. The sites (listed in the table) were selected by NASA to represent specific Earth science disciplines, and are known as Distributed Active Archive Centers (DAACs). In addition, Cooperating Data Centers (CDCs) are following EOSDIS standards in order to interoperate with EOSDIS. DAACs and CDCs are connected by an Information Management System (IMS), which provides an interface for single-point access ("one-stop-shopping") for Earth science data.

As a prototype of EOSDIS and as its first operational release, the Version 0 IMS was released in July 1995. This software package is a collaborative effort between representatives of the IMS team at GSFC and existing data center teams to take maximum advantage of existing Earth science data, information, and experience at DAACs and CDCs.

Heritage archives were developed independently, along lines of specific science disciplines. The Version 0 IMS

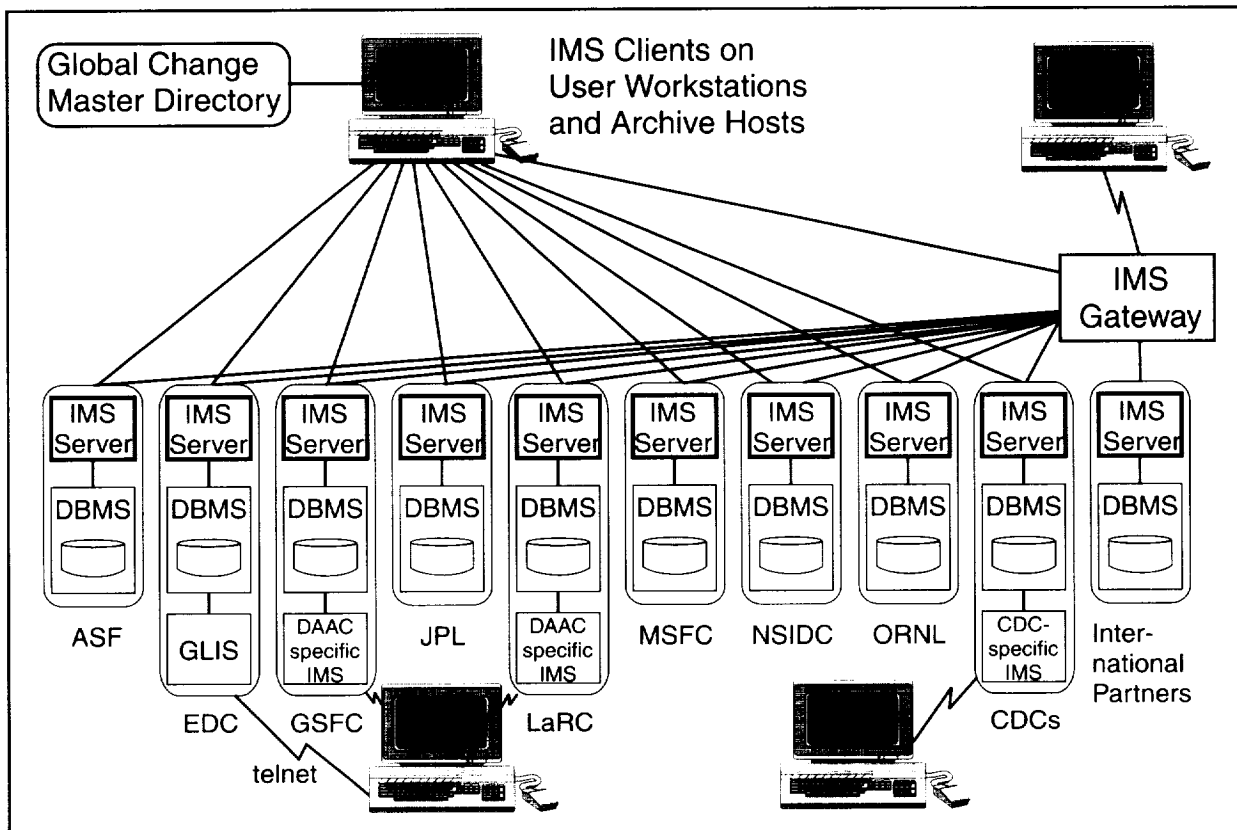
(V0) was developed to interoperate with heritage systems while maintaining the policy of noninterference with ongoing operations. This is accomplished through message passing and translation. The figure illustrates the overall system architecture, with configurations at each of the DAACs. The common thread among the archives is that each holds data described by metadata held in relational database management systems (RDBMSs). In order to provide common access to all archives simultaneously, a common layer of terminology and software was defined as the basis of the IMS client. Each DAAC developed an IMS server that translates between the common layer and their archive-specific layers. Because the implementation is generic, the IMS client can interact with any RDBMS package archive through an IMS server. An "IMS Server Cookbook" has been completed as a reference for new CDCs or for users who want to modify the client to search their own local databases in addition to the archives. While meeting the needs of multidisciplinary and interdisciplinary users through the EOSDIS IMS, DAACs and CDCs continue to meet their discipline-specific user's needs through interfaces to their local DAACs.

The IMS interface is available through graphical and character-based user interfaces and World Wide Web

*Distributed Active Archive Centers and their Disciplines*

DAAC Name	Discipline
Alaska SAR Facility	Synthetic Aperture Radar
EROS Data Center	Land Processes
Goddard Space Flight Center	Upper Atmosphere, Atmospheric Dynamics, Global Biosphere, and Geophysics
Jet Propulsion Laboratory	Ocean Circulation and Air-Sea Interaction
Langley Research Center	Radiation Budget, Aerosols, and Tropospheric Chemistry
Marshall Space Flight Center	Hydrologic Cycle
National Snow and Ice Data Center	non-SAR Cryosphere
Oak Ridge National Laboratory	Biogeochemical Dynamics
Socio-Economic Data and Applications Center	Socio-Economics

## MISSION OPERATIONS AND DATA SYSTEMS



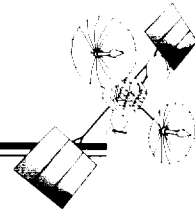
*EOSDIS IMS V0 client/server architecture.*

(WWW) browsers to accommodate a variety of user environments, ranging from simple VT100 terminals or personal computers (PCs) to sophisticated graphical UNIX Workstations. The character interface supports data search and order, and access to summary and detailed descriptive text and browse images via file transfer protocol (ftp). In addition to the functions offered through the character interface, the graphical interface and the WWW browser gateway allow geographic area selection from a map and an interactive data browse facility. The graphical interface also supports graphical coverage display.

Because of the evolutionary nature of prototyping, it was necessary to develop a modular architecture so that software could be added and deleted without affecting the remainder of the software and overall system functionality. This would allow for changes without the necessity of rewriting code. The main functionality was broken into three parts: the User Interface Manager, the Data Manager,

and the Network Manager. In the UIM there are two supported versions: an X-windows manager (a graphical user interface), and a JAM Manager (character user interface). The same Data Manager and Network Manager are used for both the graphical- and character-based user interface versions, and for the WWW browser gateway described below. In addition, a guide function that supports searching and hyperlinking of detailed text documents was implemented by integrating the Mosaic display widget and using Wide-Area Information Search indexing, hypertext mark-up language, and hypertext transport protocol.

A WWW gateway is being developed to provide access to the EOSDIS IMS through generic WWW browsers (e.g. Mosaic, Netscape), and was released as a working prototype in October 1995. Web access to V0 is designed to provide users with very simple and easy access to search for, locate, and order data. Because of limitations of



current WWW browser capabilities, some of the sophisticated interactive capabilities of the other interfaces are offered in a limited fashion, but this approach allows access to and use of the system by a wider community. The gateway provides a translation between the user's search criteria—as entered into forms from a WWW browser—to the V0 IMS. The WWW gateway accesses the existing V0 server infrastructure with no additional software development needed at the DAACs during this initial phase. If additional capabilities in the WWW gateway are developed beyond those that exist in the current V0 system, then additional software development will be needed for the V0 servers at the DAACs.

The EOSDIS Version 0 IMS team is experimenting with expansion to international communities through involvement in the Committee on Earth Observation Satellites Interoperability Experiment. This effort shows promise to provide access to Earth science data and information worldwide. Demonstrations of this functionality show that the V0 paradigm is extremely flexible and can be extended to incorporate a variety of archive structures through the gateway concepts. In FY 95, V0 servers were developed and installed in Germany, Italy, Japan, the UK, and Canada. Sites in additional countries are expected in

FY 96. Gateways from international, site-specific interfaces to the V0 system also have been developed to allow foreign access to EOS data.

The Version 0 EOSDIS system is available to the Earth science community, planners, educators, and managers for general operational use, and can be accessed [http://harp.gsfc.nasa.gov:1729/eosdis\\_documents/eosdis\\_home.html](http://harp.gsfc.nasa.gov:1729/eosdis_documents/eosdis_home.html). The prototype WWW gateway can be accessed via a WWW browser such as Netscape or Mosaic, and is available at <http://eos.nasa.gov/imswelcome>.

Contact: Robin Pfister (Code 505)  
(301) 286-1498

Sponsor: Office of Mission to Planet Earth

*Ms. Pfister currently serves as the IMS Information Engineer. She received her B.S. and M.S. degrees in Geoscience and Remote Sensing from Purdue University. She worked as a Geophysicist in the oil industry before moving to the GSFC contracting environment where she was involved in a variety of climate and Earth environment-related studies. She began working science issues in data systems with NASA's Pilot Land Data System in 1990 and began work with EOSDIS IMS in 1992.*

### GLOBE VISUALIZATION AND DATA ANALYSIS

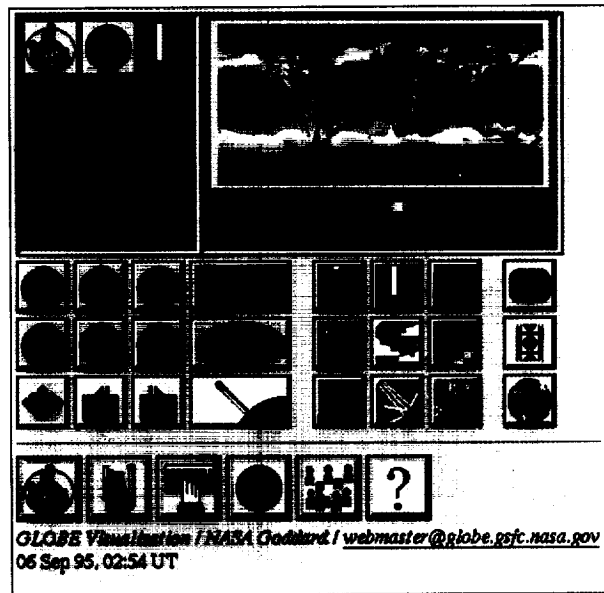
THE GLOBAL LEARNING and Observation to Benefit the Environment (GLOBE) project, under the leadership of Vice President Gore, is a collaborative effort of several government agencies, universities, foreign governments, and K-12 schools around the world, including nearly 2000 schools in the U.S. alone. In GLOBE, a worldwide network of students, teachers, and scientists works to study and understand the global environment. The GLOBE goals are to increase environmental awareness on the part of individuals throughout the world, and to contribute to a better scientific understanding of the Earth. The students' technical skills are advanced by learning to make precise scientific measurements at the school sites, and by using computers and the Internet to report their measurements to others in the network, and to analyze and understand their results.

The Scientific Applications and Visualization and the Mesoscale Atmospheric Processes Branches at GSFC have been collaborating to provide visualization and data analysis tools and products to GLOBE, including an innovative World Wide Web (WWW) interface to these products and tools. In collaboration with the curriculum developers and the Principal Investigators of the various GLOBE environmental experiments, and with regular feedback from the user community (students and teachers), we provide a variety of daily color visualizations of data obtained by students, and comparison images of a variety of reference (remotely sensed and model) data. These visualizations cover a range of physical scales, from the global to the local, thereby emphasizing that everyone's local area is, in fact, a part of the Earth as a whole. Data currently being obtained by students include daily maximum and minimum temperatures, precipitation, and cloud cover. Measurements of soil moisture at various depths, water temperatures and pH, biometric studies of selected plots near the schools, and global positioning system (GPS) localization of all data collection sites are performed at less frequent intervals. On a regular basis we also create for CNN and other broadcasters high-definition video animations, which highlight various aspects of GLOBE. Special images and advanced visualizations are provided on an intermittent basis.

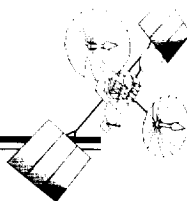
Access to GLOBE data products is through the GLOBE Visualization Server on the WWW at <http://globe.gsfc.nasa.gov/globe>. Our server incorporates a

graphical user interface that is language-independent (as this is an international project), and allows easy navigation among the different data types, global locations, dates of observation, data sources (student and reference), and observation dates. All buttons on the interface are context-sensitive (e.g., moving from maximum temperature data to minimum temperature data will give users the same view, date, and data source that they had been looking at previously). Pages of extensive, context-sensitive help are also provided to explain the interface, data sources, visualization techniques, and map projections used. These are presently in English, but could be easily translated into other languages. The interface is hyperlinked to other parts of the GLOBE project, including the GLOBE Help Desk at NASA/Ames Research Center. The first figure shows one of our WWW pages.

Because of the different data types, sources, and geographical views and resolutions, we generate hundreds of images daily. This figure will increase dramatically in the near future as the number of scientific experiments and data types increases. To support such growth, a very high



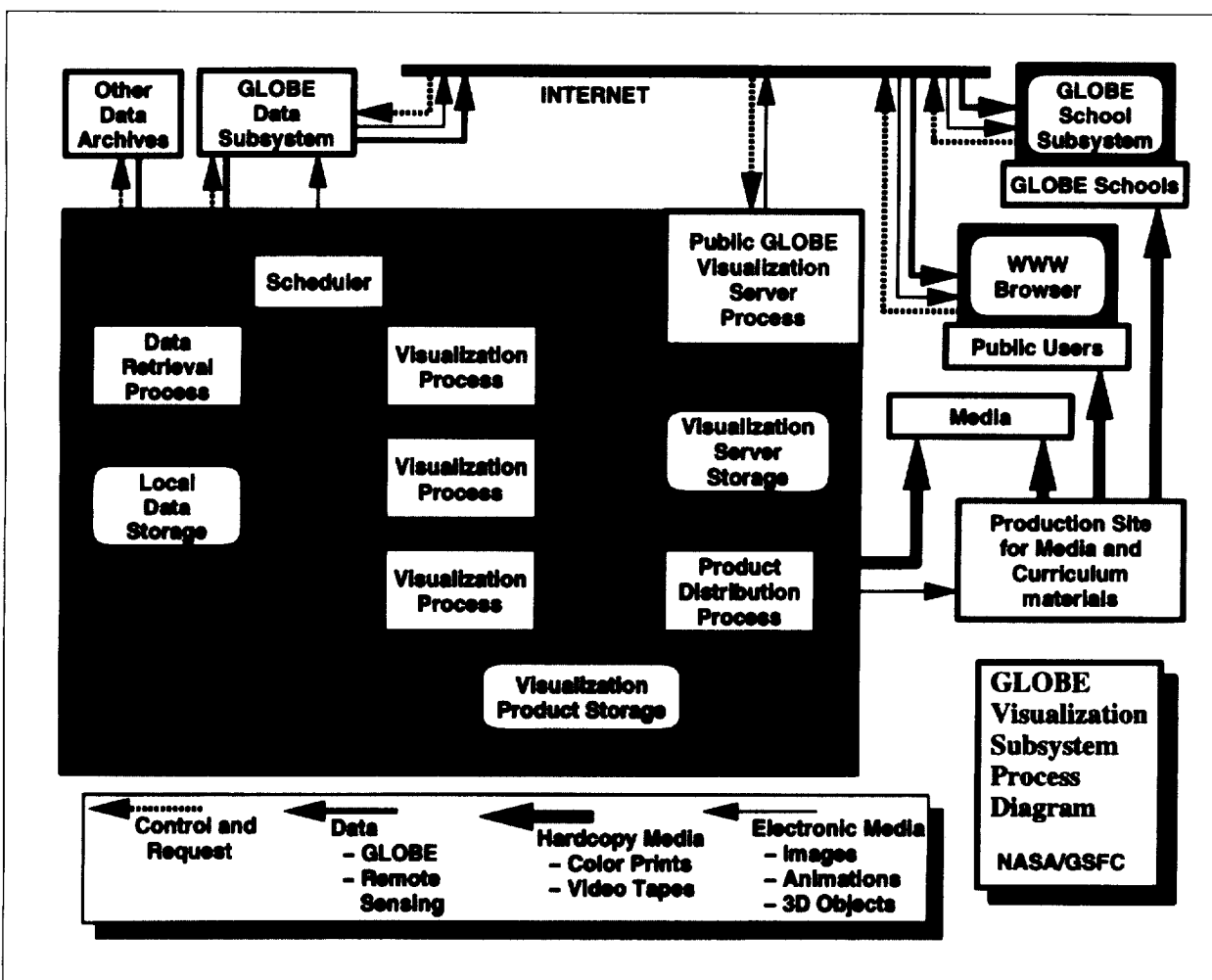
*A sample page from the GSFC World Wide Web interface. This page displays a daily image of the worldwide minimum temperature in a Cartesian projection. The language-independent, context-sensitive navigation buttons are also shown.*



degree of automation is required. We have developed a system to automatically pull data over the Internet two or three times a day, reformat it, create all the color images, embed the images in plaques with descriptive notations, move the plaques to the Web server (where they are embedded in hypertext mark-up language pages), establish the pages on the server, ship copies to the mirror sites, provide processing reports, and archive past data. This system is well-documented, and, with the exception the IBM Data Explorer software (for making the images themselves), is based on publicly available software packages. It is thus ready to be exported or commercialized, if such needs arise. The second figure shows a schematic of the

configuration in which the GSFC support activities take place.

We have had to face and surmount many technical challenges, some of which have been touched on above. Speed of Internet access is still a problem for schools, which usually have slow connections and limited daily access to the Internet. We have addressed this issue by creating a simplified, downloadable package that a teacher can access outside of regular class hours. During lesson time, the interface will run locally, avoiding problems that could be caused by spotty real-time network performance. We also provide an interface to a simple list of images (since



The GLOBE Visualization Subsystem Process Diagram. The area within the gray background shows schematically what takes place within GSFC.

highly graphical interfaces can be slow to download), so teachers can choose only what they need for the lesson that day, and can plan efficiently.

We have designed all WWW pages to fit on a 640 x 480 pixel screen, typical of low-end displays. Color scales are 8-bit, chosen from standard color tables to preclude dithering and possible hardware/software mismatches on the local systems. We have expended a great deal of effort in the design of our WWW interface, which must meet the needs of a highly varied customer base that includes K-12 and general users worldwide. Web navigation has been made language-independent and context-sensitive, to be as user-friendly and intuitive as possible. The high volume of daily processing has been addressed by automation, as described above. The high volume of user access has been addressed by load-balancing at GSFC, and automatic mirroring at other sites. We are preparing to mirror to Web sites in capital cities of other GLOBE countries, so that local schools only have to use telephone connections within their own countries, thereby avoiding overseas charges. We are also developing access methods (based on e-mail and ftp) for schools without reliable WWW connections.

Data must not only be collected, it must be analyzed. We are using the latest in network technology (e.g., Java, a new, object-oriented programming language; and Hot Java, an advanced WWW browser) to develop simple analysis tools the students can obtain over the Internet (or

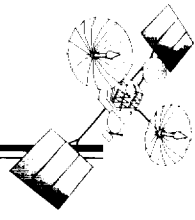
on diskette) and run on their local machines. This provides uniformity among the schools, compatibility with the formats of the data we provide, and freedom from forcing schools to buy a particular commercial package. The software is being written in compliance with a set of requirements developed in coordination with the science team principal investigators. Tools include table and spreadsheet manipulation, graphs, simple two-dimensional mapping and colorization, and some simple model fitting. Because Java is a public domain language, we fully expect that the students will jump in and enhance what we provide.

GLOBE began officially on Earth Day 1995. We expect it to grow rapidly, involving more data types, more experiments, more schools, and more countries. We are planning our system to grow with it.

Contact: Richard White (Code 932)  
301-286-7802  
Internet: [rwhite@jansky.gsfc.nasa.gov](mailto:rwhite@jansky.gsfc.nasa.gov)

Sponsor: Office of Mission to Planet Earth

*Dr. White is a member of the Scientific Applications and Visualization Branch. He earned a Ph.D. in Astronomy and Astrophysics from the University of Chicago. He came to Goddard in 1980 as an NRC research associate, and has worked on radio, x-ray, and optical studies of clusters of galaxies, COBE, and image processing and visualization.*



## MODEL-BASED VECTOR QUANTIZATION FOR IMAGE BROWSE AND COMPRESSION

OVER THE PAST SEVERAL YEARS, Vector Quantization (VQ) has been advanced as an approach to facilitate image browse and compression in large image data archives such as those being developed at various NASA centers. NASA's Distributed Active Archive Centers (DAACs), which are being built to handle data from the Earth Observing System, are expected to store some 2 to 3 terabytes of image data products per day. Image compression will be required to minimize the volume of stored data, and to produce reduced image products for quick browsing through the image data archive. VQ is attractive for this purpose because of the low computational load required for decompression, the high image quality that can be achieved at high compression ratios, and the ease of embedding VQ into a progressive compression system that integrates image browse with lossless retrieval of the original image data. However, there are certain difficulties with VQ. We have developed a VQ variant called Model-based Vector Quantization (MVQ) that overcomes these difficulties.

VQ operates on the principle that sections of image data (called vectors) can be efficiently represented by scalar indices into a list of representative image vectors. This list of representative image vectors is called a "codebook." Compression is achieved when each scalar index consists of fewer bits than the vector it represents. The best image fidelity is achieved when codebooks contain many optimally selected image vectors; more compression is achieved with larger vector sizes and fewer codebook image vectors.

The main obstacle to widespread use of VQ for image browse and compression are the difficulties encountered in generating and managing VQ codebooks. VQ codebooks are generated through a computationally intensive training process, carried out on a strategically selected set of image data, called the training data set. The codebook thus generated provides optimal performance (in the rate distortion sense) for a given size of the codebook for all the images included in the training set. However, for images outside this training set the performance is suboptimal. Nevertheless, if the training set is fully representative of the data being encoded, near-optimal performance can be achieved.

We noted earlier that the best image fidelity is achieved with larger codebooks. However, these large codebooks impose large computational and data management requirements. Fortunately, the computational requirements can be met through powerful parallel computers at the archive site, so are not of concern to the data users. However, the data users still would have to store and manage the codebooks on their local computer facilities, further limiting the utility of VQ approaches to image browse and compression.

Codebook-related difficulties are reduced somewhat by the VQ variant Mean Removed Vector Quantization (MRVQ). This is because the codebooks are more generic compared to the codebooks used in standard VQ. In MRVQ, the mean value is calculated and subtracted from each VQ vector, producing residual vectors. These mean values, which are compressed in lossless fashion separately from the residual vectors, can be reconstructed to form a first-level browse image. The residual vectors are encoded by indices into a codebook as in standard VQ.

The MRVQ codebook tends to be more consistent than standard VQ codebooks from data set to data set, as it has been observed that, in most NASA image data sets, the statistics of the residual vectors tend to be more similar from data set to data set than the statistics of the original data. While there may be fewer distinct codebooks to deal with, MRVQ still requires user involvement in the management of the residual VQ codebooks.

We have developed MVQ as a VQ variant which eliminates the need to train and manage codebooks. MVQ generates its codebook internally based on the Laplacian error model, and imposes suitable correlations. As far as the user is concerned, it is a codebook-less VQ variant.

In MVQ, as in MRVQ, the mean value is calculated and subtracted from each VQ vector, producing residual vectors. These mean values, which are losslessly compressed separately from the residual vectors, can be reconstructed to form a first level-browse image, just as in MRVQ. Unlike MRVQ, however, in MVQ the standard deviation,  $\sigma$ , of the residual vectors is calculated, and the Laplacian distribution parameter,  $\lambda$ , is computed as  $\sigma$  divided by

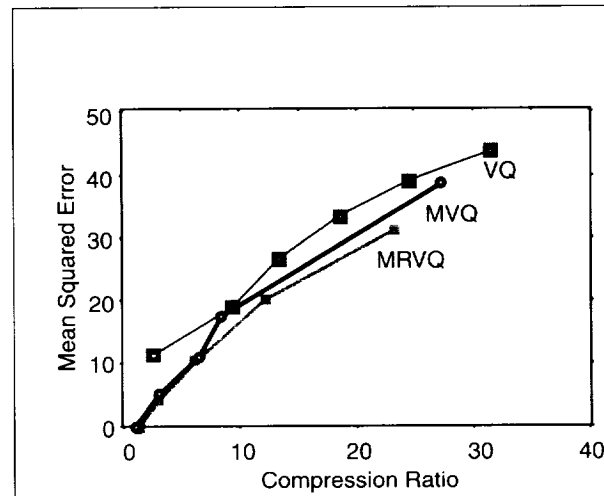
the square root of 2. The MVQ codebook is then generated by first using a random number generator to produce uniformly distributed numbers,  $u_i$ , over the range -1.0 to 1.0. These uniformly distributed numbers,  $u_i$ , are then cast into a Laplacian distribution through the formula

$$v_i = -\lambda \log_e (1-u_i)$$

where a + or - sign is randomly given to  $v_i$ . The random variables,  $v_i$ , are independent and identically distributed Laplacian random variables. However, this does not accurately model the image data residual vectors, since the elements of the residual vectors are not statistically independent, but rather have considerable correlations between them.

To impose the appropriate correlations on the independent and identically distributed Laplacian random variables, we use the characteristics of the Human Visual System (HVS) on the variables. We use the method employed by the Joint Photographic Experts Group's Discrete Cosine Transform (JPEG/DCT) compression algorithm. In JPEG/DCT, the DCT coefficients are quantized based on their significance to human perception. One way to impose HVS properties on the codebook vectors generated by the Laplacian model is to perform a DCT on the vectors, weight the result with the HVS DCT weight matrix, and perform an inverse DCT of the result. We have modified the usual JPEG/DCT coefficient weighting matrix by making the DC term 0.000 so that it is appropriate for residual vectors with 0 mean value. If the residual vector is from an image vector smaller than  $8 \times 8$  block (vector size less than 64), the corresponding subset of the HVS weighting matrix is used in the product.

The figure shows a comparison of the rate distortion performance of the VQ, MRVQ, and MVQ on a Landsat Thematic Mapper (TM) image of the Washington, D.C., area. Codebooks of four different sizes were generated for VQ and MRVQ from a suitable set of Landsat TM images that did not include the image encoded in this test. We see that the MVQ rate distortion performance (compression ratio vs. mean squared error) is better than that of VQ (i.e., for a given compression ratio, MVQ has lower distortion compared to VQ). However, MRVQ performs marginally better than MVQ.



Rate distortion performance of VQ, MRVQ, and MVQ.

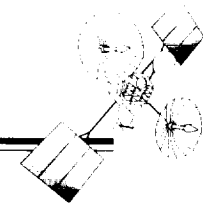
Considering how close the MVQ rate distortion performance is to VQ and MRVQ, the only drawback for using MVQ is the computational burden of computing the codebook entries. However, this computational burden is constant for any image size; for decoding large images, this constant term becomes negligibly small. The elimination of the problems arising from codebooks makes MVQ a viable approach for image browse and compression in NASA image data archives.

The primary development work on MVQ was performed by Dr. Mareboyana Manohar, Department of Computer Science, Bowie State University, with programming support from Kavitha Havanagi.

Contact: James Tilton (Code 935)  
301-286-9510  
Internet: [tilton@chrpisis.gsfc.nasa.gov](mailto:tilton@chrpisis.gsfc.nasa.gov)

Sponsor: Office of Mission to Planet Earth

*Dr. Tilton is a computer engineer in the Information Sciences and Technology Branch. He earned his Ph.D. in Electrical Engineering at Purdue University in 1981. He has been at GSFC since 1982, performing research in image segmentation, image data compression, image registration, and massively parallel software development.*



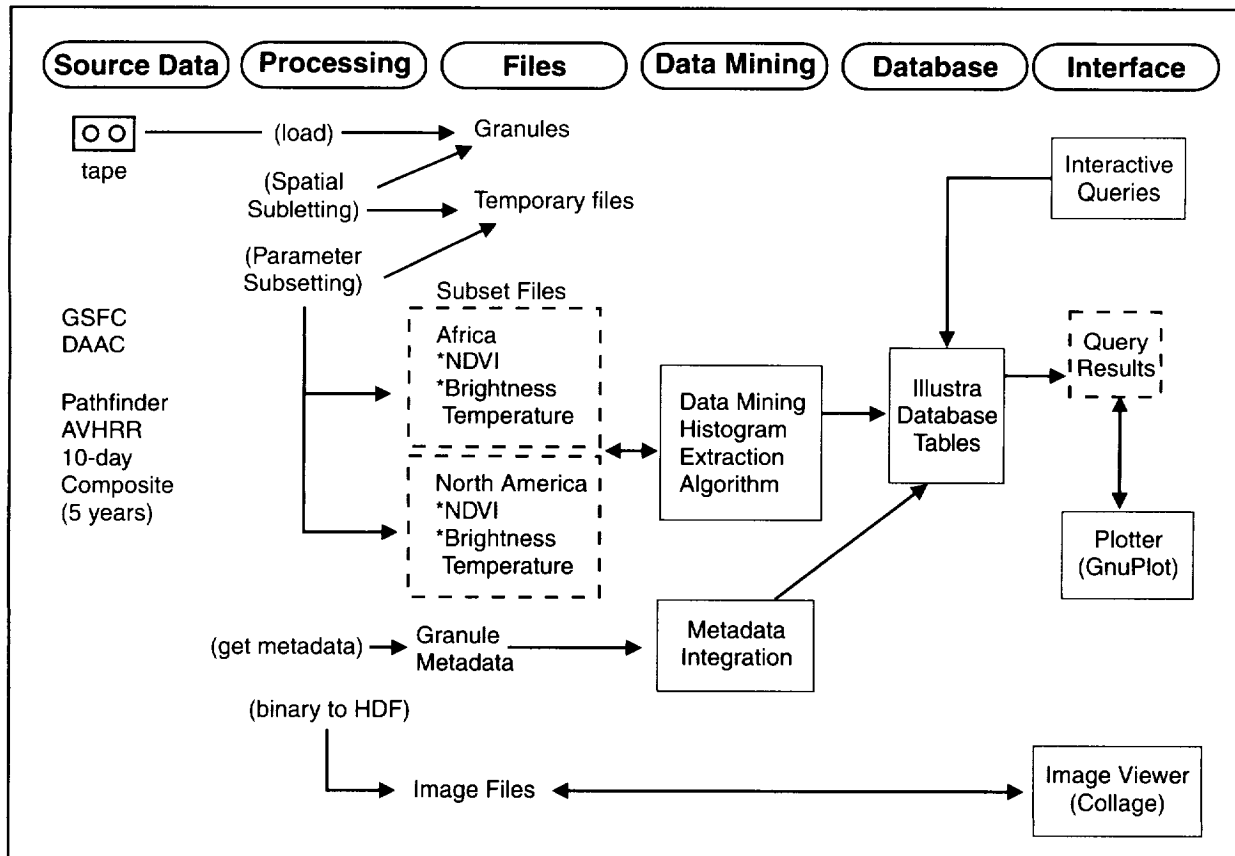
## SATELLITE IMAGE CONTENT EXTRACTION AND CATALOG AUGMENTATION: AN EOSDIS DATA MINING PROTOTYPE

THE IMAGE CONTENT extraction (data mining) and catalog augmentation prototype project is an Earth Observing System Data and Information System (EOSDIS) research project established to explore ways to enhance the information a scientist is provided about image data. This information is known as metadata. The project is comprised of a small team of scientists and system developers who have collaborated on development of a prototype that demonstrates a technique for extracting satellite image content information directly from digital imagery. This information is referred to as image content-based metadata, and is used to infer other properties of the image data, which will help investigators select appropriate images for further study.

The prototype team also explored suitable mechanisms for augmenting catalog metadata with the image content

information, and experimented with the scientific use of the information. The content-based data were cataloged with other traditional spatial and ancillary information, so that they can be retrieved from the archive, and analyzed to infer a phenomenon of interest. The study used the Pathfinder Advanced Very High Resolution Radiometer (AVHRR) Land data set to show significant events encapsulated in the extracted product. The project goals are to demonstrate technical feasibility of this process, and to gain insight into relevant designs for future EOSDIS implementations.

The prototype encapsulates an end-to-end data mining process, starting with source data and ending with interface tools for data manipulation and analysis. The figure depicts the relationship of the different parts of the prototype. It also indicates the progression of steps for



*Schematic of the Data Mining Prototype.*

preparing image data for data mining, applying a data mining technique, cataloging extracted metadata in a database, and using a set of interface tools to support the scientific use of the data mining results.

The first step in the process was the analysis and selection of the NOAA/NASA Pathfinder data set for use in the prototype. The Composite Data Set, one of the Pathfinder AVHRR Land products, was selected because it is particularly useful for studying of temporal and interannual behavior of surface vegetation, and for developing surface background characteristics for use in climate modeling. These data were ordered and received from the GSFC Distributed Active Archive Center (DAAC) on 8-mm tape cartridges. The Composite Data Set contains global 8 km terrestrial data, mapped to an equal area projection. There are three composites per month for each year of data. The first composite of each month is for days 1 to 10, the second composite is for days 11 to 20, and the third composite is for the remaining days. Data spanning a period of 5 years (1986 to 1990) were chosen for the study.

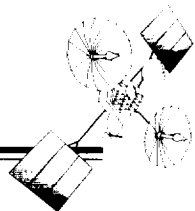
A two-step subsetting process was needed to prepare the data for data mining. Global granule data were first subset into two geographic regions, corresponding to North America and Africa. Each spatial subset was stored as a Hierarchical Data Format (HDF) file using a 'pick-a-continent' tool provided by the GSFC DAAC. Each spatial subset file was further processed into two geophysical parameter binary subset files, using a GSFC DAAC "HDF-to-binary" software tool. The selected parameter subsets were the normalized difference vegetation index (NDVI), which is related to the proportion of photosynthetically absorbed radiation, and the channel 4 brightness temperature, which is the top of the atmosphere brightness temperature in Kelvin, derived from channel 4 of the AVHRR (10.3 to 11.3  $\mu\text{m}$ ). In this manner, four binary image files were produced for each 10-day composite for each continent. A total of 720 image subset files were produced for the 5 years of data selected for the prototype.

The team developed an algorithm to extract information from an image by processing image files into counts of pixel values. The counts were subsequently grouped into different parameter range intervals, or bins. The data mining binning algorithm uses the subsetted binary NDVI

and brightness temperature image files, and screens for out-of-range values. It also checks for land pixels, which are the only pixels used in the prototype. The binary pixel values are then converted to geophysical values from the scaled 8-bit (NDVI) and 16-bit (brightness temperature) unsigned integer values. Offsets are subtracted from the scaled binary data value, and the result is multiplied by gain values provided in the Pathfinder Land Data Sets documentation. The resulting geophysical values are checked to ascertain that they are within the valid limits. If a value is within valid limits, then it is assigned to an interval (bin). Eight intervals were established for the NDVI values, and 10 for the brightness temperature values. After all valid pixels of an image have been assigned to bins, the frequency of occurrence of each interval is aggregated. Then the mean and standard deviation for the geophysical parameter is calculated, based on the total number of valid pixels in each image. Output from the algorithm is sent to a database interface that manages the population of database tables with the extracted (data mined) information.

A database schema was designed to support cataloging the data mining results and interactive queries. The schema was implemented in an Illustra object relational database management system. In addition to the data mining results, the catalog includes metadata about the source granules from which the images were subset. Granule metadata were extracted from the uncompressed HDF image file and integrated with each subset image file identifier. Relevant metadata for the subset images included the start date, end date, and source satellite name. Spatial coordinates for continental subsets, source data set, day/night flag, parameter names, and sensor were also included as database metadata. This information was then used to develop methods to support the scientific use of the data mining results using the interface tools described below.

Three basic interface components were developed to explore the scientific use of cataloged data mining information; a query interface, a tool for plotting histograms, and an HDF image viewer. An interface mechanism was required to interact with the database using search criteria based on scientific questions. A science scenario was developed to explore the capabilities, limitations, and utility of the prototype from a science perspective. The plotting tool was required to present the results of the queries to the scientist on a computer screen in the form



of a histogram. The image viewer was also used to support the interpretation of data mining results by displaying the actual subset image corresponding to spatial and geophysical parameters of interest.

For example, we wanted to find images that show characteristics of severe drought conditions over the time series available in the database. We queried the database to retrieve a few months of NDVI bin and count values. After plotting the histogram for count versus bin values, we were able to decide on the bin number to use for further analysis. Then we queried the database to retrieve only values for this bin, for the entire time series. A plot of these bin values over time allowed us to observe the trend in the data. We were able to infer that the dates where there were dips in the trend line signified periods of extremely dry conditions. Using these dates, we were able to retrieve the original data for in-depth study.

This study has demonstrated the feasibility of content-based metadata extraction and cataloging from a large satellite data collection. It has also indicated the utility of a simple histogram technique for displaying data mining results, and eventual retrieval of imagery of interest from a large database at minimal cost in both human and computer resources. The study suggests that content-based metadata extraction should best be performed after geophysical parameters are derived from the original data, before insertion of both into the database.

In the course of the catalog augmentation for data mining prototype, it has become clear that it is scientifically useful to display content-based metadata in support and response to database queries. Examples of these metadata include "quantitative browse," such as a histogram associated with each image identified in a catalog search; "trend line;" and a "feature list." A complementary effort will continue to address the problems of integration and display of image content-based metadata into an interactive interface. The team will develop this capability in a prototype interface to demonstrate how users will be able to add their own analysis routines and metadata. This approach and future work will lead to a greater understanding of the interrelationships between content-based metadata and user interface tools, from which will emerge those that will prove most useful in analysis.

Contact: Mike Moore (Code 505)  
301-286-0795

Sponsor: Office of Mission to Planet Earth

*Mr. Moore has been a computer engineer for the past 5 years in the Software and Automation Systems Branch and the Earth Science Data and Information Systems Project. He is completing a Ph.D. in Information Technology at George Mason University.*

### WORLD WIDE WEB

#### LATEST STUDY INFORMATION? CALL “HOME”

**A** PROJECT ENGINEER in search of a particular action item response is now more likely to call home rather than to try to find the latest version of the action item log. “Home,” in this case, is the project’s home page on the World Wide Web (WWW).

The Earth Observing System’s Laser Altimetry Mission Study was organized to use just such a home page. Under topics like General Mission Information, Flight Operations, Spacecraft, and Ground Segment one can find complete descriptions of the spacecraft and instrument requirements and design, including diagrams, subsystem databases and interfaces. Links are also provided to the Systems Engineering Information home page. This vast store of information is available through a common, easily accessible medium, available to the whole team (with the capability for rapid updates), just by accessing the Universal Resource Locator (URL) <http://gdglas.gsfc.nasa.gov/lam>.

At first, the page served to link the few study members in the Flight Projects Directorate, the Engineering Directorate, and the Earth Sciences Directorate across GSFC’s campus. It rapidly grew to be a tool to keep the payload scientists—and other experts at other centers—involved. Based on our recent experience with this communications medium, we have observed advantages and shortcomings, some of which will be discussed here, and which should prove instructive for others considering such methods.

Using a home page has the following advantages:

- with electronic linkage, changes and data can be loaded rapidly, almost as soon as they are generated. This means all the team members have access to late-breaking changes every time they log on. There is no significant data latency in action item responses, trade study results, or other time-sensitive efforts;
- mandating a home page early in the project cycle requires that a common format for each data item must be defined the first time it is needed. Early format definition means that generating and retrieving data gets faster with time as users get more familiar with the material; there are no surprises, nor is there time wasted wandering through information labyrinths. Data input can be free-flowing text or form-driven to standardize the presentation and for database input;

- status briefings are amazingly simple to present—they can be run right off the home page using a plasma overhead projector screen plugged into a PC connected to the WWW. Not only is it easy and slick, but there is also no question about data integrity or follow-up data; everything the Mission Study Team has done is on the page and accessible;
- the WWW exists everywhere, there is virtually nowhere on the globe where access cannot be found (or jury-rigged). This means that travelers and remote team members have the same direct data connection as local team members. In fact, “local” becomes meaningless, since where the page physically (or electronically) resides is irrelevant. This bridges time zones and makes duty hours, local holidays, and clock time meaningless with respect to accessing the information needed, whenever it’s needed;
- the breadth of the coverage is limited only by what the Study Team has decided to put on the page—information from the specialty engineers, managers, analysts, and resource staff is accessible to the whole team. This means that data gathering is no longer a sequence of phone calls and visits, nor does it require extensive group meetings; and
- since it can be chaotic and inefficient to allow each team member unlimited write privileges, it is easier and more prudent to designate a central person to administer the page and upload new information as it comes in. This provides the extra benefit of configuration management, because the administrator has the guidelines as to what can be immediately uploaded, and what should be screened and edited. Establishing the configuration management principles for what needs to be controlled and what those controls are is certainly a major benefit for any project, and should be done as early as possible.

It has not been all easy going, however. Certain disadvantages associated with home page use did arise, for example:

- any reliance on an electronic device (such as a PC) is inherently limited by whether or not the device works. Using a home page extends that risk across an undetermined number of computers and networks, most

of them unidentified (and unidentifiable), and over which the user has no control. If there is a power outage or a dropped link for whatever reason—your team is effectively deaf and dumb. Furthermore, initial access to the WWW is through an account granted by supervisors and information system managers. This access is not instantaneous, and new team members remain stalled on the information highway until the paperwork is completed, routed, and filed;

- network browsers, like Netscape or Mosaic, are mandatory for home page access. Like all software, these are subject to frequent revisions (or “improvements”). If users fall behind on the revisions, they could lose the ability to display a newly formatted table, or to print an interesting file. Further, the new software could crowd the PC to the point where the improved version runs slower than its predecessor;
- allowing everyone on the team instantaneous access to the latest Mission Study information is a great benefit few could deny. Unfortunately, everyone else on the Web (i.e., the whole world) has the same access. Passwords can be used to provide some degree of protection, but true security to protect proprietary or volatile data would first have to be established by a recognized security office before such data can be safely placed on the page;
- face-to-face contact is lost when information is transferred via Web page. This may not seem like a major drawback for some, but there is no doubt that the human connection—talking, facial expressions, body language, vocal asides, and emotion—all capture and convey significant information about what is being discussed. Indeed, much of the benefit of collaboration is lost without direct human interaction;
- configuration management is an absolute must or else there is no value to the information posted. If team

members log onto the page and see information they know is questionable, faith in the page is shattered, and the information found on the page thereafter would be highly suspect; and

- a home page does not necessarily generate a lot of new work requirements for the Project, but some maintenance is necessary to keep information current and accurate. Data checking and entry is required just as it is for any (paper) project library; it is just focussed on the home page. This means that the page administrator must also be knowledgeable in hypertext modifications, word processing, file transfer protocols, spreadsheets, and databases.

The use of a home page is a very efficient and timely way to keep a widespread project team in touch with each other if the team is willing to keep it up-to-date, impose configuration management early, and secure the information appropriately for its use. Because of all the advantages, and despite the disadvantages, the Chemistry and Special Flights Project is investigating keeping the Laser Altimetry home page operational through spacecraft contract award and development.

Contact: Bill Anselm (Code 424)  
301-286-3178  
Internet: Bill.Anselm@ccmail.gsfc.nasa.gov

Sponsor: Office of Mission to Planet Earth

*Mr. Anselm is the Special Flights Spacecraft Manager for the Earth Observing System/Chemistry and Special Flights Project. He received a B.S. in Electrical Engineering from Syracuse University, and an M.A. in Business from Central Michigan University. He has been with GSFC's Flight Projects Directorate for 5 years, serving as Instrument Manager for several of the Global Geospace Science instruments, and is now working with the Earth Observing System, managing the spacecraft definition effort for Laser Altimetry.*

### DISTRIBUTING FLIGHT DYNAMICS PRODUCTS VIA THE WORLD WIDE WEB

THE FLIGHT DYNAMICS Division (FDD) at GSFC is responsible for providing orbit, attitude, and acquisition data products to a variety of users, employing various transmission media. The primary customers of these operational products include the Payload Operations Control Center, Flight Operations Team, the Ground Network, the Space Network, Science Operation Center, and other project personnel. Traditionally, the Flight Dynamics Facility (FDF) has initiated the transfer of its data products over NASA Communication (NASCOM) lines using standard NASCOM protocols. Establishing and operating these communications lines for each new mission has incurred substantial expense. Much effort has been invested in establishing mission-unique interfaces, testing data transmissions, and responding to special data requests. With the emergence and widespread use of the Internet and its associated transmission protocols, the opportunity to provide operational FDF products in an open environment is now being realized. Many FDF customers have facilities which are connected to the Internet. The FDF has established the Flight Dynamics Products Center (FDPC), which will allow any user with an Internet connection to retrieve operational FDF products. Using a World Wide Web (WWW) browser, such as Netscape or Mosaic, the user can initiate FDF product transfers to the user's host machine. The FDPC operates on the FDD Internet server ([fdd.gsfc.nasa.gov](http://fdd.gsfc.nasa.gov)) and is accessed from the Uniform Resource Locator (URL) [http://fdd.gsfc.nasa.gov/FDD\\_products.html](http://fdd.gsfc.nasa.gov/FDD_products.html).

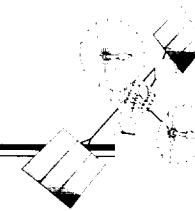
The FDPC is a multimission service that makes several standard FDF products available to any Internet user. These products include mean orbital elements in J2000 coordinates and ground trace predictions. As a non-standard service, the FDPC can offer definitive orbit ephemerides and definitive attitude solutions. These products are available via the Internet without restriction. In addition to products originating from the FDPC, other historical data (such as attitude files) and reference databases (such as Solar-Lunar-Planetary ephemeris files and SKYMAP star catalogs) are available via the Internet. All of these data products are logically grouped in Hypertext Markup Language (HTML) 3.0 documents to allow ease of navigation and retrieval via the WWW. The FDPC home page takes advantage of many of the newer features available with HTML 3.0, including forms (which support graphical selection menus) and tables (which are used to

display search results in an easy-to-read format). The FDPC includes three separate form searches: the Spacecraft Parameters Database Search, the Spacecraft Products Browser, and the Spacecraft Products Server.

The Spacecraft Parameters Database search form allows the user to display the base spacecraft parameters for FDF-supported missions. The base spacecraft parameters include spacecraft name, satellite ID, spacecraft identification code, North American Air Defense ID, semimajor axis, eccentricity, inclination, area, mass, and orbital period. Using a mouse (or equivalent pointing device), the user selects any of the 24 missions of interest from the list presented on the form. Multiple missions may also be selected; the default option is to use all missions. The user then clicks on the "Display Spacecraft Parameters" button. This directs the FDD Internet server to begin a database search for the missions that were selected. When the search is completed, the base spacecraft parameters are displayed.

The Spacecraft Products Browser lists all operational spacecraft products that leave the FDF. The browse can be restricted to specific missions, originators, recipients, delivery media, or product types by selecting the parameters of interest from the lists presented on the search form. The user may choose multiple selections from each list; the default action is to include all members from a list. The user then clicks on the "Browse Spacecraft Products" button to display the spacecraft products database information. This information includes spacecraft name, product type, originator, recipients, delivery frequency, delivery media, accuracy, and source.

The Spacecraft Products Server allow retrieval of operational spacecraft products from the FDD Internet server. Using a mouse, the user can select the 18 missions and various products desired from the lists presented, as shown in the first figure. The list of product types will be expanding as the FDPC matures, but currently it includes only mean orbital elements. Multiple selections are allowed in each list. The user then clicks on the "Retrieve Spacecraft Products" button to retrieve the products. A search results page is displayed, which provides a list of all products available that match the options selected by the user; hypertext links to the actual product are provided. The user can then click on each link to retrieve or display the desired products, as shown in the second figure.



**Netscape: Spacecraft Products Server**

Location: [http://fdp.gsfc.nasa.gov/FDPC\\_products\\_form.html](http://fdp.gsfc.nasa.gov/FDPC_products_form.html)

What's New? What's Cool? Bookmarks Net Search Net Directory Newsgroups



**Spacecraft Products Server**

These options allow retrieval of operational spacecraft products from the FTP server. Select the Missions and Products that you wish to retrieve from the lists below. Multiple selections are allowed in each list. Then click on the "Retrieve Spacecraft Products" button to retrieve the products.

All Missions	Mean Orbital Elements
ERBS	
EUVE	
GOES-7	
GRO	
HST	

**Retrieve Spacecraft Products** **Reset**

Questions? Comments? Contact the FDPC Administrator.

**Netscape: Spacecraft Products Server Search Results**

Location: [http://fdp.gsfc.nasa.gov/sgt-bin/sps\\_search.pl](http://fdp.gsfc.nasa.gov/sgt-bin/sps_search.pl)

What's New? What's Cool? Bookmarks Net Search Net Directory Newsgroups



**Spacecraft Products Server Search Results**

The following matched your search:

**ERBS**

[ERBS Mean Elements for 950822](#)— Most Current  
[ERBS Mean Elements for 950818](#)  
[ERBS Mean Elements for 950815](#)  
[ERBS Mean Elements for 950811](#)  
[ERBS Mean Elements for 950808](#)  
[ERBS Mean Elements for 950804](#)  
[ERBS Mean Elements for 950801](#)  
[ERBS Mean Elements for 950728](#)  
[ERBS Mean Elements for 950721](#)

**GRO**

[GRO Mean Elements for 950823](#)— Most Current  
[GRO Mean Elements for 950821](#)

Using a WWW browser and a mouse, the user can select one or more missions from the list presented. Clicking on the Retrieve Spacecraft Products button will initiate the product search from the FDD Internet server.

The three search forms employed by the FDPC make use of HTML form definition tags. Scripts written in the Practical Extraction and Report Language (PERL) to complete each user-directed action are transparent to the user. The Spacecraft Parameters Database and the Spacecraft Products Browser use a database search scheme to fulfill the action; the two databases are in comma-delimited text format. The PERL script takes the user-supplied search parameters and returns the relevant parameters from the appropriate database as an HTML table. The Spacecraft Products Server uses a PERL script to search for all files on the FDD Internet server that match the parameters given by the user in the search form. These files are first generated in the FDD secure computing environment, and are transferred using the file transfer protocol (ftp) to the FDD Internet server on a daily or near-daily basis. The files are uploaded to the FDD Internet server in an ftp partition near noon each day. At midnight, the server

automatically moves the files into a separate directory (according to its type), at which time the files become visible to the PERL script. Each file retains a strict file-naming convention to allow ease of retrieval by spacecraft name, product type, and date of epoch, using a PERL script. For example, a file having the name ERB\_MeanElements\_950728 uniquely identifies the mission name as ERBS, the product type as Orbital Mean Elements, and the epoch date as July 28, 1995.

This use of common communication protocols and industry-standard presentation formats will enable the FDF to continue to provide significant and useful data to its customers in a relatively inexpensive and timely fashion.

Contact: David Matusow (Code 552.1)  
 301-286-9231  
 Internet: [david.matusow@gsfc.nasa.gov](mailto:david.matusow@gsfc.nasa.gov)

## MISSION OPERATIONS AND DATA SYSTEMS

---

Mark Woodard (Code 553.1)  
301-286-9611  
Internet: [mark.woodard@gsfc.nasa.gov](mailto:mark.woodard@gsfc.nasa.gov)

Sponsor: Office of Space Communications

*Mr. Matusow is a software development engineer in the Software Engineering Branch. He received a B.S. in Computer Science from Drexel University in 1990, and has worked in the FDD for 5 years. Mr. Matusow is responsible for the development of the FDD's external*

*and internal WWW sites, as well as being involved with the software development of the SAMPEX, FAST, TRMM, and TRACE missions.*

*Mr. Woodard is an aerospace engineer in the Flight Dynamics Support Branch. He received a B.S. in Aerospace Engineering from the University of Virginia in 1985, and has worked in the Flight Dynamics Division for 10 years. Mr. Woodard is responsible for spacecraft attitude analysis and operations, and has supported the COBE, SAMPEX, FAST, and ACE missions.*

## EXPLOITING WORLD WIDE WEB TECHNOLOGY TO MAKE DATA FINDING AND ACCESS EASIER

THE WORLD WIDE WEB (WWW), which was originally conceived for document delivery across the Internet, has evolved into a medium supporting interactive data visualization and distribution.

There are several compelling advantages of using the WWW to provide access to data, which allows information providers to rapidly and economically build multimedia data and information systems that are easy to use: (1) The client ("browser") software needed to access a WWW site is freely available for almost all computing platforms. The software required to "serve" data is also freely available. (2) The WWW uses an open, nonproprietary network protocol, while the browser software supports additional network protocols such as file transfer protocol (ftp), telnet, gopher, News, Wide Area Information Search, etc. (3) The WWW supports multimedia. Thus, textual information can be served side-by-side with images, video, and audio. Indeed, WWW browsers can be easily extended to support almost any digital medium. (4) The WWW has the powerful hypertext feature that allows developers to "link" various pieces of information and data resident on widely distributed hosts into an information "space" that is much larger than what might be available locally. (5) WWW browsers are very simple to use, requiring no special knowledge (i.e., the user can simply point and click to retrieve information or perform functions). (6) The language used to develop WWW content is easy to learn.

Two WWW-based data systems, OMNIWeb and Coordinated Heliospherical Observations Web (COHOWeb), have been developed at the National Space Science Data Center (NSSDC) at NASA's GSFC to provide enhanced access to scientific data. Using only freely available WWW browser software, a researcher cannot only retrieve data but also perform interactive visualization of the data through a simple point-and-click interface.

The NSSDC OMNIWeb data system was created in late 1994 for enhanced access to the OMNI data set, which consists of 1-hour-resolution, "near-Earth" solar wind magnetic field and plasma data, energetic proton fluxes (1 to 60 MeV), and geomagnetic and solar activity indices. The OMNI data have been network-accessible via the NSSDC On-Line Data and Information Service (NODIS) (but without graphical analysis capability) for several years. OMNIWeb introduced the enhanced capabilities of

visualization, listing, subsetting, and data conversion through the WWW. Interactive visualization of the data is supported through 2-D time series plots that are dynamically generated as Graphics Interchange Format or PostScript files using the Interactive Data Language. This visualization feature aids users in finding trends and isolating areas of interest in the data. After browsing the data, users have the capability to generate ASCII listings, subsetted files, or raw binary files for further analysis.

OMNIWeb addressed the need of researchers to access a single data set with visualization and retrieval capabilities over Internet. It was designed with a generic framework in mind to support any data set conforming to the NSSDC Common Data Format (CDF) data standard (described in the *1994 GSFC Research and Technology Report*). An open architecture was developed on top of this data standard to provide a transparent, machine-independent application programming interface to store, manipulate, and access multidimensional data sets. Data stored in CDF are self-describing, such that a CDF application can provide generic data access to any CDF data file. The access tools for listing, converting, subsetting, and plotting the CDF data were not designed for any specific CDF, but for any time-ordered CDF data set with a minimum set of metadata attributes that describe the data to be accessed. A demonstration of this generalized extensibility was provided by development of another data system, COHOWeb. Within the NSSDC WWW server the same data access tools are shared by both OMNIWeb and COHOWeb, which have different underlying data sets.

The COHOWeb system was built shortly after OMNIWeb and provides similar access to the COHO data, which consist of hourly to daily averages for key heliospheric parameters selected from spacecraft ephemerides and science experiment measurements of interplanetary solar wind plasma, magnetic fields, and energetic particles. Data sources include historical and on-going deep space missions such as Ulysses, Helios 1 and 2, Pioneer 10 and 11, Pioneer Venus Orbiter (Pioneer 12), and Voyager 1 and 2.

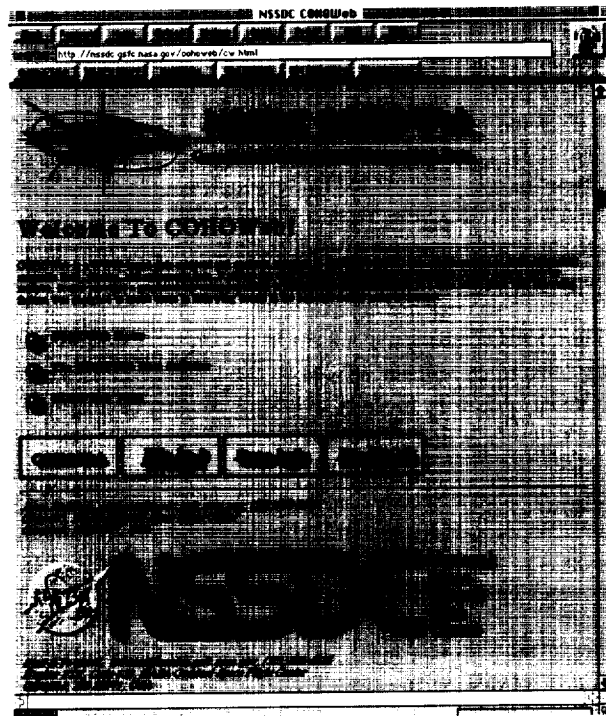
COHOWeb reuses many of the ideas and the software from OMNIWeb. However, COHOWeb represents a more evolved and generalized implementation of a WWW-based data system because multiple data sets are supported through a single interface that is generated dynamically from the data themselves. COHOWeb is easily expandable,

since data can simply be "plugged into" the system without changing the underlying software. The system can also be reused to provide access to other data, a feature that has been requested by a number of NASA projects and universities for building similar data systems.

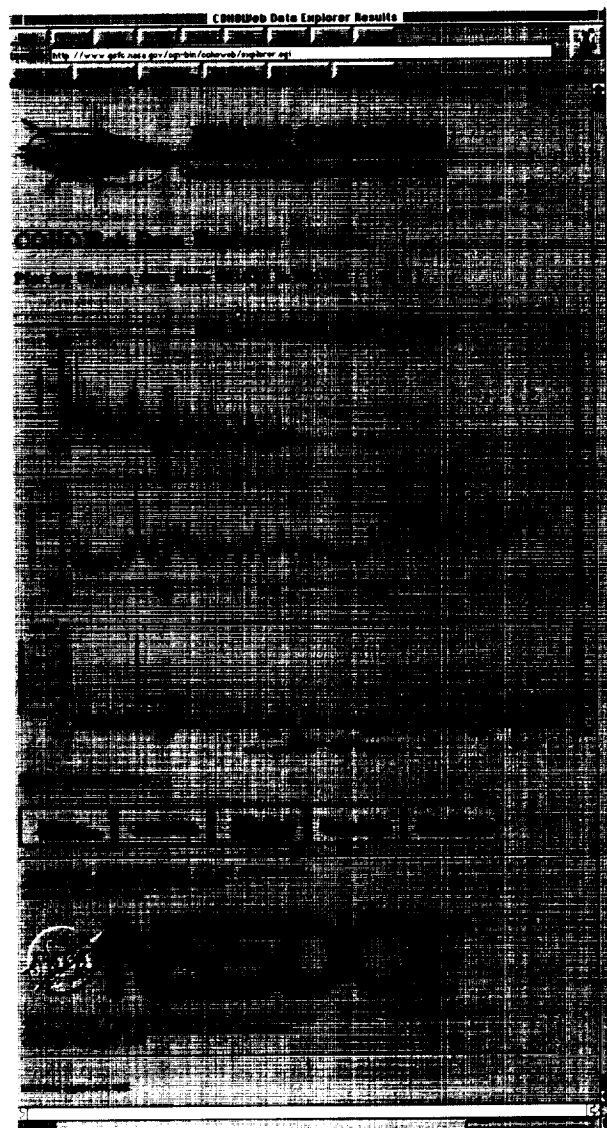
NSSDC provides "What's New" pages from the OMNIWeb and COHOWeb Home Pages to help keep users informed about what has been recently changed or added. Contact information is provided at the bottom of every page, and there is a feedback mechanism to allow users to communicate directly with the developers. Much feedback has been received, and many of the requests for enhancements, such as some advanced customization options (e.g., PostScript output, symbol and character sizes, logarithmic axes scaling), have been implemented.

OMNIWeb and COHOWeb represent a framework from which to model data systems providing interactive access to data via the WWW. These systems provide not only access to large amounts of science data, but also allow

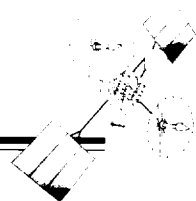
users to perform various operations on the data. For access to these systems and the corresponding data, OMNIWeb and COHOWeb are available over the WWW with the Universal Resource Locations (URLs) <http://nssdc.gsfc.nasa.gov/omniweb/ow.html> and <http://nssdc.gsfc.nasa.gov/cohoweb/cw.html>, respectively. The COHOWeb Home Page and a sample plot generated from Ulysses data by COHOWeb are shown in the figures.



The COHOWeb home page.



A sample plot generated from Ulysses data by COHOWeb.



Contact: G. Jason Mathews (Code 633.2)  
301-286-6879  
Internet: matthews@nssdc.gsfc.nasa.gov

Syed Towheed (National Space Data Center)  
301-286-4136

Sponsor: Office of Space Science

*Mr. Mathews is a computer engineer in the NSSDC Interoperable Systems Office of GSFC. He has earned a B.S. in Computer Science from Columbia University and*

*an M.S. in computer science from the George Washington University. He is interested in the development of portable and reusable software tools and has been at GSFC for 5 years.*

*Mr. Towheed is a systems programmer at the National Space Science Data Center. He holds a B.S. in Physics from Lynchburg College. His professional interests include hypermedia information systems and GUI design. He has been at GSFC for 3 years.*

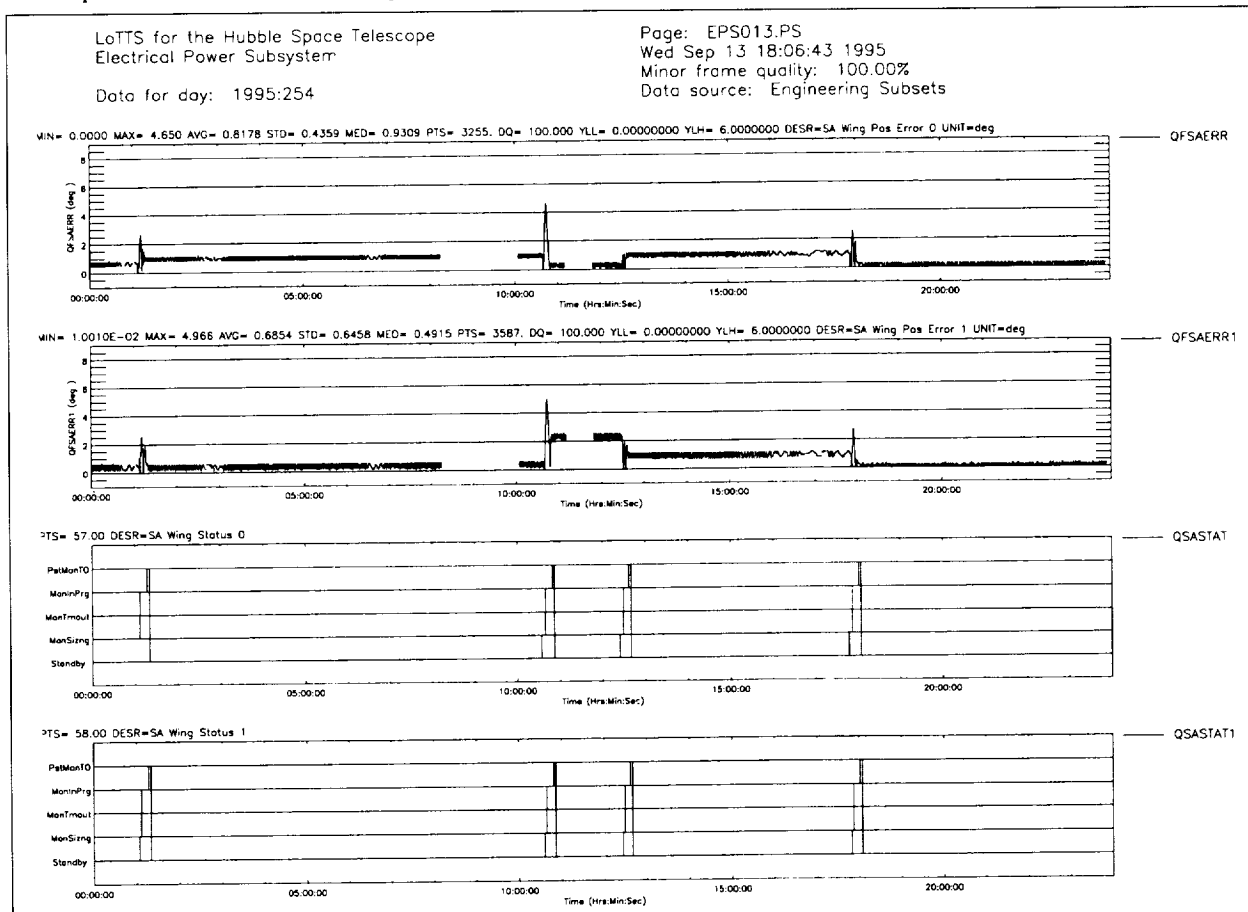
### HUBBLE SPACE TELESCOPE'S LONG-TERM TRENDING SYSTEM USES THE WORLD WIDE WEB TO DISTRIBUTE ENGINEERING DATA

**W**HEN SOMETHING GOES wrong with your spacecraft, the last thing you need is a problem getting pertinent data to your systems experts. For the Hubble Space Telescope (HST), with its geographically dispersed, international contractors, this problem can lead to delays in finding answers. To minimize the time delays in faxing or mailing data to the experts, the HST project added World Wide Web (WWW) capabilities to the Long-Term Trending System (LoTTS). This allows the experts near-instantaneous access to the data necessary to resolve spacecraft problems.

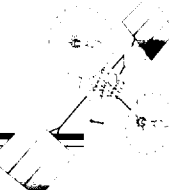
LoTTS, developed over the last 4 years, provides near-real-time and archived engineering telemetry to users. The system is hosted on a VAX 4000. The system, as originally developed, required users to go to terminals in the operations control center to request and obtain their

data. The users, our spacecraft system engineers and contractors, identified remote access as the single most desired upgrade to be made to the system.

In early 1995, Computer Sciences Corporation (CSC) developers were directed to install a WWW server on the system to provide users with access to the data analysis capabilities of the system. First, a prototype was developed, not only to get feedback on the user interface, but to learn the capabilities of the WWW browser software. A 2-month effort developed the first prototype; after another 2 months of user feedback, the system interface was finalized. The WWW server uses standard Netscape and Mosaic features—such as buttons, forms, and lists—to obtain input from the user. These data are used to generate and execute scripts that return either plots or a tabular listing of the data requested.



Sample output from LoTTS.



To establish the WWW server, the software, written in C, is downloaded to the host machine. Server software for a variety of platforms, including UNIX, VMS, Windows, and MACOS, is available via CERN on the WWW. Depending on the host and the version of the operating system, the software may need to be recompiled. One of the files downloaded is a configuration file that can be customized for a specific host. This file specifies which directories contain files that the client can read/execute, and also specifies which port the client will use to access the host.

Once the server is configured and started on the host machine, it is available to anyone with a browser (such as Netscape or Mosaic) via the WWW. The LoTTS WWW package includes hypertext markup language files containing overviews, instructions, and other static information; links to other projects; and forms that set global keys depending on user requests and links to scripts (VMS DCL files). The scripts execute programs and use the global keys as input variables. The programs generate the desired output. Depending on the output products, the output is displayed as an online image (graphic interchange format) or available to an external application in several other formats (Joint Photographic Experts Group; PostScript; etc.), as shown in the figure.

A primary function of LoTTS is to produce daily trend plots of nearly all data telemetered from the HST. Currently, these plots are printed on paper and distributed each

day to the system engineers. Since most of the HST system engineers are located off-site at a contractor facility, each day one engineer from each subsystem goes to the control center to retrieve the data for evaluation. To provide easier access to the daily trend data, these plots are now generated in electronic form and made available for viewing via the WWW server as an option on the LoTTS homepage.

The HST Project intends to increase use of the WWW for disseminating data. Plans for publishing our quarterly trending report—with hotlinks to the appropriate data plot—are being made. This will facilitate the distribution of and access to these types of data.

Contact: Andrew Dougherty (Code 441)  
301-286-5914  
Internet: andy\_dougherty@  
hstmailgw.gsfc.nasa.gov

Sponsor: Office of Space Science

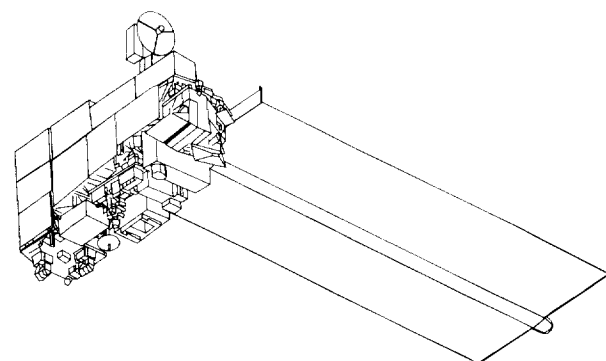
*Mr. Dougherty is the Observatory Systems Manager on the HST mission. Mr. Dougherty earned a B.S. in Aerospace Engineering from the University of Texas at Austin and is currently working on an M.S. in Computer Science at the Johns Hopkins University. He has been at GSFC for 2 years, where he works in the Operations and Ground Systems Project in the HST Operations and Ground Systems Project, managing the HST operations engineering staff.*

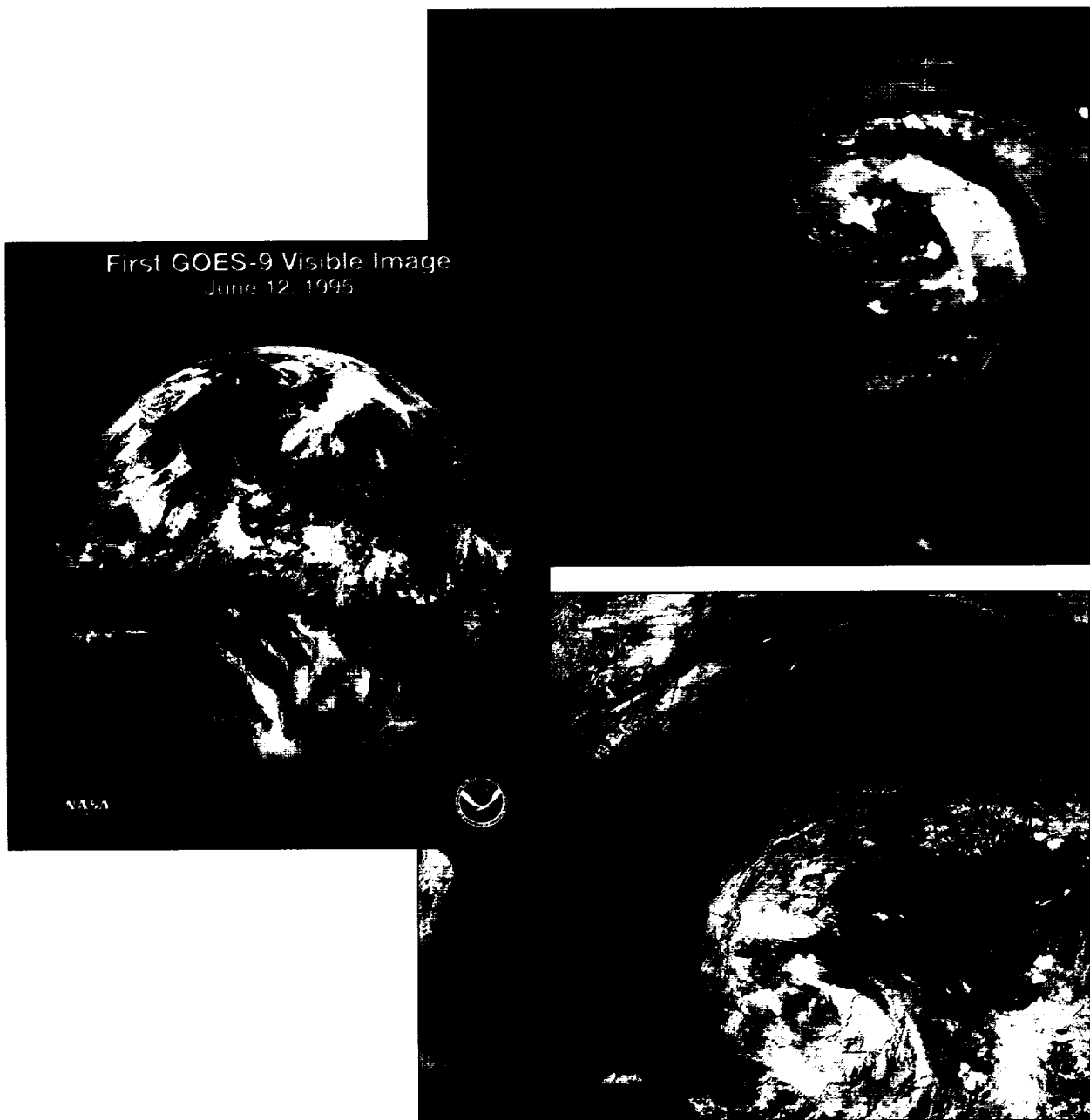


---

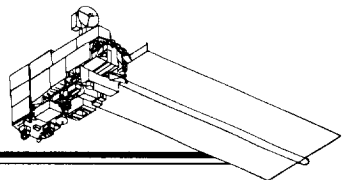
---

# ***FLIGHT PROJECTS***





Shown above are high-quality, color-enhanced images of Hurricanes Felix and Roxanne taken by the GOES-9 spacecraft subsequent to its launch on May 23, 1995. Superimposed over them is the first visible image taken by GOES-9 on June 12, 1995, of the western hemisphere.



# FLIGHT PROJECTS

THIS PAST YEAR has been a successful one for the Flight Projects Directorate. Following on the heels of the successful launch of NOAA-J on December 30, 1994 from Vandenberg Air Force Base (VAFB), 1995 ends with the successful launches of the Solar and Heliospheric Observatory (SOHO) and the X-ray Timing Explorer (XTE) from Kennedy Space Center. SOHO carries the GSFC-developed ultraviolet coronagraph spectrometer into orbit as part of a continuing campaign to study the interaction between the Earth and the Sun. The XTE will study X-rays, including their origin and emission mechanisms, and the physical conditions and evolution of compact X-ray sources within the Milky Way galaxy and in the nuclei of other galaxies which may harbor supermassive black holes. Equally successful and exciting was the flawless launch of GOES-9 (now GOES-East and West) on May 23, 1995, whose images upon reaching orbit were even better than those achieved earlier by GOES-8; the computer color-enhanced images of hurricanes Felix and Roxanne are of the highest quality.

As of this writing, the Polar Plasma Laboratory stands ready for an early February 1996 launch from VAFB. The second of two space physics laboratories in the Global Geospace Science program, Polar is using the lessons learned from the success of the Wind mission which has been operating flawlessly since its November 1994 launch. Polar's eleven science instruments will measure the entry and transport of solar plasma over the Earth's magnetic poles, and observe the energy exchange between the magnetosphere and the ionosphere. Polar will also provide global imaging of the northern aurora.

Not to be outdone by the aforementioned launches on unmanned Delta and Atlas expendable vehicles, TDRS F-7 was successfully launched on the STS-70 (Discovery) on July 13, joining its five predecessors now in orbit to form the Tracking and Data Relay Satellite System (TDRSS). Temporarily delayed when a pair of

woodpeckers tried to nest in the insulation surrounding the Shuttle's main external fuel tank, with its launch and subsequent positioning, TDRS F-7 becomes the last in a series of geosynchronous spacecraft that provide NASA with its primary means to communicate with and gather data from many of its low-Earth-orbiting satellites. These include the Hubble Space Telescope (HST), the Compton Gamma-Ray Observatory, Landsat, the Space Transportation System, and many others.

Meanwhile, a large contract has been awarded for the building of the EOS PM-1 and EOS Chem-1 spacecraft. PM-1 and Chem-1 will join the first EOS spacecraft (AM-1), for launch in 1998. EOS, the linch-pin of the Mission to Planet Earth (MTPE), is a long-term, co-ordinated program to study the Earth as a single, global system. EOS will greatly expand MTPE's scope, with benefits ranging from improved long-term weather forecasting to a greater understanding of the interactions between the Earth's various subsystems, and of the Earth's climate.

The year was not without disappointment. Technical problems with the Pegasus XL launch vehicle have postponed once again the launch of the Total Ozone Mapping Spectrometer (TOMS)-Earth Probe, Fast Auroral Snapshot Explorer (FAST), and Submillimeter Wave Astronomy Satellite (SWAS). TOMS scientists are concerned about the loss of global total columnar ozone data, particularly during the Antarctic winter, when the stratospheric ozone hole is largest. The forthcoming Satellite de Aplicaciones Cientificas-B (SAC-B)/HETE launch is also affected by the delay in the Pegasus program. At this time, the Center looks forward to 1996 and the planned upcoming launches (in addition to those mentioned above) of CLUSTER, NOAA-K, the Advanced Earth Observation Satellite (ADEOS), and, in the first quarter of 1997, the second HST servicing mission. The Flight Projects Directorate looks forward to a challenging and rewarding 1996.

*Howard K. Ottenstein*

### EOS AM-1: PROJECT UPDATE

**E**OS AM-1 is the initial component of NASA's Earth Observing System (EOS). EOS serves as the centerpiece for Mission to Planet Earth (MTPE), and is to provide satellite observations to determine extent, causes, and regional consequences of global climate change. EOS AM-1 is specifically focused on the characterization of terrestrial and oceanic surfaces; clouds, radiation, and aerosols; and the Earth's radiative balance. It carries five advanced instruments: Advanced Spaceborne Thermal Emission and Reflection Radiometer (ASTER), Clouds and Earth's Radiant Energy System (CERES), Multiangle Imaging Spectroradiometer (MISR), Moderate Resolution Imaging Spectroradiometer (MODIS), and Measurements of Pollution in the Troposphere (MOPITT). They are provided by the Ministry of International Trade and Industry of Japan, NASA's Langley Research Center, the Jet Propulsion Laboratory, GSFC, and the Canadian Space Agency, respectively. The project is currently in its C/D Phase, and is maintaining schedule for a June 1998 launch. The EOS AM-1 project is managed by GSFC.

In January 1995, the spacecraft Critical Design Review (CDR) was successfully completed. This followed the successful completion of all component and subsystem CDRs in 1994 and 1995, which included CDRs for the thermal, command and data handling, guidance navigation and control, power, structure, propulsion, harness, communications subsystems, ground support equipment, and flight software/firmware systems.

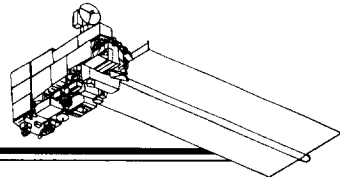
During the past year, fabrication, assembly, and testing were successfully completed for the majority of the spacecraft engineering development modules (EDMs) and engineering test modules (ETMs). These included the power equipment module EDM testing, which verified acoustic and structural mode and strength characteristics, along with fabrication and handling techniques for general application to the other equipment modules; the solid-state recorder EDM testing, which demonstrated throughput/producibility; the electrical power subsystem ETM testing, which verified subsystem performance and functionality; various direct access system component ETM (e.g., antenna, solid-state power amplifier/transmitter, upconverter, and modulator) testing, which demonstrated link margin and functionality; and science formatting equipment ETM testing, which verified compliance with critical performance requirements like high-rate science data throughput. Qualification testing of the solar array drive

and nonexplosive actuator high-gain antenna and solar array release mechanisms will be completed later this year.

The Capillary Pumped Loop (CAPL) II experiment was successfully flown on the Space Shuttle in September 1995. This rear-bay Hitchhiker payload was a capillary pumped heat transport system (CPHTS) that closely approximated the design of the EOS AM-1 CPHTS. Its purpose was to demonstrate the operation of a full-scale CAPL in microgravity, validate fluid management and startup techniques, verify operation of a heatpipe heat exchanger radiator design, study pressure losses in two-phase systems, and develop and update two-phase analytical models. Results indicate that CAPL II performed as expected, and give high confidence for the performance of the EOS AM-1 CPHTS.

All instrument CDRs were completed successfully in 1994 and 1995. ASTER's interface CDR was held in November 1994, and MISR's and MOPITT's in December 1994. MOPITT's CDR for the Canadian Space Agency held in July 1995. Engineering model functional, performance, and environmental testing have been completed for all of the instruments, with the exception of MOPITT. The MOPITT engineering qualification model is currently undergoing thermal vacuum testing, and will be sent shortly to the David Florida Laboratory in Ottawa for structural qualification testing; completion is scheduled for the end of October 1995. Spacecraft Interface Simulator (SIS) testing has been successfully completed on the ASTER, MODIS, and MISR engineering model instruments. The SIS tests provide verification of all instrument-to-spacecraft electrical interfaces, including low- and high-rate science data, command and telemetry, time mark and frequency, relay drive commands, and power and grounding. The remaining engineering model instrument SIS tests will be performed by the end of 1995. Instrument flight model hardware/software is currently being fabricated and integrated. The flight model instruments will be delivered to Lockheed Martin Astro Space for spacecraft-level integration and testing between mid-1996 and early 1997.

NASA's Lewis Research Center awarded the Atlas IIAS launch vehicle contract to Lockheed Martin Space Systems in December 1994. Payload adapter design and fabrication is underway. The launch readiness date is in June 1998, and the project is on track to achieve that goal.



Contact: Christopher Scolese (Code 421)

301-286-9694

Steven Neeck, Code (704.3)

301-286-3017

Francesco Bordi/CSC

301-464-7478

Sponsor: Office of Mission to Planet Earth

*Mr. Scolese is currently the EOS AM Project Manager responsible for the development of the five EOS AM instruments, the CERES instrument for TRMM, the EOS AM spacecraft, the interface with the Earth Science Data and Information System, and the integration and launch of these elements. Prior to assuming these duties, he served as the EOS Systems Manager responsible for the EOS system architecture and the integration of all facets of the project. Mr. Scolese obtained a B.S. in Electrical Engineering from the State University of New York at Buffalo and an M.S. in Electrical Engineering in Computer Science from the George Washington University. Mr. Scolese is the recipient of several honors including the NASA Outstanding Leadership Medal.*

*Mr. Neeck is Senior Instrument Systems Engineer supporting the EOS AM Project of the Flight Projects Directorate at GSFC. In that capacity he has overseen the design and*

*development of the ASTER, CERES, MISR, and MOPITT EOS AM-1 instrument/spacecraft interfaces during the project's C/D Phase. Prior to joining GSFC in 1986, he held related positions in academia and private industry associated with the design, development, and application of remote sensing technology. He received B.S., M.A., M.S., and M.Sc. degrees from Rochester Institute of Technology, Johns Hopkins University, University of Connecticut, and University of London (UK), respectively, and is a member of Phi Kappa Phi, Delta Phi Alpha, and Sigma Xi.*

*Dr. Bordi is a systems scientist on the EOS AM Project at GSFC and a section manager for Computer Sciences Corporation (CSC) on the Systems Engineering and Integration Management Support Services contract. Dr. Bordi joined both CSC and the EOS project in October 1988. From 1985 to 1988, Dr. Bordi was a senior analyst with ST Systems Corporation, and the leader of a team of physicists and computer scientists developing scientific data processing software for the COBE mission. Dr. Bordi received his doctorate in theoretical physics from the University of Florence (Italy) in 1980 and, until 1985, carried out scientific research at the Johns Hopkins University, the University of Geneva (Switzerland), the National Institute for Nuclear Physics (Italy), and the Massachusetts Institute of Technology.*

## ENVIRONET SATELLITE END-OF-LIFE DISPOSAL COMPUTATIONAL MODEL

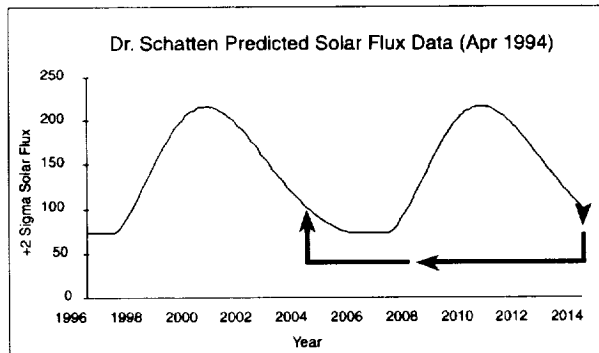
**T**O LIMIT FUTURE GENERATION of manmade debris in space, NASA adopted a set of requirements (NMI-1700), to be placed on all future satellite projects. One of the key options of the NMI-1700 is to have the satellite naturally decay into the Earth's atmosphere at the end-of-life (EOL). The need arises then to create an easy to use means of allowing mission planners to predict the amount of time it will take for their satellite to decay naturally from the mission orbit. If the time predicted is greater than 25 years, steps will have to be taken to have the satellite decay in the desired time.

Several tools have been developed to predict the time to decay for a satellite. One such program written by Dr. Philip Anz-Meador of Johnson Space Center has been available as part of the EnviroNET service for the last 4 years. This tool predicts the drag on a satellite generated by the space environment and then computes the time it would take for the satellite to decay. This model provides a very rough approximation of the time to decay. One of the reasons this model only provides a rough approximation is that as it stands, the model uses a static value of the solar flux for the entire decay period. Since the decay period of a satellite could reach 25 years or more, it became obvious that since the solar cycle is about 12 to 13 years, the satellite might see almost 2 complete solar cycles. Thus, a static value of solar flux would not be an accurate prediction, especially if the user of the program has no idea what an accurate value might be.

To solve this problem, EnviroNET has developed a version of this model that accesses the predicted solar flux values provided to NASA by GSFC's Dr. Kenneth Schatten. Dr. Schatten's predictions are considered to be the standard for predicting the future solar environment. These data are viable for use with Anz-Meador's orbital decay problem. However, since Dr. Schatten only predicts data for the next two cycles, the predicted solar flux data set only goes to the year 2014. Since most current projects (like EOS AM-1) will have an EOL of 2004 or later, a cutoff of 2014 does not provide enough data for solar flux prediction.

Observing that the Schatten data did have an obvious pattern and did repeat itself, it became clear that the data

could be extended by picking a point in the data that existed one solar cycle earlier. The first figure displays the method taken for providing predicted solar flux values beyond the year 2014 for the orbital decay model.



*Solar flux prediction for years greater than 2014.*

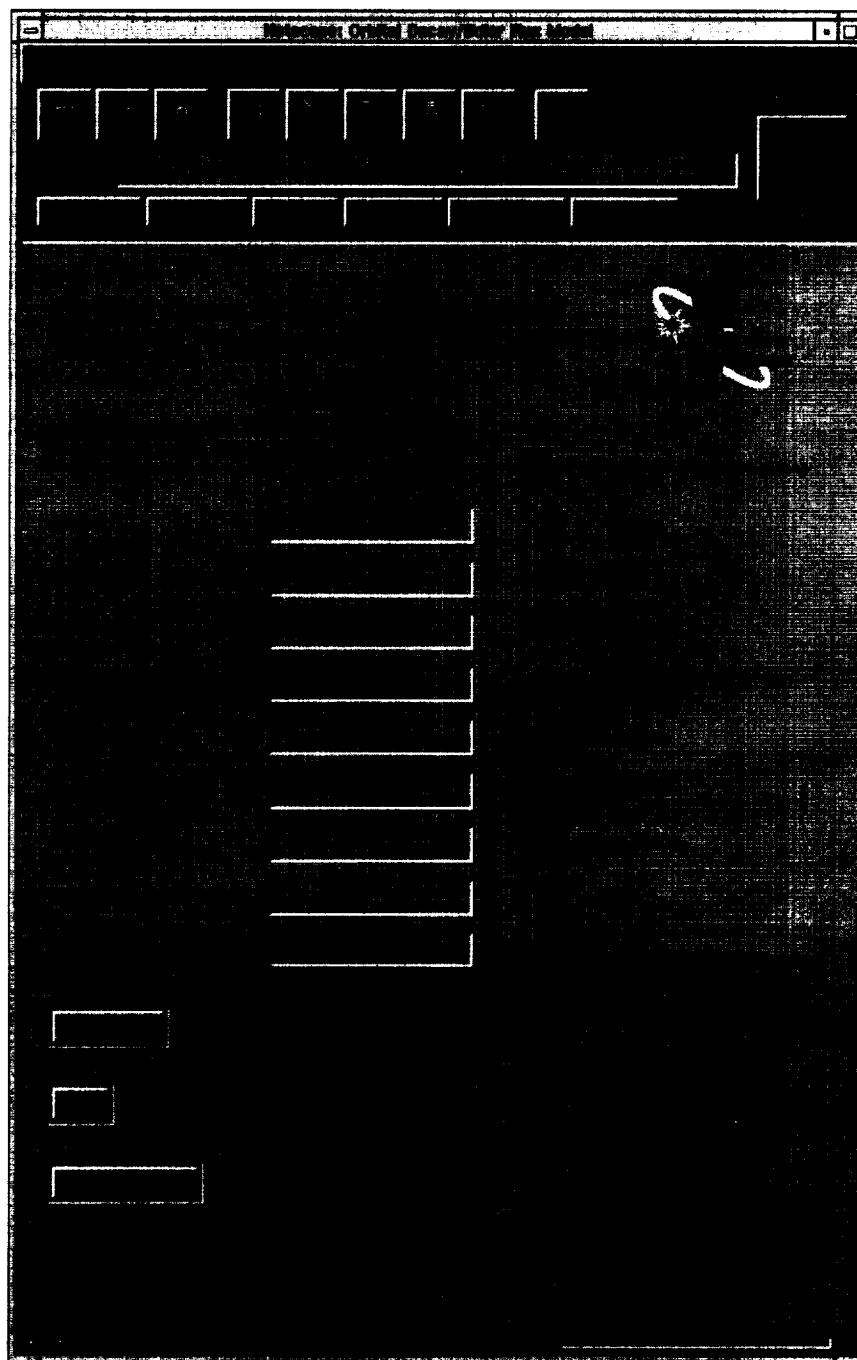
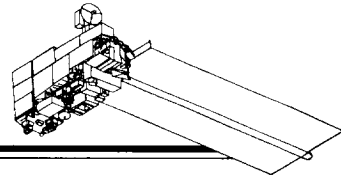
Once completed, the model was compared to analyses performed for the EOS AM-1 spacecraft, and the model produced identical results to the decay times predicted by GSFC's Flight Dynamics Branch. The model was developed for use on the World Wide Web, as shown in the second figure, to allow quick and easy access to the tool.

Currently, the model is not available to everyone on the Internet, protected by a username and password. EnviroNET is willing to perform analyses for projects requesting an EOL decay time to be predicted for them. If there is great interest in the model and after more testing, it might be made available to members of the space science community.

Contact: Michael Lauriente (Code 400.1)  
301-286-5690

Sponsor: Office of Safety and Mission Assurance

*Dr. Lauriente is Manager of EnviroNET, the Space Environment Information Service. He earned a B.S. and an M.S. from Michigan Technological University and a Ph.D. in Engineering from the Johns Hopkins University in 1955. He has been at GSFC for 13 years.*



*World Wide Web interface for mission EOL decay model.*

### NASA LESSONS-LEARNED INFORMATION SYSTEM WORLD WIDE WEB INTERFACE

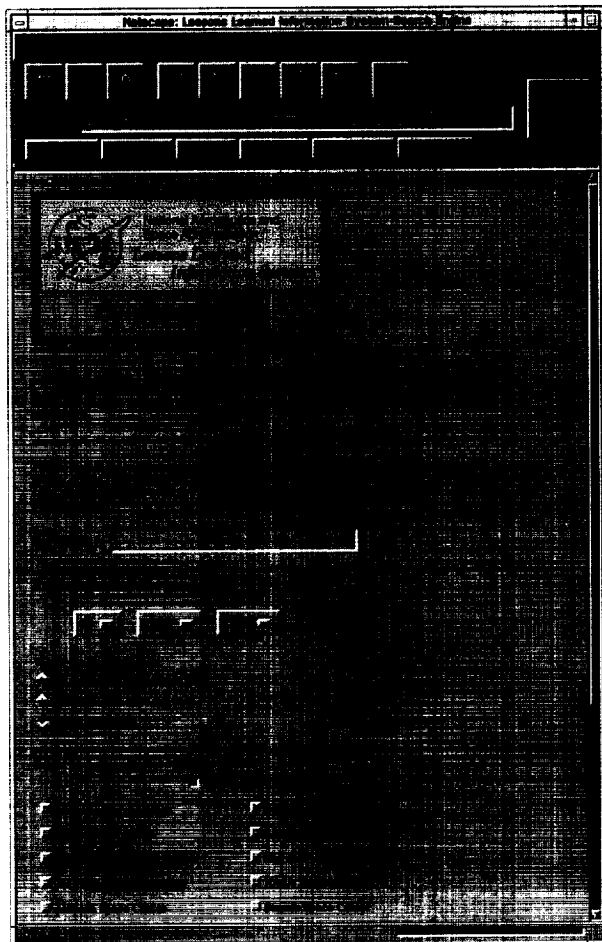
THE GOAL OF the NASA Lessons-Learned Information System (LLIS) is to collect and make available for use by all who may benefit from the experience of others, the lessons learned from almost 40 years in the aeronautics and space business. Both government and industry have long recognized the need to document and apply the knowledge gained from past experience to current and future projects to avoid the repetition of past failures and mishaps. Through the LLIS, NASA seeks to facilitate the early incorporation of safety, reliability, maintainability, and quality into the design of flight and ground support hardware, software, facilities, and procedures.

The first step in successfully implementing a system like the LLIS is the development of the interface for its use.

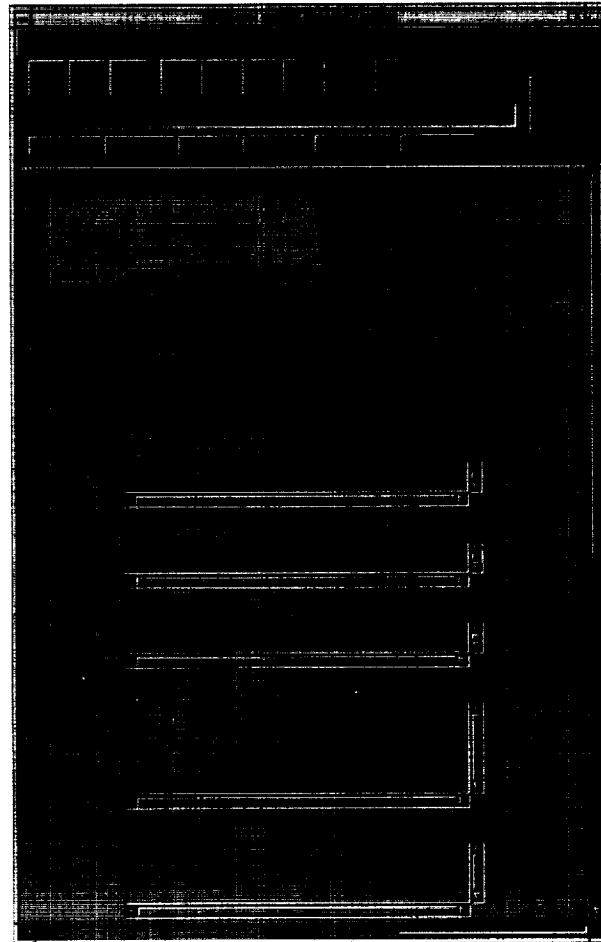
In the past, access to the LLIS has been provided in a variety of ways. Recently however, with the explosion of the Internet and the World Wide Web (WWW), it has become clear that the best place to offer the LLIS is on the WWW. EnviroNET has been commissioned to develop a fully functional interface for the LLIS database. EnviroNET was given the opportunity based on a 10-year history of developing its own system with a user-friendly interface and increasing its user community to over 5000 world wide.

The requirements for the LLIS interface were simple:

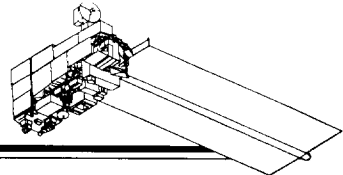
- make it easy to use and allow for ease in learning how to use it;



LLIS search engine interface.



LLIS lesson submission form.



- provide a means of performing a search based on a variety of factors on the lessons database;
- allow users to contribute to the system by submitting their own lessons to a Center Data Manager for approval and eventual inclusion into the database; and
- restrict access of the entire database to computers in the NASA Internet domain (.nasa.gov) only, and provide access to NASA contractors in other domains as necessary.

Using experience gained in the creation of the EnviroNET home page, the EnviroNET staff developed a fully functional prototype system in less than 1 month's time to present at the annual Lessons-Learned Steering Committee meeting. The members of the committee agreed that the interface did meet the requirements set forth and that it would be the interface used for the LLIS database.

The interface was created for the WWW by developing the necessary forms in the hypertext markup language and writing the necessary search routines in the Practical Extraction and Report Language (PERL), a scriptable programming language. All of the work that was done for the creation of the LLIS interface was done by EnviroNET staff, no commercial packages needed to be purchased to implement the interface. For the incorporation of each lesson into the database, a utility was written in PERL to generate an alphabetical index of every word

in every lesson. The search engine (written in PERL) executes a binary search through the word index for the keyword(s) entered by a user and returns the lessons that contain the keyword(s) for which the search was conducted. This technique allows for a very rapid search of the database.

Other features of the interface include a help utility which defines all of the inputs presented to the user. Each input's help entry can be easily accessed by selecting the input name. Users may also find out more information about what has been recently added to the system and may also submit comments on how they feel the system can be improved.

The LLIS interface now has access to the entire database. Lessons can be easily be added on a regular basis. An EnviroNET staff member is dedicated to the maintenance of the LLIS interface so that the system is guaranteed to maintain operation 24 hrs per day, 7 days per week.

Contact: Michael Lauriente (400.1)  
301-286-5690

Sponsor: Office of Safety and Mission Assurance

*Dr. Lauriente is Manager of EnviroNET, the Space Environment Information Service. He earned a B.S. and an M.S. from Michigan Technological University and a Ph.D. in Engineering from the Johns Hopkins University in 1955. He has been at GSFC for 13 years.*

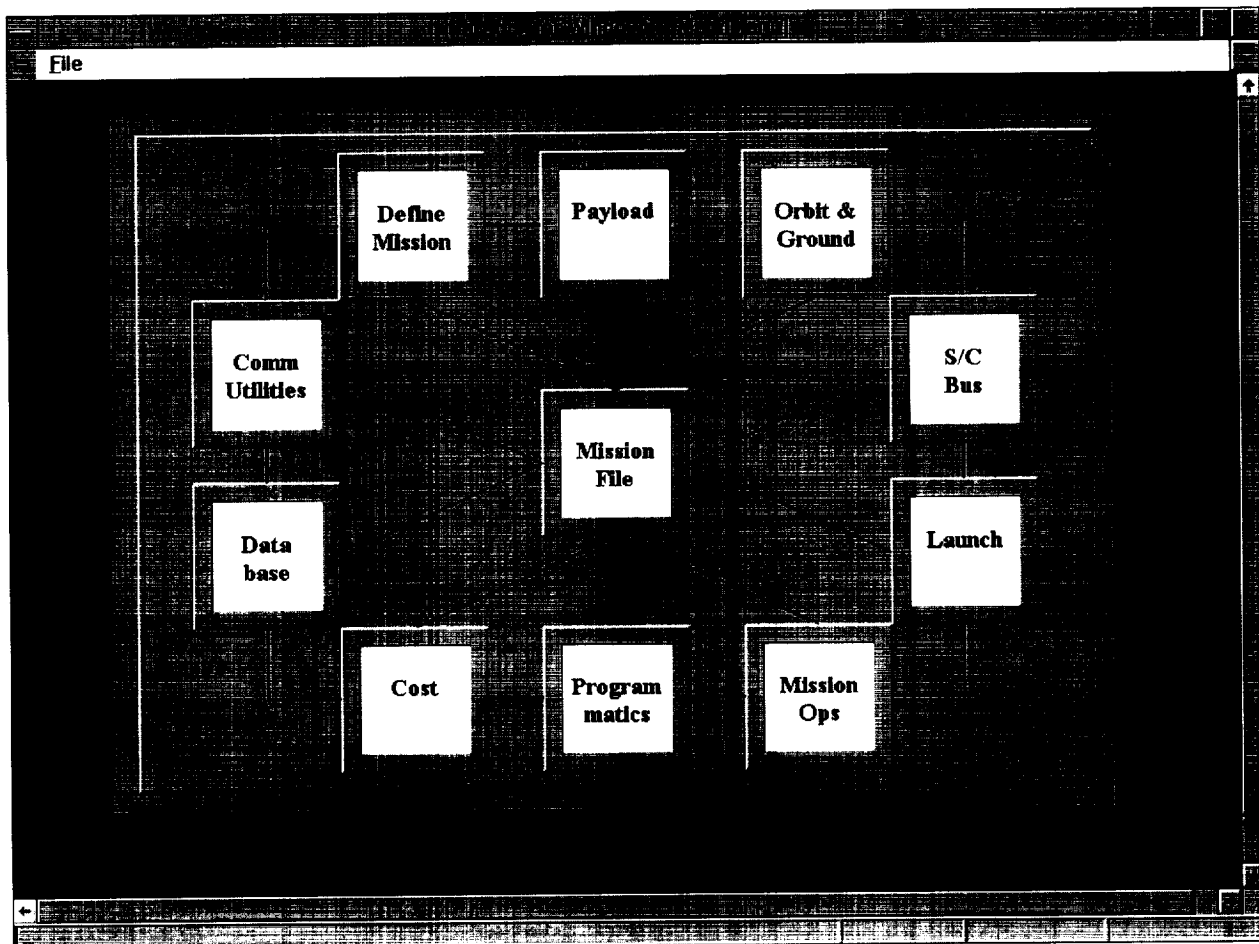
### ADVANCED SYSTEM SYNTHESIS AND EVALUATION TOOL

NASA IS CHANGING the new program start process. One change will be to streamline interactions among and between NASA centers and other teamed organizations, which can include industry, academia, and other government or government-supported labs. Being competitive in this environment requires a more structured and disciplined approach to the conceptual design process than has been applied to date. The conceptual design product must be developed to a greater level of technical and cost detail, and in a shorter time.

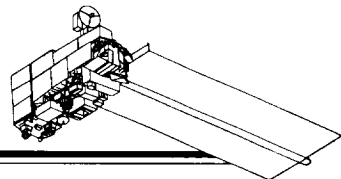
In addition to greater efficiency in conceptual design processes, NASA also must become more efficient in evaluation processes. With various organizations responding to NASA's Announcements of Opportunity,

numerous proposals must carefully be evaluated by a small, isolated group in a short time. This group must have the knowledge base and access to the tools to evaluate proposals based on scientific merit and engineering rationale.

The Advanced System Synthesis and Evaluation Tool (ASSET) is being developed to assist conceptual design teams and proposal evaluation teams in meeting the challenges described above. ASSET is being developed with a modular structure, capable of accommodating and integrating a variety of software tools, updates, and changes, as needed. The functionally related tools are grouped together, and can be executed from ASSET's Main Menu, as shown in the figure.



ASSET's main menu screen.



Upon completion of its development, ASSET shall be able to

- support a design effort in developing mission concepts and assist the proposal evaluation team by providing an engineering “sanity” check. At the same time, ASSET shall be capable of capturing the design and/or evaluation process; provide the capabilities for capturing requirements, analyzing several mission architectures based on preset criteria, capturing the rationale behind the mission concept, and analyzing the overall mission reliability;
- provide the capability to perform standard mission analyses, such as instrument viewing capabilities, orbit selection, ground communication opportunities, spacecraft subsystem analysis, mission operations analysis, and resource management analysis;
- perform preliminary costing, especially relative costing for design alternatives, and define inputs for more sophisticated cost models;
- provide a database for launch vehicle selection. This database will contain performance curves, working envelope drawings with dimensions, payload adapter drawings with dimensions, insertion errors, etc.;
- provide a database of prior sensor parameters to allow rapid development of preliminary payload requirements;
- provide a database of subsystem components for catalogue items, and a methodology for defining noncatalog subsystem components such as power supply electronics. New technology items will be included with appropriate risk/development schedule information. Special emphasis will be placed on components and new technology applicable to small spacecraft;
- provide a database of design parameters for previously flown and currently available spacecraft to give “off-the-shelf” options for the current study. Special emphasis will be placed on small spacecraft;
- provide the capability to communicate with remote data files and remote users. This can be implemented through e-mail and/or Internet browsers;
- provide an accessible “current design” data file to maintain configuration control of the design. This data file shall capture the pertinent design features so that the study can rapidly proceed into a more detailed design phase without loss of data and the need to again develop these items. In addition, the data file shall be structured such that it provides interconnectivity between all the software modules;
- provide a user-friendly interface with default values that can be used for most parameters, and a defined list of selectable values for other parameters; and
- provide the capability to generate products for studies and mission analysis reports.

Support for the ASSET development has been provided by Timothy Rivenbark of McDonnell Douglas Aerospace.

Contact: John Oberright (Code 401)  
301-286-9653

Ronald Leung (Code 401)  
301-286-9407

Sponsor: Office of Space Science  
Office of Mission to Planet Earth

*Mr. Oberright is Chief of the Mission Integration Office. He earned a B.S. in Mechanical Engineering from Catholic University in 1966. Mr. Oberright has been employed at GSFC for 29 years, where he has worked in both the Engineering Directorate and the Flight Projects Directorate.*

*Mr. Leung supports the ASSET development and new technology research for the Mission Integration Office. He earned a B.S. in Electrical Engineering from the University of Maryland in 1975, and an M.E.A. with a major in Research and Development from George Washington University in 1983. Mr. Leung has been employed at GSFC for 8 years. He worked as the Systems Manager for the Tracking Data Relay Satellite before his recent transfer to the Mission Integration Office.*

## REMOTE MANIPULATOR SYSTEM CONTROL USING FUZZY LOGIC

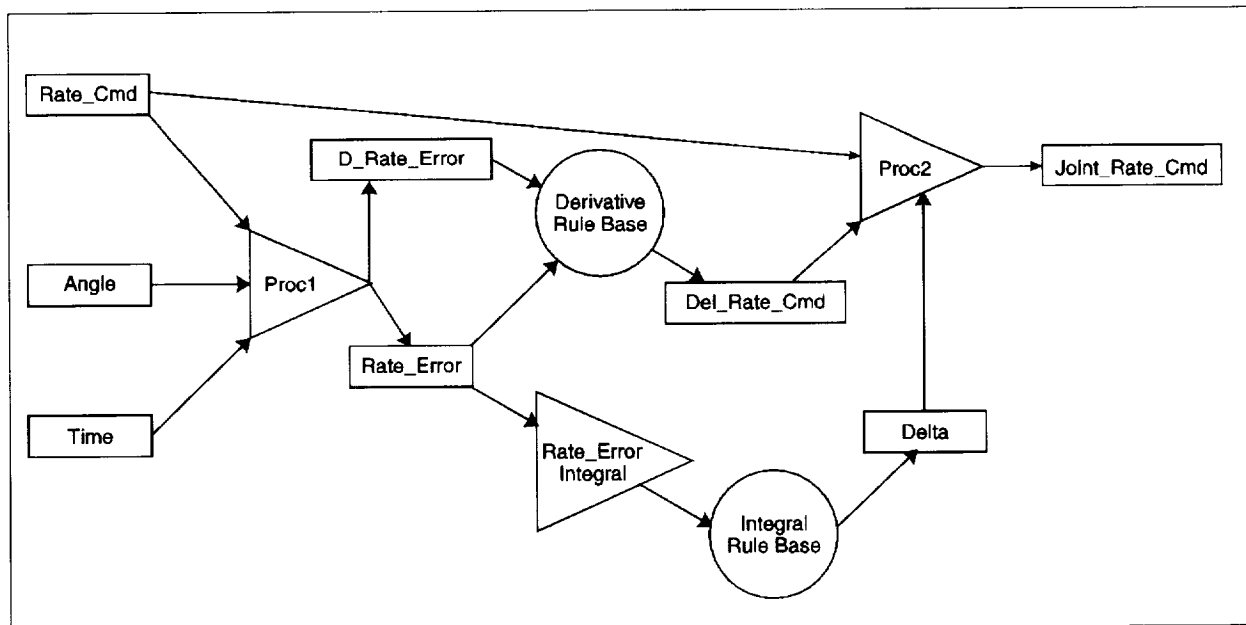
THE HUBBLE SPACE TELESCOPE (HST) Flight Systems and Servicing Project has developed and implemented a fuzzy logic system to control a remote manipulator system (RMS). The GSFC RMS consists of a 6-degree-of-freedom arm, software based on shuttle RMS Flight Software Systems Requirements (FSSR), and a fuzzy logic controller for controlling the six joint rates for the required levels generated by the FSSR software.

The FSSR system generates the joint rate command required to move the point of resolution (POR) of the robotic arm based on commands generated by remote manual operation of translational and rotational hand controllers. Since operating characteristics of robot arms can vary dramatically due to different hardware configurations and loads on the system, a command to a joint on the arm may not produce the desired rate. The function of the fuzzy logic system is to control joint rates at required levels based on feedback from joint angle encoders and their respective time tags.

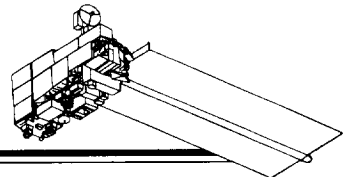
The functional flow of the fuzzy logic system for controlling the joint rates of the robotic arm at desired levels is shown in the figure. The controller design assumes that commanded rates are available to the system and that these rates, if implemented correctly, will cause the desired

motion of the end effector. Problems have arisen when certain joints of the robotic system have not responded as quickly as other joints due to design considerations, configuration of the arm, or unusual loads on the system. When some joints respond faster than other joints in a multijoint system, the end effector will not move in the desired direction until all commanded joint rates are achieved. On the other hand, if all the joints in the system reached their commanded level at approximately the same time, motion will closely match the desired trajectory, although it may be slightly slower or faster as transition to the new joint rates occur.

The fuzzy logic controller is designed to control the rate of each of six joints to match the commanded rate as computed by the FSSR. This software accepts translational and rotational rates of the POR of the arm as generated from the translational and rotational hand controllers. (For this discussion, we assume the POR is the end of the wrist roll joint.) The fuzzy logic system is being designed to take commands from an operator, convert them into joint rates required to achieve these end-effector rates through the FSSR software, and to achieve and maintain the commanded rates through fuzzy logic control, based on feedback from angle position encoders and their respective time tags, which provide the only feedback to the



RMS fuzzy logic system functional flow diagram.



control system. From these measurements, estimated joint rates are computed. From the joint rates and the Rate\_Cmd that is generated by the FSSR, joint rate errors (Rate\_Error) and changes in joint rate errors (D\_Rate\_Error) are computed. Next, Rate\_Error and D\_Rate\_Error are treated as fuzzy input variables to a fuzzy rulebase that outputs a fuzzy variable Del\_Rate\_Cmd, which is used to modify the Rate\_Cmd from the FSSR and to generate a Joint\_Rate\_Cmd as output to the joint, which will achieve the desired rate as commanded by the operator, and subsequently by the FSSR software. A second integral type correction to the input Rate\_Cmd, Delta, was introduced to smooth the commanded rate. This second delta to the Rate\_Cmd, Delta, is generated by a second fuzzy rulebase and fuzzy membership functions for the variables Rate\_Error\_Integral and Delta.

This software has been integrated into the hardware/software system. Tuning has been completed, and initial test runs have given good results. This system has performed at least as well as a PID controller, with the added important advantage of ease of modification of the rulebase, which will be required to adjust for the effects of cross-correlation of the joints during normal operation of multiple joints simultaneously. Additionally, this method

will be easily transferred to the industrial community, since this model is not strongly dependent on the size, weight, or number of joints in the arm under consideration. Initial results have indicated that commanded joint rates can be achieved and maintained with this methodology even if the transfer function is difficult to model and varies considerably with different configurations of the arm.

Contact: Joe Mica (Code 442)  
301-286-1343

Sponsor: Office of Space Science

*Mr. Mica is the Electrical Systems Manager with HST Flight Systems and Servicing Project. He earned a B.S. in Electrical Engineering from Washington University in 1978, and completed a graduate certificate in Artificial Intelligence from Washington University in 1990. Mr. Mica has been employed at GSFC for over 4 years, where he has managed the GSFC RMS Program, and was responsible for the carriers avionics systems for the first HST Servicing Mission. Mr. Mica has received awards for his outstanding contributions to the first HST Servicing Mission. Mr. Mica would like to recognize the outstanding RMS support of his colleagues, Robert N. Lea at Ortech Engineering, and Yashavant Jani at Hitachi America, Ltd.*

## THE HEMISPHERICAL RESONATOR GYROSCOPE

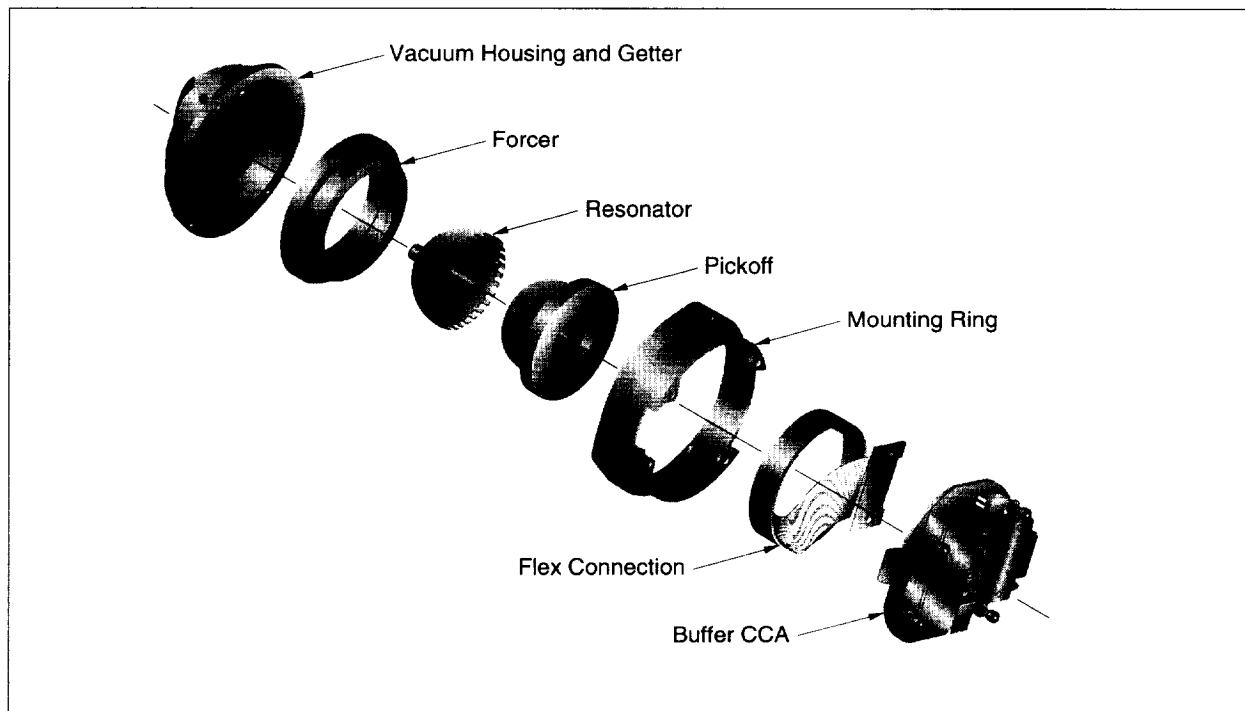
**I**N RESPONDING TO THE high-precision, low-noise gyroscope requirements of the Hubble Space Telescope (HST), Hughes Delco enhanced the mechanization of their existing commercial Hemispherical Resonator Gyroscope (HRG) to improve performance 100 times. This resulted in a 30-mm HRG that has long life, high reliability, and small size, and can be used in high-precision applications in both the government and commercial markets. The HST Project is now pursuing development of flight units for use in the 1997 and 1999 Servicing Missions.

The inertially sensitive element is a fused silica (quartz) axisymmetric shell, the hemispherical resonator. If a standing wave is established on the shell and the shell is rotated about its axis, the oscillating mass elements experience Coriolis forces that cause the standing wave to precess (rotate) with respect to the shell. The precession angle is a constant fraction of the angle the shell has rotated through. In this whole-angle mode, the HRG operates as an integrating-rate sensor. The gyro can also be caged in a force-rebalance mode and act as an angular rate sensor. Both modes have been implemented, and can be realized as two different operating modes of the same

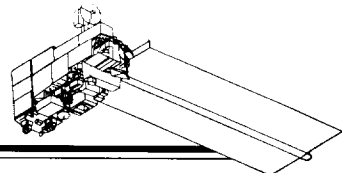
gyroscope, a unique capability among inertial sensors. Because the main structure and hemispherical resonator are fused silica, perfect matching of thermal expansion occurs.

The HRG (shown in the figure) has several advantages: it can provide full inertial quality at a fraction of the size and volume of existing gyros, it does not require a high-intensity light source (which has a limited life expectancy) or photodetectors (which are prone to radiation degradation), and it has no moving mechanical components. Since the inertial sensing is performed by the mechanics of a standing wave in the vibrating quartz shell, the HRG can "coast" through a nuclear event without loss of inertial data and in spite of temporary disabling of the electronics.

The HRG uses capacitive forcing and readout. Capacitor plates are deposited on the housing (ring forcer, discrete forcer, and pickoff electrodes). A few hundred angstroms of metallization are deposited on both the inner and outer surfaces of the shell. When the device is assembled, the shell wall comprises the second plate for a series of parallel plate capacitors.



*An exploded view of the 30-mm HRG mechanical components.*



The resonator and housings are joined with indium solder to form a hermetically sealed enclosure for the resonator. A near-vacuum is maintained in the enclosure to prevent aerodynamic damping of the resonator motion; a gas-getter maintains this vacuum. There are no moving parts other than the low-amplitude oscillation of the resonator (the peak amplitude is about 10 times the wavelength of light). Quartz was chosen as the resonator material because of its low internal damping, long-term stability, and low thermal sensitivity. These are the same properties that make quartz crystals an excellent frequency reference for radios and timekeeping.

In addition to satisfying HST's needs, the HRG's accuracy and small size make it a versatile sensor for tactical missiles and interceptors, launch vehicles and strategic missiles, and underground drilling.

The HRG can uniquely benefit drilling and surveying operations by providing a true inertial reference. The gyroscopic reference does not depend on the Earth's rotation, nor does it react to ferrous materials in the Earth. The HRG is manufactured from inherently rugged and stable fused quartz, which allows the HRG to survive severe underground forces such as vibration, shock, and high temperature.

Consisting of three pieces of quartz, its very simple construction provides ultrahigh reliability, with low maintenance and calibration requirements. The HRG is the smallest high-accuracy gyro—small enough to use in measurement-while-drilling tools. The HRG operates with the precision needed for surveying, drifting less than 0.01° per hour.

The HRG features an unparalleled angle random walk, needing only 1 second of start time and less than 2 minutes

of gyrocompassing. It offers high precision in a three-axis inertial measurement system, allowing steering of a tool to accuracy of 1 ft per 1000 ft. Its wide dynamic range makes it capable of withstanding high rpm. It can be placed close to a drill bit to optimize direction and attitude knowledge, and it can be placed in low-power mode when operational accuracy is not needed.

The HRG provides fully compensated direction and attitude outputs and performs rapid gyrocompassing, even at high latitudes. Quality control via built-in test capability gives high confidence in consistent performance. It provides digital signal processing of gyro outputs and a built-in motion detector technique.

The 30-mm Hughes Delco HRG is yet another example of how NASA requirements push industry to refine a technology, which, in turn, leads to expanded markets for that newly improved technology.

Contact: Mark Jaster (Code 442)  
301-286-9232

Sponsor: Office of Space Science

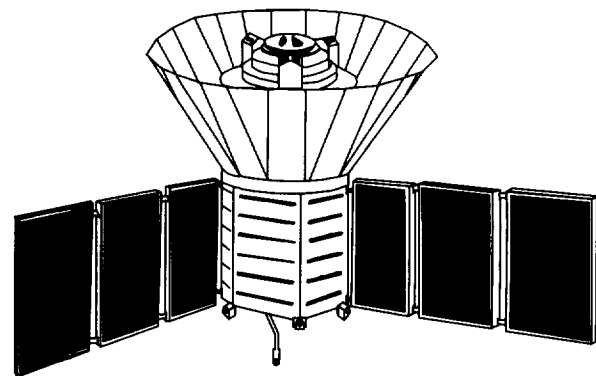
*Mr. Jaster is the Advanced Technologies Development Manager for the HST Flight Systems and Servicing Project. He earned a B.S. in Biomedical Engineering from Duke University in 1984 and an M.S. in Manufacturing Systems Engineering from Stanford University in 1990. Mr. Jaster has been employed at GSFC for 5 years, where he has managed the Servicing Aid Tool Program, led the EVA efforts supporting the HST First Servicing Mission, and is now leading an initiative to foster commercial spinoffs from the HST. He is a recipient of Goddard's Exceptional Achievement Award and the Astronaut's Silver Snoopy.*



---

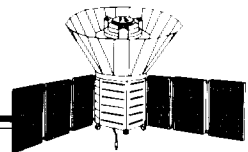
---

***SPACE  
SCIENCES***





*Spiral Galaxy Messier 101 photographed by the Ultraviolet Imaging Telescope on Astro 2.*



# SPACE SCIENCES

THE SPACE SCIENCES DIRECTORATE at the Goddard Space Flight Center investigates our space environment and the universe around us through instruments, experiments, and missions conducted by NASA and its international counterparts. In so doing, the Directorate contributes not only to scientific knowledge, but also to the advancement of cutting-edge technology.

Repeatedly, we find that the requirements of basic research drive the advancement of technology, so that solutions to practical problems often are based on engineering and physics work that has been conducted with a very different initial rationale. Two examples of work done at GSFC are particularly fitting as physicists celebrate the centennial of the discovery of x-rays by the German physicist Roentgen.

One example, the development of cadmium zinc telluride detectors for x-ray observations in space, is one of the highlights of this report. These sensors are applicable to the smaller, better, and more capable instrumentation required for progress in x-ray astronomy. Increasingly, NASA is relying on its own facilities, like those at the Goddard Center, to develop the detectors that we need, rather than counting on "trickle down" from other programs. Technology developed in the early history of x-ray astronomy has had significant application in modern society, such as for use in security scanners at airports. We can expect that the new technologies perfected by the current space program can make similar contributions.

The second example of x-ray technology developed at GSFC and that shows great future promise is the thin foil optics replication technique for x-ray astronomy. The technology was developed to advance basic research in astrophysics and cosmology, as it enables lighter and more capable focussing telescopes, operating at higher x-ray energies than predecessor methods. Typically for GSFC investigators, they are already considering how the replication technology developed here can be applied to a new generation of optics for the x-ray photolithography industry, and there are likely to be future applications of this program to medical x-ray imaging at energies higher than those usually employed.

As impressive and useful as these projects are, improvements in the technology of detectors and optics are not enough. We need progress in handling the ever-growing streams of meaningful data obtained by our space program. Favorable accounts of progress in these areas are found in several reports. For example, an area of space science that can have direct effects on our planet is space weather, an emerging discipline at the crossroads of basic science and practical applications. It deals with the phenomena of particles and fields in the region around the Earth that regularly affect operating spacecraft, the Earth's upper atmosphere and magnetosphere. These phenomena even have effects on societal infrastructure and activities on the ground, as when a utility power grid is overloaded during a geomagnetic storm, or when the electronics along a pipeline suffer interference from Earth currents induced by disturbances aloft. The new COHOWeb system provides timely access to space weather data, which, with its predecessor OMNIWeb, may provide a model for data systems that could provide interactive access over the World Wide Web.

In another article, we find a discussion of an object-oriented approach to astrophysical data bases, which provides a much better tool than the conventional relational data bases that have been in vogue until now to allow users to mine the vast treasure troves of scientific information amassed by the space program. Application of these and similar techniques can benefit other disciplines and interests, as well.

Articles in this section of the Report also provide an overview of continuing progress in astrophysics, space physics, and planetary sciences, ranging from investigations of the galactic bulge of the Milky Way and the observatory site capabilities of the South Pole, to a discussion of the presence of ammonia on Jupiter.

Based on reports such as these, we can expect that in coming years reports describing the newest missions and experiments designed and carried out by scientists at the Goddard Space Flight Center will be equally exciting and useful in areas far-removed from the space program.

*Stephen P. Maran*

## SOLAR SYSTEM

## NEW SCIENCE FROM ARCHIVED DATA: HAWKEYE OBSERVATIONS OF HIGH-LATITUDE RECONNECTION OF MAGNETIC FIELDS

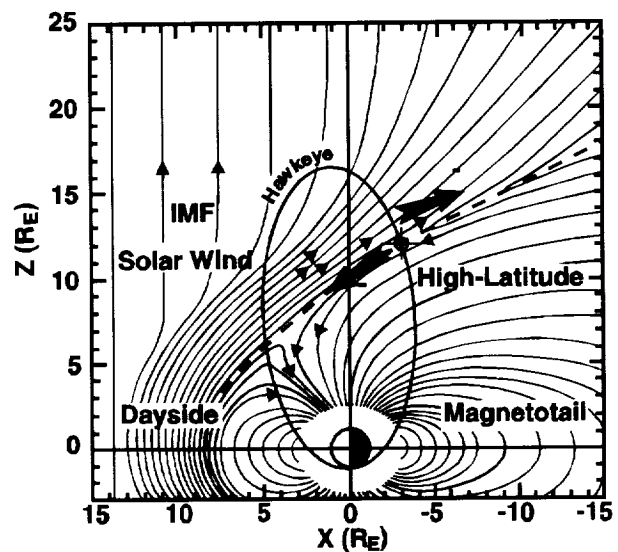
**T**HREE IS A TENUOUS stream of particles flowing from the Sun to the Earth, carrying solar magnetic fields along with them. This supersonic flow of particles is called the solar wind, and the solar magnetic fields stretching away from the Sun are termed the interplanetary magnetic field (IMF). The Earth has its own magnetic field produced from its iron core, and its own particles flowing in complicated patterns in the atmosphere and above. When the interplanetary fields and solar wind particles encounter the Earth's fields and particles there is conflict and standoff. The interplanetary fields drape around the Earth's magnetopause, a thin region separating the interplanetary and terrestrial magnetic fields. The solar particles mainly flow around the Earth's magnetopause and continue on towards the outer planets. But in a confined region on the magnetopause surface there can be an interaction: the interplanetary and terrestrial fields can "reconnect," or merge, and solar particles can flow into the Earth's magnetosphere.

Nearly 35 years ago, Jim Dungey predicted that during periods when the IMF had a southward direction, merging should take place on the equatorial magnetopause. He also predicted that during periods of northward-directed IMF, merging should move poleward of the cusps to the high-latitude magnetopause. Since that time, *in situ* observations have provided conflicting results concerning the occurrence patterns of magnetic reconnection on the magnetopause. Most of the statistical studies have been conducted at the dayside magnetopause, with some in the magnetotail (the region stretching back behind the Earth, away from the Sun), but none at the high-latitude magnetopause. Recently, however, evidence of reconnection at the high-latitude magnetopause has been revealed, from observations of the high-latitude magnetopause obtained from the Hawkeye satellite.

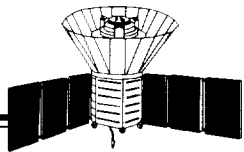
Hawkeye (Explorer 52) collected data from June 3, 1974, until April 28, 1978, supplying nearly four years of continuous coverage. Hawkeye flew in a polar orbit with an inclination to the Earth's equator of nearly 90°, an apogee of 20-21 Earth radii ( $R_E$ ), and a period of 51.3 hours. During each orbit, Hawkeye crossed the magnetopause boundary at least twice, and more often if the magnetopause was in motion. Using the data obtained from the Hawkeye satellite, direct observations of reconnection at the high-latitude magnetopause during northward-directed IMF have recently been presented.

This work was possible because the 20-year-old Hawkeye data are archived at the National Space Science Data Center (NSSDC), and are available on-line to researchers, schools, and the general public. The combination of easy access and the availability of state-of-the-art tools that have been developed in the past few years make the Hawkeye data look like those from a "new" satellite.

The first figure shows a global picture of reconnection during a period of northward IMF. The arrows indicate the flow directions. At the high-latitude magnetopause, the Earth's locally southward-directed magnetic field "reconnects" to the IMF's locally northward-directed magnetic field. At the reconnection site there is a magnetically neutral point or region (shown in the first figure as a gap) where the magnetic configuration is unstable. Plasma is accelerated as the reconnected field lines shorten, like the action of a catapult under tension. More precisely, the plasma is accelerated by an induced electric field tangential to the magnetopause, and the energy associated with the magnetic configuration is converted into particle energy. The magnetic field (just outside the magnetopause), initially is composed of open field lines,



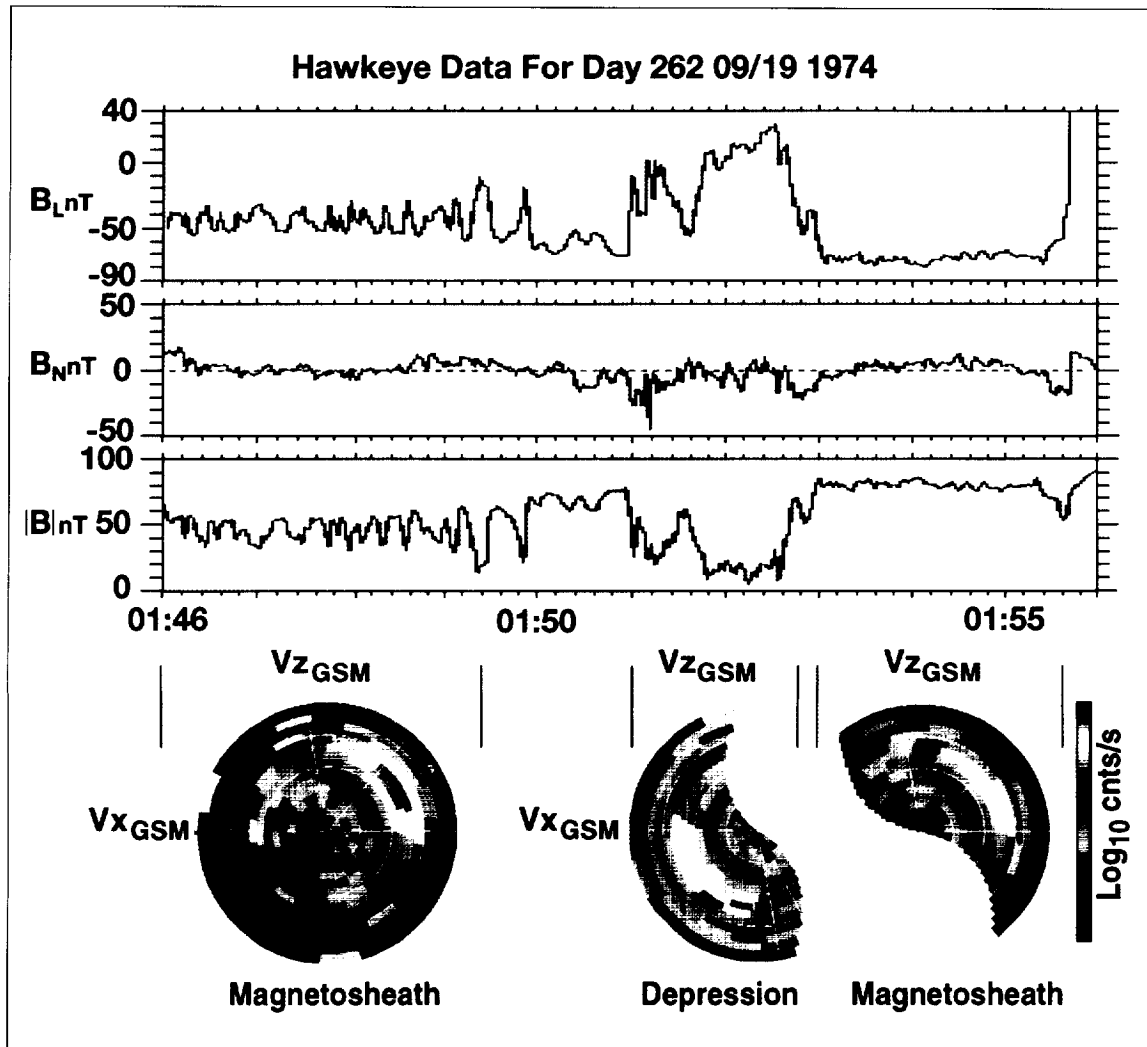
Depiction of the near-Earth magnetic field during northward IMF when high-latitude reconnection is occurring tailward of the cusp. A full Hawkeye orbit is sketched over the field lines to highlight Hawkeye's passage through the various magnetospheric regions. The arrows indicate flows near the reconnection region.



but at least one end attaches to closed field lines by the reconnection process, while the other end remains open in the solar wind. High-latitude reconnection can also create open field lines extending down the tail from previously closed tail field lines.

In a closed magnetosphere, magnetic field lines of the interplanetary medium do not connect to the Earth's field,

and the magnetopause is a tangential magnetohydrodynamic discontinuity (TD). A TD separates two regions with different flows that can only interact through diffusion. A pressure balance is maintained, but there is no component of the magnetic field normal to the magnetopause. If reconnection takes place and the magnetosphere is open, the magnetopause becomes a rotational discontinuity (RD). Plasma data can be used to check for



The top three panels display Hawkeye magnetic field observations, and include from top to bottom, respectively, the  $B_L$  component, the  $B_N$  component, and the magnitude. Partial proton distributions obtained with the Low-energy Proton-Electron Differential Energy Analyzer instrument are shown below these panels, and correspond to the three identified regions, that is, the magnetosheath (0146 UT to 0150 UT), depression (0151 UT to 0153 UT), and magnetosheath (0153 UT to 0155 UT). The radial direction represents energy, from 100 eV at the center to 40 keV at the edges; the angular direction represents measured plasma flux in that direction.

the existence of a moving frame of reference in which plasma flow is aligned with the magnetic field and has a particular speed (Alfven speed). If these conditions are met, then the discontinuity is an RD. Additionally, if the change in magnetic field across the discontinuity is proportional to the change in plasma velocity, then tangential momentum balance is maintained.

The second figure shows Hawkeye magnetic field and plasma observations near a high-latitude reconnection region. The magnetic field is in boundary-normal coordinates, in which the magnetopause is modeled as a planar surface,  $B_N$  is the component normal to this surface, and  $B_L$  is along the surface. Three regions are displayed: the magnetosheath (just outside the magnetopause), a region with depressed magnetic field strength, and another magnetosheath region. Each region exhibits a distinctly different magnetic field magnitude and orientation (identified most strongly in the  $B_L$  component). The large magnetic shear between regions along with the nonzero  $B_N$  component strongly suggests the presence of a rotational discontinuity. Partial proton distributions are shown below the magnetic field panels, and correspond to the three identified regions. The magnetosheath distributions show plasma flowing roughly tailward and northward. The middle distribution shows large numbers of sunward and southward flowing protons during the observed depression in magnetic field strength. The flow in the magnetic depression region is nearly field-aligned, approximately Alvenic, and roughly obeys tangential momentum balance, and thus is consistent with reconnection.

Hawkeye observations have provided evidence of reconnection at the relatively unexplored high-latitude

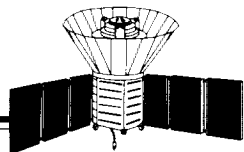
magnetopause. Because the Hawkeye data were preserved, an important discovery was possible and the way is paved for in-depth statistical studies with the entire 4-year data set. These data represent one of our national treasures, and are not easily replaceable. Even though its data are nearly 2 decades old, Hawkeye clearly remains a key data source for high-latitude magnetosphere observations.

The author would like to thank the many people who contributed to this work including S.-H. Chen, J.L. Green, S.F. Fung, S.A. Boardsen, L.C. Tan, T.E. Eastman, J.D. Craven, L.A. Frank, with thanks also to R. Kilgore for the artwork.

Contact: Ramona Kessel (Code 632)  
301-286-6596

Sponsor: Office of Space Science

*Dr. Kessel is an astrophysicist at the Space Physics Data Facility (SPDF) of GSFC. She earned an M.S. and a Ph.D., both in Physics, from the University of Kansas, and has been at GSFC for 3 years. Dr. Kessel serves as the acquisition scientist for the International Solar Terrestrial Physics Project and developed the Implementation Guidelines for International Solar Terrestrial Physics Project usage of the Common Data Format (CDF). She assists International Solar Terrestrial Physics Project scientists and programmers with CDF implementation, represents NSSDC and particularly the CDF effort to International Solar Terrestrial Physics Project investigators in various countries, and takes part in the Inter-Agency Consultative Group Science Campaigns. Dr. Kessel is presently involved in several research studies.*



## A THREE-DIMENSIONAL MAGNETOFLUID SIMULATION OF SHEAR-DRIVEN TURBULENCE: APPLICATION TO SOLAR WIND OBSERVATIONS

THE SOLAR WIND is a fast-moving (200 to 1000 km/s) flow of hot, ionized particles (plasma). This flow, primarily consisting of electrons and protons, travels from the Sun to the Earth in a few days, dragging with it the solar magnetic field. When the magnetized plasma strikes the Earth's magnetic environment, it leads to such phenomena as the aurorae in both hemispheres, and to damaging effects, like the disruption of communications and power grids due to the incident particle fluxes and to electrical currents set up by magnetic field changes. An important ingredient in the prediction of the solar wind's effects on the Earth is the proper modeling of the evolution of the heliospheric magnetic and velocity fields. This is rendered more difficult by the ever-changing nature of the Sun's atmosphere, which makes the solar wind a turbulent medium. Analysis of these complex phenomena requires high-resolution treatment.

Our group has been working for many years on the problem of computer simulation of the turbulent evolution of the solar wind. The main approach we and others have used is that of treating the wind as a fluid, with an additional force provided by the magnetic field's action on the charged particles. Although this magnetohydrodynamic (MHD) approach ignores some important details of the particle motions, it has proven very useful in understanding the main features of the flow. High resolution in computer solutions to the MHD equations has generally been obtained with spectral method codes that use Fourier or other transforms to calculate derivatives with high accuracy. The drawback, however, has been that these methods are periodic (e.g., the top and bottom of the box are equated with each other, etc.); thus, it is impossible to simulate true spatial evolution. Typically, investigators simulate a small region of plasma and assume that the spatial evolution with heliocentric distance is equivalent to the evolution in time of the (implicitly) convecting selected parcel.

This year, collaborative work between the Interplanetary Physics Branch and the High Performance Computing Branch has led to the development of an algorithm that removes the periodic restriction, thus allowing us to study true radial, turbulent evolution for the first time. The derivatives needed for the simulations are simplified by calculating the differences between nearby points, but any order of accuracy needed can be achieved at the expense of more computing time. The algorithm allows the wind

to flow in one end of the box and out the other, with time-dependent conditions at the inflow representing fluctuations and structures generated by the Sun. In the near future, we will adapt the algorithm to spherical coordinates so that the important effects of the global expansion of the wind can be included in a natural way.

The work illustrated in the figure was done with 100 x 100 x 100-grid points (close to the largest runs we have done with spectral methods), but the algorithm was efficient enough to run on a local workstation in about a day. In the figure, the wind enters the box from the right, with the middle third of the box moving faster than the outer thirds; this simulates the fast and slow streams observed in the wind. Superimposed on the streams are fluctuations that initially travel purely "outward" (i.e., to the left), as well as a structured magnetic field and density (shown in the white contours). An important and readily observable diagnostic of the evolution of the fluctuations is the degree to which inward-propagating (in the wind frame—the wind is supersonic) fluctuations are generated. This is shown by the color scale, which has the outward-propagating fluctuations as black, a mix of both directions given by intermediate colors, and nearly purely inward-propagating fluctuations in red/pink. It is clear that the turbulence generates inward-propagating waves, first at the shear layers between the streams, and later in regions associated with the structured field and density. This case is a "proof of principle" that we can study a useful radial range at sufficient resolution to model the solar wind evolution. A more detailed study of this case will show us, for example, what the relationship is between the directions of the transverse fields at the input and output ends of the box; this will give us an idea of how well we can predict conditions at the Earth from conditions measured near the Sun, such as magnetic field strength and orientation. In this way, we plan to elucidate the Sun-Earth connection and other issues, such as the effect of the solar wind on cosmic rays entering the solar system from the Sun or from the external Galaxy.

Contacts: D. Aaron Roberts (Code 692)  
301-286-5606

Melvyn Goldstein (Code 692)  
301-286-7828

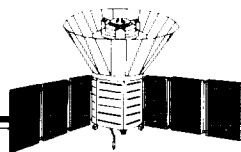
Sponsor: Office of Space Science



*Various cuts through a 100 x 100 x 100-grid point simulation of magnetic and velocity fields similar to those observed in the solar wind. The white contours represent density, and the colors represent the sense of propagation of the fluctuations with the black/blue end of the spectrum representing waves traveling outward from the Sun (i.e., to the left), and the red/pink end waves going inward toward the Sun in the frame of the wind.*

*Dr. Roberts has 9 years of experience at GSFC and holds a Ph.D. in Physics from the Massachusetts Institute of Technology. He is Co-Investigator on the Space Physics Theory Program grant to GSFC, and Principal Investigator on a NASA Code ST RTOP grant to study stereoscopic analysis methods.*

*Dr. Goldstein, Principal Investigator for the Solar Terrestrial Theory Program grant to GSFC and NASA Deputy Project Scientist for the Cluster Mission, has 23 years of experience at GSFC. Dr. Goldstein holds a Ph.D. from the University of Maryland, and has received a NASA Exceptional Scientific Achievement Medal for his work.*



## THE NONLINEAR DYNAMICS OF THE MAGNETOSPHERE AND SPACE WEATHER PREDICTION

THE SOLAR WIND is a hot, tenuous, fully ionized plasma that flows at high speed away from the Sun and collides with Earth's magnetic field with sufficient force to strongly modify its shape. Earth's magnetic field would fade away as a dipole with increasing distance from the planet, were it not for the solar wind. Rather than a dipole, Earth's magnetic field is contained in a comet-shaped region, the magnetosphere, with the field on the side of Earth facing the Sun being highly compressed, and the field on the side away from the Sun extended into a long tail whose full length is unknown.

The interplanetary magnetic field (IMF), carried by the solar wind past Earth, tends to lie in the ecliptic plane of the solar system. Because of irregularities at the surface of the Sun and in the solar wind flow, the IMF direction fluctuates both north and south of the plane. When the IMF direction is northward, the solar wind plasma and field are diverted around the magnetosphere and flow past it with little effect in its interior. However, if the IMF turns southward, field line merging can occur at the nose of the comet-shaped magnetosphere; interplanetary field lines become connected to Earth's field lines. Those field lines, then, have one end connected to the planet and the other end—in deep space—being dragged by the solar wind in the tailward direction. For as long as the IMF direction remains southward, more magnetic flux is loaded into the “magnetotail” through this “flux transfer” process. The magnetic pressure in the magnetotail increases, the tail flares out, and the ram pressure of the solar wind on the flaring tail increases.

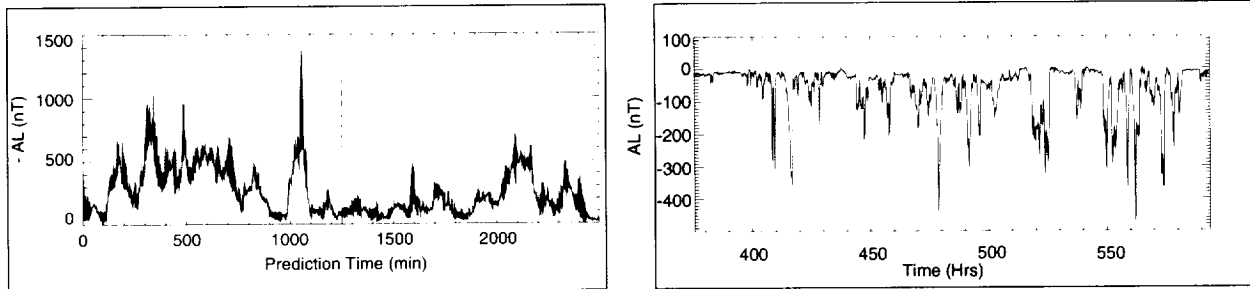
A critical state can be reached in the magnetotail when a major portion of the tail, a plasmoid, is lost in a violent plasma physical process called a substorm. The remaining portion of the tail, having been stretched during the loading part of the substorm, rebounds earthward following the plasmoid release. If the IMF direction remains strongly southward for an extended period, several substorms may take place that, collectively, are called a storm. During substorms, and particularly storms, an electric field tangent to the surface of Earth can be generated which, because of its large spatial scale, can generate a large electrical potential. Interconnected electrical power transmission lines become, effectively, antennas in which the substorm potential drives strong DC currents. These currents often do serious damage to

expensive generators and transformers and, in one case, caused a total blackout for 8 to 9 hours throughout a major portion of eastern Canada. As power-generating systems have become more interconnected, this problem has become more serious. The magnetotail rebound following a substorm plasmoid release also leads to a large increase in the flux of energetic charged particles at geosynchronous altitude. Geosynchronous satellites have been damaged and lost, and onboard data processing can be disrupted. As satellite electronics have become more sophisticated this problem has also become more serious.

There are other consequences of “space weather.” Train track transducers, which detect the positions of trains, often report the positions of nonexistent trains during storms. Pipelines can also act as antennas, and can be damaged by the large currents that flow in them. The ionosphere can be altered, leading to the failure of over-the-horizon radar and other communication methods that rely on the ionosphere. On the less serious side, homing pigeons often get lost. And, on the brighter side, phenomenal aurorae are stimulated in both the northern and southern polar regions of Earth.

More than a decade ago, it was clearly understood that southward turnings of the IMF could lead to substorms and storms. Efforts were made to predict the times and strengths of individual substorms using “linear prediction filters.” It was assumed that the substorm response of the magnetotail to the input IMF could be represented by a linear filter that was general enough to represent any linear relationship between the IMF input and the magnetotail output response. In fact, these studies showed that a linear relationship is not general enough, as the relationship is nonlinear. Since then, methods of nonlinear dynamics have been employed to study the magnetospheric dynamical response to the solar wind and to construct methods for predicting space weather.

An electrojet index, AL, is a measure of the current induced in the ionosphere by substorms in the magnetotail; it is also a good measure of the electric field strength induced at the surface of Earth. Two input-output nonlinear dynamical methods have been used to predict the AL index using solar wind data from the Interplanetary Monitoring Platform -8 spacecraft for input; the index is the output. Prediction examples are shown in the figure.



*Predictions of AL index using (left panel) the local-linear prediction method and (right panel) the Faraday loop model. The shaded area shows the difference between the predicted and measured AL. Note that -AL is plotted in the left panel.*

To obtain the results shown in panel a, a nonlinear filter technique has been used. The filter is deduced directly from the input and output data. The emphasis in this method is on the quality of the prediction, which far exceeds that of any available previously. This method is suitable for real-time prediction using real-time solar wind data from a spacecraft upstream in the solar wind. The results shown in panel b are from a nonlinear analogue model, the Faraday loop model, constructed using plasma physical reasoning. In this case, the prediction is not as good, but the physical processes in the magnetosphere that couple the solar wind input to the AL index output are revealed.

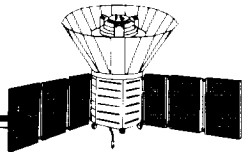
In the future, the two prediction methods discussed above will be merged. Analog models will be constructed that reproduce the output of the nonlinear filters. The analog models that result will provide a physical description of

the magnetospheric dynamics deduced directly from the measured solar wind and AL data. We anticipate improvements in prediction and understanding of the substorm process.

Contact: Alex Klimas (Code 692)  
301-286-3682

Sponsor: Office of Space Science

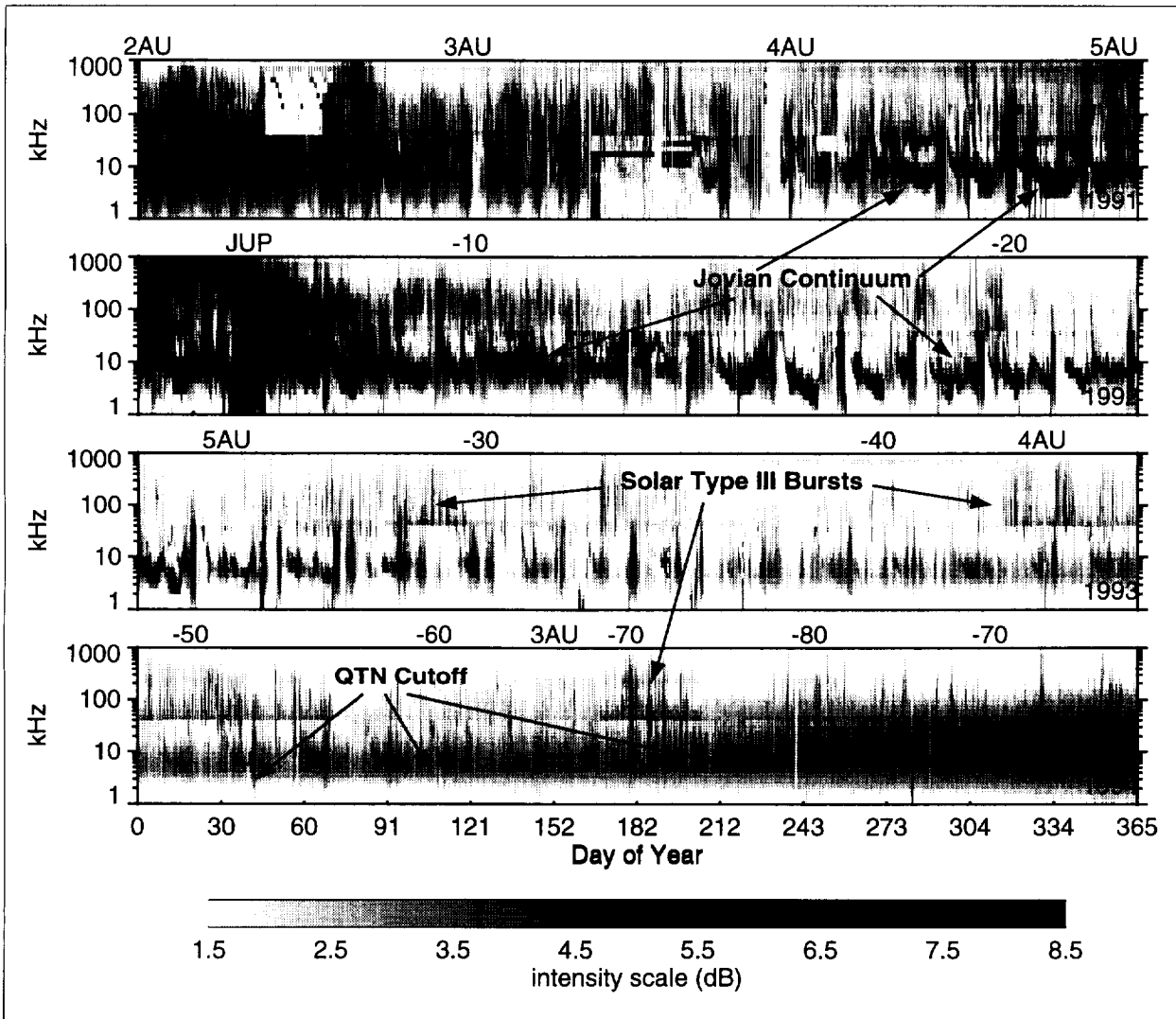
*Dr. Klimas is Principal Investigator on the NASA SR&T Program in Magnetospheric Physics, A Global Study of the Dynamic Solar Wind-Magnetosphere Interaction. He earned a Ph.D. in Physics from the Massachusetts Institute of Technology. Dr. Klimas has been at GSFC for 20 years, where he works in the Interplanetary Physics Branch studying the nonlinear dynamics of the magnetosphere.*



## ULYSSES RADIO AND PLASMA WAVE OBSERVATIONS AT HIGH SOUTHERN HELIOGRAPHIC LATITUDES

**S**ENDING A SPACECRAFT over the poles of the Sun has been contemplated since the beginning of the space program. The Ulysses mission was designed to do just that. The primary scientific objective of the Ulysses mission is to study, for the first time, the fields and particles in the Sun's polar region as a function of solar latitude.

After a gravitational swing-by, Ulysses left Jupiter, traveling southward in an elliptical orbit inclined 80.1° to the solar equator with an aphelion of 5.4 astronomical units (AU), and a perihelion 1.1 AU. Ulysses reached 70° heliographic latitude south in June 1994, and obtained a maximum southern latitude in November 1994. In June 1995, it reached 70°N latitude, and passed over the Sun's



*Data from 1991 through 1994 are shown. Selected distances from the Sun in AU and heliographic latitude are indicated. During the year 1992, Ulysses was just beyond 5 AU. Examples of intense solar type III bursts may be seen on days 0 to 60, 180 to 190, and 330 to 331 of 1994. Examples of nonthermal radio continuum and QTN low-frequency cutoffs are indicated. "JUP" indicates Jupiter flyby.*

polar cap and descend to 70°N latitude in September 1995. Ulysses will have spent 234 days above 70° latitude.

Radio and plasma wave observations obtained by the Unified Radio and Plasma Wave Investigation (URAP) aboard Ulysses provide remote diagnostics of solar and planetary radio emissions and *in situ* plasma waves resulting from wave-particle interactions. The URAP instrument measures electric fields over the frequency range of ~0 to 1 MHz, and magnetic fields from 0.22 to 450 Hz. Full polarization and source direction of emission from remote radio sources, and the intensity and orientation of *in situ* plasma waves, can be determined.

The figure shows the variability of wave phenomena related to the changing heliographic position of Ulysses along its trajectory from the ecliptic to high southern heliographic latitudes for the years 1991 (top panel) through 1994 (bottom panel). The data are 4-hour averages, displayed as dynamic spectra.

For several months surrounding the closest approach to Jupiter, centered on day 39 of 1992, the radio data were dominated by low-frequency Jovian radio emissions whose intensities are partially controlled by the solar wind conditions at Jupiter. Before mid-1991 and after 1992, solar radio emissions and quasi-thermal noise (QTN) predominated. QTN is generated by electrostatic waves produced by random motion of the ambient plasma particles. QTN spectroscopy is currently used for measuring electron parameters in space plasmas. An example of QTN can be seen in 1994, where the electron plasma frequency began the year at ~2 to 3 kHz, and gradually rose to ~10 kHz by the end of the year—a factor-of-10 density increase. Since QTN depends on electron density, it will vary with the distance from the Sun, latitude, and the level of solar activity. Thus, QTN will depend on the number of transients in the solar wind. In 1994 QTN

exhibited little fluctuation on a time scale of days, because the spacecraft was continuously in high-speed solar wind, which has less variability than the solar wind at low latitudes.

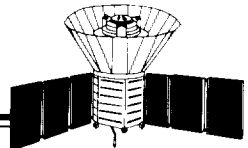
The great variability of QTN in late 1991, when the Ulysses-Sun distance was the same as in early 1994, resulted from the larger number of shocks, coronal mass ejections, and other transients in the solar wind. In late 1992 and early 1993, Ulysses was alternately in fast- or slow-speed wind as a corotating, high-speed solar wind stream repeatedly passed the spacecraft. This quasi-periodic (~25 day) variation in density caused an associated QTN variation, and a modulation of the Jovian nonthermal radio continuum reaching the spacecraft.

The radio activity diminished as the solar cycle approached minimum. For example, intense radio wave activity (above 100 kHz), observed from mid-March through June 1991, was associated with a very high period of solar activity, including a 3B/X9.4 flare on March 22, 1991. In 1994, at a similar distance from the Sun, but well into the declining phase of the solar cycle, the levels of all types of solar radio activity were greatly reduced.

Contact: Robert Stone (Code 690)  
301-286 8631  
Internet: [stone@urap.gsfc.nasa.gov](mailto:stone@urap.gsfc.nasa.gov)

Sponsor: Office of Space Science

*Dr. Stone is a senior scientist with the Laboratory for Extraterrestrial Physics. He is Principal Investigator Emeritus for the URAP Ulysses Mission. He earned his Ph.D. in physics from Yale University and has been with GSFC for 34 years where he developed the long wavelength space radio astronomy program. He received the NASA Exceptional Service Medal this year.*

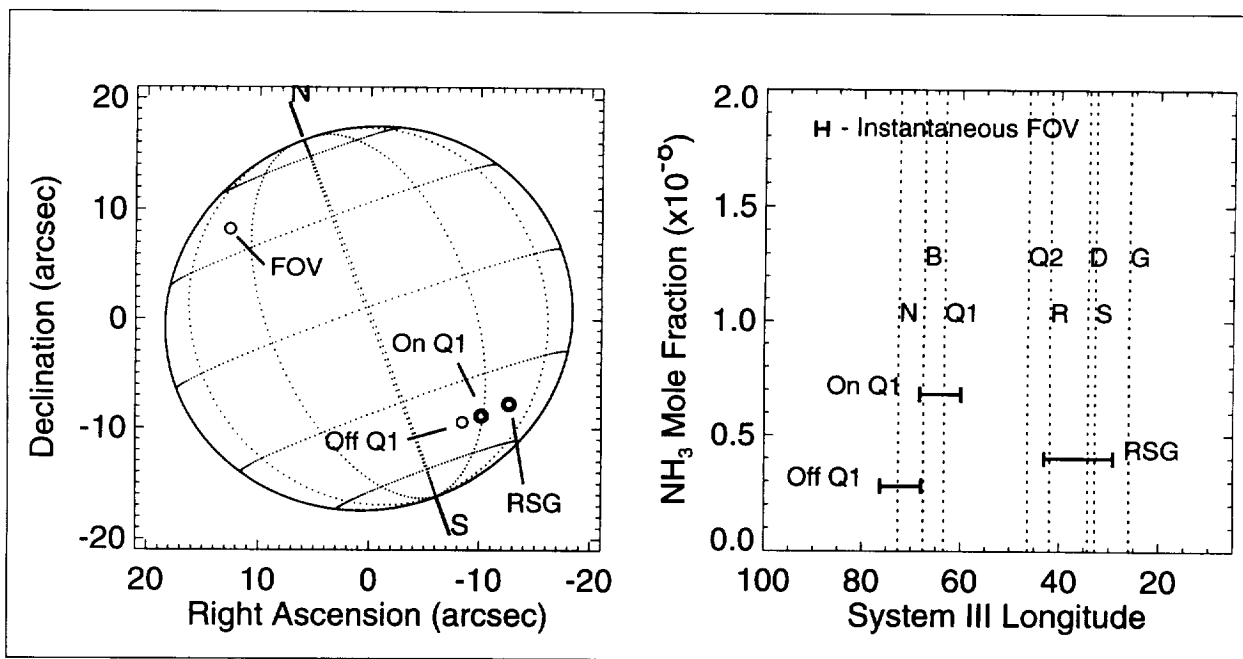


## MEASUREMENTS OF AMMONIA ON JUPITER AFTER SL9

AMMONIA IS PRESENT IN the atmosphere of Jupiter as condensed clouds below the  $\sim$ 600 millibar (mb) pressure altitude, and as a gas in the region above the clouds and below the tropopause at  $\sim$ 100 to 150 mb. The spectral signature of tropospheric ammonia is observed in the infrared as broad absorption lines. Ammonia ( $\text{NH}_3$ ) is not normally present in detectable quantities in Jupiter's stratosphere, the region above the tropopause, due to rapid photolysis by solar ultraviolet (UV) radiation, and condensation loss (cold-trapping) at the tropopause. When present, stratospheric ammonia can be observed as narrow emission lines in the infrared. The collision of periodic Comet Shoemaker-Levy 9 (SL9) with Jupiter in July 1994 injected  $\text{NH}_3$  into the planet's stratosphere. This provided a unique opportunity to study the lifetime of stratospheric ammonia for comparison with photochemical models that describe the processes of formation, destruction, and distribution of molecular species that compose the atmosphere of the largest planet in our Solar system.

The work we describe here is based on measurements of  $\text{NH}_3$  spectral line emission from two SL9 impact regions, corresponding to comet fragments Q1 and the RSG group, taken several days after the impacts. Ammonia emission line profiles were obtained at a wavelength near  $11\text{ }\mu\text{m}$ , with sub-Doppler spectral resolution. Measurements of the lineshape permit retrieval of the postimpact  $\text{NH}_3$  abundance, and constrain its altitude distribution in the stratosphere. These results can be used with those from other spectral measurements to study the temporal behavior of ammonia in Jupiter's stratosphere.

Observations were made at the NASA Infrared Telescope Facility (IRTF) on Mauna Kea, Hawaii, as part of the IRTF Comet Collision Science Team. Individual spectral emission lines of  $\text{NH}_3$  were measured with a spectral resolution of 25 MHz ( $\sim 1 \times 10^5$   $\text{cm}^{-1}$  wavelength) using the Goddard Infrared Heterodyne Spectrometer (IRHS), which has been used extensively in other studies of the composition and thermal structure of Jupiter's stratosphere.



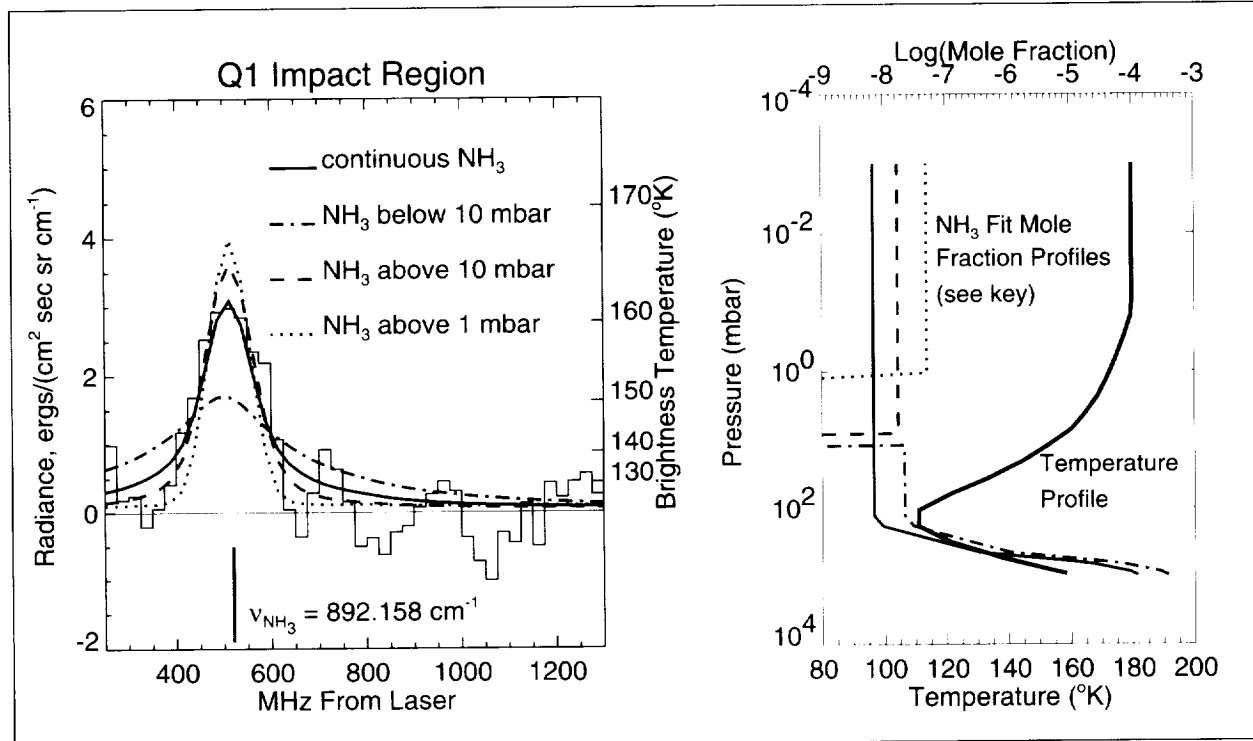
Field-of-view (FOV) of the Goddard Infrared Heterodyne Spectrometer during the measurements discussed here. The left panel indicates the positioning on the sky of the FOV for measurements of three Southern Hemisphere regions associated with the SL9 impacts, and also shows the size of the spectrometer FOV. The right side shows the longitude positioning of impact sites close to the measurement regions, and the longitude range included in each measurement; the vertical positioning of the bars corresponding to the longitude ranges indicates the retrieved  $\text{NH}_3$  mole fraction determined from the relevant spectra.

The measurements reported here were made on July 29, 1994 (Universal Time), 8.5 days after the Q1-fragment impact, 8 days after the R and S impacts, and 11 days after the G impact. The left side of the first figure shows the position of the spectrometer field-of-view (FOV) used to conduct the measurements; the right side shows the longitude range covered by the FOV as Jupiter rotated during the time required to collect the spectra. The Q1 and RSG sites both exhibited ammonia emission lines, indicating the presence of the molecule in Jupiter's stratosphere. The data were analyzed by comparing the measured spectra with theoretical spectra obtained by solving the radiative transfer equation for several candidate altitude distributions of  $\text{NH}_3$ . Candidate altitude distributions were scaled to produce the best fit between the theoretical and measured spectra.

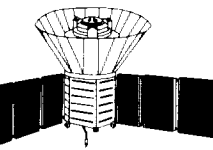
The second figure compares the measured  $\text{NH}_3$  molecular emission line from the Q1 impact site with the best-fit

spectra for each of four candidate altitude distributions, as shown in the right side of the figure. These depict, respectively,  $\text{NH}_3$  mixing ratio uniform with altitude in the stratosphere (solid line);  $\text{NH}_3$  limited to the lower stratosphere and troposphere (dash-dot line);  $\text{NH}_3$  limited to altitudes in the stratosphere above the 10 mb pressure level (dashed line); and  $\text{NH}_3$  limited to high stratospheric altitudes, above the 1 mb pressure level (dotted line). The thermal profile is derived from Voyager observations of Jupiter's quiescent southern midlatitudes, assuming that the temperature would have returned to equilibrium by several days after impact. The physical processes that contribute to the variation of the theoretical line shape are pressure-broadening of the  $\text{NH}_3$  emission line wings in the high-pressure region of the lower stratosphere, and saturation of the emission line core.

The best-fitting theoretical spectrum results from the altitude distribution limited to the region above  $\sim 10$  mb



The left side compares the measured  $\text{NH}_3$  spectrum obtained from the Q1 impact site (histogram) with model spectra from candidate altitude distributions. The right side shows the four altitude distributions considered with the temperature profile used in these analyses, based on Voyager measurements of the quiescent atmosphere.



pressure (dashed line). The spectrum from the distribution limited to very high altitude does not have enough pressure-broadening to fit; the spectrum from the distribution limited to low altitude is too pressure-broadened and saturated at line-center. The distribution with uniform NH<sub>3</sub> mole fraction fits adequately, but is too broad in the wings.

We could interpret this result as two ways: as an indication that the lower stratospheric emission of NH<sub>3</sub> is shielded from view by an opaque haze layer, or that the stratospheric NH<sub>3</sub> is limited solely to the upper stratosphere. The haze-layer interpretation is consistent with stratospheric hazes observed in the visible and UV ranges, and is consistent with high thermal continuum-emission levels and relatively low line emission for ethane (C<sub>2</sub>H<sub>6</sub>) observed at the same time and at the same impact sites. Therefore, interpretation of the postimpact photochemistry of NH<sub>3</sub> in Jupiter's stratosphere must account for the shielding effects of opaque haze found in the same altitude range as the gaseous debris from the impacts.

Follow-up observations made with the IRHS in March 1995 indicate that stratospheric ammonia resulting from the impacts had almost, if not completely, dissipated by this time. In further work, we will combine our extremely high-resolution data, which provide information about the altitude distribution of NH<sub>3</sub>, with other measurements made by a variety of techniques close to the time of impact and several weeks to months afterward. These combined data sets will form the basis for an investigation of NH<sub>3</sub> photochemistry in the period following the impact of SL9 with Jupiter.

Additional contributors to this research are Gordon Bjoraker, David Buhl, Fred Espenak, and Paul Romani in Code 693; Tilak Hewagama of the National Air and Space Museum; and David Zipoy of the University of Maryland.

Contact: Theodor Kostiuk (Code 693)  
301-286-8431

Kelly Fast (University of Maryland)  
301-805-5608

Timothy Livengood (University of Maryland)  
301-286-1552

Sponsor: Office of Space Science

*Dr. Kostiuk is an astrophysicist in the Planetary Systems Branch of the Laboratory for Extraterrestrial Physics and Chief Scientist for Exploration Programs in the Space Sciences Directorate. Dr. Kostiuk earned a Ph.D. in Physics from Syracuse University in 1973, then came to GSFC as a National Research Council Research Associate. His interests include composition, thermal structure, and dynamics of planetary atmospheres; infrared spectroscopy; and development of advanced instrumentation. He is currently on part-time detail to NASA Headquarters in the Solar System Exploration Division managing the Planetary Instrument Definition and Development Program.*

*Ms. Fast is a Faculty Research Associate with the University of Maryland, working with members of the Planetary Systems Branch under a cooperative agreement. She received a B.S. in Astrophysics from UCLA and an MS in Astronomy from the University of Maryland. Her scientific interests include ionospheric research and infrared imaging and spectroscopy.*

*Dr. Livengood received a Ph.D. in Physics and Astronomy from the Johns Hopkins University in 1991, then came to GSFC as an NRC Research Associate. He is presently working in the Planetary Systems Branch under cooperative agreement with the University of Maryland. His main research interests are in infrared and ultraviolet diagnostics of processes in planetary stratospheres and magnetospheres, including aurorae and dayglow emissions.*

## COSMOLOGY AND ASTROPHYSICS

## COSMIC MICROWAVE BACKGROUND RADIATION

WE ARE ENGAGED in a great endeavor to measure the cosmic microwave background radiation (CMBR), the relic of the intense heat of the Big Bang that started the expansion of our universe 7 to 15 billion years ago. Although the CMBR contains 99 percent of the radiant energy of the universe, it is extremely difficult to observe. It was discovered in 1965 and was quickly recognized as one of the most fundamental facts of cosmology, the study of the origin and large-scale properties of the universe. Precise tests of the CMBR require observations from space, above the interference from the Earth's atmosphere. There are two things to learn: the brightness at each wavelength (the spectrum), and the brightness in each direction (the map).

The Cosmic Background Explorer (COBE) satellite was designed, built, operated, and analyzed by GSFC to measure this radiation better than ever before, and to search for the light from the first objects that formed after the Big Bang. We delivered the main observational data from COBE to the National Space Science Data Center (NSSDC) this year; they are available on the Internet or in other formats by request. Over 1000 papers have been written by other scientists interpreting our results. For direct access to the data and documentation, see our World Wide Web (WWW) page at [http://www.gsfc.nasa.gov/astro/cobe/cobe\\_home.html](http://www.gsfc.nasa.gov/astro/cobe/cobe_home.html).

The main cosmological results from COBE are that the spectrum of the CMBR is precisely as predicted by the Big Bang theory, and that the map of the CMBR has features that differ in brightness by a few parts in 100,000. These few words have had enormous impact. The agreement of the spectrum with the prediction means that the Big Bang was simple in the sense that no other processes released significant amounts of energy more than a year after the great explosion. It had been thought that energy could have been liberated by the decay of chaotic turbulent motions, by black holes, by the decay of unstable elementary particles, by primordial cosmic strings, or by the formation of galaxies and galaxy clusters. None of these released more than about 0.03 percent of the total energy in the CMBR, which has a temperature of 2.726 K.

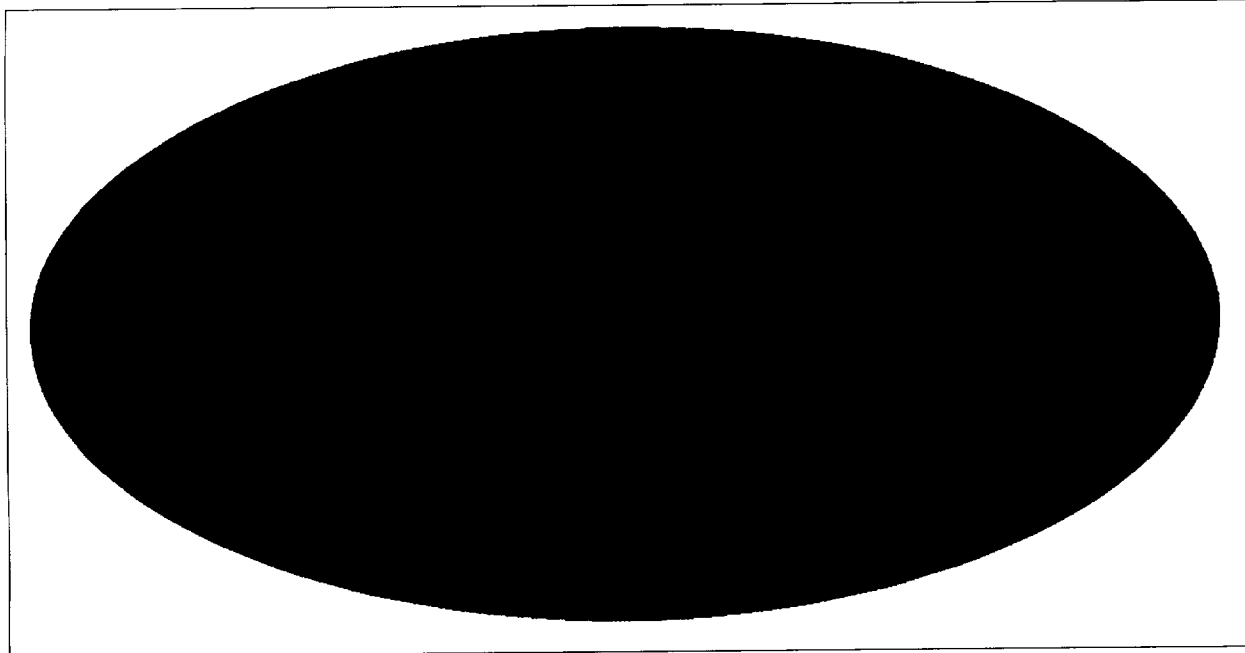
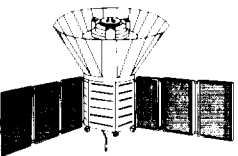
To measure the spectrum at longer wavelengths than could be seen by COBE, we have started construction of a prototype balloon-borne instrument in collaboration with P. Lubin of the University of California, Santa Barbara,

scheduled to fly in 1996. We have also begun a study for a new satellite, the Diffuse Microwave Emission Survey (DIMES), with R. Shafer as Principal Investigator (PI). DIMES will measure the spectrum of the CMBR and diffuse galactic emission at wavelengths as long as 15 cm.

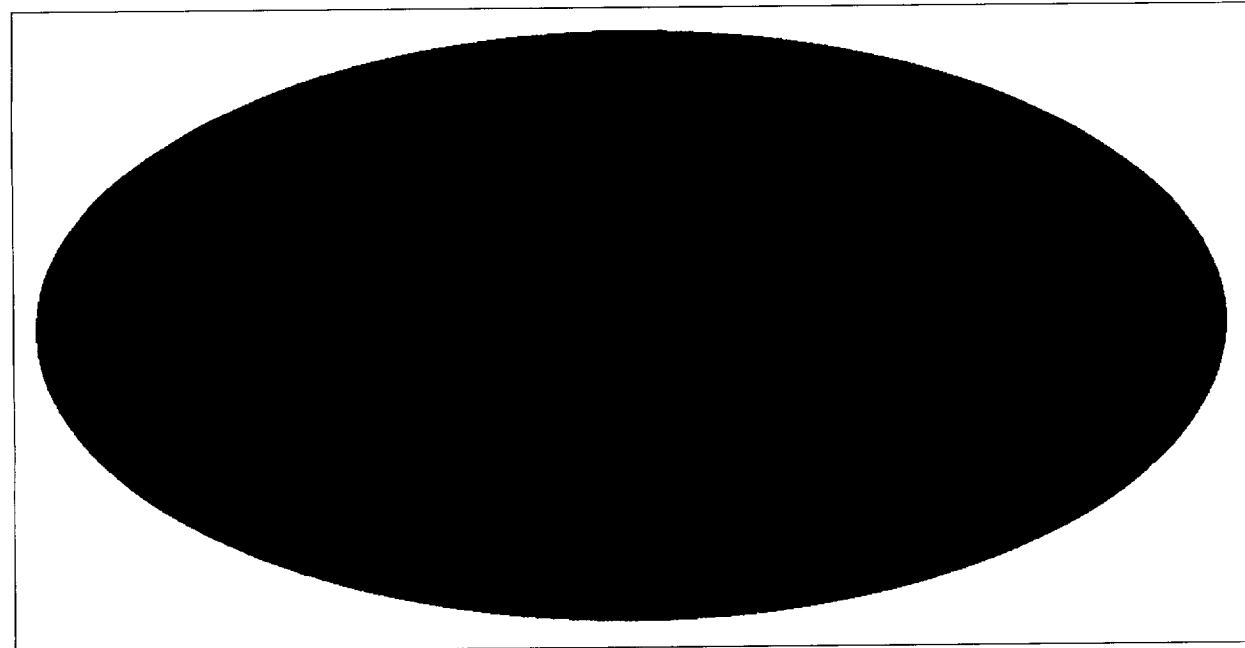
The all-sky map of the CMBR made by COBE is shown in the first figure. G. Smoot of Lawrence Berkeley Laboratory is the PI for the instrument that obtained these data; the Deputy PI, C. Bennett (GSFC), is in charge of the data analysis. There are some large features that stretch across large parts of the sky, which are the oldest objects that can ever be observed by humans (barring the faint possibility that the cosmic neutrino background can be observed). They are seen as they were  $\sim$ 300,000 years after the Big Bang. That is the moment called the Decoupling, when matter turned from an opaque plasma of hydrogen and helium nuclei and electrons into a transparent gas of ordinary hydrogen and helium. After that moment, the CMBR was free to travel until it reached our receivers, which allow us to see it as it was then. In its simplest sense, this is a map of the gravitational potential on the surface of a sphere surrounding the present location of the Earth at the moment of decoupling. The effect occurs because photons receive a gravitational redshift when escaping from a gravitating object, and effectively lose energy.

This map is important because it shows the initial conditions for the development of structure in the early universe. It is generally thought that the gravitational forces represented in this map are responsible for the movement of matter particles after the Decoupling, when they become free from the influence of the CMBR and could begin to fall towards the strongest gravitational attractors. Immense effort has been expended by theoretical astrophysicists to simulate the early universe, using the characteristics of this map to predict the appearance of galaxies, clusters of galaxies, and the enormous voids between them.

There is as yet no agreement about the best theories, but they share one common feature: all require the existence of some kind of dark matter, something with properties quite unlike ordinary matter. Dark matter has been detected only through its gravitational effects, but it nevertheless seems to provide 90 percent to 99 percent of all the matter in the universe. The existence of dark matter has also



*All-sky map of the cosmic microwave background temperature variations as measured by COBE. Red regions are 0.01 percent brighter than average; the early universe was 0.03 percent less dense than average in those regions.*



*Simulated all-sky map of the CMBR temperature with a finer beam. The dominant small speckles come from the oscillations of the primeval fluid about 300,000 years after the Big Bang.*

been inferred by measurement of the bending of light by the gravitational field of clusters of galaxies. Its nature and distribution are among the greatest mysteries of modern physics and cosmology.

More detailed maps of the CMBR would be of great value. The COBE mapping instrument has an angular resolution of  $7^\circ$ , roughly the angular distance from Boston to Washington. We made a hypothetical map with  $0.5^\circ$  resolution (shown in the second figure) to illustrate what could be learned with increased resolution. Measurements of a map with this accuracy would enable us to determine the total density of the universe, the fractions of various kinds of dark matter, and the primeval fluctuations of density. According to theory, this map shows the oscillations of the primeval fluid around the time of the decoupling, when matter first began to respond to gravitational fields. A certain characteristic size of the spots should occur as a result, giving a graphic display of the very first music of the spheres. We have recently proposed to build the instrument needed to make this measurement. Called the Microwave Anisotropy Probe, with C. Bennett as PI, it would be part of NASA's Mid-sized Explorer Satellite program.

We also carry out a vigorous balloon research program to make detailed maps of smaller areas of the CMBR. Full details are available on our Web page, <http://cobi.gsfc.nasa.gov/msam-tophat.html>. The Medium-Scale Anisotropy Measurement has flown in 1992, 1994, and 1995, with a 1-m diameter telescope and a  $0.5^\circ$  beamwidth. Two balloon flights have observed the same regions of the sky, confirming the initial observations very well. This

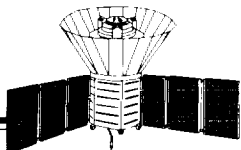
work, done in collaboration with colleagues at Princeton University and the University of Chicago, led at GSFC by R. F. Silverberg and E. S. Cheng, has reported clear detections of cosmic structure of a few parts in 100,000. Improved detectors developed at Brown University are being prepared for our next flights, and even better ones are being developed for use in long-duration balloon flights. Balloons have already been flown around Antarctica for several weeks, but payloads must have all the functions of a satellite in orbit and, as a result, construction is a challenge.

The study of the CMBR has wrought a revolution in cosmology. We have provided a firm observational basis for understanding the growth of galaxies from the nearly (but not quite) featureless primeval explosion.

Contact: John Mather (Code 685)  
301-286-7620

Sponsor: Office of Space Science

*Dr. Mather is Project Scientist and one of the three Principal Investigators on the COBE mission. He earned a Ph.D. in Physics from the University of California at Berkeley. He has been at GSFC for 19 years, where he works in the Infrared Astrophysics Branch developing new technology for cosmic background studies. In 1995, he received an honorary D.Sci. from Swarthmore College, and was selected to receive the John Scott award from the City of Philadelphia, and the Rumford Prize from the American Academy of Arts and Sciences. He is the PI for the COBE instrument that provided the CMBR spectrum.*



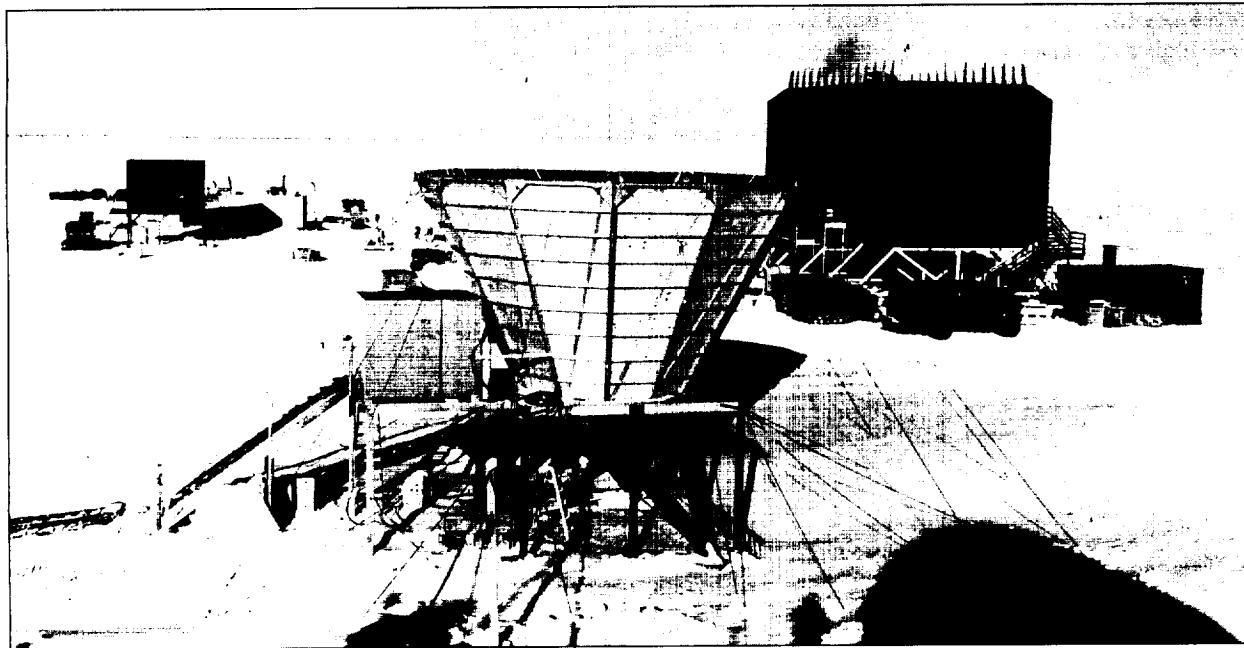
## EXPLORING THE LIMITS OF ASTRONOMY FROM EARTH

OUT OF NECESSITY, astronomers have historically sought out the most inhospitable locations on Earth from which to carry out their observations. In search of clear skies, observatories have been built on some of the driest mountain peaks in the world. Mauna Kea in Hawaii has been identified as perhaps the premier site in the world in recent years; most of the large new telescopes in the world are being built there. The skies over Mauna Kea are particularly clear in the infrared region of the electromagnetic spectrum because the air is particularly dry, which is a welcome condition for infrared astronomy because water vapor is the primary absorber of infrared light in the atmosphere. But, is Mauna Kea really the best infrared site in the world? It is very good, but there is one location which is consistently better: the South Pole! The perpetually cold temperatures freeze the water vapor from the atmosphere, so during the six-month-long Antarctic winter night, the Pole may be the best site on Earth for infrared observations.

A group centered at the University of Chicago has formed the National Science Foundation Center for Astrophysical

Research in Antarctica (CARA) to explore and develop the South Pole as a site for infrared and submillimeter astronomy. The CARA site is shown in the figure. Our group at GSFC is participating with CARA in characterizing the South Pole as an observing site for the midinfrared part of the spectrum, ranging from  $\sim 5$   $\mu$ m to  $\sim 40$   $\mu$ m. In this wavelength range, many young stars in the process of being born, and old stars shedding their mantles of elements synthesized during their lifetimes, emit most of their energy. At these wavelengths, the center of our galaxy, which cannot be seen at visible wavelengths due to intervening dust in the galaxy, is fully revealed. Although part of this spectral range can be observed from Mauna Kea, the very longest wavelengths are accessible only from the South Pole during the frigid Antarctic night.

We have built an instrument that can measure the transparency of the sky at these long wavelengths, and which can carry out astronomical observation if the transparency is sufficiently good. In a preliminary expedition in December 1994 and January 1995, measurements of sky transparency showed that some observations are possible



*Facilities for the Center for Astrophysical Research in Antarctica located in the Dark Sector of the United States South Pole station. The foreground plywood structure is the Cosmic Background Radio Anisotropy experiment facility. This photograph was taken from the roof of CARA's ASTRO building.*

even in summer, making it probable that the site will support long wavelength observations in the winter.

To carry out this exploration program, we are deploying a telescope at the Pole in January 1996 for a winter-long sojourn. Our team will spend about a month installing the instrument to assure its proper performance, after which it will be left in the hands of a technician who will "winter over" at the Pole to care for the instrument. We will control the instrument and receive data over the Internet, which will allow us to adjust and optimize our observing program according to local conditions.

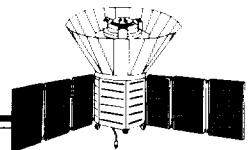
This program, funded by the GSFC Director's Discretionary Fund, has allowed us to obtain operational experience with new, far infrared focal plane arrays (also obtained with the support of the GSFC Director's Discretionary Fund); to test ideas for rapid design, construction, and testing of complex instruments; and to develop techniques for low-cost remote operations. The program will also provide the community with a clear picture of the limits of what is possible when observing from the Earth's surface. By testing ideas for low-cost, rapid instrument development, we are laying the groundwork for lower-cost, high-performance missions in the future.

By operating instruments at the South Pole, we are extending the pioneering tradition of astronomers who sought out inaccessible mountain peaks in the quest for better observing conditions. We will discover the limits imposed at the best Earthly site so that we have a clear understanding of those problems that require voyages to the much more difficult-to-reach environment of space.

Contact: Harvey Moseley (Code 685)  
301-286-2347

Sponsor: Office of Space Science

*Dr. Moseley has been at GSFC for 17 years. He received his Ph.D. from the University of Chicago, carrying out his research with the NASA Kuiper Airborne Observatory. At GSFC, he joined the Cosmic Background Explorer Science working group, and played a major role in the development of the COBE instruments. He originated the concept of using microcalorimeters as x-ray spectrometers, and is a member of the X-ray Spectrometer team which will fly such detectors on the Japanese Astro-E satellite. He continues his study of far infrared astronomy and the development of new detectors for space astronomy.*



## THIN-FOIL REPLICATED OPTICS FOR X-RAY ASTRONOMY

THE ADVANCED SATELLITE for Cosmology and Astrophysics (ASCA), presently in low-Earth orbit, is a Japan/U.S. collaborative astronomy mission that uses a 420-kg spacecraft carrying four ~4-m long, co-aligned x-ray telescopes. The telescopes are commanded daily to point, with close to arc-minute accuracy, toward astronomical targets whose x-ray spectra are of interest to observers. The use of broad-band focusing optics—as contrasted with mechanically collimated detectors—has greatly increased the sensitivity of such x-ray measurements, and has allowed the use of high-resolution focal plane detectors such as the charge-coupled devices (CCDs) used on ASCA. However, imaging in the x-ray band is done at grazing incidence, which results in long focal lengths and large instruments. ASCA best exemplifies the way conical foil mirrors have opened up this area of research, which otherwise could not have been addressed with available resources. These lightweight foil mirrors (10 kg each) were conceived, developed, and fabricated at GSFC. In spite of their simple and inexpensive construction, they perform in most ways as one would infer from computations and ray tracings, but with one important exception: image blurring is about seven times worse than what would be expected from their approximately conical geometry.

Efforts to improve imaging capability had not been fruitful through the design and launch of ASCA. Fortunately, the x-ray sky is not very crowded, so with ASCA we can generally isolate sources of interest even in the presence of the blur. Occasions abound, however, where better imaging would have resulted in more detailed information. This is particularly true for extended sources, such as supernova remnants, and for fainter sources, where the presence of a weak source signal combined with the increased background “noise” reduces the statistical significance of a result. Future imaging and spectroscopic studies in the x-ray band will invariably involve fainter and more spatially complex sources, so imaging limitations have to be taken into consideration in the design of new instruments.

More generally, in an era of rapidly decreasing opportunities for observations from space, future missions and instruments must maximize the return from each opportunity. Our best chance for enhancement with foil optics has always been to recover at least a fraction—if not all—of the lost imaging potential. We have been selected to

participate in the follow-up to ASCA project with Japan, Astro-E, partly because of the progress we have towards attaining this important goal using a modification of standard techniques.

In the case of the ASCA mirrors, we have identified midfrequency roughness (often referred to as “orange peel”) as the most significant source of imaging error. Orange peel results from shallow foil surface deformations on scales from tens of microns to several millimeters. The  $\sim 10 \mu\text{m}$  thick acrylic coating that has been used to reduce the surface micro-roughness is simply not effective in covering deformations of such large extent. A search for a smoother foil supply has not resulted in any significant improvements. For this reason, we have been exploring a promising alternative surface smoothing process, which we call “surface replication.”

Replication, as historically used in connection with x-ray optics, is the process of transferring the characteristics of super-smooth mandrels to mirror surfaces. When, in addition to surface smoothness, shape integrity is also of primary importance (as it has been in past applications of this concept), the substrate must be sufficiently stiff to accurately maintain the shape of the mandrel. An extension of this technique to thin and easily flexible foil reflectors would be counterproductive because the added stiffness requirement would work against the most attractive feature of such reflectors, which is their light weight. In addition, it would be absurd to plan on having as many mandrels available as would be required to form the hundreds of different-size reflectors that make up a typical foil mirror (e.g., 240 for ASCA).

We have developed a variation of this process that allows us to maintain the key characteristics of foil mirrors while simply replacing the lacquer coat with a very thin epoxy replica of the smooth mandrel surface. The basis for this approach is as follows: The substrate is an uncoated foil reflector, a preformed conical segment made of resilient 0.127 mm thick aluminum foil. We can make small changes to the shape and curvature of such a segment by bending it elastically about its symmetry axis. Such changes are needed to effect complete contact between it and a mandrel of similar—but not necessarily identical—curvature. In practice, the mandrel in question can be either a cone or a cylinder. Gold is first sputtered onto the mandrel, and then a thin layer of epoxy is applied before

the reflector is pressed against it. The epoxy acts as a buffer that allows a transition of surface characteristics from the relatively rough raw aluminum to the smooth surface of the mandrel. When the epoxy hardens, the reflector is pulled off the mandrel; the gold layer now acts as the release agent and as the reflecting surface of the finished reflector. If the epoxy is uniformly applied, and if its thickness is small compared with that of the foil, the finished reflector will spring back to approximately its original conical shape. We have developed a process for applying the epoxy so that both these conditions are met. Using this approach, we have accomplished two major simplifications to the replication process: we have drastically reduced the number of mandrels needed, since one mandrel now can accommodate a range of sequential reflector sizes; and we use smooth cylindrical mandrels which are much easier to obtain than conical ones. For example, we have successfully used glass cylinders as mandrels, which have been selected and cut from commercially available extruded Pyrex tubing, whose surface is comparable in micro-roughness to float glass.

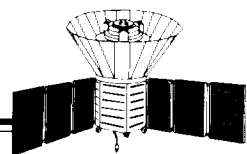
We are presently entering the Astro-E flight hardware development stage using this new surface preparation

technique for the thousands of reflectors that will make up the five Astro-E mirrors. Preliminary x-ray beam tests with small groups of reflectors have shown that we have gone roughly half the way toward bridging the gap between imaging potential and actual performance. We have not yet made a detailed analysis of the source(s) of the remaining imaging errors, but we are certain that most of them are due to large-scale figure and alignment errors. Nevertheless, the improvements we have made are significant, and will play a key role in helping us achieve the scientific objectives of the Astro-E mission.

Contact: Peter Serlemitsos (Code 666)  
301-286-5255

Sponsor: Office of Space Science

*Dr. Serlemitsos is an astrophysicist at the Laboratory for High Energy Astrophysics at GSFC. Dr. Serlemitsos earned a Ph.D. in Physics from the University of Maryland. He has been at GSFC for over 30 years, where he works in the X-Ray Astrophysics Branch.*



## CdZnTe HARD X-RAY SEMICONDUCTOR DETECTOR DEVELOPMENT

THE TREMENDOUS SCIENTIFIC output of the Compton Gamma-Ray Observatory (CGRO) has shown that there is a great scientific benefit from flying new instrumentation for x-ray and gamma-ray astronomy. However, there is a need for smaller, more convenient, hard x-ray (5 to 200 keV) payloads that still provide measurements at high sensitivity and high energy resolution. A convenient, compact, low-power, light-weight, room temperature, hard x-ray detector array with good position resolution, sensitivity, and energy resolution is very desirable.

A new semiconductor material, cadmium zinc telluride (CdZnTe), shows great promise for use as hard x-ray detectors in that it has a high density and high atomic number, so that thin (2 mm) detectors are efficient up to 100 keV. Thin detectors can result in a more compact, light-weight detector package. Volume-dependent detector background contributions will also be reduced for thin detectors, resulting in improved instrument sensitivity. The wide band gap of CdZnTe allows room temperature operation, so that no cryogenic cooling systems are required. The recent commercialization of CdZnTe detectors for medical and environmental applications has resulted in a reduction of the material cost to the point where large arrays of detectors are now financially feasible. The needs of the high-energy physics community have also led to the development of integrated linear electronics chips that allow analysis of large numbers of electronics channels within space flight power constraints. These new developments, coupled with CdZnTe's high stopping power, good-energy resolution, low-bias voltages, and room-temperature operation, make CdZnTe an ideal technology for the next generation hard x-ray imaging instruments.

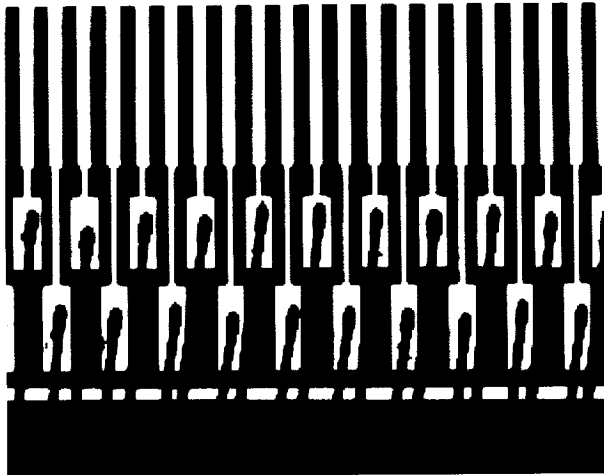
One exciting application of such an instrument would be the precise localization of gamma-ray bursts. Every day, the Earth is bombarded by intense flashes of gamma radiation, lasting from a fraction of a second to several minutes, and, at times, more than 1000 times brighter than all other gamma-ray sources in the sky. Despite the concerted efforts of many scientists over the past 25 years, the mystery of the origin of these gamma-ray bursts remains unsolved. Sensitive new instrumentation on CGRO has shown that gamma-ray bursts originate at great distances from us and are isotropically distributed on the sky. Recent CdZnTe detector research and development

work at GSFC has been aimed at the development of very high resolution CdZnTe strip detectors for use in the proposed Burst ArcSecond Imaging and Spectroscopy (BASIS) gamma-ray burst instrument. A large array of < 100  $\mu\text{m}$  position resolution CdZnTe strip detectors will be used in BASIS to determine the positions of gamma-ray bursts to within an unprecedented  $\pm 3$  arcsec. Large arrays of unsegmented CdZnTe detectors will also provide spectroscopic information about the bursts. Such accurate burst positions will be used to search for gamma-ray burst counterparts at other wavelengths. The discovery of a burst counterpart may lead to the solution of the gamma-ray burst puzzle.

The GSFC CdZnTe detector development program represents a successful partnership between astrophysicists in GSFC's Nuclear Astrophysics Branch and engineers in the GSFC Solid-State Device Development Branch. Detectors are fabricated from cut CdZnTe material received from commercial vendors. Except for mechanical polishing, the detector processing is done in GSFC's microelectronics clean room facility, with its capabilities for wet chemical processing, photolithography, and thin film deposition. The material is mechanically polished, chemically etched, and then contacted with various metal films. Fine strip patterns are produced through photolithography techniques.

The fabrication of CdZnTe detectors with 100  $\mu\text{m}$  pitch strip contacts is a new development at both GSFC and commercial laboratories. A one-dimensional, 100  $\mu\text{m}$  pitch, 50  $\mu\text{m}$  width CdZnTe strip detector has been successfully produced at GSFC. The figure is a photograph of the strip pattern laid down on the CdZnTe crystal; it shows the wire bonds to a very large-scale integration (VLSI) circuit chip (the SVX) used to read out the electronics signals from the strips. Note that features on even the smallest size scale in the pattern (25  $\mu\text{m}$ ) were well reproduced. Thus, we have successfully fabricated a one-sided, 100  $\mu\text{m}$  pitch CdZnTe strip detector, wire bonded it to both discrete electronics and an existing VLSI readout chip, and have shown that 60 keV photons can be localized to less than 100  $\mu\text{m}$  with these devices.

The CdZnTe detector development work at GSFC has progressed very quickly thus far. We have nearly reached our next milestone: the fabrication of two-dimensional strip detectors with 100  $\mu\text{m}$  position resolution in both



*Photograph of a portion of a 100  $\mu\text{m}$  pitch, 50  $\mu\text{m}$  width CdZnTe strip detector wire bonded to a VLSI readout chip.*

dimensions, as read out by an optimized VLSI chip. Our final milestone is to construct small array modules that can be used in conjunction with the prototype BASIS imaging system (coded aperture mask) to demonstrate source positioning accuracy on the order of a few arcsec.

Without knowledge of the material-dependent background rates in CdZnTe, it is very difficult to determine the sensitivity of such an imaging instrument. Therefore, we have flown the Piggyback Room Temperature Instrument for Astronomy (PoRTIA) on a small balloon to measure the background rates of an unsegmented CdZnTe detector in the balloon environment. The PoRTIA instrument was successfully flown on June 1, 1995, from Palestine, TX, and measured the CdZnTe background rates for a 6.45- $\text{m}^2$  area, 1.9-mm thick CdZnTe detector during a 10-hour observation at an altitude greater than 115,000 ft. This same detector will be flown once again in the fall of 1995, along with an additional high-spectral-resolution 1.44- $\text{cm}^2$   $\times$  5-mm CdZnTe detector for further background measurements.

CdZnTe detector technology has certainly captured the interest of the hard x-ray astrophysics community as a promising new technology for future astrophysics missions. Since CdZnTe hard x-ray imaging instruments also

have important applications in medical imaging and other fields, work done at GSFC to develop the technology for gamma-ray burst instruments such as BASIS has great relevance to industries outside NASA. The success of the CdZnTe detector development is the result of dedicated individuals within the Solid State Device Development Branch, and within the Laboratory for High Energy Astrophysics including Peter Shu, Carl Stahle, Jack Shi, Lyle Bartlett, and Casey Lisse, Bonnard Teegarden, Scott Barthelmy, David Palmer, Louis Barbier, John Krizmanic, and Frank Birsa.

Contacts: Ann Parsons (Code 661)  
301-286-1107  
Internet: [parsons@lheavx.gsfc.nasa.gov](mailto:parsons@lheavx.gsfc.nasa.gov)

Neil Gehrels (Code 661)  
301-286-6546  
Internet: [gehrels@lheavx.gsfc.nasa.gov](mailto:gehrels@lheavx.gsfc.nasa.gov)

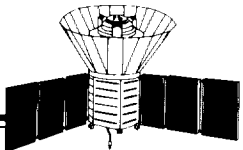
Jack Tueller (Code 661)  
301-286-4678  
Internet: [tueller@tgrs.gsfc.nasa.gov](mailto:tueller@tgrs.gsfc.nasa.gov)

Sponsor: Office of Space Science

*Dr. Parsons is an astrophysicist working on CdZnTe detector development projects and CGRO data analysis. Dr. Parsons earned a Ph.D. in Physics from the University of California, Berkeley, and has been at GSFC for 2 years, where she works in the Low Energy Gamma-Ray Group in the Laboratory for High Energy Astrophysics.*

*Dr. Gehrels is an astrophysicist working as the Project Scientist for the CGRO. Dr. Gehrels earned a Ph.D. in Physics from the California Institute of Technology, and has been at GSFC for 14 years, where he works in the Low Energy Gamma-Ray Group in the Laboratory for High Energy Astrophysics.*

*Dr. Tueller is an astrophysicist working as Principal Investigator for the GRIS project. Dr. Tueller earned his Ph.D. in Physics from Washington University in St. Louis, and has been at GSFC for 16 years, where he works in the Low Energy Gamma-Ray Group in the Laboratory for High Energy Astrophysics.*



## THE NEW SHAPE OF THE GALACTIC BULGE

**E**DWIN HUBBLE'S DETERMINATION in 1924 of the distance to M31, the Andromeda galaxy, closed a long debate in the astronomical community about the nature of the fuzzy "nebulae" seen in astronomical images. As Immanuel Kant had postulated in 1755, these nebulae proved to be "island universes," much like our own Milky Way galaxy, but far outside of it. Thus, they provided us with a view of what our own Galaxy might look like to an outside observer. Many of these nebulae, including the Andromeda galaxy and our own Milky Way, contain a component where stars are found in spiral arms within a relatively thin disk. Such galaxies are referred to as spiral galaxies. A common characteristic of all spiral galaxies is a central bulge, which in some galaxies can dominate their luminosity and physical appearance. In others the central bulge is hardly noticeable. Could our Galaxy have a similar feature in its center? And if it does, what is its size, shape, and luminosity? These questions have proved difficult to answer, since the center region of our Galaxy is heavily obscured at visible wavelengths by interstellar dust.

In 1944, Baade was able to distinguish individual stars in the bulge of M31. He found the stars to be red K giants, very similar to the ones found in the Sagittarius star cloud, which was known from Shapley's studies of globular clusters to be located near the center of our own Milky Way galaxy. From these comparative studies, Baade concluded that our Galaxy possesses a middle-sized bulge, probably similar to the one in M31.

The discovery of the bulge in our Galaxy raised a number of compelling questions. How does the bulge fit into an evolutionary picture of the Galaxy? How is the bulge related to other known galactic components, such as the halo, the thin disk, or the thick and extended disk?

To address these questions, scientists performed numerical studies that followed the evolution of a rotating disk-like distribution of stars influenced by the presence of a centrally condensed spherical halo resembling an extended bulge. As this rotating system evolved under the influence of gravitational forces, the stars in the central region of the disk gathered and formed a thick, bar-shaped structure that can be described as a triaxial spheroid with one elongated axis and two, roughly equal, shorter axes. Viewed edge-on, the bar could appear peanut-shaped, but it could appear box-shaped or even round from different

viewing angles. The immediate question arising from these computer simulations was whether there is any observational evidence to suggest that the Milky Way bulge is bar-shaped. The existence of a bar in our Galaxy would have important implications for understanding the dynamics of the Galaxy. A bar would provide a mechanism for sweeping gas from the disk into the galactic center, feeding a central black hole. It would also provide a mechanism for generating spiral arms, and a basis for estimating the mass of the halo relative to that of the disk.

The presence of a bar in the center of our Galaxy can be inferred from observations in several different ways. First, a bar-like distribution of stars has a gravitational potential that is quite different from an axisymmetric distribution of stars. Stellar orbits in such a potential will not be circular; rather, they will fall into several orbital classes with distinct shapes and orientations with respect to the bar's major axis. Searches for these orbital characteristics are an active field of research. So far, the limited data on the motions of the stars in the galactic bulge are consistent with it being an oblate spheroid.

A bar will also affect the dynamics of the gas in the galactic center region. Studies of the motions of the molecular and atomic hydrogen gas show that the gas does not move in the circular orbits expected in the presence of an axisymmetric potential. One possible explanation for these peculiar motions is that the gas is expanding. Such large-scale expansion could be caused by some violent event associated either with activity in the nuclear region or with supernova explosions of massive stars. However, theoretical studies have shown that a nonaxisymmetric potential, such as one created by a bar, similarly could cause such noncircular motions, eliminating the need for explosive events to explain the peculiar gas orbits. These studies also suggested that the bar would have to be oriented in such a way that its nearest side is in the first galactic quadrant, creating a viewing angle of about  $16^\circ$  between its major axis and the line of sight from the Sun to the galactic center. Furthermore, the studies show that the bar would be rotating in an opposite direction to the disk material, with a rotation period of about 80 million years.

A bar with such an orientation would give rise to a third observational effect, an asymmetrical appearance between its left and right sides (i.e., between its projected intensities

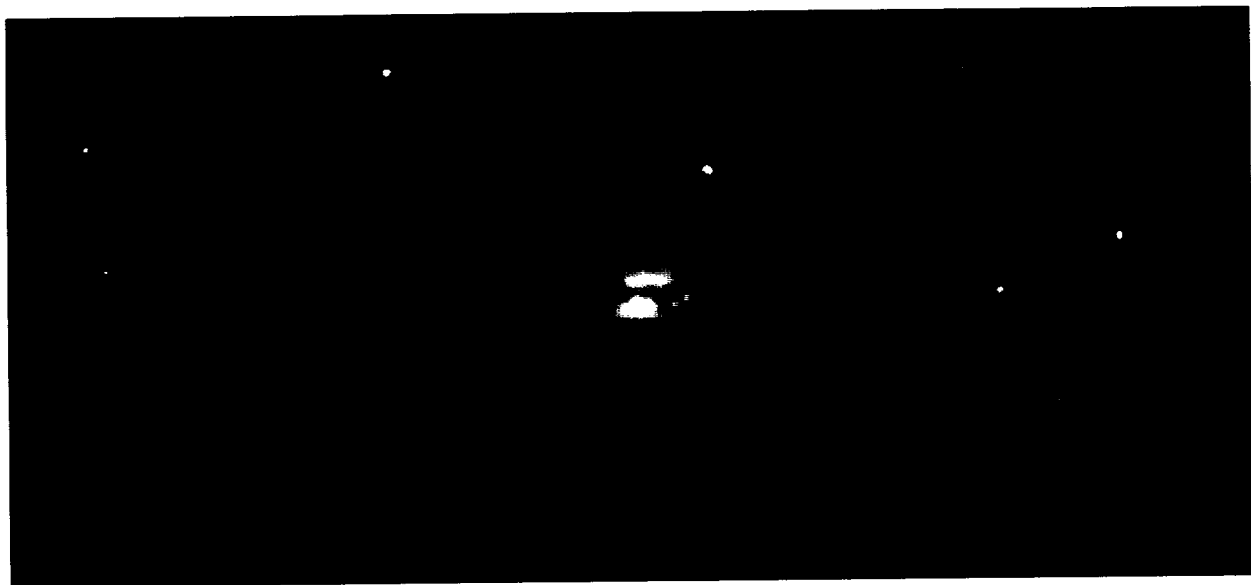
in the first and fourth quadrants of the Galaxy, respectively). Any asymmetrical appearance of the bar is purely a geometric effect. Lines of sight intersecting the near side of the bar at sufficiently large galactic longitudes will encounter more stars than their symmetric counterpart at negative galactic longitudes.

Searches for this asymmetry have included studies of the spatial distribution of stellar objects that trace the bulge population and studies of the projected light intensity of the bulge. Since the large-scale structure of the bulge is obscured by intervening dust, many of the studies have concentrated on stellar objects that are readily observed at infrared wavelengths. These studies were pioneered by the Dutch astronomer Harm Habing using data obtained by the Infrared Astronomical Satellite (IRAS), a joint project between the Netherlands, the United States, and the United Kingdom. The IRAS conducted an all-sky survey in four infrared bands centered at 12, 25, 60, and 100  $\mu\text{m}$ . The stellar sources detected at the two shortest wavelengths provided a rich database for studying the bulge morphology. The IRAS catalog included a population of long-period variable stars with cool circumstellar

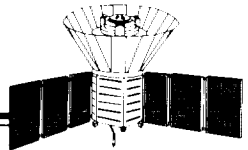
dust shells associated with the bulge. Detailed studies revealed that the projected distribution of these stars implies that the left side of the bulge (which is at positive galactic longitudes) is closer to us than its right side. The three-dimensional distribution of these sources was consistent with a bar oriented at a viewing angle of about 45° to the observer.

Another source of information on the morphology of the bulge was provided by a Japanese survey carried out from a high-altitude balloon in 1980, which mapped the projected light intensity of the galactic center region at 2.4  $\mu\text{m}$ . Recent analysis of this map showed various distinct features expected from a bar-shaped bulge, including a longitudinal asymmetry in the infrared brightness of the bulge. The near-side of the bar was found to be in the first galactic quadrant, consistent with the findings from the distribution of stellar tracers. The shape and orientation of the bulge remained poorly determined.

Fascinating new data were provided by the Diffuse Infrared Background Experiment (DIRBE) on NASA's Cosmic Background Explorer (COBE) satellite, which was



*This figure presents a new view of the Milky Way Galaxy obtained by the DIRBE on NASA's COBE satellite. This image combines images obtained at near-infrared wavelengths of 1.2, 2.2, and 3.5  $\mu\text{m}$  represented, respectively, as blue, green, and red colors. The image is presented in galactic coordinates, with the plane of the Milky Way Galaxy horizontal across the center, the galactic northpole at the top, south pole at the bottom, and galactic center at the center. The region covers galactic longitudes from 264° (right) to 96° (left).*



launched in November 1989. NASA/GSFC was responsible for the design, development, and operation of COBE, under the scientific guidance of the COBE Science Working Group. DIRBE conducted an all-sky survey in ten infrared bands, and provided the striking new image of the Milky Way shown in the figure. The picture is a composite image of our Galaxy at 1.25, 2.2, and 3.5  $\mu\text{m}$ . These wavelengths provide an almost unobscured view of the galactic bulge. The orange colored regions along the galactic disk delineate the lines-of-sight where the emission, primarily at 1.25  $\mu\text{m}$  and 2.2  $\mu\text{m}$ , is still strongly absorbed by intervening dust.

The improved sensitivity and the simultaneous wavelength coverage of the DIRBE instrument make the DIRBE data ideal for studying the bulge morphology. The DIRBE image shows that the bulge has a box-like, perhaps peanut-shaped, appearance. A more careful inspection suggests that the bulge appears larger at positive galactic longitudes than at negative longitudes.

A more quantitative analysis of the bulge morphology requires the removal of confusing foreground emissions and absorption from the image, which brings out the asymmetry in the light distribution in this "corrected" view of the bulge. Furthermore, the DIRBE bulge images show that the peanut-shaped appearance was largely an artifact created by the presence of a heavily obscuring dust cloud in front of the bulge, and that the bulge has more of a box-like appearance. Detailed numerical modeling of the light distribution of the bulge at these wavelengths confirms that the bulge is bar-shaped, with its near-side in the first galactic quadrant. The major axis of the bulge is rotated by 10° to 30° from the line of sight to the galactic center, consistent with earlier estimates. The relative brightness of the bulge at the various near-infrared wavelengths is also consistent with previous bulge observations in the direction of Baade's window, suggesting that

most of the stars that give rise to the near-infrared emission are K and M giants. The total infrared luminosity from these stars is about six billion solar luminosities, about 15 percent of the total energy output from the Galaxy. From the integrated light from the bulge, the total number of K and M giants can be estimated, and with the aid of stellar evolutionary theory, the total mass of bulge stars that are still on the main sequence can be derived. The mass of the bulge obtained by this photometric method is between 8 and 15 billion solar masses, accounting for about 5 percent of the total mass of the galactic disk, consistent with the bulge mass derived from stellar dynamics.

The DIRBE observations provide astronomers with a new means for studying the nature of the Milky Way bulge. These data will continue to be a source of valuable information which will undoubtedly lead to new questions regarding the nature and evolutionary history of this remarkable feature in the center of our Galaxy.

Contact: Eli Dwek (Code 685)  
301-286-6209

Sponsor: Office of Space Science

*Dr. Dwek is an astrophysicist in the Laboratory for Astronomy and Solar Physics at NASA/GSFC, and a member of the COBE Science Working Group. Born in Israel, he received a Masters in Nuclear Physics from the Hebrew University in Jerusalem in 1973, and a Ph.D. in Astrophysics from Rice University in Houston. He held postdoctoral fellowships at the Kellogg Radiation Lab. at Caltech (1977-1979) and at the Astronomy Department at the University of Maryland (1979-1981). His main research interests are cosmology, stellar and galactic evolution, the evolution of supernovae and supernova remnants, and studies of the interstellar medium.*

## AN OBJECT-ORIENTED MULTIMISSION AND MULTISPECTRAL ASTROPHYSICS DATA CATALOG

**A**STROPHYSICAL DATA analysis demands efficient access to large volumes of complex data, which are often stored in disparate mass storage systems, and in different formats. This is largely a historical development, reflecting the evolution of computers and mass storage technology over the past 30 years. These data are products of space missions and, hence, are stored in archives according to mission-specific parameters. These astrophysics databases constitute a huge investment, and the information in them a key NASA (and national) asset. Facilitating access to them is a key concern.

Scientists often wish to conduct research that cuts across mission boundaries, and would do so more often were it not so challenging to locate and understand unfamiliar data sets. It is generally advantageous, for example, to use multiwavelength observations to interpret a class of celestial objects. Yet it is currently necessary to learn the specific structure of each NASA mission data archive before one can determine whether the relevant data exist and then access them. The user has to know *a priori* which data archive to search. Some mission archives have built interfaces to make the underlying database structure transparent to the users. Nonetheless, the search is conducted one data set at a time and one mission at a time, and the researcher must integrate information gleaned from the various catalogs. The problem is exacerbated if the user is unfamiliar with the data products generated by a particular mission, and thus does not even know where to begin. A uniform, multimission user interface is needed to support *global* searches, to make these heterogeneous, distributed data holdings behave as if they formed part of a single database.

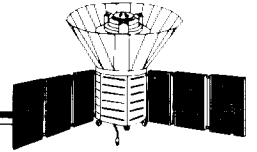
There are other problems for the astrophysical investigator. For example, scientific databases share a distinctive characteristic, their basic structure (schema) evolves as new views need be examined, new techniques and calibration algorithms are developed, and new interpretations of the same raw data are being derived. At the same time, the old schema must be maintained to support previous applications, algorithms, and access methods. Even for a single mission, it often happens that the same data files are moved several times to satisfy the different database schema employed at various phases of the mission. A penalty is incurred for this inefficient procedure: the total physical storage requirement for the mission is multiplied and there is a considerable cost in wasted personnel time.

It would be both economical and useful to store the files once and adapt the interface as the access requirements to the data evolve.

Traditionally, relational databases are used to represent the astrophysics catalogs. But their rigid organization is ill-suited to handle the necessary schema evolution. Also, a significant fraction of the metadata are in semistructured form, e.g., documentation in free text, which cannot be exploited by traditional relational database technology. A better solution to these problems may be found in object-oriented database (OODB) methodology. The hierarchical nature of many of the scientific data relationships favors an object-oriented approach, which more closely mirrors the structure of the data. The OODB technique allows much greater flexibility in characterizing classes of "objects" (astronomical objects as well as "objects" in the OODB sense) and can provide a scientific view into the heterogeneous data archive without changing the existing underlying mission-oriented structure.

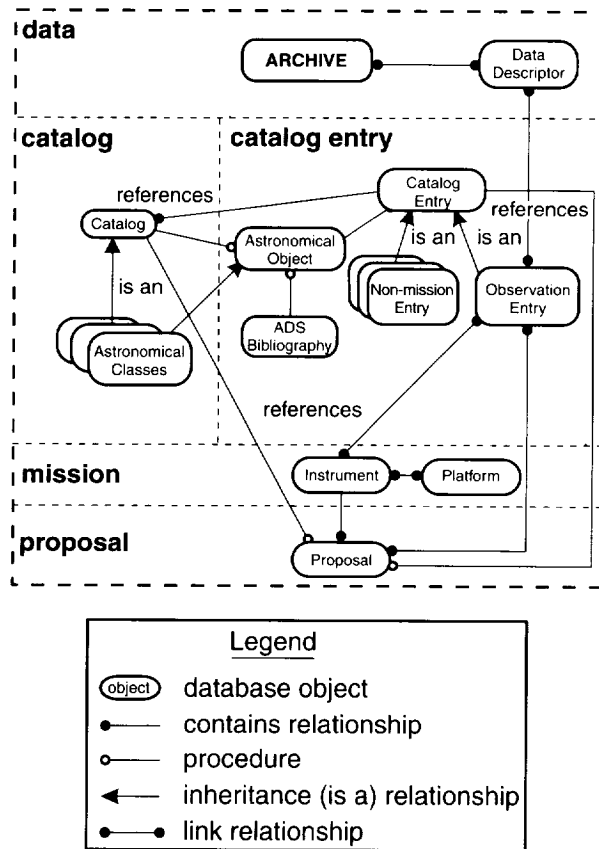
To address these problems, the GSFC Astrophysics Data Facility is developing the Astrophysics Multispectral Archive Search Engine (AMASE), an on-line data catalog that consists of scientific reference pointers to enable scientists to locate appropriate low-level archival astrophysics data across catalogs by specifying scientific (as opposed to mission) parameters. A central tenet of our approach to building AMASE is that it is impractical to require the existing databases to be ported to new systems, with application programs rewritten to operate against new interfaces, or to require unstructured data to be moved from flat file systems into a database. OODB techniques are being used to classify data products with scientific attributes. An automated data cataloging system is also being developed to glean the scientific attributes directly from the mission data files. This ensures that the metadata (i.e., descriptive data about the data) are consistent with the data. The metadata are then merged using OODB methodology to form the multimission and multispectral catalog. The catalog uses World Wide Web (WWW) browsers as the major user interface.

We seek to encapsulate the existing data, metadata, associated documentation, and analysis software into "objects" in our catalog, anticipating the complex requirements that arise in the course of scientific inquiries. The scientific attributes include fundamental astronomical



measurements such as name of object, position, coordinates, flux, spectral bandpass, surface brightness, color, velocity, proper motion, redshift, and astronomical classification. These attributes are generally available in published astronomical catalogs. The AMASE is being designed to capture relevant information from the astronomical catalogs and use it as criteria to search the mission data archives. The mission data are described using attributes gleaned from the mission timelines, target lists, and observation logs that are generated directly from the FITS headers of data files in the archives. These attributes include pointing position, observation time, instrument configuration, and name of primary target. Other information, such as the instrument field of view, spectral coverage, and operation time span, is also captured and used in algorithms to aid the search. In AMASE, all the scientific attributes and mission data attributes are linked by OODB techniques to an "Astronomical\_Object." An "Astronomical\_Object" can be a single astronomical object, a class of astronomical objects, or an abstract class with well-defined scientific attributes. A hierarchy of astronomical "classes" has been defined in the OODB so that a child class inherits all the attributes of the parent class. For example, an active galaxy is characterized by all the attributes of the "galaxy" class, plus some additional attributes that are specific to the "active galaxy" class. When a user queries for science data, the search criteria are issued against the "Astronomical\_Object," and the query results are returned in terms of mission data descriptors. The mission data descriptors identify the names of the relevant mission data sets, archive location, and retrieval information, as shown in the figure.

For the prototype effort undertaken during this past year, two missions that examined different wavelength bands and with different mission operations philosophies were selected to demonstrate multimission and multispectral search capabilities. The Roentgen Satellite (ROSAT) is an x-ray mission that is still operating, with data gathered from pointed observations by guest investigators. The Infrared Astronomy Satellite (IRAS) was an infrared mission that was operated mainly in the scanning mode. The available data products from these missions were reviewed and parameterized for input to AMASE. The team decided to store only fundamental astronomical measurements that will help locate low-level data. Other derived quantities will either be generated dynamically by algorithms stored in the OODB, or referenced via



High-level database design of AMASE.

hypertext pointers to the actual data products in the archives. There is an on-going tradeoff in the design process between database performance and data storage capacity. Typical user scenarios are used to guide the development of the query engine and its optimization.

AMASE uses the hybrid object-relation database product, Illustra, to provide the benefits of object-oriented technology and to support access to existing relational databases using Standard Query Language (SQL). The system hardware consists of a Silicon Graphics Indigo-2 workstation, with a 40-GB magneto-optical jukebox and a standalone DLT tape drive as secondary storage. The system is being used initially to process and extract metadata for ROSAT and IRAS. Subsequently, it will become a server on the Internet for the scientific community to access the astrophysics data archive through AMASE.

## SPACE SCIENCES

---

The AMASE project is a collaboration between the GSFC Astrophysics Data Facility and the Computer Science Department of the University of Maryland, College Park. Other team members at GSFC are Dr. David Leisawitz, Dr. Gail Reichert, Mr. David Silberberg and Mr. Jim Blackwell. The University of Maryland team is headed by Dr. Nicholas Rousoupoulos.

Contact: Cynthia Cheung (Code 631)  
301-286-2780  
Internet: [Cynthia.Y.Cheung.1@gsfc.nasa.gov](mailto:Cynthia.Y.Cheung.1@gsfc.nasa.gov)

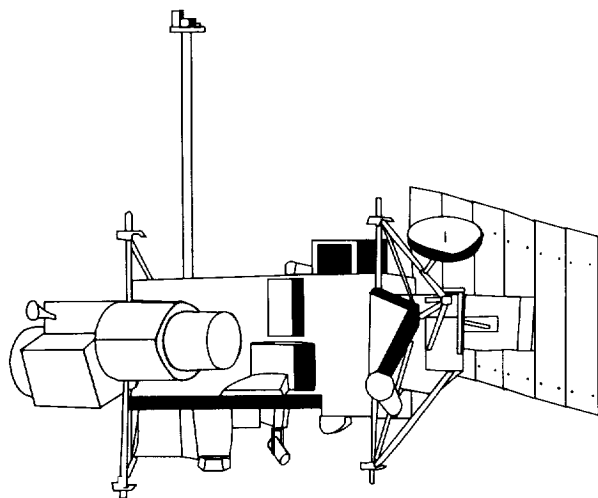
Sponsor: Office of Space Science

*Dr. Cheung is an astrophysicist at the GSFC Astrophysics Data Facility. She is responsible for using advanced technology to develop better user interfaces to the public astrophysics data archive. She has an A.B. in Astronomy from the University of California at Berkeley and a Ph.D. in Astronomy from the University of Maryland.*

---

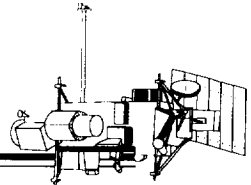
---

*EARTH  
SYSTEM  
SCIENCE*





*Colorized map view of the 100 m scale topographic ruggedness of Iceland in the North Atlantic. This image depicts how rugged the landscapes of Iceland are at 100 m length scales (shown in colors, with hot colors being more rugged than cool ones) in order to illustrate the kinds of measurements that are now possible from Earth Orbit using echo recovery laser altimetry methods as demonstrated by the recently completed Shuttle Laser Altimeter experiment. The data shown here were derived from digital elevation models, but emulates how orbital laser altimeter echoes could be used to quantify the vertical ruggedness of complex landscapes. Low-lying gravel outwash plains in front of active glaciers are extremely smooth (southern coast of Iceland) in contrast with volcanically active uplands and the margins of icecap glaciers (interior of Iceland). The oldest fjord-like regions of Iceland are severely eroded and indicate high relative ruggedness value in this sort of image. Iceland is an important oceanic hot-spot at a major divergent plate boundary in the mid-Atlantic Ridge system and has a long geologic history extending many millions of years. This image suggests that ruggedness can be used to classify landscapes in terms of degree of erosion, relative age and formation process history.*



# EARTH SYSTEM SCIENCE

OVER THREE DECADES AGO, humans obtained their first comprehensive view of the Earth from space. From this perspective, it became increasingly apparent that phenomena and processes on the Earth—and within it—are interconnected: oceans play a role in determining climate and weather patterns; climate affects the land surface and vegetation; volcanoes can affect climate; and, perhaps most importantly, it has become apparent that humans are becoming a significant force in determining the state of the Earth's environment.

The activities dedicated to understanding this interconnectivity has been termed *Earth System Science*, which involves studying the processes that link the biosphere, lithosphere, atmosphere, and hydrosphere, and includes modeling these processes and testing the models. To fully encompass the global nature of these interactions observations from the vantage point of space are required. This forms the basis for the Earth science research and technology development carried out at GSFC, and the central theme of the articles in this section (and, where appropriate, in other sections of this volume), offered as current and major examples of this R&D effort.

We regard the various spheres of the Earth as a continuum. In this report, we might think of starting at one end of this continuum at the higher reaches of the Earth's atmosphere—the “mesosphere”, as dealt with in the paper on periodic oscillations generated by gravity waves in the middle atmosphere. This paper contains themes also discussed in other papers: gravity waves are also an important factor in terms of global climate models, and quasi-biennial oscillation effects are observed in the Earth's surface temperatures and its outgoing longwave radiation.

At the other end of this continuum are studies of the Earth's interior. GSFC has been noted for its accurate and detailed numerical models of the Earth's gravity field, as discussed in a paper that gives yet another way to improve such models using TDRSS satellites. Space geodesy has also allowed us to consider observing the rise of the land surface after removal of the load imposed by the Ice Age, or the tilt in the Earth's inclination, which may be caused by climate change.

At the Earth's surface, our scientists are monitoring soil conditions in the northern Tibetan Plateau, developing and evaluating techniques for measuring snow and snow depth, and mapping urban sprawl.

But our research hinges, in large measure, on our ability to make new observations and to conceive, design, and develop new techniques for making these observations and analyzing the data. Laser altimetry is an exciting new technique which will be able to determine topographic elevations with high precision; such instruments have already been flown aboard aircraft, and have been designed and are now scheduled to fly aboard the Shuttle. Other instruments are being designed with novel detector systems, such as the diode array, which has also been incorporated into an aircraft spectrometer. In order to handle these and other high-volume data sets quickly and efficiently, new parallel-processing workstations have been designed.

The papers that follow are but a few examples of the interdisciplinary research and development efforts being carried out at GSFC in our effort to understand the Earth as a comprehensive system.

*Lou Walter*

**WATER****ESTIMATES OF SENSIBLE AND LATENT HEAT FLUX  
OVER GLOBAL OCEANS**

THE STUDY OF CLIMATE requires accurate observations of the components of the climate system (e.g., atmosphere, land, ocean, cryosphere) and numerical models capable of simulating the physical and dynamical processes in the system. Observations traditionally have been obtained through *in situ* measurements from land-based stations, buoys, ships, balloons, and aircraft. However, over most of the globe, observations with high spatial resolution are obtainable only by satelliteborne sounders, which measure outgoing radiation from the Earth-atmosphere system.

As part of the Pathfinder program, a version of the Goddard Laboratory for Atmospheres' interactive forecast-retrieval-analysis system has been used to retrieve surface and atmospheric fields from radiances measured by the TIROS Operational Vertical Sounder (TOVS) High Resolution Infrared Radiation Sounder 2/Microwave Sounding Unit (HIRS2/MSU), on board National Oceanic and Atmospheric Administration polar-orbiting satellites. The retrieved fields include land/ocean surface temperature, profiles of temperature and moisture, cloud parameters, outgoing longwave radiation, and precipitation. The data are gridded on a  $1^\circ \times 1^\circ$  grid, on a daily, 5-day, and monthly basis, for ascending and descending orbits. The data set is ideal for the study of climate variability on global and regional scales.

One dominant global scale climatic phenomenon that often has adverse socioeconomic impacts in many parts of the world is the El Niño/Southern Oscillation (ENSO). This oscillation is driven by instabilities in air-sea interactions in the tropical Pacific Ocean. The means by which the atmosphere and ocean interact is through exchanges of quantities such as heat, water vapor, and momentum.

In this study, TOVS HIRS2/MSU surface skin temperature, surface air temperature, and surface specific humidity are used in conjunction with European Center for Medium Range Weather Forecasting data on surface winds to estimate the air-sea latent and sensible heat fluxes during 1987 (an El Niño year) and 1988 (a La Niña year). The fluxes are computed on a 5-day basis using the Bulk Aerodynamic method.

TOVS HIRS2/MSU surface skin temperature and vertically-integrated water vapor have been compared to

Climate Analysis Center sea surface temperature (SST) data and Special Sensor Microwave/Imager water vapor data. Over the global oceans, the SST data generally agree to within 1 K. TOVS water vapor data are within 0.2 cm of SSM/I estimates.

Panels a and b in the figure show the time series of 5-day, zonally averaged latent heat (LH) and sensible heat (SH) flux from January 1987 to December 1988. The magnitude of the fluxes is determined, in part, by the wind speed, while the direction is dictated by the air-sea gradients of temperature and moisture for SH and LH, respectively. Generally, the LH is positive (from the ocean to the atmosphere) except over the polar oceans, where it is negative from October to February. The SH has a similar distribution, except that the ocean south of  $60^\circ\text{S}$  has high ocean-to-atmosphere flux during the southern hemisphere winter, when the ocean remains warmer than the overlying air. Both fluxes have a dominant seasonal cycle, with overall global maxima during the northern hemisphere winter. There is a local minimum at the equator which is especially pronounced from June to September.

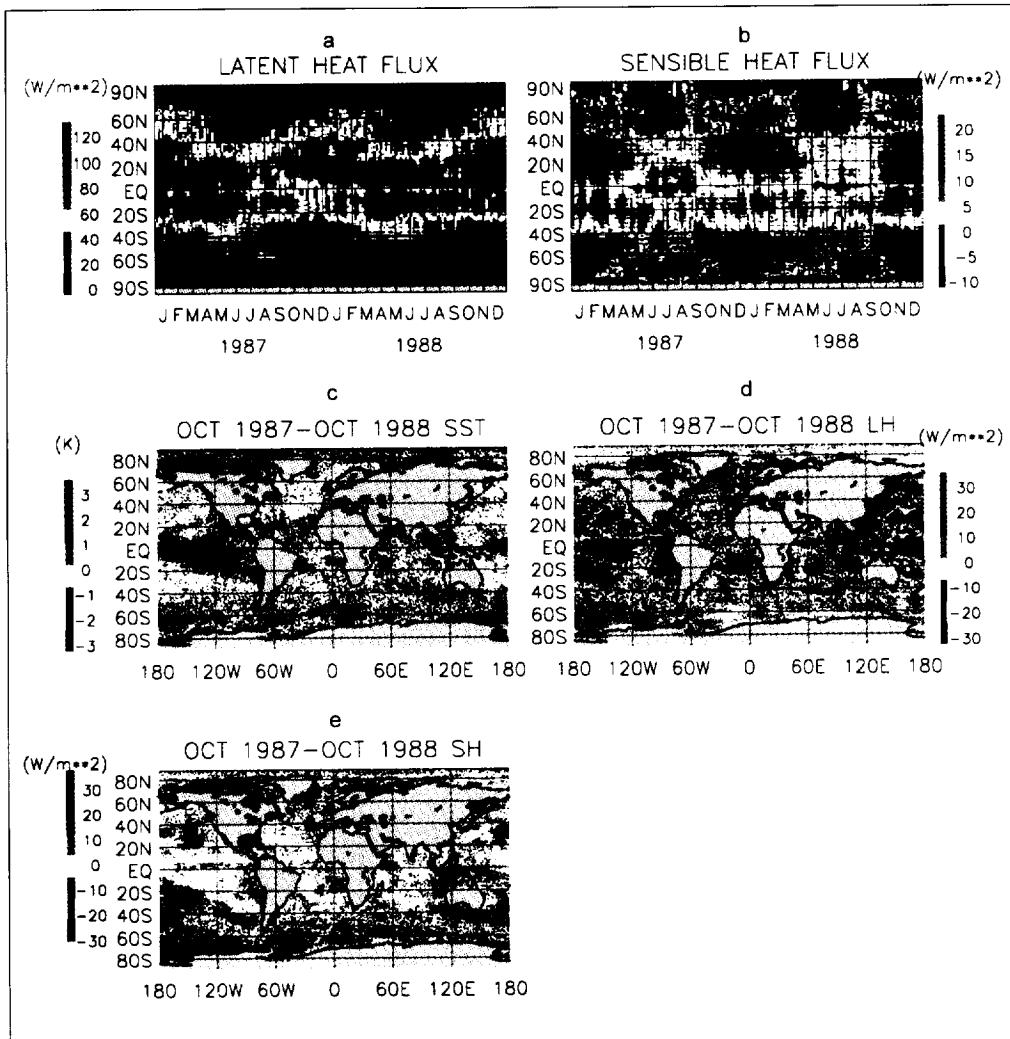
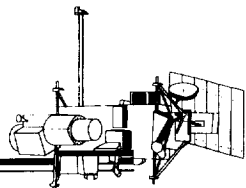
Comparisons between 1987 and 1988 have been made. Panel c shows the difference between the SST in October 1987 and October 1988. In the Equatorial East Pacific, 1987 was warmer than 1988 by at least 2 K during this month. Panels d and e show the corresponding differences in LH and SH, respectively. It is clear that the area of maximum warming does not necessarily coincide with maximum positive fluxes. This is because of the dependence of the fluxes on gradients of moisture, temperature, and wind speed. Generally, the spring, summer and autumn of 1987, though warmer and moister, had weaker winds and weaker air-sea temperature and moisture gradients than 1988.

The ability to make comparisons such as these will help us understand the mechanisms underlying many Earth system phenomena.

Contact: Joel Susskind (Code 910.4)  
301-286-7210

Ebby Anyamba (USRA)  
301-286-7430

Sponsor: Office of Mission to Planet Earth



*Time series of zonally-averaged 5-day mean (a) latent heat flux, (b) sensible heat flux over the global oceans for 1987-1988, (c) the difference between October 1987 and October 1988 SST, (d) the difference between October 1987 and October 1988 latent heat flux, and (e) the difference between October 1987 and October 1988 sensible heat flux.*

*Mr. Susskind is Head of the Satellite Data Utilization Office and Senior Scientist at GFSC. He is also the METSAT Project Scientist, NASA Co-chairman of the Integrated Sensor Working Group (for NOAA/DOD/NASA convergence activities) and AIRS Team member. His research interests lie in theoretical and experimental infrared and microwave molecular spectroscopy, atmospheric radiative transfer, and infrared and microwave satellite meteorology.*

*Ms. Anyamba is a research associate in the Satellite Data Utilization Office. She received her B.S. and M.S. from the University of Nairobi, Kenya, and Ph.D. in Atmospheric Sciences from the University of California-Davis. Her research involves use of satellite data in the study of short-term climate variability. She has been at GSFC since February 1995.*

## DIURNAL VARIATIONS IN TROPICAL ATMOSPHERIC CONVECTION OVER OCEANIC REGIONS

OVER CONTINENTAL REGIONS, studies have established that thunderstorms often occur in the late afternoon due to strong surface heating, while over open oceans the strongest convection and maximum rainfall tends to appear in the late evening due to atmospheric radiation-cloud interactions. Other mechanisms, like orographic forcing and land-sea contrast, are also known to contribute to diurnal variations in various geographic regions.

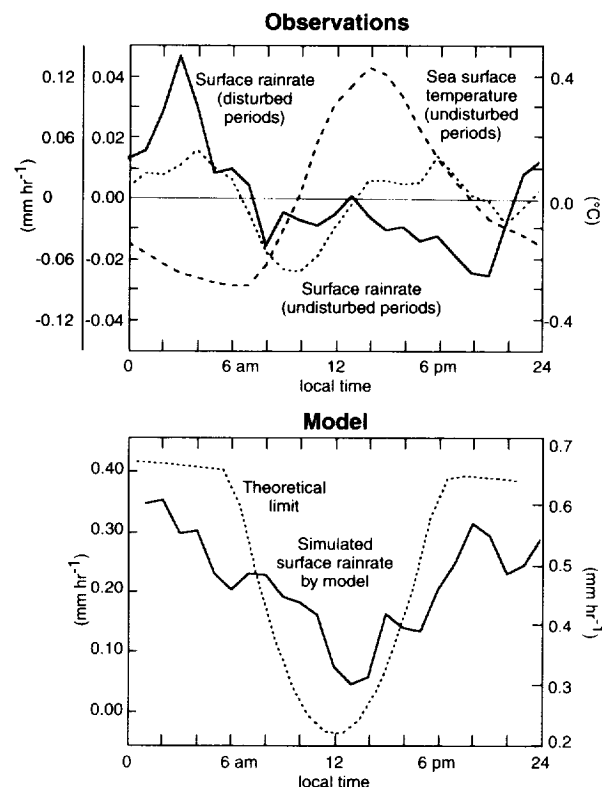
In this study, we focus on oceanic regions free from continental influence to analyze diurnal variations of atmospheric convection (and rainfall) over the oceans to identify the mechanisms for producing the diurnal variations.

A proposed basic mechanism has attributed the nocturnal mode to a thermodynamic response of the atmosphere to solar heating and infrared cooling, such that clouds are reduced during the day and enhanced in the evening. A more sophisticated mechanism emphasized the radiative heating differential between cloudy regions and clear regions. The first mechanism works whether vertical motions exist or not, while the second mechanism is more applicable when vertical motions are strong. In this study, the diurnal variations are analyzed separately in large-scale disturbed and undisturbed periods. A two-dimensional cloud-resolving model and an ocean-mixed-layer model are further used to identify the relevant mechanisms.

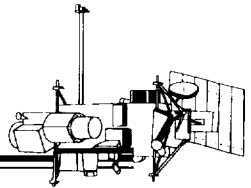
We analyzed observations collected in a recent field experiment, the Tropical Ocean Global Atmosphere/Coupled Ocean Atmosphere Response Experiment (TOGA-COARE), in the tropical western Pacific region. The observational analysis includes rainfall and cloud statistics based on surveillance scans by two shipborne radar and satellite measurements, and mass, heat, and moisture budgets based on upper-air soundings within the special observation array.

The rainfall and cloud statistics reveal that most active convection appears between midnight and sunrise. This nocturnal mode accounts for 43 percent of the total

variance in area-mean rain rate. As shown in the top panel of the figure, the diurnal composite results show that the nocturnal mode exists in both disturbed and undisturbed periods, but is more easily distinguished in the disturbed periods. In addition to the nocturnal mode, a secondary peak appears in late afternoon. The afternoon mode is much better defined in the undisturbed periods, when sea-surface temperature (SST) shows a strong diurnal cycle.



As shown in the top panel of the figure, the diurnal composite results show that the nocturnal mode exists in both disturbed and undisturbed periods, but is more easily distinguished in the disturbed periods. As shown in the lower panel of the figure, experiments with constant SST (to eliminate the diurnal surface forcing), pronounced nocturnal rainfall maxima are simulated.



Analysis of divergence, vertical velocity, heat and moisture budgets further indicates that the development of nocturnal convection is associated with the establishment of thermodynamic instability in the early evening. This destabilization arises due to the radiative cooling in the troposphere, and moistening in the lower troposphere. Our analyses also show that afternoon convection is preceded by enhanced boundary layer buoyancy. Cloud structure, stability, divergent circulation, and heat and moisture budgets further indicate that afternoon thunderstorms are shallower and more convective, and nocturnal convection is higher and more stratiform.

Several numerical experiments were carried out to study the responses of the cloud-resolving model to two different large-scale forcings (in terms of imposed mean vertical motion, horizontal wind, and SST), representative of disturbed and undisturbed conditions. In experiments with constant SST (to eliminate the diurnal surface forcing), pronounced nocturnal rainfall maxima are simulated; an example is shown in the lower panel of the figure. The amplitude of the diurnal cycle appears to be insensitive to the cloud-radiative forcing. The amplitude of the nocturnal cycle in rainfall can be explained by the time-rate-of-change of saturation of total precipitable water as a function of diurnally varying temperature, as shown in the lower panel in the figure. This suggests a fundamental mechanism for producing nocturnal maximum rainfall (i.e., the atmospheric sustainability of moisture as a function of temperature due to the Clausius-Clapeyron relationship). In experiments with diurnally varying SST, the amplitude of the nocturnal peak is reduced, and a secondary peak appears in the afternoon.

The present study leads us to conclude that the diurnal cycle of the radiative heating within the atmosphere leads to nocturnal convection, and the diurnal cycle of the radiative heating at the surface leads to afternoon showers. The fundamental mechanism that contributes to maximum nocturnal rainfall is a direct thermodynamic response to the heating-induced destabilization in the night and stabilization in the day.

In the disturbed periods, cloud-radiative interactions may act to intensify the diurnal variations through the horizontal heating gradient due to heating in the cloudy regions relative to clear regions, and the vertical heating gradient between the cloud tops and cloud bases.

Contact: Chung-Hsiung Sui (Code 913)  
301-286-2122

William K.-M. Lau (Code 913)  
301-286-7208

Xiaofan Li (Code 913)  
301-286-3070

Sponsor: Office of Mission to Planet Earth

*Dr. Sui works in the Climate and Radiation Branch of the Laboratory for Atmospheres. His current research effort focuses on analysis and modeling of the water cycle in the climate system. His research interests included Tropical Meteorology and Climate Variations. Dr. Sui earned a Ph.D. in Atmospheric Sciences from the University of California, Los Angeles.*

*Dr. Lau is Head of the Climate and Radiation Branch. His research areas cover theoretical, observational, and modeling aspects of the climate system. He is the Principal Investigator of the Earth Observing System/Global Hydrologic Processes and Climate Interdisciplinary Science Investigation. Dr. Lau received his Ph.D. in Atmospheric Sciences from the University of Washington.*

*Dr. Li is working with a coupled model to study the role of high-frequency air-sea interaction in climate variations. Dr. Li received his Ph.D. in Atmospheric Sciences from the University of Hawaii.*

## COMPARISON OF DAO AND NMC REANALYSES WITH SATELLITE DATA OVER TROPICAL OCEAN DURING 1987 AND 1988

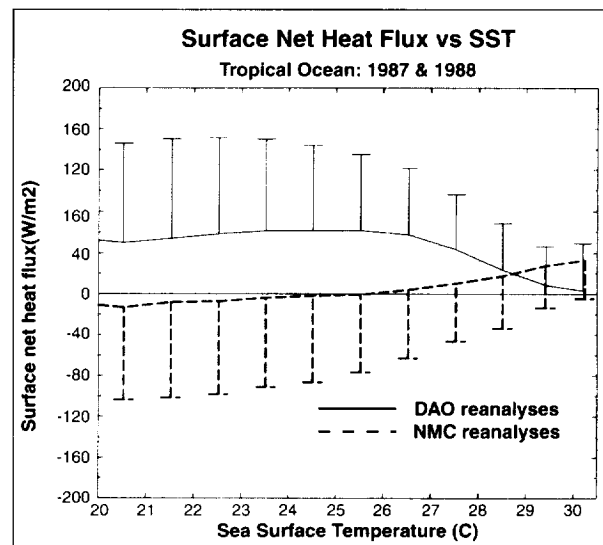
IN A FOUR-DIMENSIONAL data assimilation system (DAS), the atmospheric data are assimilated in such a way that consistency between the dynamical and physical fields is maintained everywhere within the constraints of the resolution of the model. Since observational data are ingested quite frequently (every 6 hr), the DAS products are often used as best estimates of observations. Nevertheless, these data sets cannot be viewed as "truth" because they are affected by DAS biases. Consequently, different analysis centers using different analysis systems are bound to produce somewhat different analyses. Changes to a DAS naturally follow research and development; however, a "frozen" DAS will produce temporally consistent analyses. Recently, the National Meteorological Center (NMC) and the Data Assimilation Office (DAO) at GSFC each completed an 8-year (1985 to 1993) reanalysis of data by ingesting *in situ* and satellite observations using frozen versions of DASs. We have examined the differences between these DAO and NMC reanalyses over the tropical ocean ( $30^{\circ}\text{S}$  to  $30^{\circ}\text{N}$ ) regions for the period from 1987 to 1988, and compared them with the monthly satellite data, wherever possible. Such an investigation is vital if the analyzed data are used in research applications and/or forcing other models, such as ocean general circulation models.

For temperature and humidity distributions, we used TIROS Operational Vertical Sounder (TOVS) Path A data produced at the Laboratory for Atmospheres at GSFC. For precipitation, we used three satellite-data-based estimates: (1) (Microwave Sounding Unit (MSU) measurements, (2) TOVS-Path A infrared retrievals, and (3) Global Precipitation Climatological Project (GPCP) data on the International Satellite Land-Surface Climatology Project NASA-Distributed Active Archive Center (DAAC) CD-ROM. For radiation fluxes at the top of the atmosphere, we used Earth Radiation Budget Experiment data. For the surface radiation, we used satellite-data-based radiation fields produced at NASA/Langley Research Center. We also used sea surface temperature (SST) analysis data produced at NMC.

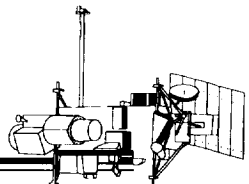
In the annual averages, a good agreement is evident among DAO and NMC reanalyses and satellite data products. Nevertheless, some common (and model-specific) biases are noteworthy. The common bias is in the dryness (low specific humidity) of the lower troposphere. In the NMC reanalyses, this is partly caused by a cold bias in the lower

troposphere. Such a dry bias leads to reduced trapping (water vapor greenhouse effects) of infrared radiation emitted to space. Longwave cooling at the ocean surface is overestimated because the down-welling infrared radiation emitted by water vapor gets reduced. The shortwave cloud radiative forcing, a measure of the reflected shortwave radiation by clouds, also shows significant differences as compared to the ERBE data. The DAO reanalysis underestimates it in the cold subtropical regions, and overestimates it in the warm (highly convective) tropical regions; the NMC reanalysis overestimates it everywhere. Such biases induce large errors (10 to 50  $\text{W/m}^2$ ) in the solar radiation absorbed at the surface.

Latent and sensible heat fluxes at the ocean surface are also quite different between the DAO and NMC reanalyses (often differing from observations by  $20 \text{ W/m}^2$  and  $3 \text{ W/m}^2$ , respectively). Together with the shortwave cloud-radiative forcing differences discussed earlier, the net surface energy into the ocean is quite different between the two reanalyses (as shown in the first figure). This must be duly recognized by the ocean modelers intending to use DAO and/or NMC reanalyses to force their models, because large analysis biases can produce vastly different forcings of the ocean circulation. The satellite-data-based



Mean surface Net Heat Flux derived from DAO and NMC reanalyses over tropical ocean for the period 1987 - 1988 as a function of the SST. Vertical bars represent the standard deviation.



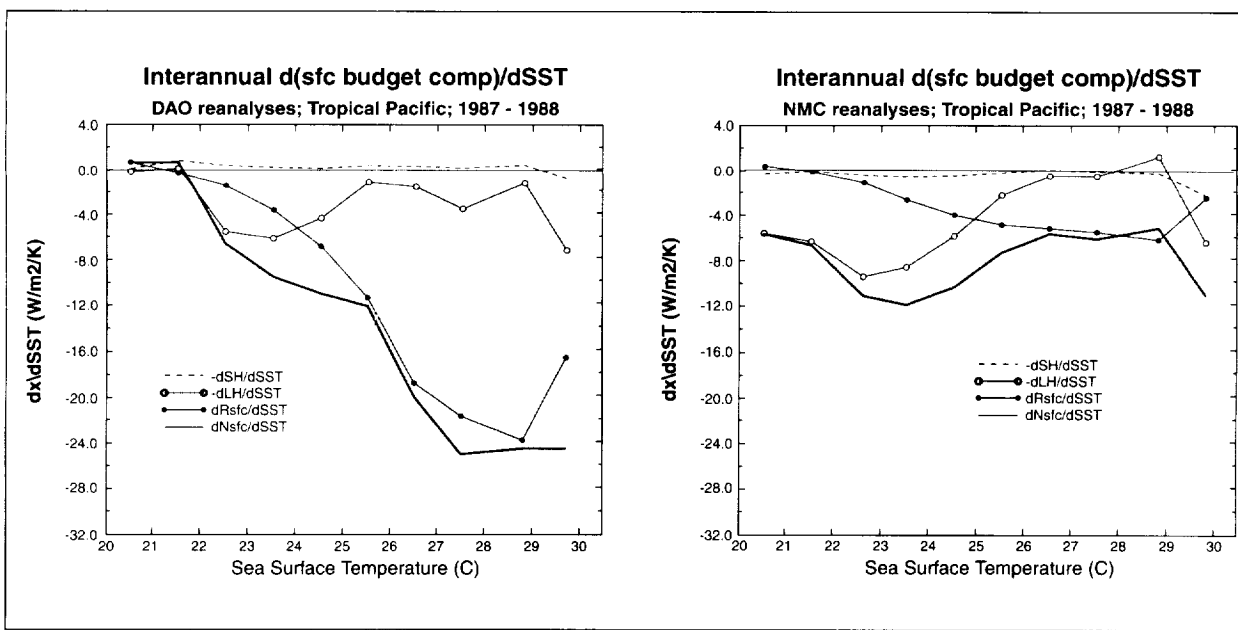
estimates of precipitation also differ somewhat among the MSU, TOVS, and GPCP data sets; GPCP estimates are generally larger than TOVS estimates, but smaller than MSU estimates. However, on the average, the DAO precipitation is in much better agreement with GPCP data, while the NMC precipitation shows comparatively larger errors.

We have also compared the interannual anomalies of physical and dynamical fields in the DAO and NMC reanalyses for the chosen period. In general, these anomalies are in good agreement with the satellite-derived observations. However, the magnitude of the interannual variability is overestimated in DAO reanalyses, while it is comparatively well-reproduced in the NMC reanalysis, even though the NMC anomaly patterns are shifted eastward as compared to models. The interannual variability of the different components of the surface energy budget is qualitatively similar in both reanalyses, although quantitative differences appear, as shown in the second figure. In the cooler subtropical regions, the surface evaporation increases with SST, and the evaporative cooling of the ocean is larger than the radiative cooling induced by the cloud-cover anomalies. Conversely, in the warm tropi-

cal regions, the evaporation anomalies are small, and the warming tendency of the ocean is largely countered by enhanced screening of the solar radiation by clouds. However, the magnitude of the interannual anomalies of the net atmospheric heat flux into the ocean is quite different between the reanalyses.

Despite above differences in the heating fields, the dynamical fields on the monthly to interannual time scales are quite similar. For example, the spatial distribution and the occurrence of different large-scale circulation regimes (binned by vertical velocity) is very similar in both reanalyses. The contrast in the comparisons of the physical (particularly radiation) and dynamical fields is easily explained by recognizing that the analysis increments are applied so as to relax the dynamical fields to the observations, while the physical fields continue to suffer from parameterization biases.

Our investigation reveals that further improvements are needed in the physical parameterizations involving water vapor, clouds, and cloud-radiation interactions. Nevertheless, the main characteristics of the observed climate variability, particularly in the dynamical fields, are well-



Linear regression coefficient between SST anomalies (regional monthly anomalies between 1987 and 1988) and anomalies in the different components of the surface energy budget over tropical ocean. LH: Latent heat flux; SH: Sensible heat flux; Rsc: surface net radiation; Nsfc: surface net heat flux (units:  $W/m^2/K$ ).

reproduced in both analyses. Consequently, the assimilated products constitute useful tools to better understand the physical and dynamical processes that govern climate variability. With ongoing research to improve DASs, future data are likely to be even more powerful research tools than those currently available. Despite the above deficiencies, the reanalyzed data can be used to study the interactions among atmospheric temperature, water vapor, and radiation, as shown in a companion article, elsewhere in this report.

Contact: Sandrine Bony (Code 913)  
301-286-4910  
Internet: bony@lmd.ens.fr

William K.-M. Lau (Code 913)  
301-286-7208

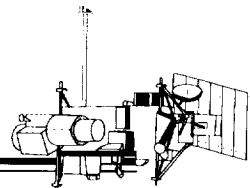
Yogesh C. Sud (Code 913)  
301-286-7840

Sponsor: Office of Mission to Planet Earth

*Dr. Bony is a visiting scientist with the Climate and Radiation Branch of GSFC. She is a visiting scientist from the Laboratoire de Meteorologie Dynamique (LMD) du CNRS in Paris, France.*

*Dr. Lau is Head of the Climate and Radiation Branch. His research areas cover theoretical, observational, and modeling aspects of the climate system. He is the Principal Investigator of the Earth Observing System/Global Hydrologic Processes and Climate Interdisciplinary Science Investigation. Dr. Lau received his Ph.D. in Atmospheric Sciences from the University of Washington.*

*Dr. Sud has been a scientist at the Climate and Radiation Branch laboratory since 1980. Dr. Sud uses numerical models and satellite data to understand the influence of physical processes on the behavior of the climate system.*



## IMPROVING AND EVALUATING REMOTELY-SENSED SNOW/MICROWAVE ALGORITHMS AND SNOW OUTPUT FROM GENERAL CIRCULATION MODELS

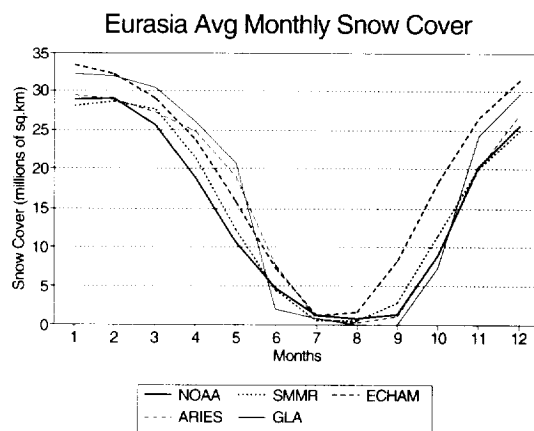
**C**ONFIRMATION OF THE ability of general circulation models (GCMs) to accurately represent snow cover and snow mass distributions is vital for climate studies. There must be a high degree of confidence that what is being predicted by the models is reliable, since realistic results cannot be assured unless they are tested against results from observed data or other available data sets.

In this study, snow output from a number of GCMs and passive-microwave satellite snow data, derived from the Nimbus-7 Scanning Multichannel Microwave Radiometer (SMMR), are intercompared. National Oceanic and Atmospheric Administration (NOAA) satellite data are used as the standard of reference for snow extent observations (as shown in the first figure), and a snow depth climatology (SDC) is used as the standard for snow mass (as shown in the second figure). The reliability of the SMMR snow data must be verified as well, because this is the only available data set that allows for yearly and monthly variations in snow depth, needed to estimate the snow mass. The three GCMs employed in this study are the Max Planck Institute for Meteorology/University of Hamburg GCM, the Goddard Laboratory for Atmospheres GCM, and the Goddard Coupled Climate Dynamics Group GCM. Data for both North America and Eurasia are examined in an effort to assess the magnitude of spatial and

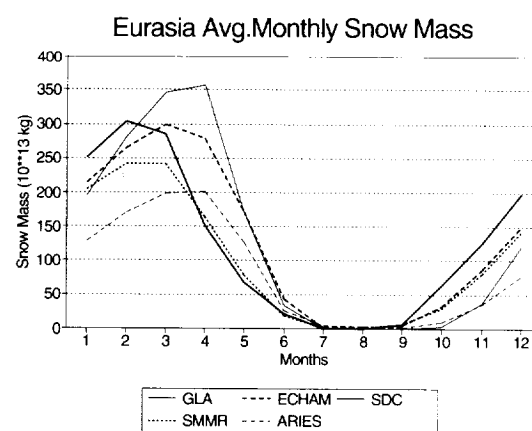
temporal variations that exist between the standards of reference, the models, and the passive microwave data.

Results indicate that both the models and SMMR represent seasonal and year-to-year snow cover distributions fairly well. However, neither the models nor SMMR accurately portray the snow mass in each season. With the SMMR data, dense vegetation and differences in snow crystal size affect the microwave response. Where forests occur, snow mass estimates using the passive microwave approach are generally underestimated. A vegetation index and information on crystal size have now been incorporated in the microwave algorithms developed for North America and Eurasia, and estimates of snow mass can be more reliably used to gauge the performance of the GCMs. Other problems remain that must be accounted for, which, to some degree, influence snow cover and snow mass derivations. These include wet snow (liquid water in the snowpack), signal saturation (very deep snow), mixed pixels (microwave contributions from varying sources), effects of snow metamorphism (melt and re-freeze), and crystal shape.

With the GCMs, the models perform better during the winter months than during the transition months. There is a lack of realism in simulating the snow mass at this time of year due primarily to inaccuracies in modeling



*Intercomparison of snow cover data from NOAA, SMMR, and the Max Planck/University of Hamburg (ECHAM), Goddard Coupled Climate Dynamics (ARIES), and the Goddard Laboratory for Atmospheres general circulation models.*



*Intercomparison of snow mass data from SDC, SMMR, and the Max Planck/University of Hamburg (ECHAM), Goddard Coupled Climate Diagnostics (ARIES), and the Goddard Laboratory for Atmospheres general circulation models.*

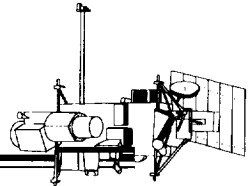
precipitation and temperature fields in the early fall and late winter. For instance, in October the models underestimate the snow mass, and in April the models overestimate snow mass when compared to the SDC data.

These types of intercomparisons are important not only for showing where and to what degree differences exist between the modeled snow amounts and remotely sensed snow estimates, but also for determining why differences exist. This must be known before the models can be refined and improved.

Contact: James Foster (Code 974)  
301-286-7096  
Internet: [jfoster@glacier.gsfc.nasa.gov](mailto:jfoster@glacier.gsfc.nasa.gov)

Sponsor: Office of Mission to Planet Earth  
Goddard Research and Study Fellowship  
Program

*Dr. Foster received his B.S. and M.A. in Geography from the University of Maryland in 1969 and 1977, respectively, and his Ph.D. in Geography from the University of Reading in England in 1995. Since 1973, he has worked at GSFC, and has been employed by NASA since 1978. His professional interests include the remote sensing of snow, global determination of snow cover and snow volume, and the influence of snow on climate. He is a member of the American Meteorological Society (serving on the Hydrology Committee) and of the Eastern Snow Conference (serving as President from 1988 to 1989). Research projects and field work have taken him to locations in Antarctica, Alaska, Greenland, Spitsbergen, and the Northwest Territories of Canada.*



## MONITORING SOIL CONDITIONS IN THE NORTHERN TIBETAN PLATEAU USING SSM/I DATA

**A** MAJOR CHALLENGE in the remote sensing of soil parameters is the development of a robust algorithm that can effectively distinguish the freeze/thaw condition of the soil. Microwave radiometry has been used with success in the Northern Plains of the United States to infer soil freeze/thaw conditions. The usefulness of microwave techniques derive from the fact that the thermal microwave radiation emerging from an object depends on its physical temperature, composition, and physical structure. The large differences between the dielectric properties of water, soil, and ice make it possible to deduce the freeze/thaw condition of soil using microwave measurements, since the dielectric constants of water (~30) and of dry soil (~3.5) at about 20 GHz differ so greatly. In addition, there is strong dependence on thermal emission from soil and its moisture content. This dependence provides a means for remotely sensing the moisture content in a surface layer less than ~5 cm thick.

The high elevation of the Tibetan Plateau exerts a strong barrier effect on the global atmospheric flow, and constitutes an elevated heat source that generates a temperature contrast with the surrounding free atmosphere. A growing body of modeling and observational evidence suggests that the slowly varying surface boundary conditions, such as the freeze and thaw of soil in this region, can influence the interannual variability of the atmospheric circulation of this region and of the Indian monsoon. The freeze/thaw state of soil is not only important in determining the energy exchange between the air and ground through the latent heat of fusion and vaporization, but also in inferring snow depth. Due to its remote geographic location, measurements of these surface parameters are not routinely made, so remote sensing data would be useful in supplementing conventional observations to provide soil condition information.

The Tibetan Plateau covers some 2.5 million km<sup>2</sup>; about 70 percent of this area consists of high pastures. The desolate northern area (Chang Tang), north of about 32°N latitude, is mostly uninhabited or only sparsely populated. It is a place so remote that even nomadic herdsmen do not venture there. The ground observation network in Chang Tang is clearly limited. Remote sensing may be the only way to monitor the soil and snow condition for this inaccessible area on a routine basis.

There is very sparse surface vegetation in this region; the coverage is usually less than 20 percent. The most widely distributed soil type is sand having less than 1 percent organic material; the surface soil moisture content is low most of the time. Due to strong solar radiation, continuous winds, and long duration of sunshine, surface evaporation is very high. Due to low relative humidity (annual average 33 percent) and sparse vegetation coverage, any surface soil moisture will evaporate very quickly. Permafrost underlies much of this area at a depth of 1 to 2 m. Because of the difficulty in obtaining ground truth data, climatology data from Gerze station (32°09'N, 84°25'E), which is located at the edge of Chang Tang, were used to represent the entire Northern Tibetan Plateau in this study.

Freezing influences the measured brightness temperature ( $T_B$ ) of the ground. Usually it will (1) lower the thermal temperature, (2) increase emissivity due to tighter binding of the free soil moisture, and (3) provide a negative brightness gradient. Lower thermal temperature will decrease brightness temperature, and tighter binding of soil moisture will increase brightness temperature. Changes of brightness temperature that result from freezing may either be positive or negative, depending upon soil moisture content. Thus, the combination of (1) and (2) may not support unambiguous characterization of frozen ground. A two-parameter freeze indicator had been tested using Nimbus-7 Scanning Multichannel Microwave Radiometer data. The two parameters were (1) 37 GHz brightness temperature below 247 K, and (2) the 10.7 to 37 GHz spectral gradient having values lower than -0.3 K/GHz. The behavior of the 37 GHz brightness temperature and the dominant characteristics of the spectral gradient can be explained by a one dimensional half-space model for moist soil.

The present study used data from the Special Sensor Microwave/Imager (SSM/I), which is a four-frequency (19.35, 22.235, 37, and 85.5 GHz) microwave radiometer flown in a near-polar Sun-synchronous orbit on a Defense Meteorological Satellite Program satellite. The first SSM/I was launched in June 1987; because it is an operational instrument, additional SSM/I data should be available in the foreseeable future.

The 37-GHz radiation, emerging mainly from the top layer of soil, could provide information on the soil temperature. A regression between soil temperature and 37-GHz brightness temperature gives a correlation coefficient of 0.9. However the standard error of estimate is 5.1 K; thus, 37-GHz brightness alone may not provide an accurate estimate of frozen soil conditions.

The normalized brightness temperatures of morning passes were slightly lower than those of evening passes for both 19 and 37 GHz. This is because the surface moisture at 6 a.m. is usually slightly higher than that found at 6 p.m., owing to percolation of moisture from the lower soil layer during the previous night. The 19-GHz normalized brightness temperatures were systematically higher than the 37-GHz temperature by a few percent for both morning and evening measurements. This is probably due to stronger volume scattering at 37 GHz, which results in a lower brightness temperature.

When the soil freezes, the normalized brightness increases because of changes in the dielectric constant of water with the change in state. The shift in emissivity with freezing is most pronounced at the lower microwave frequencies. At 19.35 and 37 GHz, no significant changes in the normalized brightness temperature were observed when soil state changed from frozen to thawed, and vice versa. This is because the soil is mostly dry, so there are no changes in the dielectric constant or the normalized brightness temperatures.

The figure shows scatter plots of 37-GHz brightness temperature as a function of soil temperature for morning and evening satellite passes. When the soil temperature was less than 0°C, the 37-GHz brightness was lower than 231 K and 238 K for morning and evening passes, respectively. The chosen 37-GHz brightness threshold of 247 K for frozen soil definitely will not work for this area.

The probability of detection gives a sense of the ability of the scheme to find the "freeze" case. However, a given scheme could indicate many more frozen soil cases than are actually found and yet still give a good probability of detection. A high probability of detection should be

accomplished with a small false-alarm rate in order to be meaningful. The percent error is representative of the error in "freeze" delineation with respect to the total number of cases to which the method is applied. The percent error could be small even when the probability of detection is low and the false-alarm rate is high, especially when there is a small number of freeze cases. For a more objective evaluation of the classification scheme, all statistics should be considered.

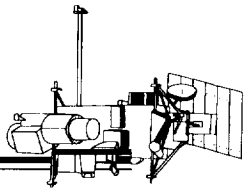
By adopting 231 K and 238 K as the  $T_B$  threshold for the morning and evening cases respectively, classification accuracy improved greatly. These brightness thresholds also happened to be the mean annual brightness temperature for the grid box. Based on this observation, we might be able to generalize the algorithm by selecting the annual mean brightness temperature as the threshold for different regions.

Frozen soil volume scatter decreases  $T_B$  at 19 and 37 GHz, much as is observed for dry snow. Scattering centers, such as ice lenses embedded in the underlying permafrost layer, produce lower microwave signatures throughout the year. These signals would complicate the detection of the freeze/thaw state of soils with snow cover; however, snow cover should not be a major factor. In 1988, as a typical example, there were only 30 days with snow cover, with just a few centimeters of snow reported. With shallow snow cover, the algorithms used in this study can accurately describe soil condition to 90 percent accuracy.

Contact: Alfred T.C. Chang (Code 974)  
301-286-8997

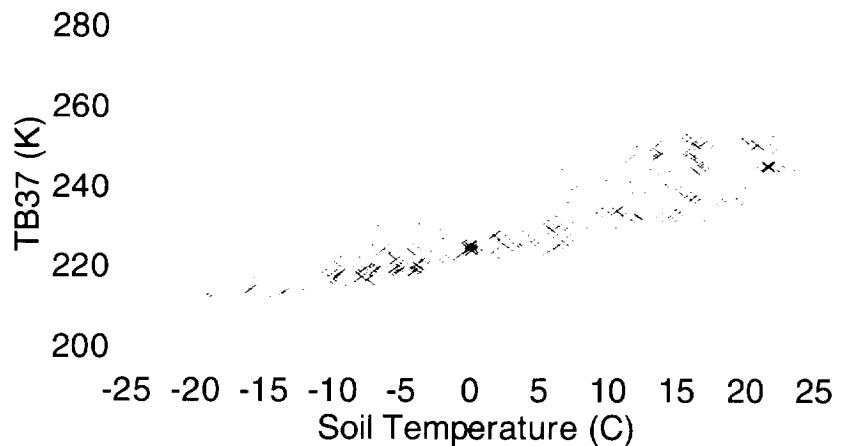
Sponsor: Office of Mission to Planet Earth

*Dr. Chang is a remote sensing specialist in the Hydrological Sciences Branch, Laboratory for Hydrospheric Processes. He received a Ph.D. in Physics from the University of Maryland, College Park. He has been at GSFC for 21 years. His interests include radiative transfer calculations and microwave interactions with precipitation, snow, soil, and vegetation.*



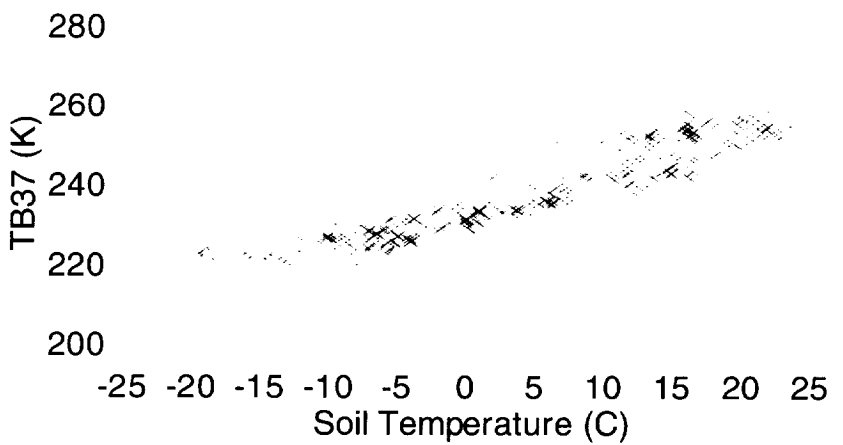
## Scatter plot

(TB37 vs Soil Temperature, am.)



## Scatter plot

(TB37 vs Soil Temperature, pm.)



*Scatter plot of soil temperature and 37-GHz brightness temperature, (top) morning passes and (bottom) evening passes.*

## AIRBORNE LASER/GPS MAPPING OF ICE SHEET TOPOGRAPHY FOR MONITORING ICE SHEET MASS BALANCE

THE ICE SHEETS OF Greenland and Antarctica contain enough water to raise Earth's sea level by some 70 m, were they to melt. Recent data indicate that sea levels are rising, but it is not clear whether changes in these ice sheets are contributing to the current rise.

Ice sheet mass balance estimates can be obtained by monitoring the topography of selected Arctic regions. The Arctic Ice Mapping (AIM) Project is a continuing program designed to provide a record of the absolute height of representative Arctic ice sheets. Using the Global Positioning System (GPS), aircraft flight lines may be duplicated with sufficient tolerance to provide aircraft-borne laser-based elevation measurements over reproducible locations from one year to another. The raw GPS measurements are reprocessed after missions to provide sub-10-cm trajectories for each aircraft flight. This program began in 1991 with a proof-of-concept mission to Greenland. The data from this mission demonstrated repeatability, but only at the 20-cm level, principally due to the limited GPS constellation then available. Refinements in all phases of the program (software, laser and GPS hardware, and a complete GPS constellation) have yielded 10-cm repeatability in data from subsequent years, which includes probable geophysical change in the surface due to storm events and wind drift.

Two major field missions to Greenland in 1993 and 1994 have resulted in an extensive surface topography characterization of the major portions of the island. The 1993 data set consists of ~1,000,000 surface elevation measurements over representative portions of the southern one-third of Greenland. The resultant data set has undergone extensive scrutiny, and demonstrates repeatability at the 10-cm level (16). This data set has been made available to the scientific community via the National Snow and Ice Data Center (NSIDC). Additionally, the 1993 data set is being incorporated into the latest digital contour map of Greenland, produced by the National Survey and Cadastre of Denmark, which has responsibility for surveying and mapping in Greenland. The 1994 field mission consisted of 12 flights of 5 to 7 hrs duration each from Thule Air Force Base, with two additional missions from Sondrestrom. This effort resulted in ~32,000 km of data

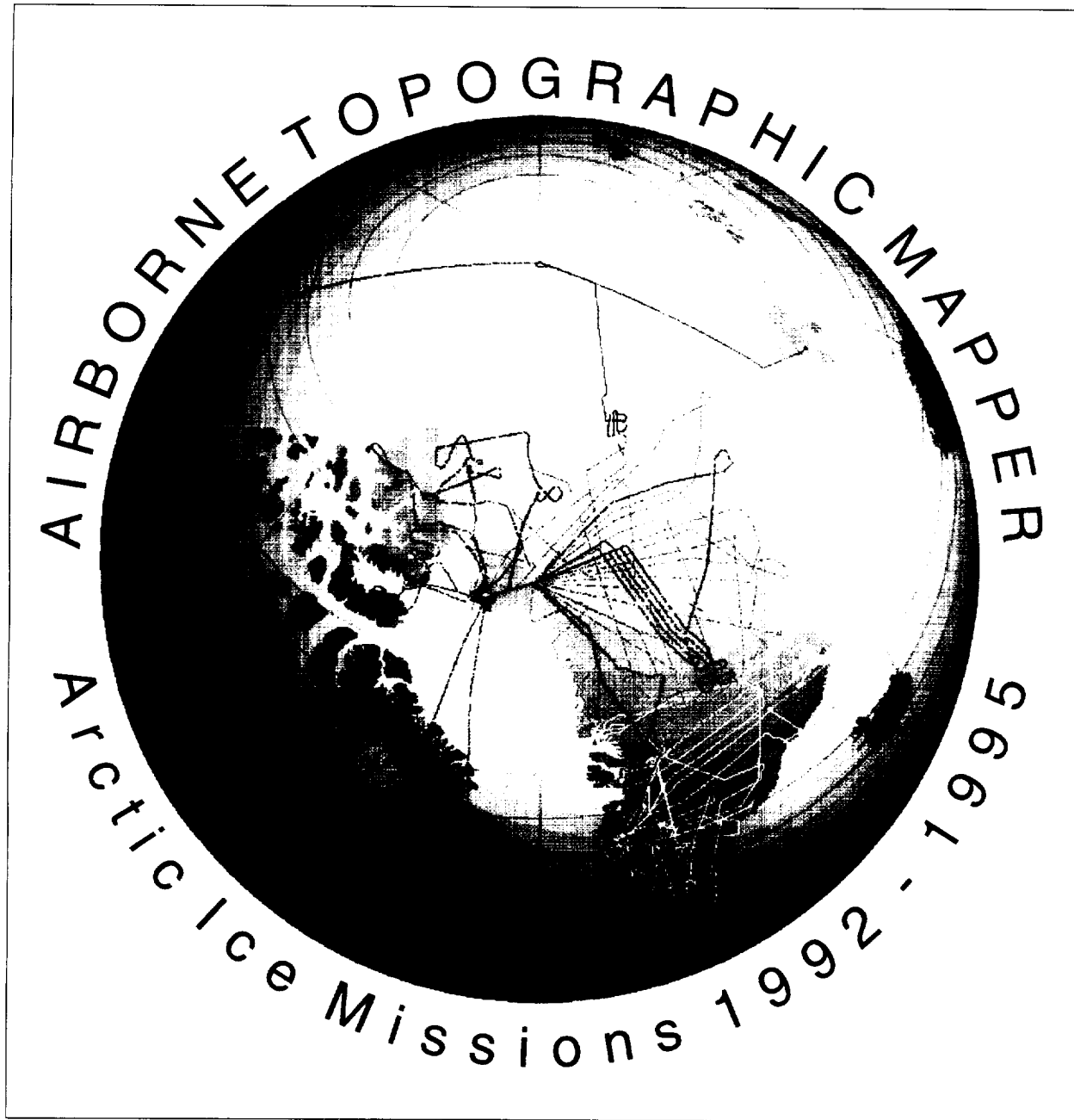
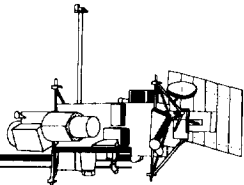
in a swath 135 m wide, containing ~1 billion surface elevation measurements, mostly over the northern two-thirds of Greenland. Processing of the 1994 data set is nearly complete, and will be made available to the scientific community through the NSIDC.

For the 1995 field mission, the project returned to Thule, Greenland, and accomplished a series of flight tracks over northern Greenland and northeastern Canada. Most of the specific flight lines were at the request of the National Survey and Cadastre of Denmark and the Geological Survey of Canada. The map shown in the figure displays the ground tracks associated with the AIM missions from 1992 to 1995. Planning is underway for the 1996 field mission, which will collect data in Iceland, Svalbard, and Arctic Basin sites in Russia.

All of the AIM Project measurements prior to 1994 were made using the Airborne Oceanographic Lidar (AOL). The AOL is a flying laser laboratory designed to be flexible for multiwavelength, active-passive laser/optical remote sensing applications. The need for a dedicated, advanced, state-of-the-art scanning system for ice sheet topography measurements led to the development of a new sensor package, which is optimized for collecting high-resolution altimeter data. The old AOL configuration for topographic mapping operated at a data rate of 800 Hz and a scan rate of 5 Hz. The first generation of the new instrument, called the Airborne Topographic Mapper (ATM), operates at 2000 Hz and scans at 10 Hz; development of a second-generation model is well underway; it will pulse at 5000 to 8000 Hz and scan at 30 Hz. The system takes advantage of new laser transmitter technology available in the form of a Tightly Folded Resonator (TFR). The TFR provides pulse rates up to 10,000 Hz, with excellent pulse-to-pulse stability. Calibration techniques have been developed for this project which yield range measurements with an accuracy of 2 to 3 cm from the ATM.

Contact: William Krabill (Code 972)  
804-824-1417

Sponsor: Office of Mission to Planet Earth, Polar  
Research Program



*This map displays the ground tracks associated with the AIM missions from 1992 to 1995.*

*Mr. Krabill is the Principal Investigator of the AIM Project. He has 28 years experience with tracking systems and airborne remote-sensing technology. For the past 10 years he has been a leader in the application of the Global Positioning System (GPS) for precision aircraft*

*positioning. His publications and projects have demonstrated the ability to position an aircraft, and subsequently infer surface measurements from airborne remote sensors, to the 10-cm level. Mr. Krabill has a B.S. in Mathematics from Salisbury State University.*

**LAND****PRECISION ORBIT DETERMINATION AND GRAVITY FIELD IMPROVEMENT DERIVED FROM TDRSS**

**N**ASA'S TRACKING AND Data Relay Satellite System (TDRSS) is a constellation of six geosynchronous spacecraft that provide tracking and communications support to a host of Earth-orbiting spacecraft and other ground-based vehicles.

The Bilateration Ranging Transponder System (BRTS), which supplies S-band range and range-rate tracking data, is used operationally to determine the TDRS positions. BRTS tracking has a number of deficiencies. The BRTS range is ambiguous, the range-rate is largely insensitive to the subtle motions of the geostationary spacecraft, the four BRTS ground stations do not provide a robust tracking geometry, and the S-band signal suffers from ionosphere path delays. Furthermore, each TDRS is treated as a homogeneous sphere when evaluating force and measurement models in the process of determining operational orbits. Consequently, the operational TDRS trajectories are limited to total position accuracies of 30 to 40 m. These errors propagate into the TDRSS-user satellite ephemerides, and represent one of the largest contributions to the TDRS orbit error budget. These deficiencies can be addressed largely by incorporating more detailed satellite force and measurement models, performing simultaneous TDRS-user solutions, and exploiting the knowledge of the precise position of another spacecraft where such information is available.

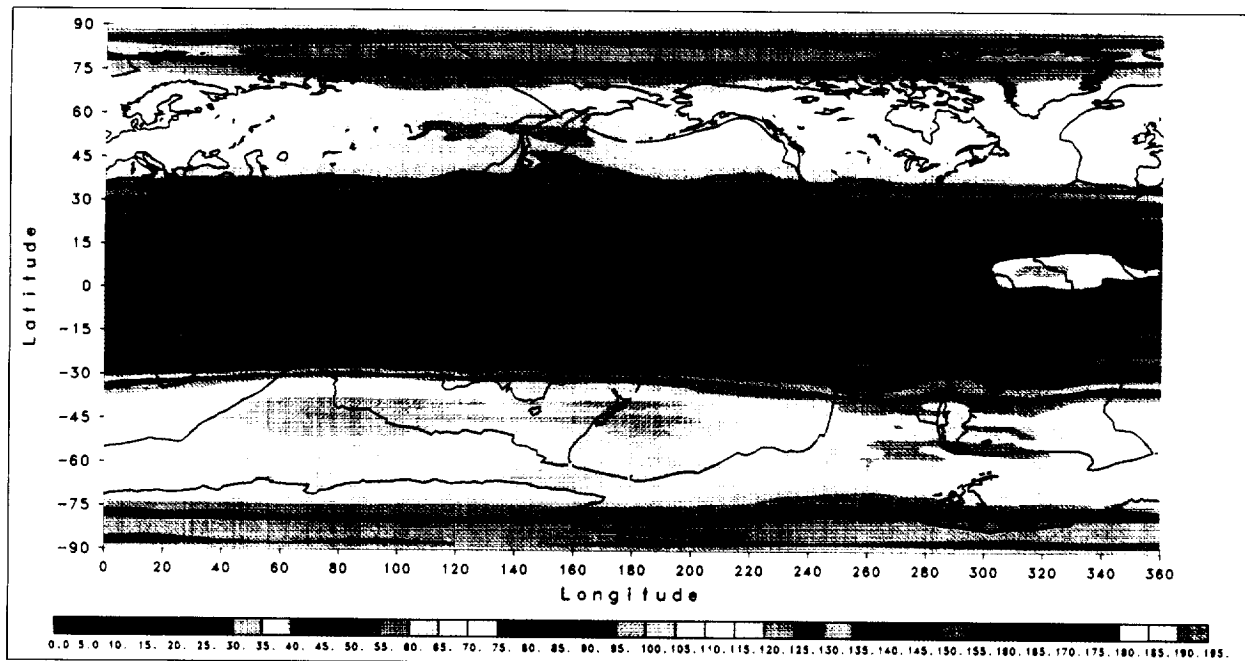
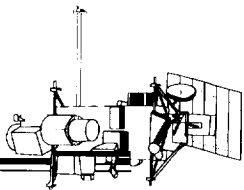
Such precision position information is available for TOPEX/Poseidon (T/P). T/P uses four distinct tracking data types: (1) Satellite Laser Ranging (SLR), (2) Doppler Orbitography and Radio Positioning Integrated by Satellite (DORIS), (3) Global Positioning System (GPS), and (4) TDRSS. The T/P orbits on the mission geophysical data records are routinely produced with less than 3 cm radial root mean square (rms) error and 15 cm rms total position accuracy over the 10-day orbit repeat period using SLR and DORIS tracking data. Consequently, these independent, SLR/DORIS-based, precise ephemerides can be used to create a "roving ground station" for TDRSS. The T/P orbit is held fixed and the TDRS and user satellite orbits are determined simultaneously from the one- and two-way range and range-rate TDRSS tracking data. This technique capitalizes on the extensive geometry T/P provides to position the TDRS. For a limited test case, this orbit determination methodology, including the force and measurement model improvements, yielded 3 to 5 m and 25 cm total position orbit accuracies for TDRS and

for a second, imaginary T/P duplicate, respectively. TDRS and user satellite ephemerides computed in this manner are of sufficient accuracy to further augment and refine gravity field, atmospheric density, and nonconservative force models. To date, these techniques have been applied to the Extreme Ultraviolet Explorer (EUVE) and Landsat-4 and -5 spacecraft.

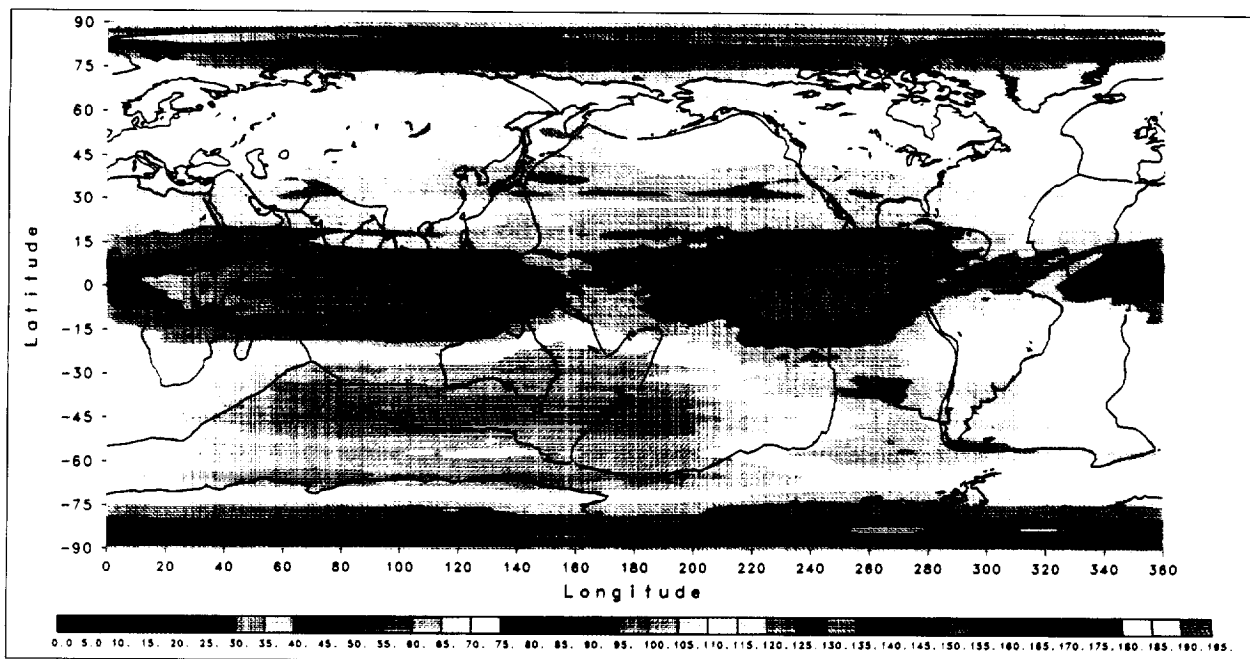
The EUVE spacecraft is in a 510-km altitude circular orbit at an inclination of 28.4°. Landsat-4 and -5 share a 702-km, circular, Sun-synchronous (98.1°) orbit with a relative phasing of approximately 160° to 170°, and a 16-day repeating ground track. With the SLR/DORIS T/P orbits fixed, simultaneous solutions for EUVE and the TDRSSs were performed. The resulting EUVE orbits were judged to be accurate to 2 to 3 m in total position, which is consistent with the unmodeled antenna offset. Positions for TDRS-4 and -5, which are tracked by T/P, are known to better than 5 m. Using the same methodology as EUVE, simultaneous solutions for the TDRSSs and Landsats were generated. Tests demonstrated that the Landsat ephemerides were known to better than 1 m (<30 cm radially) and the TDRS to better than 5 m. Parameterization, modeling, and data weight changes are expected to further improve the orbit accuracies for both EUVE and Landsat-4 and -5. Nonetheless, the current trajectories are significantly better than those generated for operational purposes.

With this more precise knowledge of the low-altitude TDRSS-user spacecraft positions, information on the characteristics of the Earth's gravity field can be inferred. Preliminary combination gravity solutions were generated by adding least squares normal equation matrices generated in the aforementioned orbit determination process to the JGM-2 gravity field model. A new gravity model was created for each additional satellite.

The improvements realized through the TDRSS tracking data are primarily at long wavelengths and confined to spherical harmonic degrees less than 40 and spherical harmonic orders less than 10. This can be attributed to the long, continuous observation passes and the high-low observation geometry between TDRS and the user satellites. The long continuous observation passes increase sensitivities to the short orbital perturbation frequencies, and thus improve the separability of lower-order harmonic geopotential coefficients. The high-low observation



Errors in the JGM-2 satellite-only geoid heights with respect to the complete geoid model, which incorporates satellite altimetry and surface gravity data.



The same information for the JGM-2+EUVE solution.

geometry allows for more radial observations of the satellite motion and, hence, provides better estimation of odd degree spherical harmonic geopotential coefficients. The inclusion of the TDRSS tracking data reduces the radial orbit errors (compared to JGM-2) at or near the inclination of the specific user satellites by as much as 55 percent (from 110 cm to 50 cm) for EUVE, and 20 percent (from 13.7 cm to 11.5 cm) for Landsat.

While the addition of any significant new data set is likely to improve the formal error statistics of a gravitational model, it is important to confirm these improvements independently. This is accomplished through comparisons with independently observed gravity anomalies and geoid undulations. The results of these comparisons demonstrate that relatively small improvements are obtained from Landsat-4 and -5. This can be attributed to the small amount of data, the low data weights, and the fact that satellites with similar inclinations are already present in the JGM-2. However, significant improvements—greater than from any other single satellite—are realized with the addition of TDRSS-EUVE tracking data. This is due to the low altitude and unique inclination of EUVE, which is not represented in JGM-2. This impact is best visualized by examining plots of the geoid height errors. The first figure shows the errors in JGM-25 (determined from satellite tracking only) geoid heights from the calibrated covariance matrix of the JGM-25 gravity solution. The second figure displays the same information for the JGM-2+EUVE solution. Note the striking improvements, especially directly below the TDRSS-4 and -5 positions (41°W and 171°W). Geoid height errors are currently the limiting factor in oceanographic analysis of the T/P altimetry data; these results bode well in that regard.

Clearly, TDRSS is a powerful tracking system and can be used for precision orbit determination and gravity model improvement. Increased understanding of the performance and peculiarities of the various tracking data types, enhanced nonconservative force modeling of the TDRSSs, and alternative orbit determination strategies have made

the realization of the system's potential possible. The quality of TDRSS tracking data is high, as is evidenced from the analysis of these data acquired on T/P, EUVE, and Landsat-4 and -5. With sufficient two-way range-rate tracking, and T/P held fixed to its independently determined SLR/DORIS trajectory, TDRS orbits accurate to 3 to 5 m can be attained via TDRSS-T/P tracking. Preliminary analysis of EUVE and Landsat-4 and -5 tracking data yields orbit knowledge to better than 3 m and 1 m, respectively. Further improvement is anticipated with the optimization of the relative data weights and more sophisticated modeling of the spacecraft attitude and nonconservative forces.

Even at this current level of accuracy, TDRSS provides a high-low observation geometry and long, uninterrupted tracking passes that are well-suited to gravity field model improvements. Improvements in the current orbit determination solutions and the addition of more data from both these and other user satellites bodes well for further gravity field model refinement.

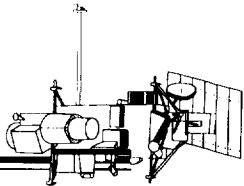
Contact: Andrew Marshall (Code 926)  
301-286-3044

Frank Lemoine (Code 926)  
301-286-2460

Sponsor: Office of Space Communications

*Mr. Marshall is an aerospace engineer in the Space Geodesy Branch and has been at GSFC for over 3 years. He holds an M.S. in Aerospace Engineering from the University of Colorado. His primary focus while at GSFC has been precision satellite orbit determination.*

*Dr. Lemoine is a geophysicist in the Space Geodesy Branch and has been at GSFC for over 1 year. He graduated from the University of Colorado with a Ph.D. in Aerospace Engineering from the University of Colorado. He specializes in planetary geodesy and has actively pursued gravity model development for the Moon, Mars, and the Earth.*



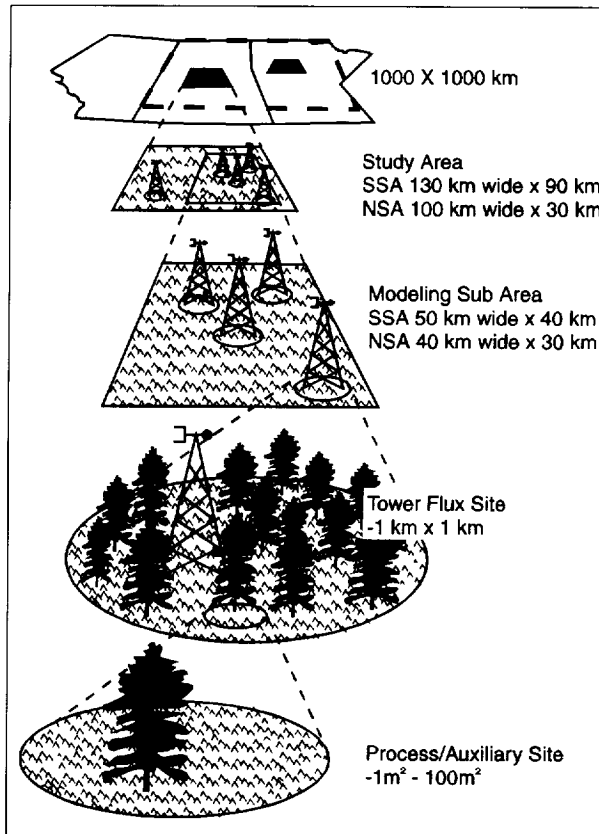
## BOREAL ECOSYSTEM ATMOSPHERE STUDY (BOREAS)

THE BOREAL (northern geographic region) ecosystem girdles the Earth above about 48°N latitude and covers about 17 percent of the Earth's land surface. It consists primarily of aspen and coniferous forests, and is second in areal extent only to the world's tropical forests. The role of the boreal ecosystem in influencing global climate and weather patterns is poorly understood.

It is well-accepted that variations in the ratio of reflected sunlight to that absorbed by land surface vegetation can influence local and global atmospheric circulation. Light reflected back to space has little effect on the weather or climate. On the other hand, light absorbed by vegetation either heats the surface, in turn heating the lower atmosphere (sensible heat), or is released as evaporation (latent heat), which eventually condenses into clouds. The ratio of heat energy release to evaporative energy release can have very different effects on the dynamics of the lower atmosphere and, thus, the weather.

The role that the boreal ecosystem plays in global carbon dynamics, and possible resultant effects on weather and climate, is only just emerging. Theoretical studies suggest that these forests play a strong role in cleansing the Earth's atmosphere of excess carbon dioxide by removing nearly 20 percent of the annual emissions from fossil fuel combustion. Other studies suggest, however, that these forests might be greatly reduced in extent by rapid climatic change resulting from global warming. If so, these forests could quickly release the vast stores of carbon that they have accumulated since the last ice age and potentially accelerate global warming.

The Boreal Ecosystem Atmosphere Study (BOREAS) was instigated to improve our understanding of the interactions between the boreal forest biome and the atmosphere to clarify their roles in global change. Of particular interest to BOREAS is the rate of carbon uptake and release from the forests, water, and heat exchange between the forest and the lower atmosphere. In 1994, the GSFC Biospheric Sciences Branch led coordinated ground, aircraft, and satellite field campaigns involving over 85 teams of scientists from around the world. As shown in the figure, BOREAS employed a multiscale experiment design permitting physiological, ecological and other information obtained at the leaf, plot, and study area level



*Multiscale experiment design for the BOREAS study.*

to be translated, via remote sensing and process models, to regional, and, ultimately, global scales.

The field measurements portion of BOREAS took place in the Canadian boreal forests during five 20-day intensive study periods during all four seasons in 1994. While nearly 200 scientists in the field used a variety of instruments to measure plot-level biophysical characteristics and energy, water, and gas emissions from the trees and soils, 11 aircraft flew coordinated missions overhead using a battery of sensors to measure reflected light patterns and gas emissions at scales ranging from 1 to 1000 km. During the experiment, Earth resources satellites documented the patterns of reflected and emitted radiation from the forest and the overlying atmosphere. These light and radiation patterns, in combination with energy, water and carbon process models, will be analyzed for clues to the

forest's structure, condition, temperature, rate of growth, and the energy flow between the atmosphere and the boreal land surface.

This large and complex set of data will be stored in a database at GSFC, to which scientists from around the world will be electronically linked. These data will be analyzed to determine how a warmer climate might change the forest's composition, and what these changes might mean for the boreal ecosystem and the Earth's climate. The measurements and analysis will concentrate on two  $\sim 80 \times 100$  km research study areas (one near Prince Albert, Saskatchewan; the other near Thompson, Manitoba), but the results will be extended to similar forests, which cover a large fraction of the Earth's land surface above  $48^{\circ}\text{N}$  latitude.

To fund and obtain the international cooperation required for a project of this scale required the collaboration of several U.S. and Canadian agencies and other organizations from around the world. NASA and the Canada Center for Remote Sensing (CCRS) led the study, with additional support from other U.S. agencies, including the National Oceanic and Atmospheric Administration and the National Science Foundation, and Canadian agencies, including the National Science and Engineering Research Council of Canada, Environment Canada, Agriculture and Agri-Food Canada, Canada Forest Service, and the National Research Council of Canada. Significant support was obtained from research agencies in the United Kingdom and France.

The last field campaign ended in September 1994; the first science workshop was held in December of that year. Even at this early stage in the experiment, a fascinating picture is emerging of the energy, water, and carbon dynamics of the boreal ecosystem, and its strong coupling to the boreal soils and forest species types. Results are showing that the composition of the boreal forests and soils may be as much a determinant of boreal climate as the boreal climate is of the nature of the boreal ecosystem.

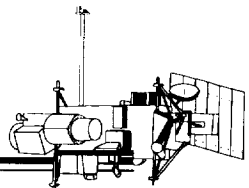
Much of the boreal forests of central Canada grow on a nearly flat terrain composed of mineral soils deposited by glaciers and lakes during the last ice age. These soils are overlain by a thin layer of live and decomposed moss, to which the tree's root systems are largely confined. Because annual precipitation exceeds evaporation, the

moss layer and soil surface generally stays saturated, even throughout the summer. With an abundant water supply and the warm summer temperatures of central Canada, trees should be capable of sustaining large growth rates, and a correspondingly large capacity to transpire water to the atmosphere, humidifying the atmospheric boundary layer.

Instead, tower and aircraft measurements of evaporation and heat release show that the forest behaves more like a desert than a wetland. The transpiration rates observed from the forest were low ( $<2$  mm/day) on most days throughout the growing season. In the spring and early summer, frozen soils limited surface evaporation. In mid- to late summer, low evaporation rates (observed on many days) resulted from leaf stomatal closure, which, by midmorning, were responding to falling humidity as the atmospheric boundary layer expanded and dried from solar heating. The boundary layer expansion was accelerated by the evaporative shutdown of the vegetation. This positive feedback between the vegetation physiology and lower atmosphere resulted in deep convection by midmorning, creating boundary layer heights greater than 3000 m, similar to those observed over deserts.

The key to understanding this unexpected picture of an atmospherically arid wetland ecosystem appears to lie with the low photosynthetic capacity observed for the boreal vegetation. Measurements show that the boreal species have considerably less photosynthetic capacity than temperate forests to the south. This is reflected in low rates of annual carbon dioxide exchange with the atmosphere and associated low carbon fixation rates. In turn, low photosynthetic capacities may be related to the limited root volumes of the forests and low soil temperatures, with correspondingly low rates of nutrient cycling. Because transpiration of water from boreal vegetation is strongly coupled to photosynthetic rates, the boreal soils themselves and the adaptation of boreal vegetation to these harsh conditions may provide a key to understanding boreal climatology and the effects of future climate change.

These and later findings should have significant implications for our understanding of how this important ecosystem influences weather, climate, and other global processes. In an earlier, similar study of the grassland prairies of the U.S., known as the First ISLSCP Field



Experiment, scientists showed that correctly accounting for the stored soil moisture and evaporative heat release in operational weather forecast models permitted more accurate predictions of the 1993 floods that inundated portions of the U.S. Central Plains. Current weather models do not realistically represent the boreal ecosystem; thus, it is anticipated that the BOREAS results, when incorporated into operational forecast models, will greatly improve weather forecasts in the short term, as well as longer term climate simulations.

Contact: Forrest Hall (Code 923)  
301-286-2974

Piers Sellers (Code 923)  
301-286-4173

Sponsor: Office of Mission to Planet Earth

*Dr. Hall is at NASA/GSFC's Laboratory for Terrestrial Physics, where he currently serves as research scientist and Co-Project Manager for the BOREAS. Dr. Hall has an undergraduate degree in Mechanical Engineering from the University of Texas, and an M.S. and Ph.D. in Physics from the University of Houston.*

*Dr. Sellers is Co-Project Manager/Scientist for BOREAS. He also works in the Biospheric Sciences Branch at GSFC. He has a B.Sc. in Ecology from Edinburgh, Scotland, and a Ph.D. in Bioclimatology from Leeds, UK.*

## MAPPING URBAN SPRAWL FROM SPACE: EVALUATING LAND USE CHANGE WITH NIGHTTIME VIEWS OF THE EARTH

THE EXPLOSIVE GROWTH of human populations is generating a new phenomenon—megacities, urban centers with 2.5 million residents or more. By the year 2025, estimates indicate that there will be almost 100 megacities on Earth; 31 of them will have populations of more than 8 million, and some will have populations of 20 million or more, constituting a new ecophysiological and sociological phenomenon. The potential impact of the process of urbanization on Earth's biological and geochemical systems is a subject of current debate and the object of numerous modeling efforts and scientific investigations. As more land is converted to urban use, the question arises as to whether or not we are systematically reducing our ability to produce food by placing our urban infrastructure on the most productive soil resources. Since a logical outcome of this process is a growing dependence on more distant regional, continental, or even globally distributed food resources, a rapidly growing number of regional populations are at risk with respect to sociopolitical and economic instability and its effect on the food supply.

While the reality of some agricultural land loss is accepted, both the magnitude and the potential effect is hotly debated. What is needed are data to support modeling and decision making. The use of satellite remote sensing is an obvious choice for detecting, monitoring, and classifying land transformation, including urban expansion. However, coarse resolution data sets (pixels  $> 1 \text{ km}^2$ ) have inadequate spatial and spectral resolution for reliably determining urban infrastructure, while the high-resolution data sets ( $10^2$  to  $10^3 \text{ m}^2$ ), while capable of showing infrastructure, present problems of analysis because of the vast volumes of data necessary for processing and the high costs of data acquisition.

Nighttime images of the Earth acquired at visible wavelengths by the Defense Meteorological Satellite Program's Operational Linescan System (DMSP/OLS) provide a dramatic picture of urbanization through the detection of city lights, as seen in the top "slice" in the figure. The contrast provided by this type of image, and the intermediate spatial resolution (0.6 to 2.6 km), makes it an interesting choice for mapping and classifying the transformation of land to urban and suburban uses over large areas. Using OLS images of the U.S. and image thresholding techniques, a bit map was created having two

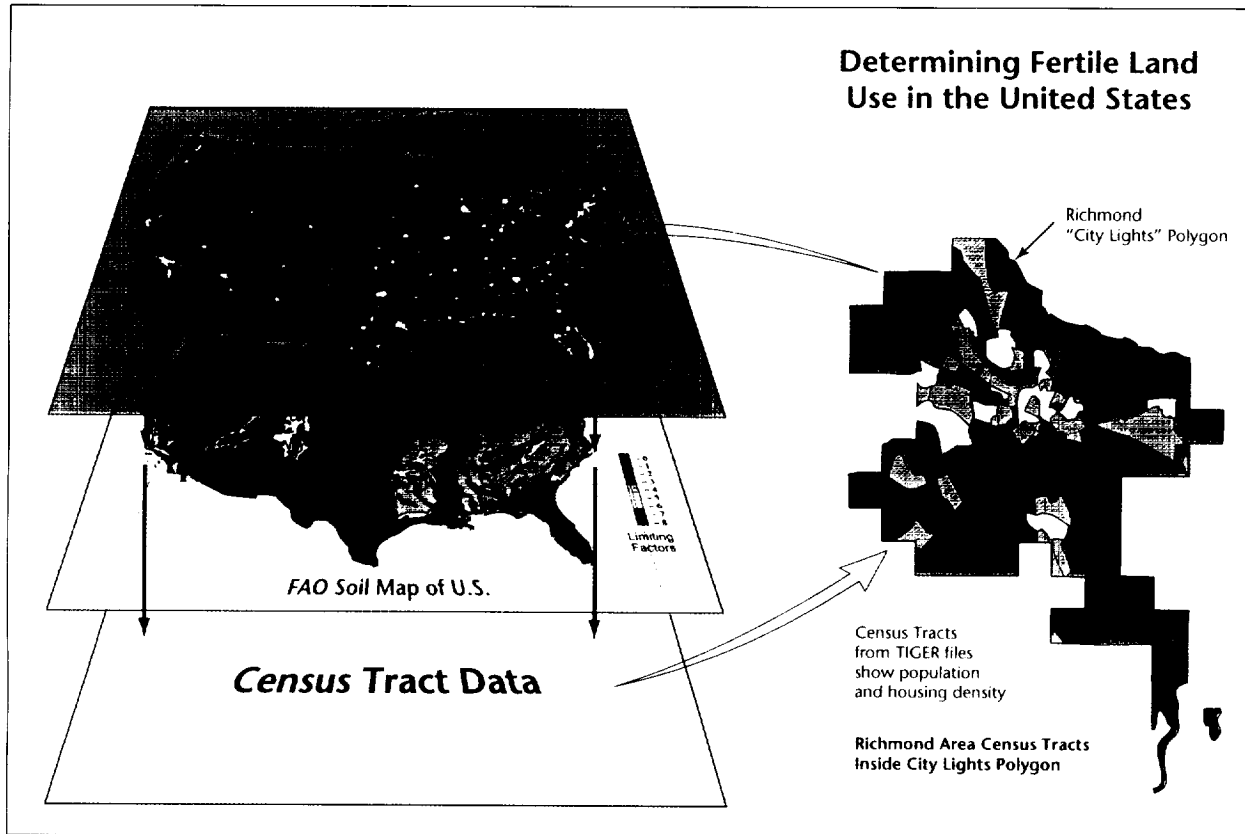
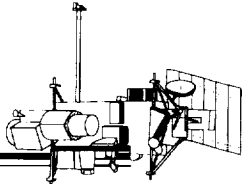
classes: lights (classified as urban/suburban) and no lights (classified as other).

Demographic values were assigned to the urban/suburban (lit) areas by projecting census data on population and housing onto the "city lights" image in a geographic information system, as shown in the figure. Average population and housing density values were calculated for the lit areas. The mean housing density for lighted pixels was 290 housing units/ $\text{km}^2$  (~three houses per hectare); the mean population density was 711 persons/ $\text{km}^2$  (7.11 persons per hectare), or about 2.45 persons per housing unit. This density of housing would preclude large-scale mechanized agriculture.

To assess the impact of urbanization on soil resources, the "city lights" image was merged with the United Nations Food and Agriculture Organization (FAO) Digital Soils Map of the World, which contains approximately 315 soil units for the U.S. The soil units were ranked using an agronomically-based fertility index, which lists condition modifiers, or factors limiting agricultural production to each soil type. This served as an economic rating scale of the costs required to produce crops for each soil. The best soils are those with the fewest limiting factors, or factors most economically overcome. In our soil evaluation, the units were ranked according to the number of limiting factors present, with 0 being the most potentially productive class (in terms of least cost of production), and 7 or 8 being nearly impossible to cultivate due to adverse conditions; high salt content, high acidity, high slope, etc.

An estimate of the impact of urbanization on agricultural soil resources was made by overlaying the "city lights" image on the FAO soils map and calculating the fraction of soil surface area for each of the soil units that is under city lights, and therefore considered to be unavailable to mechanized agriculture. Soil units were assessed individually (the middle "slice" in the figure), or grouped by number of physical factors limiting agricultural production (data not shown).

The continental scale overview of the data shows that a substantial amount of land has been converted to urban use in the conterminous U.S., with nearly 5.3 percent of the total land surface now under city lights. If coalesced,



Use of a geographic information system can help interpret DMSP/OLS-based categorization of urban sprawl. "City lights" image of the continental U.S. acquired by the DMSP/OLS in 1994, is shown being overlaid on the FAO Soils Map for the U.S. The soils are rated as to the number of factors limiting agriculture. The "city lights" data are indexed to population and housing density using the U.S. Census Topologically Integrated Geographic Encoding and Referencing System Line Files and the Summary Tape Files-1B files.

the urban/suburban land use class would be approximately equal to the size of the state of California. Urbanization seems to be relatively evenly distributed across soil types with limiting factors ranging from 0 to 5. The only clear trend at this scale is that the least amount of urbanization is taking place on soils with the greatest number of limiting factors. Results, however, for four states with the highest agricultural production (California, Illinois, Wisconsin, and Florida) are considerably less ambiguous, and show a strong relationship between soil fertility and urban sprawl. In those states, urban development is definitely taking place on the soil groups best suited to agriculture.

As a means of reference, we compared our estimates of urban sprawl to those made by the 1990 Census of Population and Housing. Estimates derived from our 1993 city lights imagery shows that 407,742 km<sup>2</sup> are in urban use, while the 1990 Bureau of the Census has 226,304 km<sup>2</sup> registered in urban land use. The 1990 Census figures represent a more conservative estimate, as they include only the area of incorporated towns and cities. In addition, 3 years of additional growth took place between the 1990 Census and our satellite survey. While our "city lights" approach may overestimate urban areas due to pixel blooming, saturation, etc., the census figures almost certainly underestimate the full extent of urbanization or

built-up land. Together, these two figures provide an upper and lower boundary for the estimate of urban areas or built-up land in the U.S.

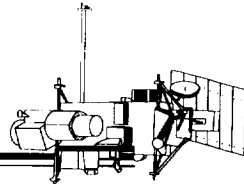
The conversion of potentially productive soil resources to nonproductive urban land can now be monitored through the application of synoptic satellite data sets and existing global soils maps. When four agronomically important states in the U.S. were examined, a pattern emerged showing development definitely occurring on the soils best suited to agricultural production. The economic incentives, then, are negatively synergistic, where "good" soils bring economic wealth encouraging development, but are also themselves attractive soils on which to build. Short-term economic forces may tend to undervalue agricultural use relative to infrastructure development, especially when production can be economically shifted to distant areas due to inexpensive transportation. Some analysts estimate that, in the next century, population and economic growth in China will reach the point where the demand for grain imports will exceed the current export capability of the leading grain-producing countries. If this

indeed happens, it is likely that agronomic land use will then have greater economic value, but the question remains as to whether we will have enough soil resources left to respond.

Contact: Marc Imhoff (Code 923)  
301-286-5213

Sponsor: Office of Mission to Planet Earth

*Dr. Imhoff is currently in the GSFC Biospheric Sciences Branch and was awarded a Research and Study Fellowship to Stanford University. During his 15 years at GSFC, Dr. Imhoff has played key roles in the Shuttle Imaging Radar-B program, the Landsat-4 Data Quality Assessment Team, and the EOS Project Office. Dr. Imhoff holds a B.S. and an M.S. from The Pennsylvania State University and a Ph.D. in Biological Sciences from Stanford University. His research interests include human population growth and how it affects the Earth's natural systems particularly in the areas of biodiversity, ecosystem services, and global carrying capacity.*



## NITROGENOUS FERTILIZERS: GLOBAL DATA SETS OF CONSUMPTION AND ASSOCIATED TRACE-GAS EMISSIONS

**N**ITROGEN (N) FIXATION converts unreactive N<sub>2</sub> to reactive nitrogen usable by biotic systems. Nitrogen fixed via human activities is currently equal to or greater than that fixed in undisturbed terrestrial ecosystems. Fertilizer production accounts for about one half of the ~140 Tg N (1 Tg = 10<sup>12</sup> g) fixed annually through human activities. Other anthropogenic sources include energy production and cultivation of legumes (nitrogen-fixing crops).

Large-scale consumption of chemical fertilizers began about four decades ago. Global growth rates of fertilizer N use averaged about 10 percent per year from 1960 to 1980, and about 3.5 percent per year during the 1980s. Nitrogen fixation and consumption in the form of chemical fertilizers increased from 57 Tg N in 1979 to almost 80 Tg N a decade later. Although some developed regions experienced declining growth trends in the latter period, high growth rates continued in many developing tropical and subtropical countries supported by increases in production capacity within those countries.

Consumption of nitrogenous fertilizers, followed by redistribution via gaseous emissions from soils, leaching to ground water, and transport to rivers, alters the nitrogen cycle in many ways. Enhanced ammonia and nitrous oxide emissions are among the deleterious effects of N fertilization. Others include possibly large emissions of nitrogen oxide (NO) and nitrogen dioxide (NO<sub>2</sub>), and nitrate pollution of groundwater. Increased deposition of ammonium to terrestrial ecosystems has been linked to soil acidification and to forest decline, while reduction of species diversity and stimulation of carbon uptake are possible related effects of inadvertent N fertilization.

Biosphere models of carbon and nitrogen cycles that incorporate climate and/or ecological parameters such as precipitation, temperature, or soil characteristics require that input data sets capture the environmental and ecological settings in which fertilizer N is consumed. In addition, 2-D and 3-D atmospheric chemical models require geographic accuracy in input data sets of trace-gas exchange. Therefore, considerable effort was devoted in this work to capturing the geographic distribution of cropland and associated fertilizer consumption. Geographic accuracy facilitates the treatment of fertilizer consumption across the range of climatic, ecological, and management environments in which it takes place and which differentially affect trace-gas emissions.

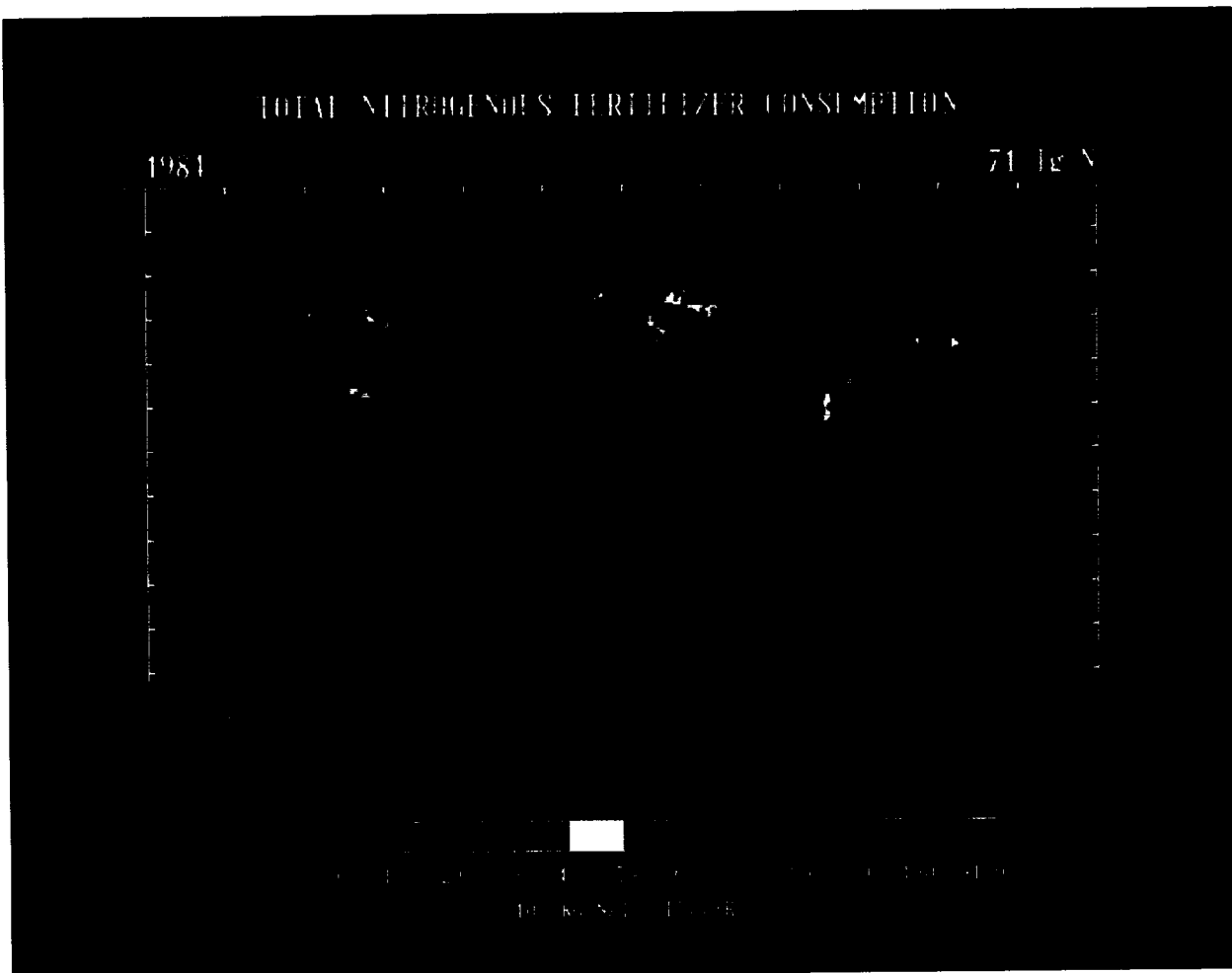
We focussed initially on estimating emissions of nitrous oxide and ammonia from the use of nitrogenous fertilizers to illustrate major regional patterns and uncertainties in emissions. Nitrous oxide (N<sub>2</sub>O) is a greenhouse gas whose concentration in the atmosphere is increasing at about 0.25 percent per year. Causes of the increase are not understood. Although the magnitude of individual sources is uncertain, emissions from undisturbed soils, particularly in the tropics, appear to dominate; other sources include land clearing, biomass burning, fossil fuel combustion, nitrogenous fertilizer use, and oceans. Stratospheric destruction removes ~10 to 11 Tg N<sub>2</sub>O-N annually. The stratospheric sink, combined with the atmospheric increase of 3 to 4 Tg N per year, indicates a large imbalance in the nitrous oxide budget; calculated sinks exceed estimated sources by ~40 percent.

Ammonia (NH<sub>3</sub>) is the major neutralizing agent for atmospheric acids. The larger ammonia sources include decomposition of animal excreta, release from fertilized agricultural soils and from undisturbed soils, biomass burning, and oceanic fluxes. Atmospheric NH<sub>3</sub> is removed primarily by wet and dry deposition and by reaction with acidic sulphates. The latter converts NH<sub>3</sub> to ammonium-containing aerosols deposited by rainfall and dry fallout. Ground-level measurements of atmospheric ammonia and ammonium concentrations in England show that local sources are strongly reflected in elevated levels of ammonia, while ammonium concentrations are more uniform owing to formation during transport. Field measurements and estimates of ammonia volatilization following fertilization of temperate agricultural lands range from 1 to 46 percent of applied fertilizer N. Measurements in flooded rice fields of Australia, China, Malaysia, and the Philippines indicate that ammonia volatilization accounts for losses of 2 to 56 percent of applied N, and that the higher rates are consistently associated with urea treatment. A recent assessment of the global ammonia budget suggests that ~10 percent of fertilizer N may be lost to the atmosphere as volatile ammonia; this value equals ~10 to 15 percent of the global ammonia emission, estimated at 45 to 75 Tg N annually.

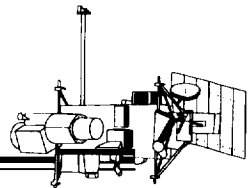
The global distribution of nitrogenous fertilizer consumption, at 1° x 1° (latitude/longitude) resolution, was derived by integrating several data sources. Information on total nitrogenous fertilizer use by country and by fertilizer type was extracted from fertilizer yearbooks published by the United Nations Food and Agriculture

Organization (FAO). Area of agricultural land (by country) was derived from FAO's production yearbooks. The geographic distribution of agricultural locations in which fertilizer is used was developed from a global, digital land-use database. Country statistics on fertilizer and crop area were located within appropriate political boundaries using a digital database of countries of the world. To reduce uncertainties in fertilizer distribution within several large countries with regionally variable agricultural activities and/or large fertilizer consumption, more detailed information on fertilizer use for political subdivisions and by fertilizer type was acquired for China, India, the United States, the former Soviet Union, and Brazil.

The first figure shows the distribution of total fertilizer consumption in millions of kg N in the  $1^{\circ}$  cells. The second figure collapses these data into latitudinal totals. East Asia, where fertilizer use grew at  $\sim 10$  percent per year in the 1980s, accounted for  $\sim 37$  percent of total N consumption in the mid-1980s. Central America, South America, Oceania, and Africa together account for less than 8 percent of total N use in the mid-1980s. Nitrogenous fertilizer use is stabilizing in North America and Europe which together accounted for 30 percent of 1984 use. Former centrally planned economies of Europe consumed one-fifth of the 1984 total, but consumption trends are variable; a downward trend is apparent at the end of the decade.



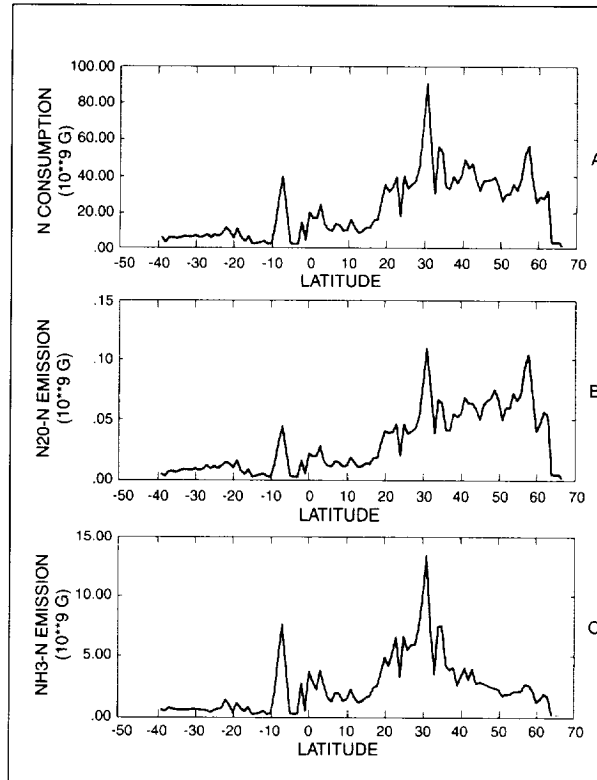
*Global distribution of 1984 nitrogenous fertilizer use showing total N consumption in  $1^{\circ}$  cells.*



Almost every country consumes urea, which accounted for 40 percent of the world's total fertilizer N use in the 1980s. Ammonium nitrate, used primarily in the former centrally planned economies of Europe, in West Asia, and in Africa, accounted for about one quarter of global consumption. The remainder was composed of a suite of eight other fertilizer types. Regions display characteristic profiles with respect to the suite of fertilizer types consumed. For example, urea accounts for 75 percent of East Asia's use while ammonium sulphate (AS), ammonium nitrate (AN), ammonium phosphate (AP), other nitrogenous fertilizers (ON) and other complex fertilizers (OC) each account for 1 to 10 percent of use. This contrasts with former CPEs of Europe where 63 percent of consumption is in the form of AN, 22 percent in urea, and 5 percent each in AS, AP, ON, and OC. Because trace-gas emissions may vary among fertilizer types and environments, differences in regional fertilizer consumption exert differential impacts on regional trace-gas emissions. Furthermore, regional profiles evolve over time in response to prices, trade, agricultural policies, and development of fertilizer production capacity.

We estimated ranges for  $\text{N}_2\text{O}$  emission from chemical fertilizer consumption using the distribution of total N usage among fertilizer types, together with median, low- and high-emission coefficients for types derived from the literature; the second figure shows the latitudinal distribution of the median estimate. The median emission of 0.1 Tg N emitted as  $\text{N}_2\text{O}$  ( $\text{N}_2\text{O-N}$ ) equals 0.14 percent of global fertilizer N use, with lower and upper ranges of 0.01 percent and 2.8 percent of N consumption. Urea and AN, which account for almost 65 percent of total fertilizer N use, account for 73 percent of estimated  $\text{N}_2\text{O}$  emission. In addition, urea is a significant component in the fertilizer complement of East Asia, which is a large consumer, with high decadal growth rates.

Applying  $\text{NH}_3$  emission coefficients from two studies to the suite of fertilizer types consumed in 1984 gives emission totals of 5.5 to 7.1 Tg  $\text{NH}_3\text{-N}$ , indicating that ~8 to 10 percent of fertilizer N may be released to the atmosphere as volatile ammonia. The second figure shows the latitudinal distribution of the higher estimate. Although urea and AN are the two largest contributors in both studies, emission coefficients for the individual fertilizers vary by factors of two to four between the studies, producing large differences in proportional contributions



*Latitudinal distribution of (a) total fertilizer user consumption and associated emission of (b)  $\text{N}_2\text{O}$  emission and (c) ammonia emission.*

of fertilizer types to the total emission. For example, AN and urea account for 24 percent and 40 percent, respectively, of global fertilizer N consumption. Using identical consumption statistics with the suite of emission coefficients from two studies, ammonium nitrate and urea account for 6 percent and 80 percent, respectively, of ammonia emission based on one study and for 31 percent and 52 percent, respectively, of ammonia emission based on the other. Presently, we are unable to determine which coefficients reflect actual field conditions and interactions.

In broad geographic terms, temperate regions (poleward of  $35^\circ$ ) and tropical/subtropical regions (within  $35^\circ$  of the equator) account for 61 percent and 39 percent, respectively, of commercial fertilizer consumption. In initial estimates of N emissions, these regions contribute 69 percent and 31 percent, respectively, of  $\text{N}_2\text{O}$  emissions, and 45 percent and 55 percent, respectively, of ammonia emissions.

At present, there are no published measurements of  $\text{N}_2\text{O}$  fluxes from fertilized agricultural fields in tropical or subtropical sites despite large and increasing consumption in these environments. Therefore, the contribution of low-latitude fertilizer use to  $\text{N}_2\text{O}$  emissions is considered highly uncertain. A forest fertilization study conducted in Brazil suggests that temperate studies may not be applicable to the climate, ecology, and management characteristics of tropical and subtropical environments. This uncertainty may also apply to estimates of fertilizer-related ammonia fluxes due to the scarcity of measurements in geographically and ecologically representative environments, although measurements of ammonia volatilization in flooded rice fields in Asia and Australia indicate that these climatically and agriculturally diverse environments exhibit emissions comparable to the high rates measured from nonflooded temperate crops.

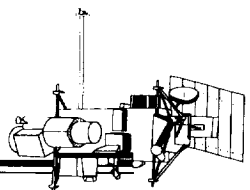
Contact: Elaine Matthews (SSAI)  
212-678-5628

Inez Fung (Code 940)  
212-678-5590

Sponsor: Office of Mission to Planet Earth

*Ms. Matthews is a research scientist with SSAI, resident at the Goddard Institute for Space Studies (GISS). She pioneered the development of high-resolution, global land-surface data sets for global climate models, and biospheric and atmospheric chemical models. Ms. Matthews received an M.A. in Geography from Columbia University.*

*Dr. Fung has studied the global carbon cycle through a combination of global modeling, remote sensing and synthesis of field observations. Dr. Fung received a Sc.D. from MIT.*



## REMOTE SENSING OF RECENTLY ACTIVE VOLCANOES IN THE MIDDLE ATLANTIC REGION

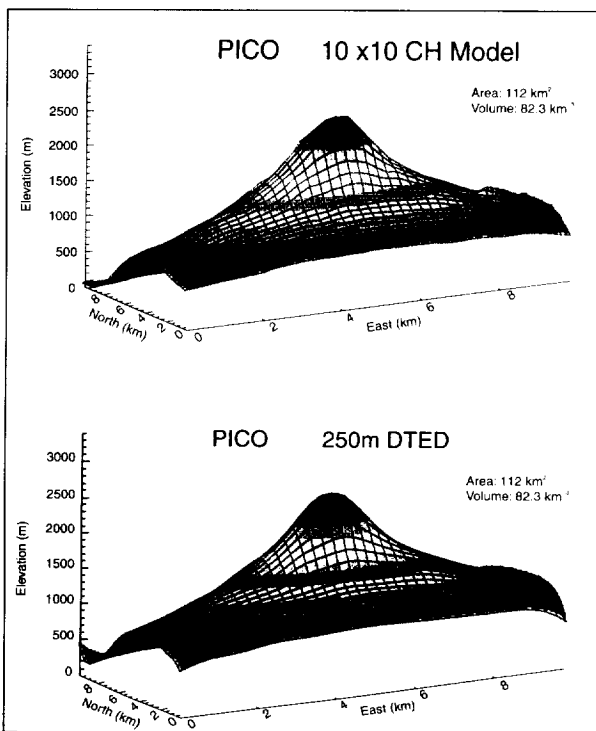
WHILE VOLCANOES dominate specific regions of the Earth, and the Pacific "Rim of Fire" is well known to many geographically aware people, a lesser-known, yet frequently active, chain of volcanoes extends as a series of islands from above the Arctic Circle to the vicinity of the Antarctic. This group of both undersea and subaerial volcanoes includes Jan Mayen, Iceland, the Azores, the Canaries, the Cape Verde Islands, Ascension, Tristan da Cunha, and Bouvet Island, many of which are very poorly studied, especially relative to their more famous "cousins" in the Pacific region, such as Hawaii, Mt. Fuji (Japan), and many others.

Since the time of the Vikings (circa 1000 AD), there have been hundreds of documented eruptions of the Middle-Atlantic island volcanoes, yet only a few have been extensively studied. Those which have most recently occurred in Iceland (Hekla, Krafla, Surtsey, Heimaey) may have been investigated to the greatest extent. Often overlooked are those volcanic island groups (i.e., the Azores archipelago and the Cape Verdes) for which the most recent eruptions (i.e., twentieth century) have only inconvenienced a few local inhabitants. However, violent eruptions have been documented in the Azores and Cape Verde Islands several times over the past 500 years, and most recently (April 1995), a relatively mild, effusive eruption commenced in the Cha Caldera on the Cape Verdean island known as Fogo.

GSFC scientists and engineers are actively developing remote sensing methodologies to characterize and directly quantify the various forms of activity associated with potentially explosive—and, hence, dangerous—Middle-Atlantic island volcanoes. As examples, the relatively inaccessible volcanoes of the Azores and Cape Verde Islands are ideally observed by means of air- and space-borne sensors. Efforts by GSFC scientists and engineers to quantify the complex topographies and surface textures of potentially active and recently active volcanoes on these midocean islands have included airborne multibeam laser altimeter surveys conducted within the Azores archipelago (September 1994), orbital imaging radar polarimetry of Azores volcanoes by means of the Shuttle Radar Laboratory (SRL-2, October 1994), orbital panchromatic high-resolution time-series imaging via the Satellite pour L'Observation de la Terre (SPOT) of the Fogo eruption in the Cape Verdes, and upcoming digital imaging surveys of both island groups from aircraft and spacecraft.

One of the two largest volcanic edifices in the Middle-Atlantic region is Pico, on the Azorean island of the same name, which rises some 2000 m above its submarine base to sea level, and over 2300 m above sea level. Pico is ~14 km in diameter at its sea-level base, and displays a total edifice volume of ~84.5 km<sup>3</sup>, as determined by mathematically modeling the three-dimensional shape of the volcano as constrained by geodetic aircraft laser altimeter data.

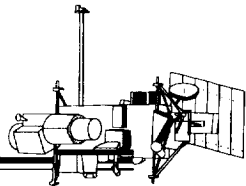
The first figure illustrates the result of modeling the complex topography of the subaerial portion of this major volcano, and demonstrates the severely oversteepened nature of its summit slopes, which average over 28° at local scales. Using GSFC multibeam laser altimeter data, acquired in September 1994 from the Wallops Flight Facility P-3B aircraft platform, it is possible



*Models of the topography of the Pico edifice located in the Azores. The Cylindrical Harmonic mathematical model illustrated below fits the known shape of the volcano to within a few tens of meters using only approximately one hundred coefficients and serves as the basis against which future changes can be observed and quantified (i.e., volume changes).*



*False-colored SRL imaging radar image of Pico volcano, which clearly illustrates the various flank collapse and slump deposits to the east of the uppermost cone and the lavas from the 18th century summit eruptions.*



to intercompare Pico with other types of volcanoes, including the simple lava shield varieties of Iceland, and the unstable, yet dormant behemoths of the Cascades, including, for example, Mt. Rainier.

The laser altimetry data suggests that the uppermost 1200 m of the Pico edifice shows strong evidence of repeated slope failure episodes, and that there is an historic tendency for potentially dangerous debris avalanches and even summit lava flow eruptions in such regions. The huge volume of material and quasi-stable local slopes indicate the possibility of future flank collapse events, which could have serious consequences for the local population, most of whom reside less than 20 km from the peak of the volcano. The SRL-2 imaging radar polarimetry of Pico was acquired in early October 1994, and reduced in early 1995. GSFC scientists have concluded from the orbital radar imaging data (shown in the second figure) that multiple episodes of summit slope failures are evident in the spatial pattern of surface textures derived from the radar backscatter data. Lava flows from the last major eruption are clearly distinguished on the basis of radar backscatter signatures. Continued topographic and high-spatial-resolution monitoring of the summit region of Pico is suggested, as local deformation due to mass wasting is probably locally frequent. The scars from ancient flank collapse events attest to the probability of future catastrophic events as well.

In another study, a time series of 10 m per pixel resolution panchromatic satellite images of the lava flow eruption on the Cape Verdean island of Fogo is under development. Stereogrammetry of stereo pairs of this image data is planned, once suitable incidence angles and minimal cloud obscuration are available. The Fogo eruption commenced in April of 1995; by late June, active effusions of lava were almost nonexistent. SPOT

panchromatic coverage during the active eruption phase was frequently acquired, but cloud-cover problems indicate that only a few of the images are suitable for stereo analysis. Using derived digital elevation model data, it will be possible to measure the erupted volume of materials (at least surficial ones) rather accurately, and the effective productivity of the eruption can then be computed.

Volcano monitoring of relatively inaccessible Middle-Atlantic volcanic islands will require annual topographic surveys and a continuing time-series of cloud-free images from instruments on satellites such as SPOT, Landsat, and others (i.e., radar-imaging satellites such as RADARSAT), and instruments that are planned but not as yet launched (such as the Moderate Resolution Imaging Spectroradiometer (MODIS)). Using locally accessible research aircraft platforms, such as those at Wallops Flight Facility, greatly facilitates short-duration laser altimeter survey missions to these otherwise somewhat inaccessible islands, which represent an important yet often overlooked component of the global Earth inventory of active and dormant volcanoes.

Contact: James Garvin (Code 921)  
301-286-6565

Sponsor: Office of Mission to Planet Earth  
GSFC Director's Discretionary Fund

*Mr. Garvin is a staff geophysicist at NASA/GSFC where he has worked for 10 years. He is the science team leader on the Shuttle Laser Altimeter experiment scheduled for its maiden flight aboard STS-72, a co-investigator on the Mars Orbital Laser Altimeter experiment which is to be launched to Mars in 1996 aboard the Mars Global Surveyor, a NASA Co-Investigator on RADARSAT, and a team member on the NASA Laser Altimeter Facility.*

## USING VERY LONG BASELINE INTERFEROMETRY TO MEASURE CONTEMPORARY POSTGLACIAL REBOUND

THE LAST GREAT ICE AGE peaked about 21,000 years ago; by 7000 years ago the ice in the northern hemisphere was gone. At its peak, the ice sheet covered virtually all of Canada, a northerly strip of the U.S., northern Europe, Greenland, and a section of the Arctic Ocean north of Siberia. The average thickness of the ice was more than 1 km, and the peak thickness was about 3.5 km. So much water was locked in the ice sheets that the global sea level was reduced by about 80 m.

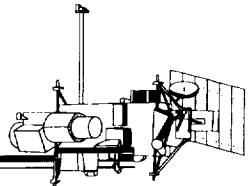
In the presence of this massive load of ice, the surface of the Earth responds like a sphere with a deformable skin (the crust) overlaying a very heavy, very viscous fluid (the mantle). The weight of ice causes the mantle to be displaced from under the thickest ice sheets and into areas of less ice and the adjacent unglaciated regions. Since the average density of the mantle is three times that of ice, approximately one-third of the ice sinks below the level of the undeformed Earth. The behavior of the Earth's surface in the adjacent regions is quite complex; nearby land may be pulled down, while that further away is lifted by the displaced fluid. The picture is complicated still further because the water in the ice sheets is removed from the oceans, thus causing a small rise in coastal plains. The ice load also causes horizontal motions in which the crust is pulled in the direction of the ice sheets. After the ice has melted, the displaced mantle migrates back into the deglaciated region and the vertical and horizontal displacements are reversed. The process is most rapid immediately after the ice has melted and tapers off exponentially, but even today lingering effects persist.

Predictions by James and Lambert, based on a postglacial rebound model by Tushingham and Peltier, show predictions of present-day vertical motions of the Earth's surface over North America and Europe. In both regions, the peak motion is between 10 and 15 mm/yr. In Europe the peak is reached over the northern end of the Gulf of Bothnia, and in North America it is centered over an area just northeast of James Bay. The predicted horizontal motions are nearly a factor of 10 smaller than the vertical and are greatest along the edges of the now-disappeared ice sheets. As with all predictions, observational data must be obtained to ascertain their validity. Very long baseline interferometry (VLBI) is well-suited to such a task.

VLBI is a technique in which vector baselines between two widely separated locations can be measured with great accuracy, routinely on the order of one part per billion. Two radio telescopes use VLBI hardware to measure delays, which are the time-of-arrival differences of radio noise signals from extragalactic objects. The delays can be measured routinely with an extremely high accuracy of less than 20 psec, or a distance of less than 6 mm, compared with the distance across of the U.S. of more than 4,000,000,000 mm. Regression analysis is applied to the delays to infer the positions and velocities of the telescopes.

Our group at GSFC, in conjunction with our contractor and university colleagues, developed the Mark III geodetic VLBI system starting in the late 1970s to address problems in measuring global plate motion and Earth rotation. During the 1980s, as a part of NASA's Crustal Dynamics Project (CDP), we measured baselines between sites on the North American, Pacific, Eurasian, Australian, and African plates. Our measured plate motions are in such close agreement with theory that many scientists consider the verification of plate motion theory a "solved" problem. As a part of NASA's Space Geodesy Program we continue to measure the Earth with VLBI for a variety of scientific objectives, and are developing hardware and analysis methods to advance the VLBI technique.

Along with our colleagues in Europe and Canada, we have begun to interpret our measurements looking for the effects of postglacial rebound. This problem is much more difficult and subtle than looking for tectonic plate motion. Tectonic plates slide horizontally on the Earth, thereby changing the lengths of baselines connecting sites on different plates. These changes are scalar quantities, which are relatively easy to measure because they are not affected by difficulties in defining an inertial, three-dimensional reference frame for the Earth. Thus, plate motions can be detected with VLBI's most robust measurement capability, the measurement of baseline length. Moreover, the motions are large. The expected motion between the VLBI sites on the island of Kauai in Hawaii and in Kashima, Japan, is 69 mm/yr; with the 10 years of VLBI data we have on hand we can estimate that motion with an uncertainty of 0.7 mm/yr, a ratio of 100 to 1.

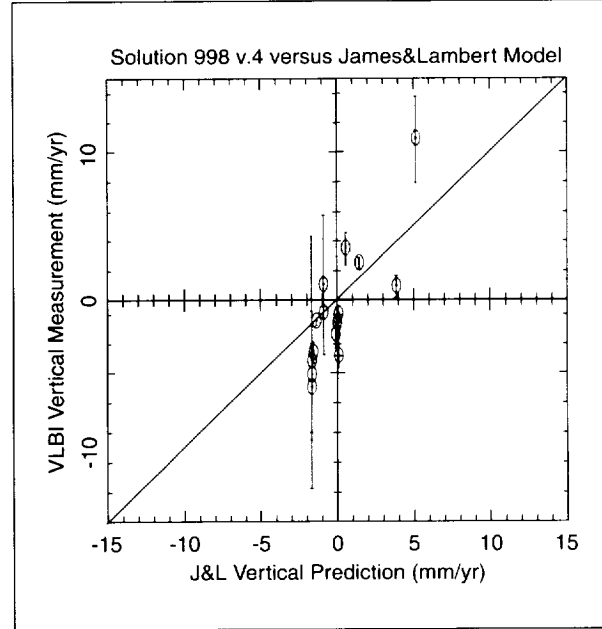


Postglacial rebound is difficult to measure because it is primarily a relatively small motion in the vertical direction, predicted to be less than 6 mm/yr for any site we have used. The horizontal motions of postglacial rebound are much smaller, predicted to be less than 3 mm/yr for all of our sites. Only vertical results will be discussed here.

Two recent papers give rebound model predictions for VLBI sites. James and Lambert's 1993 work gave estimates using their algorithms applied to the Tushingham and Peltier Ice-3G model, published in 1992. Recently, Peltier gave predictions based on his new Ice-4G model, which he tailored for making site motion predictions. Formal errors in the estimates for 10 sites in North America and five sites in Europe are not provided in either paper, but the root-mean-square difference between the two sets of predictions is 0.4 mm/yr. This value is an indication of the errors in the models, and for the balance of this paper it will be used as the formal error for the rates from both models.

Our VLBI-measured rates come from a recent reduction of our geodetic VLBI data set (Solution GLB998, version 4). The data set spans August 1979 through March 1995, and contains more than 1.5 million observations from 2474 one-day observing sessions over 127 globally distributed sites. This is virtually all the data obtained by NASA's CDP, by both the U.S. Navy and the National Oceanic and Atmospheric Administration (NOAA) Earth rotation monitoring programs, and all geodetic VLBI data from the SGP and cooperating foreign agencies. The terrestrial reference frame was defined by two conditions. First, the NUVEL-1 plate motion model, published by C. DeMets *et al.* in 1990, was used as an *a priori* model for motions of the sites on the surface of the Earth. Second, the free translation and rotation of the frame was stopped by constraining the motions of a selected set of well-represented sites to have, on average, a null adjustment from the NUVEL-1 model. This constraint results in a frame which is robust in both translation and rotation, but one in which no *a priori* vertical information has been imposed.

Comparison of the vertical motion estimates from our solution with James and Lambert's and Peltier's scaled



*Correlation plot for James and Lambert vertical predictions versus VLBI measurements.*

sigmas leads us to postulate three cases: that there is no postglacial rebound, that Peltier is correct, or that James and Lambert are correct. Considering our VLBI measurements as observed truth, detailed statistical analysis shows that either model fits the data much better than the "no rebound" assumption. The figure is a correlation plot of James and Lambert's vertical rate predictions versus our VLBI rate measurements. The VLBI points show 1  $\sigma$  formal error estimates, which are equal to the formal error produced in our analysis system, multiplied by 1.5 to account for unmodeled systematic errors. The line from lower left to upper right is the line of perfect correlation. Clearly there is a strong correlation between the two sets of values; only one point is in the wrong quadrant. The correlation plot suggests that the VLBI rates may be related to the predicted rates by a scale factor greater than 1; however, further analysis showed that the differences are not due to a simple scale factor.

VLBI shows significant negative motion at sites far away from the glaciated areas, specifically in Italy and Maryland.

These are areas where the rebound models predict virtually no motion. Either the models are in error, or there are effects not related to rebound causing vertical motion. Rising sea level and ground water withdrawal are two such effects. VLBI sites with large vertical estimate sigmas may be in error because their sample sizes are not yet large enough. Yellowknife, a site in northwest Canada which is a critical for North American rebound detection, has participated in only 21 sessions spanning 5 years.

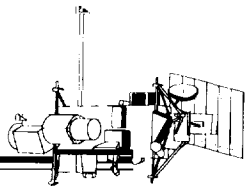
VLBI has successfully detected the effects of postglacial rebound in the vertical velocities of sites in North America and Europe, confirming both the James and Lambert and Peltier model predictions. The VLBI measurements fit the Peltier predictions slightly better than the James and Lambert predictions. We are also investigating the VLBI measurements of the much smaller horizontal rates. VLBI

results will continue to improve as more sites join the VLBI global network, the time spans for existing sites increase, and more sensitive hardware is brought to bear.

Contact: James Ryan (Code 926)  
301-286-9020  
Internet: [jwr@leo.gsfc.nasa.gov](mailto:jwr@leo.gsfc.nasa.gov)

Sponsor: Office of Mission to Planet Earth

*Mr. Ryan is a member of the Space Geodesy Branch of the Laboratory for Terrestrial Physics. He has been involved with VLBI at GSFC since the mid-1970s, and has been a key person in the development of the Mark-III VLBI Analysis System. He joined GSFC in 1963, and worked in manned flight orbit determination during the Mercury, Gemini, and Apollo programs. He holds an M.S. in Mathematics from the George Washington University.*



## SHUTTLE LASER ALTIMETER: A PATHFINDER FOR SPACE-BASED LASER ALTIMETRY AND LIDAR

THE SHUTTLE LASER ALTIMETER (SLA) was completed during 1995 and integrated into a space shuttle Hitchhiker bridge assembly for its first flight during the STS-72 mission on the Space Shuttle Endeavour in early 1996. Detailed SLA test objectives for the STS-72 mission are the acquisition of sample data sets for land topography and vegetation height, test of waveform digitizer performance, and verification of data acquisition algorithms.

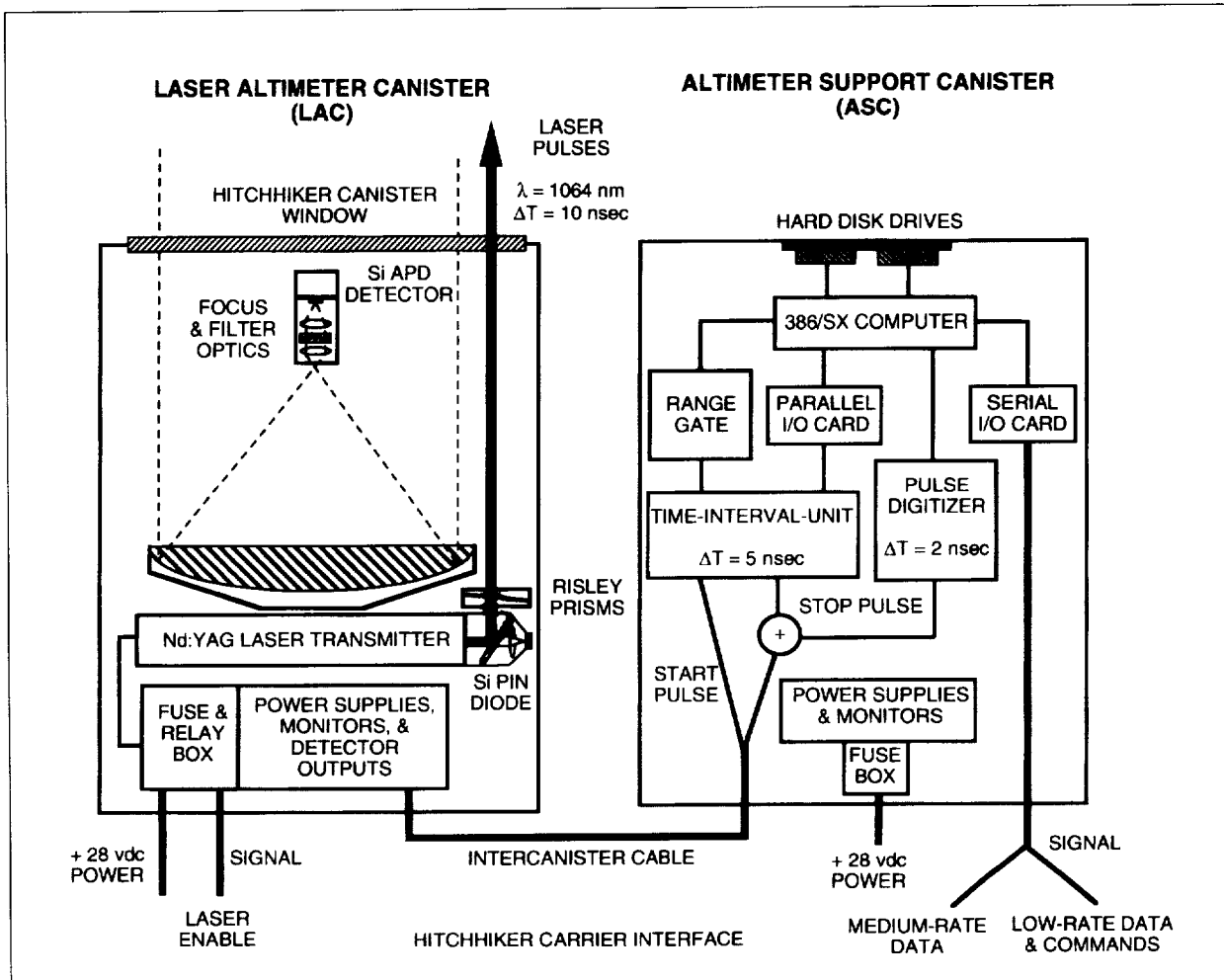
The SLA was developed at GSFC by a small team of engineers and technicians from a mixture of spaceflight spare parts and assemblies, an airborne optical system, and commercial electronics. The Hitchhiker carrier was used for its standard interfaces to space shuttle systems. Together, the SLA and Hitchhiker carrier constitute a low-cost experiment payload capable of topography and lidar measurements from Earth orbit. On-orbit operations of the SLA result in a series of sensor footprints stretched in a measurement profile along the nadir track of the space shuttle. Full interpretation of the SLA distance measurement data set in terms of Earth surface topography also requires meter-level knowledge of the space shuttle trajectory, and better than  $0.1^\circ$  knowledge of the space shuttle pointing angle. These ancillary data sets will be acquired with an on-board Global Positioning System receiver, S- and K-band range- and range-rate-tracking of the space shuttle, and use of shuttle gyroscopes and star trackers.

The SLA is an active optical instrument based on timing the two-way propagation of short ( $\sim 10$  nsec duration) 1064 nm laser pulses for their round-trip between the space shuttle and the Earth's surface. In an optically clear atmosphere, essentially all the initial laser pulse energy reaches the surface, where it is spread into a 100 m diameter spot. Distance between laser spots on the Earth is  $\sim 750$  m, due to the laser pulse rate of 10 pps and the shuttle's orbital velocity. Typically, one part in  $10^{12}$  of the reflected laser pulse is collected by the SLA receiver telescope on the space shuttle, since the surface reflection scatters the pulse into a broad angular pattern. In addition, the laser pulse is spread in time from its initial value to several tens-of-nsec as a result of nonnormal incidence angles, rough surfaces, vegetation, and surface slopes inside the laser footprint. Under cloudy conditions, the laser pulse is scattered, attenuated, and further broadened in time by several orders of magnitude.

The SLA detection and analysis electronics for these weak and broadened pulses produce time interval measurements (i.e., range data) and waveform digitization measurements that record the temporal shape of the laser echo. Waveform digitization enables lidar measurements relevant to both the surface and the atmosphere. Used at full resolution (2 nsec samples), the digitizer configures the SLA into a high-resolution surface lidar sensor; used at lower resolution (20 to 100 nsec samples), the SLA can function as a cloud lidar sensor.

The SLA instrument design requires the use of two adjacent Hitchhiker instrument canisters that are connected by a cable for data transmission. A functional block diagram of the SLA showing both canisters is shown in the figure. The two assemblies are the Laser Altimeter Canister (LAC) and the Altimeter Support Canister (ASC), each of which is separately connected to the Hitchhiker avionics through signal and power ports. The transmitter and receiver subassemblies of the laser altimeter instrument are located in the LAC canister, which is equipped with a Hitchhiker motorized door assembly and a 25.4 mm-thick optical window for operation of the laser altimeter instrument with a clear aperture diameter of 390 mm. Both canisters are pressurized at one atmosphere of dry nitrogen. Each SLA Hitchhiker canister has a mass of about 45 kg, and each canister consumes about 30 W of prime +28 V DC power.

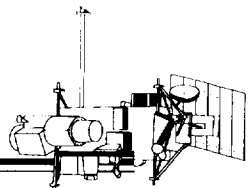
The laser source is a neodymium yttrium aluminum garnet (Nd:YAG) device that pulses at a fixed, continuous rate of 10 pps throughout the SLA operational periods. Its output is derived from linear arrays of thousands of aluminum gallium arsenide laser diodes that are driven electrically to optically excite the Nd:YAG laser crystal. A lithium niobate crystal in the laser cavity holds off lasing for the duration of the laser diode pump pulse (150 usec), and then releases the 1064 nm laser radiation in a giant pulse, called a Q-switch pulse, at the end of the pump pulse. A silicon diode receives  $\sim 1\%$  of the outgoing laser pulse, and provides a start signal for the pulse timing and data acquisition. The outgoing laser pulse is rotated  $90^\circ$  at the output, and passes through a Risley prism pair that is adjusted to align the laser beam to the fixed pointing receiver telescope. Approximately 40 mJ of laser pulse energy is transmitted.



*Functional block diagram of the two-canister Shuttle Laser Altimeter.*

The SLA telescope is a gold- and nickel-plated aluminum parabolic mirror. A sensitive silicon avalanche photodiode (Si APD), with 40% quantum efficiency at 1064 nm, is used to detect the weak laser pulse at the telescope mirror prime focus and to produce an electronic stop signal. An optical bandpass filter and focusing lenses in the mirror focal plane assist the detector by reducing broadband optical noise due to daytime solar illumination, and by reducing the size of the image spot to less than one-half of the 0.8 mm diameter Si APD.

The time-interval unit, digitizer, and computer data system are the principal data acquisition electronics in the ASC. The time-interval unit design is based on a 4-channel, matched-filter, and discriminator bank that precedes a 100 MHz counter. Matched filters, originally developed for the Mars laser altimeter instrument, are optimized for best signal-to-noise ratio in detection of 20-nsec-, 60-nsec-, 180-nsec-, and 540-nsec-wide pulses; a range of values that encompasses the expected pulse spreading from the surface. The SLA data acquisition



algorithm can accommodate a variable detection noise level by an automatic threshold tracking loop and a range gate. The payload computer, a based on a 386/SX central processing unit, is a single-board device with a single 512 Kbyte EPROM and 2 Kbyte of RAM. The computer bus, a ribbon cable, extends to three expander cards necessary for pulse waveform digitization, parallel input/output operations with the altimetry electronics, and the serial input/output communication connections to the Hitchhiker electronics for commands and data. A key innovation of the SLA design is power cycling of the waveform digitizer, which reduces its power dissipation to only 2 W.

An initial on-orbit cool-down period of 24 hrs prior to SLA activation is planned to achieve optimum operation of the LAC at 0°C. During this period, thermostatically controlled replacement heaters will activate if the LAC falls below -5 °C or the ASC falls below +5 °C. Astronauts then enable laser power by two switches, and the LAC door is opened by ground control. With an open door and acceptable operating temperatures in both the LAC and the ASC, the power-on command will be given to the ASC to initiate SLA operation for a verification of medium- and low-rate telemetry and command capability. Activation of the LAC canister is permitted only when the orbiter is in the bay-towards-Earth orientation, and no extra-vehicular activity or spacecraft release/retrieval operations are underway.

There are several SLA commands and 38 data acquisition parameters that modify the preprogrammed flight software operational modes and default parameter values. When first activated, the on-board SLA computer boots from the EPROM and enters the flight software in a safe (i.e., standby) mode, in which both medium-rate and low-rate telemetry packets are generated, but no laser pulses are generated. Upon receipt of the fire command, the laser transmitter begins operation, and pulse data are processed, formatted, recorded, and sent by both telemetry channels to the ground. All laser altimeter data are stored on the twin 260 Mbyte hard disk drives in the ASC. These are commercial units used in laptop computers. The complete data set is continuously sent via the Hitchhiker medium-rate data channel at 19.2 Kbaud and reaches the ground when that link is available. The LAC operates continuously until the *safe* (i.e., laser off) command is

issued. The total planned data take for a space shuttle mission is about 100 hours.

Four flights of SLA are planned over the next few years. They are aimed at the transition of the GSFC airborne laser altimeter and lidar technology to low-Earth orbit as a pathfinder for operational space-based laser remote sensing. Future laser altimeter and lidar sensors—such as the Geoscience Laser Altimeter System (an Earth Observing System facility instrument) and the Multibeam Laser Altimeter (the land and vegetation laser altimeter for a NASA topography mission)—will utilize laser and detector technology, data acquisition electronics, and algorithms being tested with SLA. This first SLA instrument shares laser, detector, and electronics technology with the Mars Orbiting Laser Altimeter, which is now under development for flight in 1996 on the Mars Global Surveyor Mission.

The SLA development is the result of many long hours contributed by Bryan Blair, John Cavanaugh, James Garvin, David Harding, Dan Hopf, Ken Kirks, David Rabine, James C. Smith, Glenn Staley (retired), and Nita Walsh of the Laboratory for Terrestrial Physics. Dick Aldridge and Gerry McIntire (Wallop Flight Facility) of the Laboratory for Hydrospheric Processes also contributed significantly to the payload electronics and cabling.

Important contributions came from the Engineering Directorate at GSFC where this effort originated a number of years ago as a Director's Discretionary Fund Task. Paul Weir (retired) designed the structure, while Bill Schaefer and James Fitzgerald developed the altimetry electronics. Personnel of the Special Payloads Division also made significant improvements and contributions to SLA development.

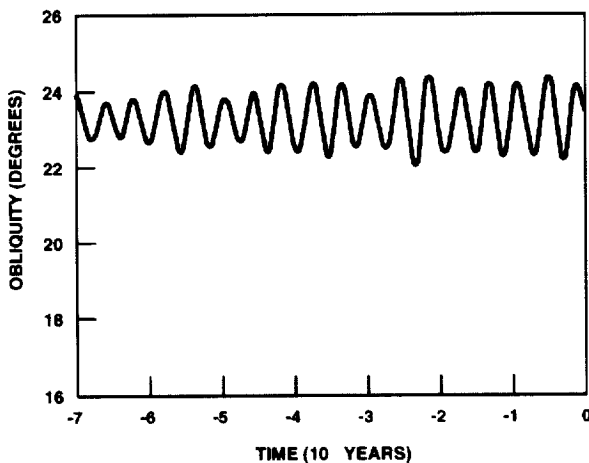
Contact: Jack Bufton (Code 920)  
301-286-8591

Sponsor: GSFC Director's Discretionary Fund

*Dr. Bufton is Instrument Manager for the Shuttle Laser Altimeter. He earned a Ph.D. in Electrical Engineering from the University of Maryland. Dr. Bufton has been at GSFC for 29 years, and is currently the Associate Chief for Sensor Physics of the Laboratory for Terrestrial Physics.*

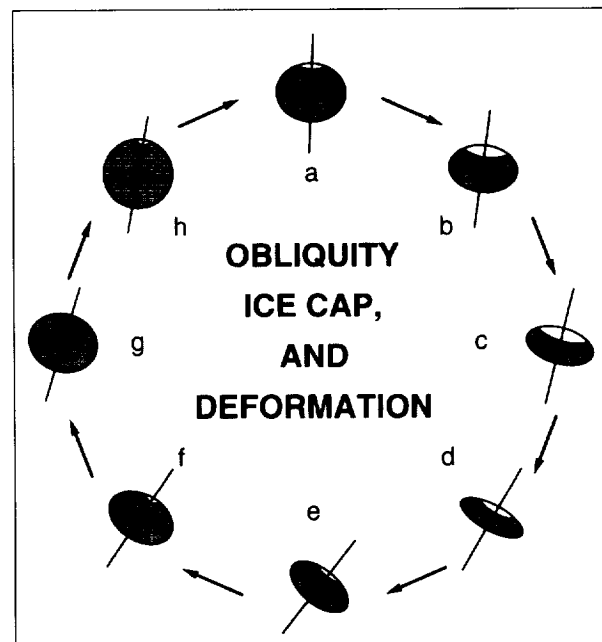
## HAS CLIMATE CHANGED THE EARTH'S TILT?

THE NAME "CLIMATE FRICTION" is given to the mechanism whereby climate changes can cause a long-term change in the tilt of a planet with respect to its orbit about the Sun. The name comes from an analogy with tidal friction, which can also generate secular (i.e., long-term) changes in orbital parameters. For example, over the eons tidal friction steadily pushes the Moon away from the Earth, while simultaneously decreasing the Earth's rotation rate and increasing its obliquity (the technical term for axial tilt); currently the Earth's obliquity is  $23.5^\circ$ . Unlike tidal friction, climate friction does not alter the Moon's orbit or the Earth's rotation rate; but climate friction can alter the Earth's obliquity, increasing it slowly over the age of the solar system just like tidal friction can. The operation of climate friction depends crucially on the obliquity cycle, which is one of the Milankovitch cycles. The obliquity oscillates by about a degree or so around its average value with a period of about 40,000 years (as shown in the first figure).



*The Earth's obliquity variations for the last 700,000 years. The obliquity oscillates about an average value, which is close to the present value of  $23.5^\circ$ .*

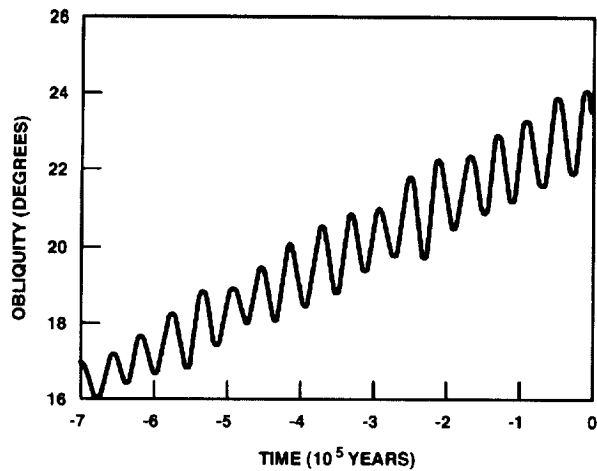
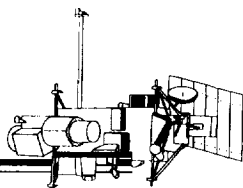
The way climate friction works is illustrated in the second figure. When the axial tilt is low, the poles cool due to decreased sunlight, and an ice cap forms. The ice cap squeezes the Earth, making it more oblate. The combination of the ice cap growth and deformations in the Earth changes the Earth's dynamical flattening, altering the torques on the Earth due to the Sun and the Moon. Similarly, when the obliquity is high, there is increased



*The interplay between the obliquity, ice cap, and deformation of the Earth, all greatly exaggerated. The obliquity is lowest at a and greatest at e, as indicated by the tilt of the axis. The ice cap is smallest at g and greatest at c. The ice cap lags the obliquity forcing by  $90^\circ$ . The deformation is arbitrarily shown here to lag the ice by  $45^\circ$ ; the exact amount depends on the Earth's viscosity.*

insolation at the poles, and the ice melts; the deformed Earth undergoes postglacial rebound, and the torques change once again. This constant cycling of the torques with the obliquity cycle can cause the average tilt of the Earth to slowly shift with time (as shown in the third figure). The waxing and waning of the ice cap with the obliquity cycle is crucial to the mechanism of climate friction: an ice cap that just sits there without fluctuating, no matter how large, produces no secular change in the Earth's tilt. The extent to which climate friction changes the tilt depends on the size of the ice caps, the phase of the ice cap mass with respect to the obliquity oscillation, how long the ice ages last, and the nature of the Earth's interior structure, particularly the viscosity of the mantle.

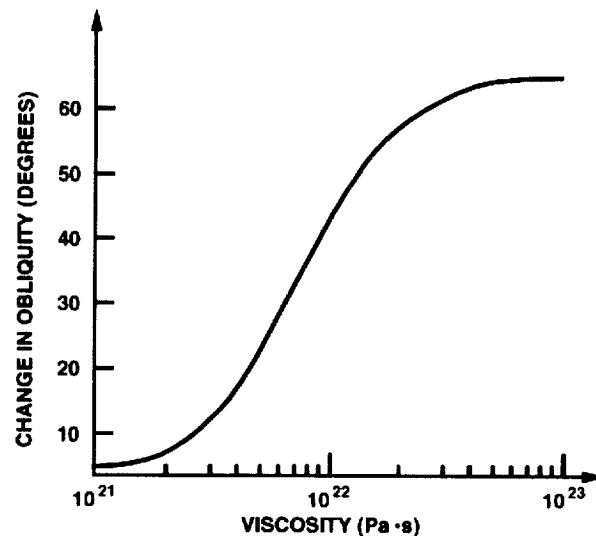
In a recent study of the interplay between these parameters, the Earth was assumed to be a homogeneous, viscous sphere of constant density and viscosity; the presence of the Earth's core and any viscosity variation with depth



*A possible secular trend in the Earth's obliquity, greatly exaggerated. This figure should be compared to the first figure. The obliquity still oscillates, but the average steadily increases. For models considered here, the average would increase by only  $0.1^\circ$  at most over the 700,000 years shown in this figure. Over hundreds of millions of years, the tilt could increase by many degrees.*

was ignored. Other assumptions were that the ice cap mass lagged the obliquity oscillation by  $90^\circ$ , as observed for the Quaternary period based on oxygen isotope ratios obtained from deep ocean sediments. This phase lag means that climate friction can only increase the average obliquity, and never decrease it. In other words, it tips the Earth over more and more as time passes, so that the Earth's tilt would have been smaller in the past due to this mechanism. It was also assumed that the ice caps cycled with the obliquity cycle for a grand total of 450 million years of Earth's history, and that the maximum ice cap size was the same as observed for the Quaternary. These last assumptions probably maximize the amount of climate friction which could have taken place; ice caps during ice ages prior to the Cenozoic era may not have waxed and waned with the obliquity cycle, and those that did may have been smaller than the Quaternary caps. For example, geologic evidence from the Miocene epoch suggests that the obliquity caps were smaller than those of the Quaternary, and the ice caps during the Huronian ice age 2 billion years ago may not have fluctuated at all. Evidence one way or the other is lacking.

Climate friction also depends on the Earth's viscosity, or resistance to flow. If the viscosity were as low as that of water, for example, then the Earth would compensate for the ice cap load immediately; there would be no change in the dynamical flattening of the Earth and, consequently, no climate friction. If the viscosity were infinite, then the cap would be completely uncompensated, allowing a large amount of climate friction. The actual value of the viscosity of the Earth is poorly known, with suggested values ranging from about  $10^{21}$  Pa-s to  $10^{23}$  Pa-s for the lower mantle. The maximum possible change in obliquity has been calculated and plotted as a function of viscosity in the fourth figure.



*The maximum probable amount of secular increase in the Earth's obliquity as a function of viscosity for a homogeneous Earth. This figure assumes that the obliquity ice caps behaved in all previous ice ages as they did in the Quaternary and went on for a grand total of 450 million years. The actual change in obliquity lies somewhere below the curve; the exact value is unknown.*

The figure shows that climate friction might explain all of the presently observed tilt of  $23.5^\circ$  if the viscosity of the Earth is about  $6 \times 10^{21}$  Pa-s or greater, even if the primordial obliquity were low. It is conceivable that at onetime the obliquity was higher than its present value due to climate friction, and then decreased to its present value due to core-mantle coupling or some other mechanism, but this seems unlikely. More likely, climate

## EARTH SYSTEM SCIENCE

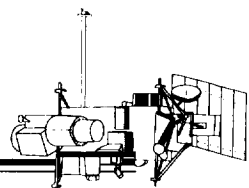
---

friction increased the obliquity by an unknown amount somewhere between zero and its present value, with the remainder being accounted for by tidal friction. Further research will be needed to sort out the various mechanisms that may have changed the Earth's tilt. Investigations are continuing by David Rubincam and Bruce Bills in the United States, and by Takashi Ito and his coworkers in Japan.

Contact: David Rubincam (Code 921)  
301-286-5107

Sponsor: Office of Mission to Planet Earth

*Dr. Rubincam has worked in the Geodynamics Branch at GSFC for 17 years. He obtained his Ph.D. from the University of Maryland. His interests include solid-Earth geophysics and celestial mechanics.*



---

## CLIMATOLOGY

### SEMIANNUAL AND QUASI-BIENNIAL OSCILLATIONS GENERATED BY GRAVITY WAVES IN THE MIDDLE ATMOSPHERE

Earth system scientists have long believed that wave interactions play a critically important role in our understanding of the dynamics of Earth's middle atmosphere.

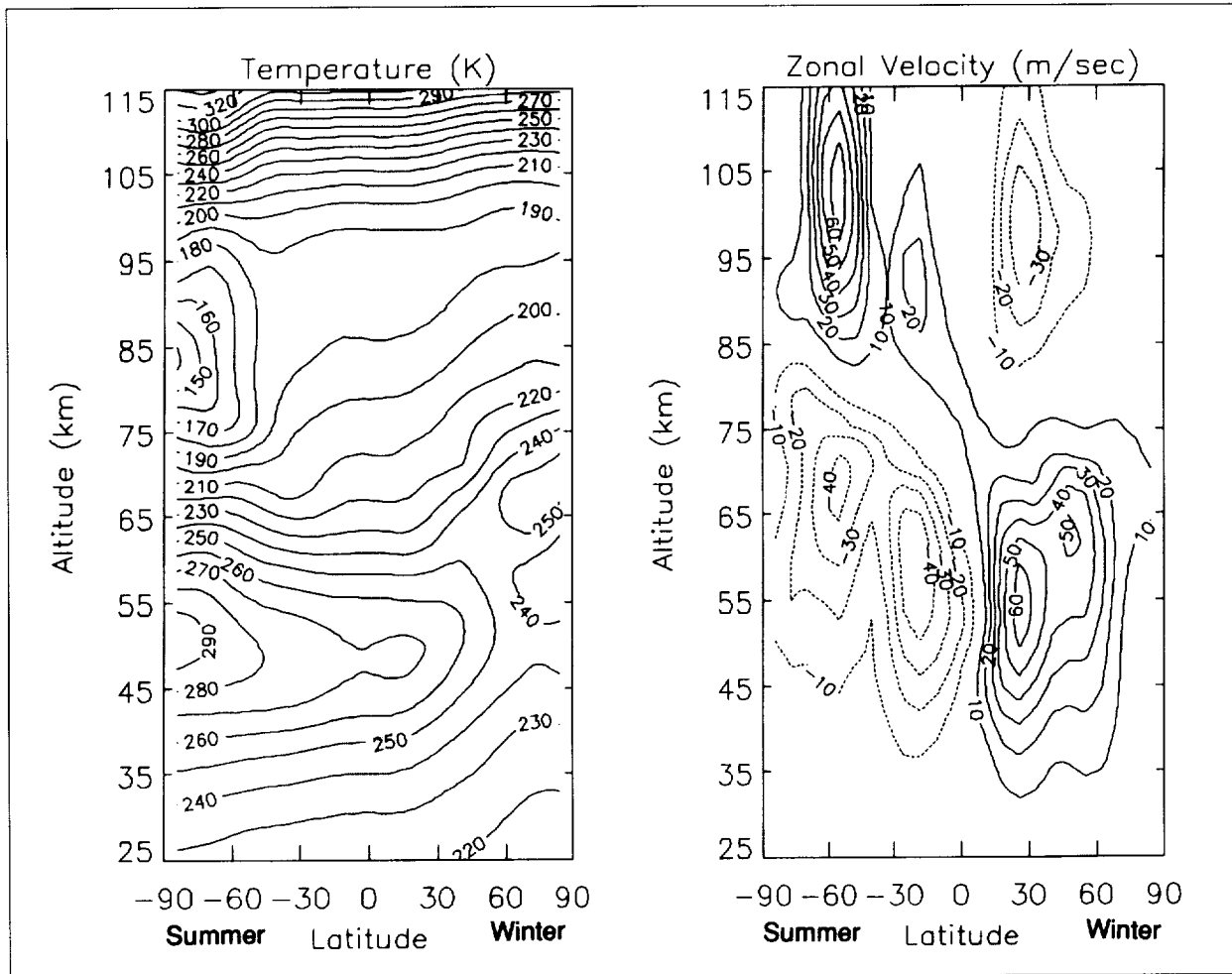
In the late 1960's and early 1970's, Lindzen and Holton demonstrated that tropical planetary-scale waves can accelerate the zonal circulation to produce the Quasi-Biennial Oscillation (QBO), which is observed at low latitudes in the stratosphere with a period of approximately 24 months. Their theory was later extended to explain certain characteristics of the Semiannual Oscillations (SAO), also observed at low latitudes in the upper stratosphere and lower mesosphere, but with a period of 6 months. The SAO cannot be accounted for by the radiative forcing and momentum advection associated with meridional circulation. In the early 1980s, momentum deposition by breaking small scale gravity waves (GWs) had been invoked by Lindzen to produce the atmospheric motions that can explain the anomalous temperatures in the upper mesosphere, which are lowest in summer rather than in winter, contrary to expectations based on radiative considerations.

Hines has recently developed a parameterization scheme for GW momentum deposition based on his Doppler Spread Theory. This formulation differs from others in that it deals with a spectrum of waves, and accounts in self-consistent form both for the interactions between the waves and the background wind field, and between the waves themselves. It also provides a self-consistent description of the eddy viscosity. This GW parameterization has now been incorporated into the two-dimensional version of a nonlinear, numerical spectral model that was originally developed at GSFC for solar and planetary applications. The adopted spectral approach has the well-known advantage of being more efficient in low and moderate resolutions. Unlike the finite difference method, it does not break down in the polar regions. Moreover, the spectral approach naturally decomposes the variable fields into separate zonal components that can be studied individually and interactively. This model is very efficient and computationally stable, and is capable of integration periods extending over several years.

At this early stage of exploring the new GW formulation, the waves are simply assumed to be generated isotropically in the four cardinal directions to the east, west, north, and

south. The wave flux originating in the troposphere is assumed to be independent of latitude and season. The GW flux was constrained such that the model reproduced the observed anomalous variations in the temperature and zonal winds of the upper mesosphere, as shown in the first figure. These numerical results correctly describe the salient features that characterize the observations. Near 50 km, where the maximum absorption of ultraviolet radiation by ozone occurs, the temperature peaks in the summer polar region. Due to geostrophic balance, zonal winds are built up that are eastward and westward in the winter and summer hemispheres, respectively. At altitudes above 70 km, however, the temperatures are lower in summer than in winter, consistent with the observations. Above 85 km, the zonal winds reverse direction, turning eastward in summer and westward in winter. As demonstrated in earlier models, these reversals in the latitudinal temperature variations and zonal winds are the direct consequence of the gravity wave interaction. In our model, the GWs propagate through the thermally-driven zonal circulation of the stratosphere near 50 km where they suffer critical-level absorption. Entering the mesosphere, the waves then have a net momentum in the direction opposite to that of the stratospheric circulation. This momentum is deposited in the upper mesosphere above 60 km due to wave breaking, which causes the zonal circulation to reverse; self-consistently, the latitudinal temperature variation reverses. Without the GW momentum source, the computed temperature and wind fields above 65 km have virtually no resemblance to those shown here; the reversals in the zonal jets do not occur, and the temperature up to 100 km is higher in summer than in winter.

The contribution of GW in generating the large oscillations in the zonal circulation at low latitudes is shown in the top panels in the second figure, covering the altitude range between 35 km and 80 km for a period of 6 years. At these altitudes, the dominant periodicity is 6 months; the fitted Fourier component, or SAO, is shown in dashed lines. Near the stratopause, at 50 km, the SAO amplitude in the zonal wind approaches 20 m/s, which is consistent with the observed values of 20 to 30 m/s. At higher altitudes, near 85 km, the computed SAO reaches a secondary maximum exceeding 10 m/s, compared with the observed values of 20 to 30 m/s. This oscillation has a phase opposite to that computed near 50 km, and the computed phase of the SAO descends in altitude with an average rate of about 8 km/month, both in agreement with

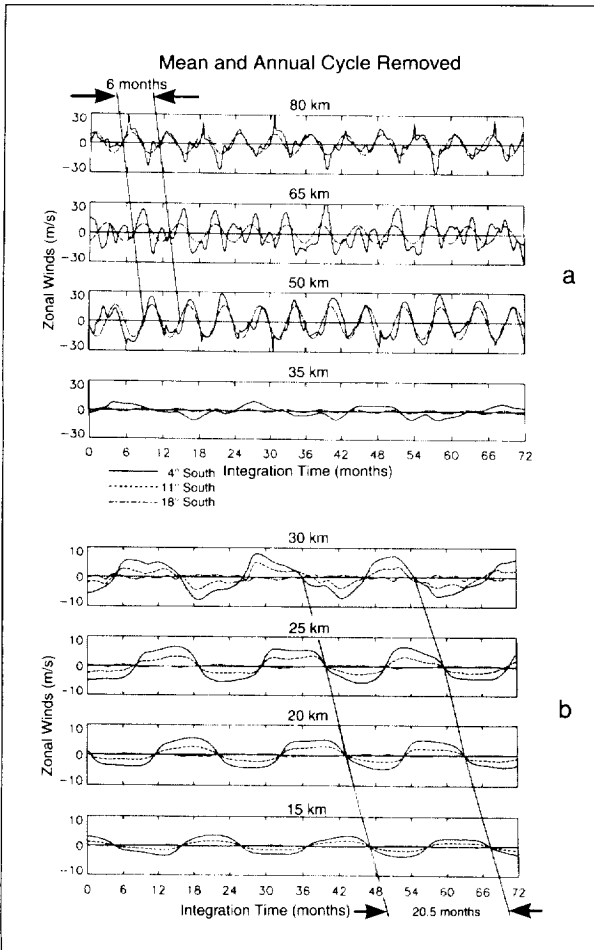
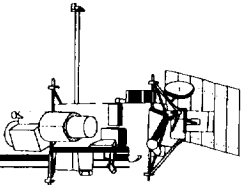


Computed zonal winds and temperatures during solstice with eddy viscosity and momentum deposition resulting from upward-propagating small-scale gravity waves. The model reproduces the observed reversals both in the latitudinal temperature variations near 80 km (with minimum temperature in the summer polar region) and in the zonal winds above that altitude.

observations. As observed, the computed amplitudes of the SAO in the mesosphere and upper stratosphere peak near the equator, and fall off rapidly with latitude.

In the stratosphere below 40 km, the computed variations in the zonal circulation take on an entirely different character, as shown in the second set of panels. Here, the winds exhibit a periodicity of more than 20 months, which approaches the lower end of the observed QBO period of

22 to 34 months. The computed wind velocities reach almost 10 m/s (maximum), about half of what is observed. As expected, the QBO generated in the model is solely the result of GW interactions (i.e., when the GW momentum source is turned off, the QBO disappears). The downward phase progression in the computed QBO of about 1.6 km/month is consistent with the observed value of about 1.3 km/month and, much like the observations, the computed QBO is again confined to low latitudes. While



Computed time series of the zonal winds, with the mean and annual cycles removed. Top: Above 35 km, the SAO dominates, with the 6-month Fourier component shown in dashed lines. Note the large amplitude at 50 km, and the phase reversal between 50 and 80 km, consistent with observations. Bottom: At lower altitudes, the computed time series of the zonal winds is presented at 4°, 11°, and 18°S. A pronounced periodicity of about 20 months is evident, which approaches that of the observed QBO; the wind amplitudes of about 8 m/s are significant compared to the observed values of 20 m/s in the QBO. The computed QBO-like oscillation rapidly falls off towards higher latitudes, consistent with observations.

the model thus reproduces many of the observed characteristics, the differences in amplitude and periodicity are significant. This suggests that planetary scale waves also should play an important part in generating the QBO (as originally suggested by Lindzen and Holton), although general circulation models have recently shown that these waves only produce QBO wind amplitudes of less than 2 m/s.

Numerical results obtained from the model presented here show that GW can describe, as expected, the anomalous summer-to-winter temperature reversal in the upper mesosphere. Such waves also contribute significantly to the generation of the large equatorial oscillations, the SAO and QBO, observed in the zonal circulation of the middle atmosphere.

Contact: Hans Mayr (Code 916)  
301-286-7505

John Mengel (ARC)  
301-286-4516

Colin Hines (NRC)  
301-286-5216

Sponsor: Office of Space Science

*Dr. Mayr has been with Goddard for 27 years and is presently a member of its Chemistry and Dynamics Branch. He received his Ph.D. from the University of Graz, Austria, and has been involved in the development of empirical and theoretical models of ionospheres and atmospheres in terrestrial, planetary, and solar settings.*

*Dr. Mengel is with the Applied Research Corporation, in Landover, MD. He received his Ph.D. from Yale University and has worked on computer models of terrestrial and planetary atmospheres.*

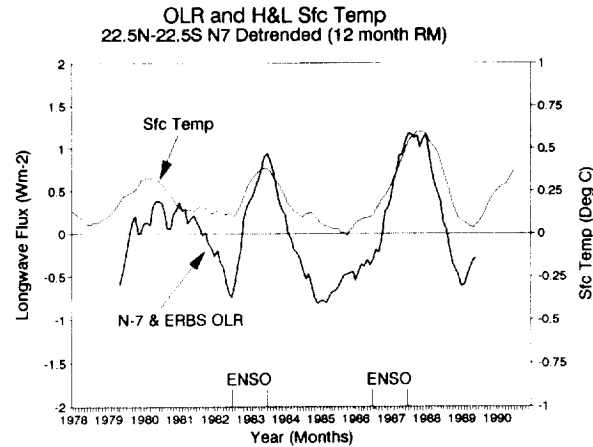
*Dr. Hines is a visiting scientist holding a National Research Council fellowship. He received his Ph.D. from Cambridge University, England, and is recognized for his pioneering work in theoretical fluid dynamics covering topics that range from the solar wind interaction with the magnetosphere to gravity wave processes.*

## IN-PHASE, QUASI-BIENNIAL OSCILLATIONS OF THE TROPICAL SURFACE TEMPERATURE AND OUTGOING LONGWAVE RADIATION

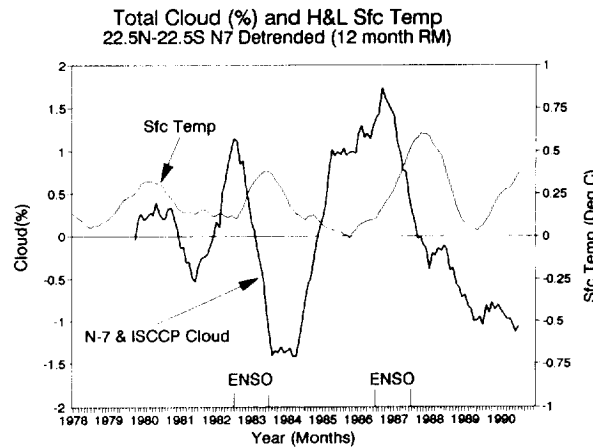
QUASI-BIENNIAL tropical climate oscillations have been studied for some time. In the context of this study, a major feature is the alternate interannual warming and cooling of the tropical surface water in the central and eastern Pacific. The larger amplitude cycles are known as El Niño/Southern Oscillation (ENSO) events; they can cause major flooding in some regions and concurrent droughts in others. Cycles with smaller amplitudes sometimes occur between ENSO events. The data indicate that not only are there regional shifts in the temperature, but that the mean tropical temperature oscillates over a range of about  $0.5^{\circ}\text{C}$ . The present study shows that for the period from 1979 to 1989, the top of the atmosphere outgoing longwave radiation (OLR) underwent a similar in-phase oscillation that was physically influenced by variations in the total cloud cover and by the surface temperature. This interannual behavior runs counter to that of the mean tropical seasonal cycle, where both the surface temperature and the cloud cover increase but the OLR decreases over the oceans, near the subsolar point. This seasonal decrease in the emitted longwave radiation is driven by the large increase in the amount of high clouds when the subsolar point is near a particular latitude.

The mean annual tropical ( $22.5^{\circ}\text{N}$  to  $22.5^{\circ}\text{S}$  latitude) surface temperature and OLR variations are shown in the first figure, for the period from 1979 to 1989. The original data, which consisted of monthly means and 12-month running means, were calculated to examine the mean annual variations. Twelve-month markers (July to June) are shown at the bottom for the 1982/83 and 1986/87 ENSO events. The top curve shows the surface air temperature anomalies compiled by Hansen and Lebedeff at the Goddard Institute for Space Studies. The bottom OLR curve was obtained by joining the measurements of the Nimbus-7 and the Earth Radiation Budget satellites; this required some bias adjustments, detrending and averaging. The OLR anomalies are departures from the mean of the combined OLR data set.

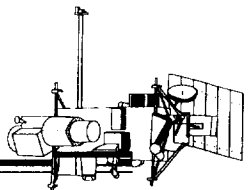
The second figure shows the 12-month running means of the tropical total cloud amount and the surface temperature variations. The Nimbus-7 cloud measurements were first joined to those of the International Satellite Cloud Climatology Project (ISCCP) to obtain a continuous cloud



*Mean tropical ( $22.5^{\circ}\text{N}$  to  $22.5^{\circ}\text{S}$  latitude) interannual (12-month running mean) surface air temperature and OLR anomalies for the period from 1979 to 1989. The temperature curve shows deviations from the 1951 to 1980 average as derived by Hansen and Lebedeff (H&L) and coworkers at the Goddard Institute for Space Studies. The OLR curve was obtained by combining measurements from the Nimbus-7 and the Earth Radiation Budget Satellite, and the anomalies are departures from the mean.*



*Tropical interannual surface air temperature and total cloud anomalies are shown. The cloud curve was obtained by combining the Nimbus-7 and the ISCCP data sets. A linear detrending was applied to the Nimbus-7 product before the two were combined. Cloud anomalies are departures from the mean of the combined data set.*



estimate starting in April 1979; some bias adjustment and detrending were required. Variations from the mean are shown. The 1982/83 and 1986/87 ENSO events start with a warming in the central and eastern Pacific, and a shift of the deep convection rain regions eastward from their normal center in the western Pacific. There is some decrease in the cloud amount in the western Pacific, but only moderate cooling.

Data in the first figure indicate that the mean tropical surface temperature and OLR start to rise fairly early in the ENSO period, but do not peak until the end of the period. Later, as the surface temperatures in the eastern Pacific cool down again, so do the tropical mean temperatures. The total cloud amount (shown in the second figure) shows a negative correlation with the surface temperature and the OLR from the beginning through the end of the main ENSO phase. However, positive cloud-vs-surface temperature correlations are noticeable in other years. It should also be noted that the interannual stability of the cloud measurements appears to be less than those of the OLR and temperature measurements.

The in-phase interannual oscillation of the surface temperature and the OLR is, of course, a mean statistical phenomenon. Regions in the tropical oceans, which develop extensive surface warming and deep convective activity only during ENSO events, show a negative correlation between interannual OLR and surface temperature variations. In the mean, these are cancelled out by larger regions that show an increased longwave emission as the mean surface temperature increases.

The normal warm water pool in the western Pacific and around Indonesia is an interesting case. During an ENSO event, there is a slight cooling of the surface temperature, but a large decrease in both total and high-altitude clouds. This results in a marked increase in the OLR. Thus, regionally there is a negative correlation between the surface temperature and the OLR. But, since the OLR

signal is large and the temperature signal is small, this region helps keep the mean tropical OLR and temperature variations in-phase. Tropical land areas also make an important contribution. In-phase oscillations occur over both land and ocean, but the amplitude of the oscillations is larger over the land than over the oceans.

In the mean tropical seasonal cycle, a super greenhouse effect occurs. That is, as it gets warmer, the high clouds build up, and the amount of heat (OLR) escaping to space actually decreases. The presence of many thin cirrus clouds keeps the input of solar energy high. These clouds pass most of the incoming solar energy, but block the escape of most of the surface-emitted longwave radiation. The eventual cooling is caused by a decrease in the input solar heat as the subsolar point moves to other latitudes. In the interannual cycle no mean super greenhouse effect occurs; as the surface temperature increases, so does the cooling OLR. This acts as a check on the increasing surface temperature. Currently we do not have enough information to determine what the OLR (greenhouse) feedback effect would be for long-term temperature changes in the tropics.

Contact: H. Lee Kyle (Code 902.3)  
301-286-9415  
Internet: lkyle@daac.gsfc.nasa.gov

Sponsor: Office of Mission to Planet Earth

*Dr. Kyle was manager for 15 years of the recently completed Nimbus-7 Clouds and Earth Radiation Budget (ERB) data sets preparation programs; he was also a member of both the Nimbus-7 ERB and the follow-on Earth Radiation Budget Experiment science teams. Dr. Kyle received a Ph.D. in Atomic Physics from the University of North Carolina. For 36 years, he has been at GSFC, where he works in the Global Change Data Center; he is presently working with the Goddard Distributed Active Archive Center to develop an Interdiscipline Data Collection for general climate studies.*

## THE SUPER GREENHOUSE EFFECT AND CLOUD RADIATIVE FORCING IN THE TROPICAL ATMOSPHERE

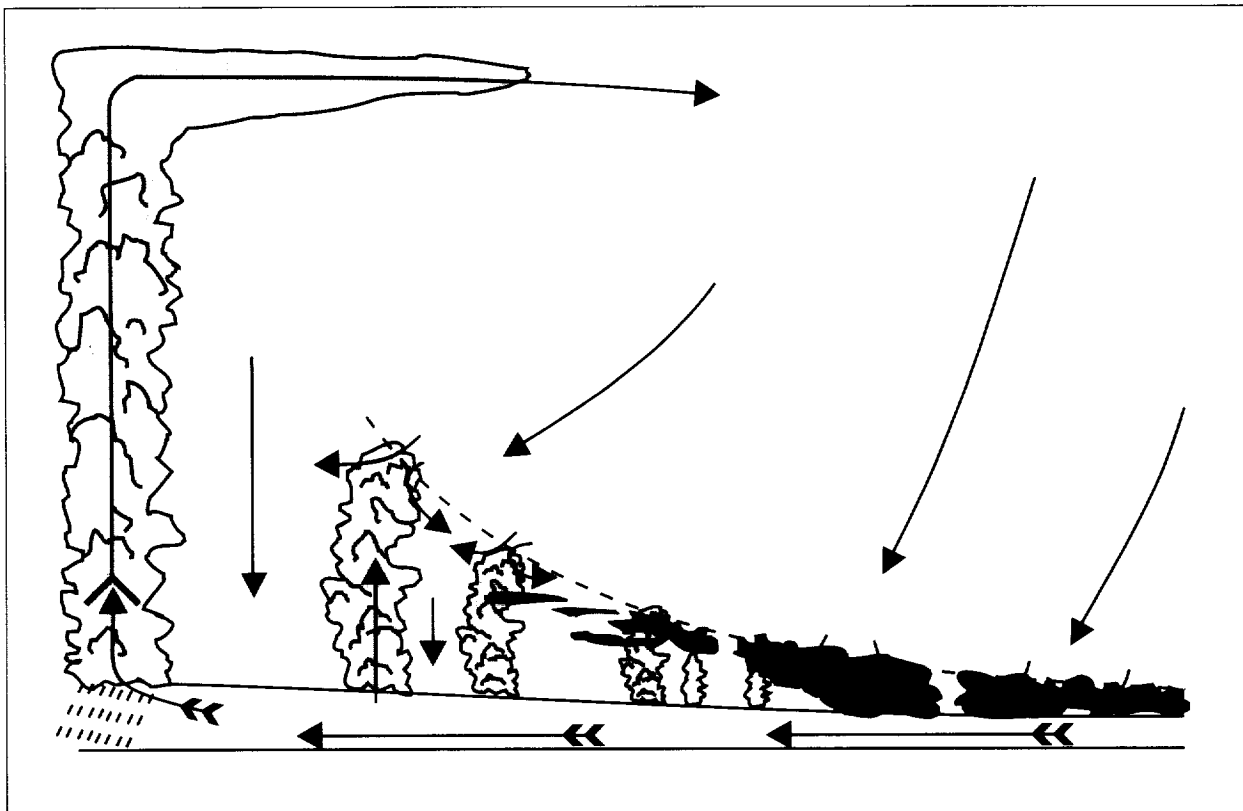
WATER VAPOR and clouds play a fundamental role in influencing climate variability. Therefore, it is important to understand the physical processes that govern water vapor and cloud distributions and their impact on the Earth's radiation budget.

Recent observational studies show that over warm tropical oceans (sea-surface temperature (SST)  $> 25^{\circ}\text{C}$ ), the clear-sky outgoing longwave radiation (OLR) often decreases with increasing SST. This situation is referred to as the "super greenhouse effect." The decrease in OLR is caused by a large increase in the water vapor amount in the atmosphere (particularly in the upper troposphere) that strongly traps longwave radiation emitted by the warmer SST beneath. In this way, the influence of water vapor absorption can completely offset the radiative effect of a warmer ocean surface and warmer lower troposphere. The dependence of cloudiness and water-vapor distribution on

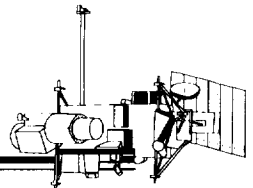
SST and large-scale circulation can be inferred from a schematic diagram such as that shown in the first figure, which shows how SSTs are related to moist-convection, clouds, and large-scale circulation.

We have investigated the variability of water vapor, clouds and radiation, and their relationships with SST and large-scale atmospheric circulation over the tropical ocean by employing satellite data to analyze data products of two four-dimensional data assimilation systems (DAS) for the 2-year period from 1987 to 1988.

We used several satellite data sets: Earth Radiation Budget Experiment (ERBE) data for radiation at the top of the atmosphere, TIROS Operational Vertical Sounder (TOVS) data for water vapor and cloud fraction (a GSFC product), and International Satellite Cloud Climatology Project (ISCCP) data for cloud fraction and cloud optical

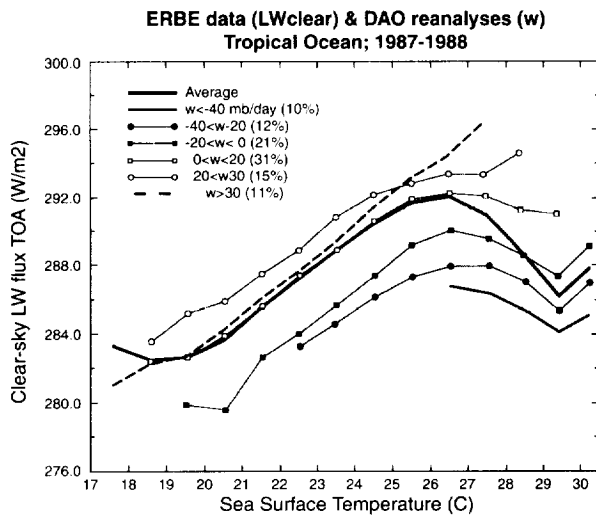


*Schematic representation of the structure of the tropical atmosphere, showing the various regimes as a function of sea surface temperature (from Kerry Emanuel).*



properties. For SST, we used National Meteorological Center (NMC) data produced by R. Reynolds. We took dynamical fields from two reanalyses: one produced by the Data Assimilation Office (DAO) at GSFC and the other produced by NMC. We have designed a methodology based on a simple flow-regime classification, which uses the vertical velocity at 500 mb as a proxy for the large-scale circulation. We found that the spatial distribution and occurrence of the different circulation regimes (strong convergence, strong divergence, etc.) are quite similar for DAO and NMC reanalyses; therefore, we show figures here for DAO analyses only.

We examined the spatio-temporal relationships between the SST and the clear-sky longwave radiation at the top of the atmosphere for different large-scale circulation regimes, and found that for a given SST, the clear-sky OLR decreases as the large-scale rising motion increases, as shown in the second figure. This is supported by TOVS data, which show that water vapor amount and upper-level relative humidity are larger in convective regions as opposed to subsidence regions. Considering the clear-sky



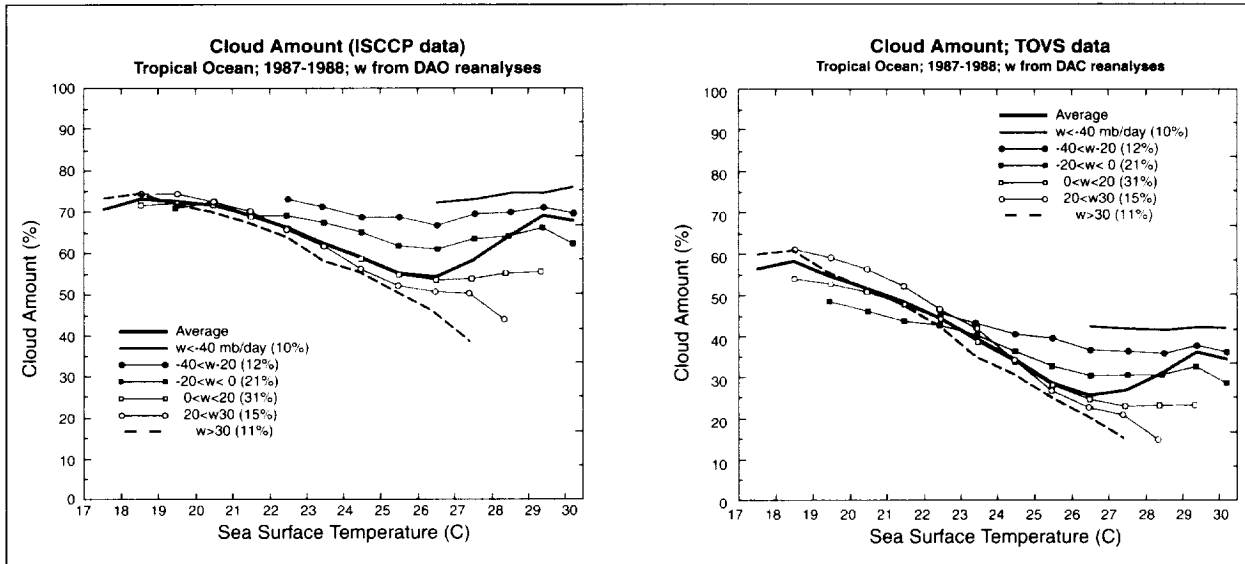
*Mean relationship between the ERBE clear-sky OLR and the SST during 1987-1988 for different regimes of large-scale circulation (defined by the analyzed vertical velocity at 500mb). Negative values of the vertical velocity correspond to rising motion (convergence) while positive values correspond to sinking motion (subsidence). The thick black curve represents the mean curve obtained by averaging all the regimes.*

OLR for a given circulation regime, we found that it always increases with SST in subsidence regimes, while it decreases only slightly with SST in convective regimes. However, because the incidence of convection is much larger in warm SST regions, the weighted average in space and time shows a large decrease in the OLR for warmer SSTs. This result is further confirmed in the regional interannual anomalies of the clear-sky greenhouse effect, which shows that the incidence and intensity of the super greenhouse effect is strongly modulated by the large-scale circulation.

We have demonstrated that the SST itself is not enough to generate clear-sky super greenhouse effect conditions. Neither the impact of SST on the local vertical velocity, nor the highly nonlinear water-vapor temperature relationship of Clausius-Clapeyron, are the dominant factors in the vertical structure of moistening of the tropical atmosphere over warm SSTs. The incidence of the super greenhouse effect is primarily controlled by large-scale circulation and the associated water vapor transports. These are strongly affected by large-scale horizontal gradients in SST, as compared to local SST changes. These results hold for both DAO and NMC analyses and earlier modeling studies performed at GSFC and elsewhere.

We used the above classification method to examine the variability of the cloud cover and its impact upon radiation budget at the top of the atmosphere. The cloud cover is found to be generally larger in convective regions as compared to subsidence regions, as shown in the third figure. In subsidence regions, there is a negative correlation between the SST and the following cloud variables: the shortwave cloud radiative forcing (derived from ERBE data), the cloud cover (derived from either ISCCP or TOVS data), and the cloud water path and cloud optical thickness (both derived from ISCCP data). In warm convective regions, the cloud cover and cloud radiative forcing appear to be less sensitive to the local SST, but much more sensitive to the variability of the large-scale circulation.

By examining the spatio-temporal variability of water vapor, clouds, and radiation for different large-scale circulation regimes, we have inferred the influences of SST and large-scale dynamics on the behavior of the Earth's radiation budget. This should motivate further process studies that must be devoted to the understanding of



Same as the previous figure but for the cloud fraction derived from ISCCP data (left panel) and TOVS data (right panel).

water vapor and cloud feedback, their interactions with large-scale circulation, and their validation in numerical climate models.

Contact: Sandrine Bony (Code 913)  
301-286-4910  
Internet: bony@lmd.ens.fr

William K.-M. Lau (Code 913)  
301-286-7208

Yogesh C. Sud (Code 913)  
301-286-7840

Sponsor: Office of Mission to Planet Earth

Dr. Bony is a visiting scientist with the Climate and Radiation Branch of GSFC. She is a visiting scientist from the Laboratoire de Meteorologie Dynamique (LMD) du CNRS in Paris, France.

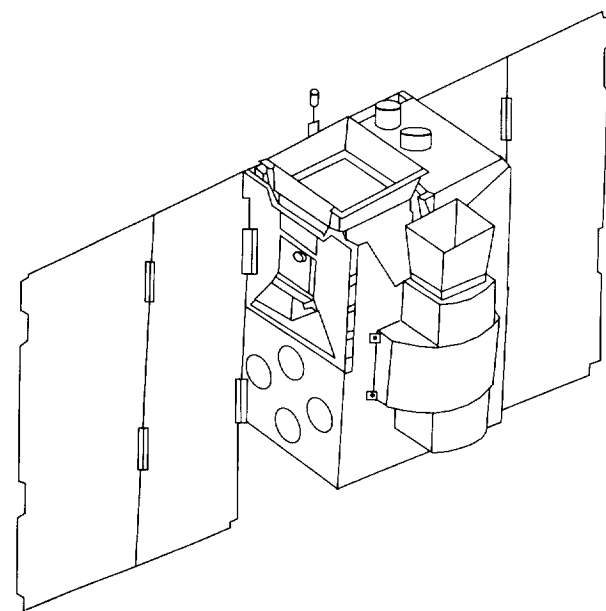
Dr. Lau is Head of the Climate and Radiation Branch. His research areas cover theoretical, observational, and modeling aspects of the climate system. He is also the Principal Investigator of the Earth Observing System/Global Hydrologic Processes and Climate Interdisciplinary Science Investigation. Dr. Lau received his Ph.D. in Atmospheric Sciences from the University of Washington.

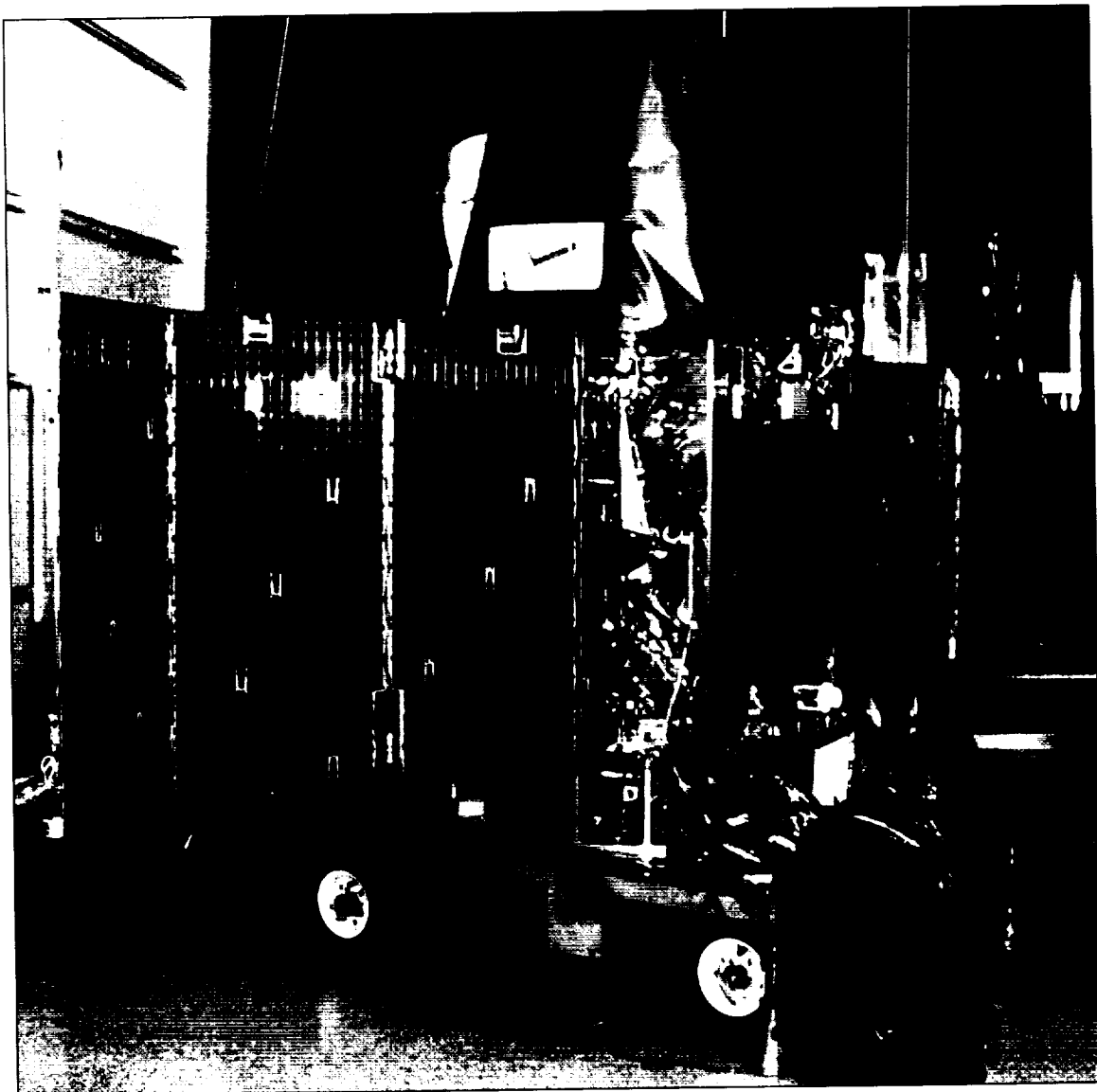
Dr. Sud has been a scientist at the Climate and Radiation Branch laboratory since 1980. Dr. Sud uses numerical models and satellite data to understand the influence of physical processes on the behavior of the climate system.

---

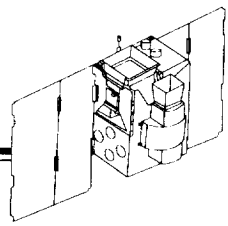
---

# ***ENGINEERING AND MATERIALS***





*The Submillimeter Wave Astronomy Satellite (SWAS) is a pathfinding mission that will study the chemical composition of interstellar galactic clouds to help determine the process of star formation. The SWAS spacecraft is a three-axis stabilized, stellar-pointed observatory with a pointing accuracy of 38 arcseconds and jitter less than 19 arcseconds. The spacecraft can point the science instrument at typically 3 to 5 targets per orbit. The SWAS instrument is a submillimeter wave telescope that incorporates dual heterodyne radiometers and an acousto-optical spectrometer which are used to investigate the composition of dense interstellar clouds. SWAS is the third mission in the Small Explorer program. SWAS has completed integration and testing at the Goddard Space Flight Center in Greenbelt, MD, and is now scheduled for a fall 1996 launch.*



# ENGINEERING AND MATERIALS

**I**N MANY WAYS, today's programmatic, scientific, and technological demands are similar to those that played a part in GSFC's early days. During GSFC's first decade, the Center was responsible for 112 scientific spacecraft—approximately one per month—yielding tremendous scientific and technological progress. GSFC's engineers and scientists thrived in that era of vision, great expectations, and hands-on involvement, despite significant constraints. These conditions fostered innovation in the Center's first decade; such a spirit of innovation will infuse our own efforts as we move into our next.

This section of the 1995 Research and Technology Report includes 11 articles that are representative of the wide range of activities conducted in GSFC's Engineering, Suborbital, and Operations Directorates, with the addition of several articles that derive from technology developments in other directorates across the Center. Although our primary focus is to support the science mission of the Center, carried out by the Center's Space and Earth Sciences Directorates, these activities also have significant impact on the growing community of space systems developers and users.

The first set of articles deals with improved spacecraft subsystems and components, and demonstrates the impact that the use of new technology and innovative design has on overall mission cost and performance. The use of high-performance solar cells, the development of innovative solutions to thermal control, and the incorporation of fiber optic busses and miniaturized high-performance spacecraft data systems will reduce the cost of both science and commercial spacecraft. Advances in optics technology will allow us to explore previously inaccessible portions of the electromagnetic spectrum.

Under Cryogenic Developments and Applications, a commercial application of cryogenic technology developed for improving the performance and duration of spaceborne science instruments is discussed. This technology, coupled with emerging high-temperature superconductor material technology, is being employed to facilitate the tremendous growth in cellular telephone communications. A second article discusses the application of cryogenic technology to scientific balloon flights to improve platform stability and mission duration.

A discussion of new tools and how we are using them includes a description of progress made over the last year in our new Detector Development Laboratory. This section also contains two articles which discuss new approaches to engineering information management to improve data access and dissemination. The last article in this section describes a new, innovative, and cost-effective way to detect lightning, which will help to reduce the cost and improve the quality of launch range support.

The final section describes technologies that directly support the science mission of the Center, with articles that describe the synergy that results from appropriate integration of commodity hardware to provide new data analytical capabilities, development of hardware and techniques to advance the growing field of x-ray astronomy, and the use of a new Shuttle-based laser altimeter.

These articles provide a sample of the many ways GSFC's engineering community is meeting today's challenges, while enabling a future of lower-cost, higher-performance space systems.

*Mitch Brown*

### SPACECRAFT SUBSYSTEMS

#### COST-EFFECTIVENESS OF ADVANCED SOLAR CELLS

OVER TIME, MANUFACTURERS of solar cells have introduced (and continue to introduce) solar cells with increased efficiency in converting sunlight to electricity. These cells are more expensive than typical cells by a factor of five. Surprisingly, GSFC has shown them to be extremely cost-effective for spacecraft that have rigid deployable solar arrays, because the new cells dramatically decrease the area and, hence, the mass of such arrays. Decreasing spacecraft subsystem mass allows more of this scarce resource to be allocated to science payloads. The cost of launch and basic spacecraft support, in relation to the mass of the science payload, is so high that increasing the science payload mass—while reducing the spacecraft mass—can be very cost-effective. The new arrays, while more expensive on the component level, reduce the overall cost to meet our scientific objectives. To quantify the potential savings, a study was performed for three types of solar cells: silicon, gallium arsenide, and multijunction.

Silicon cells, which have been used for many years, have test efficiencies on the order of 15 percent, and were used as the basis of comparison for the study. Manufacturers have offered gallium arsenide cells for several years now. These cells have test efficiencies on the order of 18 percent, and cost about five times what silicon cells cost. Manufacturers will soon offer multijunction solar cells for use on spacecraft.

They have already produced the cells in prototype quantities on production equipment. These cells will have test efficiencies on the order of 24 percent, and will ultimately cost about five times what silicon cells cost on the basis of power produced, although initially the cells may cost much more. In a typical low-Earth-orbit application, the efficiency of the newer cells is significantly greater than for silicon, but still lower than for test cases. The efficiencies of the silicon, gallium arsenide, and multijunction cells are 9.4 percent, 13.3 percent, and 18.0 percent, respectively; the multijunction cells are almost twice as efficient as the silicon cells.

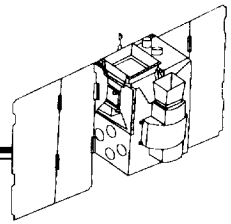
The study determined which of these cell types would have offered an overall performance and price advantage to the Tropical Rainfall Measuring Mission (TRMM) spacecraft. The study showed that the TRMM project, less the cost of the instrument, ground systems, and mission operations, would spend approximately \$552,000 per kg to launch and support science in the case of a spacecraft equipped with silicon solar cells. In the case of gallium arsenide solar cells, TRMM could carry an additional 31 kg of science at a price of approximately \$90,000 per kg. If the silicon solar cells are changed out for multijunction solar cells, at five times the cost per watt, TRMM could launch an additional 45 kg of science at a price of approximately \$58,000 per kg. A sensitivity analysis shows that even if the multijunction cells are priced at 10 times that of silicon cells, a price that is much higher than can be realistically projected, the additional 45 kg of science are launched and supported at \$182,000 per kg. This is still much less than original \$552,000 per kg to launch and support the science objectives.

Because the multijunction cells will likely be an outstanding value for spacecraft, GSFC will fly a solar cell experiment on the Lewis spacecraft. This experiment will verify the performance of the multijunction solar cells by measuring the operating temperature, current-voltage characteristics, and power output of these devices for a complete characterization of the product. If the multijunction cells are proven effective in this orbital test, GSFC will specify their use on spacecraft, thereby increasing the amount of science payload NASA can fly, and reducing the cost of flying it.

Contact: Edward Gaddy (Code 734.4)  
301-286-1338

Sponsor: Office of Space Access and Technology

*Dr. Gaddy is Head of the Energy Conversion and Analysis Section in the Space Power Applications Branch, which provides solar array engineering support to GSFC flight projects. He has over 25 years experience with spacecraft solar arrays. In 1994, NASA awarded Dr. Gaddy the Exceptional Engineering Achievement Medal.*



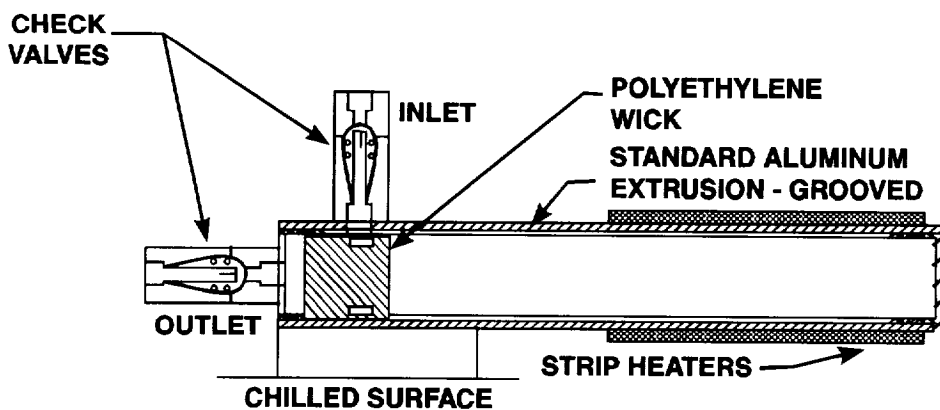
## DEVELOPMENT OF A HEAT-DRIVEN PULSE PUMP

THE REQUIREMENT for a long-lived, high-reliability pump is a serious weakness when dealing with one- or two-phase flow systems—such as those used for thermal control—in space. There are a number of mechanical pumps developed for use on Earth that have been modified for space applications, but these pumps have moving parts that eventually wear out or fail due to other mechanical problems; they also require heat-generating electronic control circuits. If a pump could be designed with no (or few) moving parts, capable of producing the pumping head for low flowrates needed for a variety of tasks, it could function over the long periods required by current spacecraft, without maintenance or replacement. The heat-driven pulse pump (HDPP) is one approach to meeting these requirements.

The basic concept for the HDPP is to use the fluid itself to create the pumping pressure. The pump consists of a grooved cylinder (whose size is dependent on the application), two check valves (one on the inlet and one on the outlet), a wick, and strip heaters (see the figure). The cylinder is initially filled with the liquid to be pumped. To begin pumping action, preset power is applied to the heater for a preset time interval (a pulse). As power is applied, the liquid heats up, vaporizes, and creates a pressure head exceeding the pressure drop in the system. This

pressure head forces the liquid in the cylinder out through the wick, past the outlet check valve; the inlet check valve closes due to the pressure difference. As the liquid in the cylinder is displaced, the liquid in the grooves is wicked towards the heater and sustains vaporization until the heater is turned off. The pump temperature must be slightly below the saturation temperature of the loop; this causes the vapor inside the pump to condense, drawing liquid through the inlet check valve, and forcing the outlet closed. As the liquid reaches the wick, the higher resistance of the wick forces the liquid to enter the grooves first and then spill over to fill the cylinder. After a specified time, the heater is again pulsed, and the process repeated, thus providing a pressure head for the fluid flow. Three pumps are used in parallel to provide continuous operation: while one pump is pulsed, the other two pumps are recovering.

A test loop was constructed that consisted of three HDPPs, a flowmeter, a reservoir, a tube-in-tube condenser, absolute and differential pressure transducers, a throttling valve, and tubing to interconnect the components. The transducers measured the absolute pressure in the loop and the pressure drop across the three pumps. The reservoir was used to set the system saturation pressure by heating and cooling the reservoir as required. The condenser was used to remove any parasitic heat acquired by



*The pump consists of a grooved cylinder (whose size is dependent on the application), two check valves (one on the inlet and one on the outlet), a wick, and strip heaters.*

## ENGINEERING AND MATERIALS

---

the fluid. Thermocouples were placed at strategic points around the loop to monitor the temperature changes. One of the three HDPPs was fabricated with a viewing port on the end so that the fluid level in the pump could be observed during testing. Power to the heaters was controlled by using an individual variable output transformer for each pump. The working fluid was anhydrous ammonia.

The loop was evacuated and then filled with a calculated amount of ammonia. Then, a temperature controller, connected to a heater on the reservoir, was used to set the loop saturation temperature and pressure. Heating the reservoir caused the ammonia to vaporize, increased the pressure, forced the liquid out, and hard-filled the loop. Finally, a chiller was used to set the pump cold-bias temperature. A series of tests was then performed to determine the operating characteristics of each pump, including power level, cooling temperature required for cold-biasing the pump, time needed to vaporize the fluid in the pump, and time needed to refill it. Once these parameters were determined, the three pumps were ready to begin their cycle. Power was applied to the first pump for a specific amount of time, then was turned off. Power to pump two was turned on when the ammonia in the first pump vaporized. This cycle was repeated for each pump. When the power was turned off to a heater, the vapor in the pump began to condense due to the pump cold-bias. The pump filled quickly, because the cold-bias created a lower pressure environment, and the cool liquid was forced into the vapor space by the fluid being displaced in the next pump in the cycle. This significantly reduced the pump recovery time.

Several power settings, timing sequences, and sink temperatures were investigated. The best combination for this preliminary stage of testing was to set the sink temperature to 15°C, and the system saturation pressure to 28 psia. The most constant flow rate was obtained by applying 50 W to pump 1, waiting for vaporization to occur, and then partially depleting the liquid in the pump. Once the pumping sequence was established on all three pumps, 50 W was pulsed sequentially to each pump for 30 sec, although a lower power setting may be capable of sustaining flow. The timing sequence never allowed any

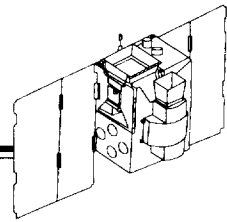
pump to fully flood before power was applied again. As a result, when power was reapplied, the pump very quickly expelled liquid. Under these conditions, we observed a flow rate averaging around 14 g/min. Due to the variation in flow, it appears that flow rate was proportional to power. During each power pulse, the pressure in the pump increased until it could overcome the 0.3 psid pressure drop caused by the spring force of the check valve. This caused a momentary increase in flow rate, followed by a more constant flow rate. The pattern is similar to that of a human heart beat. The temperatures of the pumps varied sinusoidally from about 29°C to 35°C. Although preliminary testing shows promise, there are still a number of parametric combinations that must be explored, operating conditions that must be tried, and changes in hardware that must be implemented before the HDPP concept can be tested in an actual operational situation.

Mr. Mario Martins (of Jackson & Tull) is co-investigator for the project and shares in equal measure with the GSFC Contact listed below. Ms. Donya Douglas of the Advanced Development and Flight Experiment Section was instrumental in developing the data acquisition software for testing. Testing during the summer was done by Susan Welsh (GSFC Summer Academy) and Craig Farnham (UMBC Research Fellows Program). Alex Brown (GSFC summer high school program) also contributed to this project. The project was funded under the 1995 GSFC Director's Discretionary Fund.

Contact: Steve Benner (Code 724.2)  
301-286-4364  
Internet: steve.m.benner.1@gsfc.nasa.gov

Sponsor: Office of Mission to Planet Earth  
Office of Space Science  
GSFC Director's Discretionary Fund

*Dr. Benner is an aerospace engineer and has worked with the Thermal Engineering Branch since joining GSFC in 1988. Dr. Benner received his Ph.D. in Chemical Engineering from Ohio State University in 1979. He is currently the experiment manager for the Return Flux Experiment due to fly aboard STS-72.*

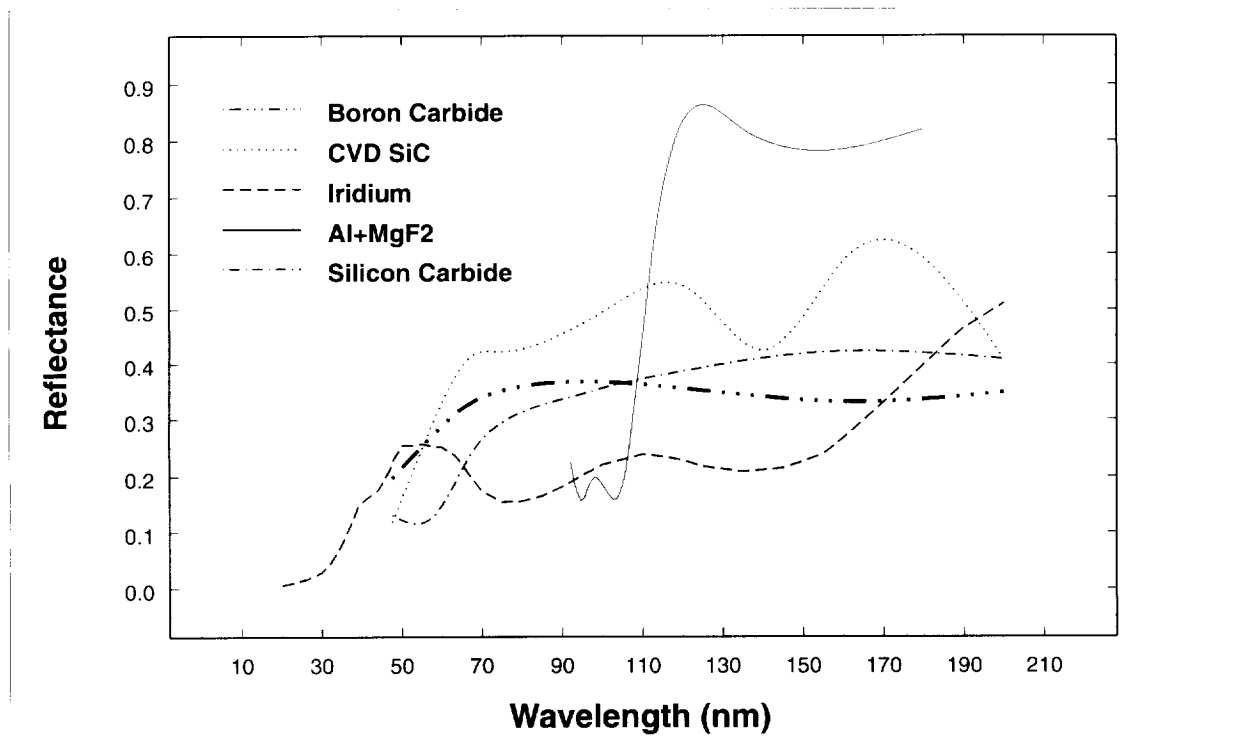


## BORON CARBIDE AS A HIGH-REFLECTANCE COATING FOR EXTREME ULTRAVIOLET OPTICS

ADVANCES IN ASTROPHYSICS often rely on the development of new instrument technologies that give astronomers better access to unexplored parts of the electromagnetic spectrum. Recent improvements in optical coating and materials technology have made possible the development of instruments with substantially enhanced efficiency in the extreme ultraviolet (EUV) spectral region. The development of high-reflectance coatings and materials extends the useful range of normal-incidence optical technology to EUV wavelengths (as shown in the figure). Historically, aluminum, coated with either magnesium fluoride or lithium fluoride, provides high-reflectance down to absorption cutoffs at 115 and 105 nm, respectively. In the EUV spectral region, below 105 nm, the normal-incidence reflectance of all conventional mirror coatings is low. This imposes severe constraints on space-based astronomy, since the alternative—glancing-incidence optics—is much more difficult and costly to fabricate.

In recent years, polished chemical-vapor-deposited (CVD) silicon carbide (SiC) has demonstrated a high normal-incidence reflectance (40 percent or greater) above 60 nm. However, the high temperatures associated with the CVD process ( $\sim 900^\circ\text{C}$ ) make it an unsuitable candidate for conventional mirror components and diffraction gratings. Silicon carbide thin-film coatings have also been developed to provide broader application of SiC to EUV instrument development. Research in the Optics Branch at GSFC on other carbide materials for normal-incidence reflective applications has led to the discovery that boron carbide ( $\text{B}_4\text{C}$ ) thin-film coatings have a high normal-incidence reflectance in the EUV, as well. Results indicate that  $\text{B}_4\text{C}$  is an attractive coating for normal-incidence EUV optical components, particularly for applications below 100 nm.

Thin film  $\text{B}_4\text{C}$  coatings have been produced by a relatively low-temperature ( $< 50^\circ\text{C}$ ) ion-beam-deposition



Reflectance of various UV coatings and materials.

## ENGINEERING AND MATERIALS

---

process. Initial studies were performed using a 3 cm diameter ion gun in a relatively small (0.5 m) deposition chamber.  $B_4C$  was sputtered with an argon ion beam incident on a sintered  $B_4C$  target. Normal-incidence reflectances of 38 percent at 92 nm, and as high as 28 percent at 54 nm, have been achieved for a newly deposited coating, substantially higher than that achieved with any conventional coating. We have initiated studies of ion beam deposited  $B_4C$  films in our 2 m facility, using a 16 cm diameter gun, which will enable us to uniformly deposit this material over a greater surface area and at higher beam energies. This facility was recently used to deposit a  $B_4C$  coating on a 30 cm diameter primary mirror for a University of Colorado sounding rocket experiment.

The improvements in normal-incidence EUV reflectance achieved through the development of  $B_4C$  coatings have been particularly important to the enhancement of diffraction grating efficiency in the 40 to 120 nm region. Although the films suffer some initial decrease in reflectance, they have generated interest in the science community for use in flight experiments. In support of various institutions in the scientific community, these coatings have been deposited on diffraction gratings and other optical components, resulting in enhanced instrument efficiency. Recently, we applied this coating on two diffraction gratings for the Ultraviolet Spectrograph Telescope for Astronomical Research instrument aboard the International Extreme Ultraviolet Hitchhiker, which flew on shuttle flight STS-69.

The resistance of  $B_4C$  to damage from atomic oxygen in low-Earth orbit is being investigated by flying several

samples on a shuttle-launched flight exposure experiment. The Surface Effects Sample Monitor, a German space exposure experiment flown on the CRISTA-SPAS mission on STS-66, carried several  $B_4C$  samples placed at various angles to the ram direction. This experiment will provide insight into the sensitivity of this new material to the space environment—information that will be valuable to astronomers selecting candidate materials for future flight programs. Preliminary data suggest that the reflectance of the  $B_4C$  samples flown on this mission did not suffer any additional degradation due to atomic oxygen exposure.

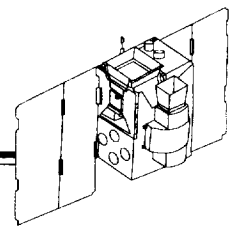
Contact: Gerry Blumenstock (Code 717)  
301-286-2416  
Internet: [gerry.blumenstock@gsfc.nasa.gov](mailto:gerry.blumenstock@gsfc.nasa.gov)

Ritva Keski-Kuha (Code 717)  
301-286-6706  
Internet: [ritva.keski-kuha@gsfc.nasa.gov](mailto:ritva.keski-kuha@gsfc.nasa.gov)

Sponsor: Office of Space Science

*Mr. Blumenstock is an electronics engineer in the Optical Research Section of the Optics Branch. He has been at GSFC for 4 years. He received both an M.S. and a B.S. in Physics from The University of Maryland at College Park. His research interests include thin-film coatings and EUV optics.*

*Dr. Keski-Kuha is Head of the Optical Research Section in the Optics Branch. She earned a Ph.D. in Physics from St. Louis University and has been at GSFC for 13 years. Her research interests are in optical coatings and X-ray and EUV optics.*



## SPACEFLIGHT FIBER OPTICS IN THE X-RAY TIMING EXPLORER SPACECRAFT

THE GSFC X-RAY Timing Explorer (XTE) is a scientific observatory whose mission is to study the structure of compact X-ray sources. XTE is designed with three distinct, dedicated, fiber optic buses for communications. A fiber optic data bus network is a distributed, multimode interconnect system consisting of a star coupler and fiber optic cabling. The network provides the optical transmission path for 850 nm optical transmitter and receiver assemblies, which are configured to meet MIL-STD-1773 communications protocol and requirements, including redundancy. The fiber optic data bus network is referred to as the network, 1773 bus, or the bus. A complete 1773 optical system consists of optical transmitters, optical receivers, multimode cable assemblies terminated with either contacting or noncontacting fiber optic connectors, and a star coupler.

The three buses used in XTE are the spacecraft component, instrument, and attitude control subsystem. In contrast to single bus designs, the use of several smaller, dedicated buses offer the benefits of lower optical losses, reduced message traffic, and utilization flexibility. Each of the three buses is redundant, which means that there is an identical back-up star coupler (to prevent a single-point failure) with fiber optic cabling. Since MIL-STD-1773 includes redundancy in a basic network and there are two identical networks for each of the three buses, the system is sometimes considered dual redundant. The most important element of the 1773 bus is the 16 x 16 fused biconical taper star coupler manufactured by CANSTAR. It is the optical device that distributes bus communications to every user in a network.

Only standardized optical transmitters and receivers with identical fiber optic connector interfaces are used on the spacecraft. Every component that interfaces with the bus is required to use a Honeywell HFT-4811-014 transmitter and Honeywell HFR-3801-002 receiver. The Honeywell parts have FSMA 905 fiber optic interface connectors.

The multimode cable assemblies were fabricated by GSFC using a Brand Rex cable with radiation-hard Corning fiber. The cables use 100/140  $\mu\text{m}$ , graded index fiber. They are terminated with contacting MIL-T-29504/4 (pin) or MIL-T-29504/5 (socket) fiber optic termini from Amphenol or noncontacting FSMA 905 fiber optic connectors from AMP, Inc. FSMA connectors are referred to as *noncontacting* because the connector ferrule never

comes in contact with or touches another optical assembly. In contrast, the 29504 termini are referred to as *contacting* because the pin/socket ferrules always contact each other via a controlled spring force. During cable assembly fabrication, the FSMA connectors receive a flat polish while 29504 termini receive a convex or physical contact polish. The MIL-T-29504 termini are used on cable ends that interface with the star coupler. MIL-T-29504 termini are installed in a low outgassing connector from Amphenol to form a complete multicable fiber optic connector. The low outgassing connectors, suffix 453, are equivalent to MIL-C-38999 series III connectors. The FSMA 905 (MIL-C-83522/2-04) connectors are used on cable ends which interface directly with the transmitters and receivers. Hereinafter, these connectors and termini will be called *FSMA, multicable 38999 or 29504*.

XTE is the first GSFC spacecraft to use multicable 38999 fiber optic connectors in a spaceflight application. Previously, up to 32 FSMA connectors were individually mated and torqued when a single star coupler was integrated, and the FSMA optical power losses were always  $> 0.5 \text{ dB}$  (typically 0.7 dB to 0.9 dB). The multicable 38999 connector provides an efficient means of mating up to 16 fiber optic cables simultaneously and reduces the optical power loss to  $< 0.5 \text{ dB}$  (typically 0.2 dB) when physical contact polishing techniques are used. The reduction in connector losses by use of physical contact polishing is important because the system optical power margin increases as connection losses are reduced.

The integration and test of the fiber optic system is key to its success. The integration and test process consists of three major steps: component transmitter and receiver optical performance verification, bus verification, and system-level optical performance verification.

The first step is performed by measuring receiver sensitivity and transmitter output power. These acceptance level tests verify that all spacecraft optical interfaces meet the specific requirements with a 100/140  $\mu\text{m}$  fiber (i.e., optical power output  $> -9.4 \text{ dBm}$  and a receiver sensitivity threshold of  $< -30.0 \text{ dBm}$ ).

The second step is performed by measuring the insertion loss of the integrated fiber optic cabling and star coupler prior to FSMA/component integration. This acceptance level test verifies optical power loss of the bus. It is

## ENGINEERING AND MATERIALS

---

critical that this test be passed, as it ensures that all connectors are properly mated, that cables are not broken during installation, and that the optical links have a loss value within specified limits.

The third step is performed by determining the optical power margin in the completely integrated flight optical system via a test connector. The test connector, located on the spacecraft skin, contains one transmitter and receiver link from each star coupler. The test is similar to the component power output and receiver sensitivity threshold tests, except that the performance of all components is verified from the test connector using an external bus controller. The bus controller interrogates each component individually via its remote terminal address. The test is performed without breaking any flight interfaces and is repeated upon completion of spacecraft environmental testing.

An additional verification test, using an Optical Time Domain Reflectometer (OTDR), was performed on the 1773 buses because of unacceptably high multicable 38999 connector losses that were discovered during initial bus verification testing.

The OTDR test was made possible because the star coupler uses an innovative design feature implemented by GSFC. Internal fiber lengths from the fused star to the interface connector vary for each port. They differ in length by a fixed amount, ~13 cm. When a 16 x 16 star coupler with "staggered leads" is tested with an OTDR, the OTDR display will show a series of 16 pulses corresponding to Fresnel reflections from each of the termini/connector interfaces. Without "staggered leads," an OTDR display would show a single, wide pulse because all the Fresnel reflections from each of the termini/connectors are superimposed.

The OTDR test results showed that inadvertent contamination of the 29504 termini endfaces or overly tight alignment sleeves caused large reflections, with subsequent high connector losses. High losses due to tight alignment sleeves occurred because excessive friction prevented contact of the 29504 ferrules, which, in turn, created a large air gap in the optical path and attenuation.

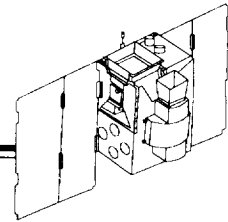
The OTDR test has proven invaluable, as it readily determines the quality of the star coupler connections and

can surface problems such as contamination and small air gaps due to tight alignment sleeves. Small air gaps can result in slight, but needless, optical losses (~0.3 dB) which may not be detected by optical power tests. The test is recommended as part of the standard verification process. As a result of the OTDR test and GSFC findings, the 29504 manufacturer has implemented improved screening tests of the alignment sleeves.

Typical handling procedures used for electrical connectors do not apply to fiber optic connectors, as contamination can be a problem. Significant amounts of contamination can increase optical connector losses by more than 4.0 dB and cause cracking, pitting, or scratching of the glass fiber. Fiber optic connectors do not, however, have to be perfectly clean or flawless to function properly. The cardinal rule at GSFC is to visually inspect a fiber optic connector for contamination (at ~100X magnification) and clean it, if necessary, before mating. Integration of a fiber optic network does not require a spaceflight hardware clean room environment.

Fiber optic integration procedures consisted of receiver sensitivity, transmitter power output, and optical bus power loss measurements. In contrast, electrical integration procedures consist of resistance, open circuit voltage, stray voltage, waveform, milli-ohm continuity, and 500 V insulation resistance measurements. In the final analysis, fiber optic procedures proved to be less complex and shorter in length than electrical procedures because fewer tests are required and fewer (typically four) interfaces require verification. Test time was decreased as a result of the shorter, simpler fiber optic procedures, and the reduced number of interfaces requiring testing. Time savings related to decreased testing had a beneficial effect on the schedule and reduced overall test costs.

Interface standardization via the use of fiber optics has resulted in significant time savings to the project. Procedure development time is reduced as a result of standardization because one integration procedure is applicable to many components. This advantage cannot be overemphasized. In addition, the document review cycle time is reduced, and changes are easier to process as only one document is affected. Moreover, the fiber optic procedures developed for XTE can be used on other projects with little modification. Finally, wasted time associated with the "learning curve" when a test is run for the first time is



eliminated by standardized fiber optic tests, in contrast to nonstandardized electrical tests requiring numerous learning curves.

In summary, when used for spacecraft applications such as the XTE, fiber optics

- reduce spacecraft integration and test time and costs;
- standardize hardware and software interfaces;
- simplify and standardize tests and procedures;
- reduce integration and test procedure development time;
- reduce harness weight, as compared to copper equivalents;
- eliminate system level harness electromagnetic interference problems; and
- increase data rate capabilities, as compared to copper equivalents.

There are also some disadvantages to using fiber optics for spacecraft applications, specifically

- connectors are vulnerable to contamination or damage due to mishandling.
- the technology is new to avionics and space applications, which means that

- personnel training is required;
- there is a limited number of mature procedures available;
- there is a limited number of flight-qualified fiber optic components; and
- there is a limited amount of test and support equipment available.

XTE demonstrated that fiber optics will play a key role in future spacecraft design by reducing integration and test time and cost. Furthermore, fiber optics is the natural solution to meeting the ever-increasing demand for higher-data-rate systems in applications such as solid-state recorders, video and imaging devices, and sophisticated new spacecraft.

Contact: John Kolasinski (Code 733.1)  
301-286-6109

Sponsor: Office of Space Science  
Office of Mission to Planet Earth

*Mr. Kolasinski is the Electrical Subsystem Manager for the XTE mission. Mr. Kolasinski earned a B.S. in Electrical Engineering from the University of Maryland. He has been at GSFC for 6 years, where he works in the Electrical Systems Integration Branch and is responsible for the development of fiber optics in spaceflight applications.*

## CRYOGENIC DEVELOPMENTS AND APPLICATIONS

## LOW-COST CRYOCOOLERS FOR HIGH-TEMPERATURE SUPERCONDUCTOR FILTERS

**H**IGH-TEMPERATURE superconductor (HTS) materials have proven useful for ultraselective radio-frequency filters. Interest in these filters in both commercial and government applications has spurred a GSFC-supported program at Superconductor Technologies Inc. (STI), in which the company develops HTS materials, filters, and cooling systems.

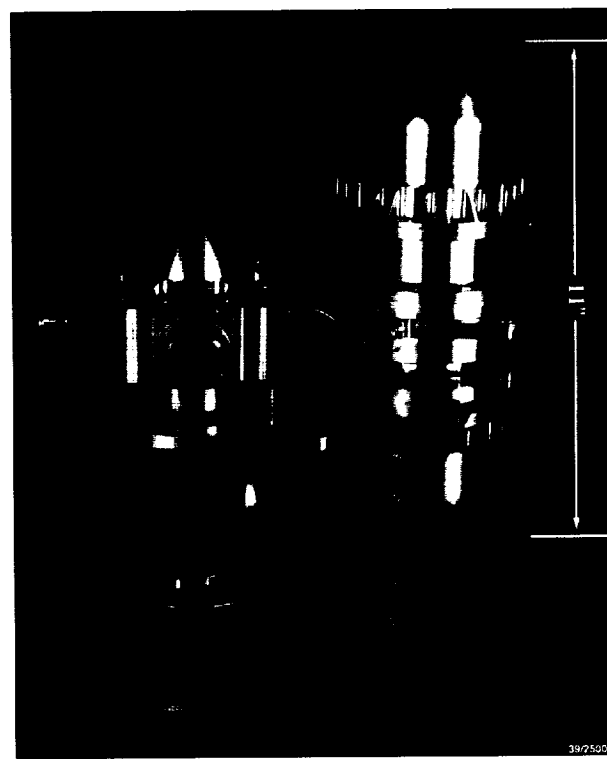
One specific problem addressed by this technology involves the separation of desired and undesired signals in cellular base-station receivers. With the increased numbers of cellular callers in recent years, base stations must be equipped with high-performance filters. Specifically, competing communications systems (i.e., cellular, personal communications systems satellite communications, and point-to-point microwave systems) interfere with each other whenever an undesired high-power signal is radiated near a sensitive base-station receiver. This high-power signal generates distortion in the receiver, which can block or distort reception of the desired lower-power signals.

The new filters under development employ thin-film HTS lumped-circuit elements, which are packaged in a vacuum dewar for heat insulation. The filter is currently cooled by a low-cost linear Stirling cooler under development at STI. The cooler is designed for 4 W lift at 77 K with 100 W of electrical input power. The key to the commercial success of this technology is the cost and reliability of the cooler. The mean time to failure (MTTF) must exceed 40,000 hr. Because traditional Stirling coolers have MTTF levels of less than 10,000 hr, cooler development is a major focus for the program.

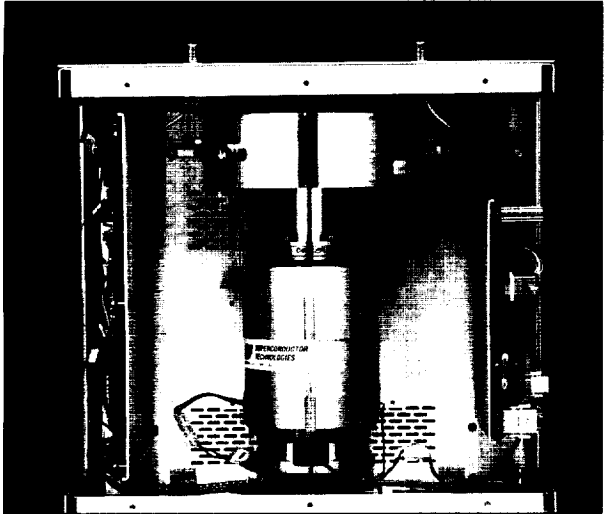
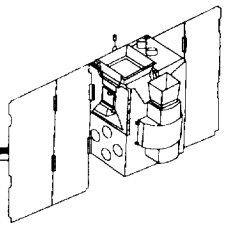
STI has addressed the cooler need by first developing a prototype linear Stirling cooler with an in-line free-moving piston and a passive displacer. Gas bearings are employed to center the piston and to eliminate wear of the moving parts. The cooler uses a moving magnet linear motor, with the magnet on the piston.

In the second phase of cooler development, under a NASA cooperative program, Lockheed Martin, the National Institute of Standards and Technology (NIST), and GSFC

are collaborating with STI to replace the presently utilized Stirling cooler technology with the pulse tube system. This will further increase the reliability and reduce the cost by eliminating the displacer, which is one of the few moving parts. (A pulse tube cooler replaces the displacer with a hollow tube, in which a pressure wave is created whose phase is shifted with respect to the piston by carefully designed orifices.) Two low-cost commercial approaches for the compressor that drives the pulse tube are being developed under this NASA cooperative contract. The first is the current STI approach, used in their Stirling cycle machine and employing gas bearings (as shown in the first figure); the second approach uses a compressor with flexure bearings (as shown in the second figure), being developed at the Lockheed Martin Research Laboratory.



Low-cost cooler with flexure bearing.



*Low-cost cooler with gas bearing.*

The flexure bearing approach is a proven technique that maintains nonwearing clearance gaps for the moving piston by flexures, rather than the gas-bearing approach used by STI. It is being developed with emphasis on low production costs. Both compressors will be tested with the pulse tube. NIST, with preeminent experience in pulse tube systems, is leading the development of the pulse tube; GSFC, with broad knowledge and expertise in cryocooler technologies, is providing consultation on the complete system.

Through 1995, several key milestones have been reached:

- two proof-of-concept Stirling coolers passed 12,000 hr each on a continuous life test;
- a revised prototype Stirling cooler was constructed with 4 W cooling and reliability enhancements;

- the first cellular receiver filter assembly was demonstrated; and
- a prototype gas-bearing compressor was put under test.

In 1996, the project should attain the following milestones:

- enter pilot production of refined Stirling cooler design and verify cooler reliability;
- qualify first cellular system for field use; begin production; and
- qualify first pulse-tube cooler for system integration and phase into production.

Collaborators on this project include T. Nast (Lockheed Martin), V. Loung (STI), and R. Radebaugh (NIST).

Contact: Stephen Castles (Code 713)  
301-286-5405

Sponsor: Office of Space Access and Technology

*Dr. Castles is Head of the Cryogenics, Propulsion, and Fluid Systems Branch at GSFC. He received his Ph.D. in Physics from the University of Florida and joined GSFC in 1978. He has participated in the development of the cryogenic systems for several flight programs. His areas of technical interest encompass closed cycle coolers, adiabatic demagnetization refrigerators, space-based helium dewars, superconductor-based detectors, and SQUID-based technologies.*

## **CRYOGENIC GAS REPLENISHMENT SYSTEM FOR LONG-DURATION BALLOONS**

**N**ASA USES LARGE helium-filled scientific balloons to conduct important research in the middle and upper stratosphere. These balloons can carry over 3000 kg of scientific experiments to altitudes of 40 km. The performance goal of a scientific balloon is to lift as much payload as possible as high as possible for as long as possible. Solar and environmental heating and cooling of the balloon gas causes changes in the balloon volume, with subsequent gains and losses in altitude; day-to-night altitude excursions of 10 km or more are not unusual. These altitude excursions are not normally desirable from a scientific standpoint, so the Balloon Program at GSFC has a continuing project to improve this aspect of balloon performance. Traditionally, balloons have used released ballast, in the form of steel or glass shot, to compensate for the vehicle's loss of buoyancy during the night. This approach, however, has two major disadvantages. First, the ballast-to-lift ratio is only 1:1 (i.e., for each kilogram of ballast dropped, the balloon gains one kilogram's worth of lift). Second, during a flight, ballast is not a renewable resource. Therefore, long-duration flights must carry prohibitive amounts of ballast to maintain working altitudes.

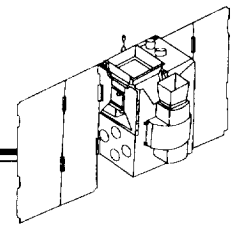
Raven Industries, under NASA contract, performed a study to determine the feasibility of using cryogenic helium to augment the balloon's lift during flight. Since 6.23 kg of lift are provided for each kilogram of cryogen evaporated, this concept overcomes the first disadvantage of traditional ballast. The cryogenic system does not avoid the second disadvantage of ballast but even with its higher tare weight, a cryogenic replenishment system shows significant advantages. Although not a new concept, employment of some new technology and several innovative features have resulted in a system concept with high potential for use on long-duration flights.

The system consists of a dewar filled with liquid helium, a heat exchanger to turn the liquid to gas, valves and miscellaneous piping, and the ducting to carry gaseous helium to the balloon. The dewar is a standard aluminum design, which will survive the 10 g terminate loads and have a loss rate of less than 3 percent per day. Since the operational helium extraction rate will greatly exceed the normal vent rate, the weight and complexity of an inner shield for vent gas recycling is saved.

Many of the innovative features of the system are related to the design of the heat exchanger. The balloon

environment and system operating requirements combine to create a challenging design problem. From a heat collection and dissipation standpoint, the balloon environment is essentially identical to the space environment. The low atmospheric pressures (300 to 500 Pa) rule out the use of convection unless a very large surface area is available. With radiation as the dominant heat transfer mode, heat exchanges with the Earth, space, and the Sun are the only alternatives. Additionally, the balloon-operating profile requires that the cryogenic system replenish lost balloon gas during the early evening and night. Since the balloon is operating at or near maximum volume and pressure during the daytime, any gas injected during the day will be almost immediately vented as excess. Thus, the heat exchanger must collect solar energy during the day, store that energy until evening, efficiently transfer that heat to the cryogenic helium when required, and not lose its stored energy to the surrounding environment in the interim. All these operational design criteria had to be achieved while still minimizing weight and maintaining balloons as low-cost, low-complexity scientific platforms. The heat exchanger design described here accomplishes all these goals.

The heat exchanger/storage unit consists of an annular aluminum ring attached with fiberglass standoffs to the outer wall of the dewar. The ring is completely filled with 8 percent density, 10 pore/in aluminum foam. It is insulated on three sides with glass foam insulation and left bare on the outer vertical surface. This outer side is painted flat black to enhance heating of the aluminum mass during the day. The heat exchanger is warmed by the Sun during the day, and will reach a temperature of 353 K after 6 hrs of exposure. When gas replenishment is desired, either in response to a manual command or from an automatic system, liquid helium is fed into one side of the aluminum foam. The evaporated gas emerges from the diametrically opposite side of the thermal mass with a minimum exit temperature of 188 K. The gas is then ducted into the balloon to provide the required lift. In terms of standard ballast amounts, the system can be sized to provide ballast flow rates of up to 0.34 kg/sec with a total daily limit of 200 kg. These statistics are comparable to current operating practices. This design has the advantages of very fast heat transfer from the aluminum to the helium (especially at high altitudes), and the simple plumbing and absence of moving parts that help keep reliability very high.



Significant performance analysis of the proposed cryogenic system and a traditional (hard-ballast) system was performed to provide a comparison and break-even analysis. Conventional, or zero-pressure, scientific balloons are open to the atmosphere at the bottom, similar to common hot-air balloons. Recent research and development efforts have resulted in an operational balloon system which is a slightly pressurized version of the conventional balloons. Both these types of balloons had to be considered during the study, making a common comparison difficult. A common basis was developed by first simulating a zero-pressure balloon's diurnal cycle, while dropping 7 percent of the system mass in ballast. This operational rule-of-thumb represents an amount which will eliminate almost all altitude excursions under nominal conditions. Simulations of the pressurized systems were then conducted, with each system dropping an amount of ballast that would result in the same altitude excursion as that of the zero-pressure system. Finally, each of these cases was simulated using a cryogenic system that would provide the same ballasting characteristics as the hard-ballast system it replaced. The figure shows the essence of the simulation results. Based solely on weight criteria, the break-even point between hard-ballast systems and

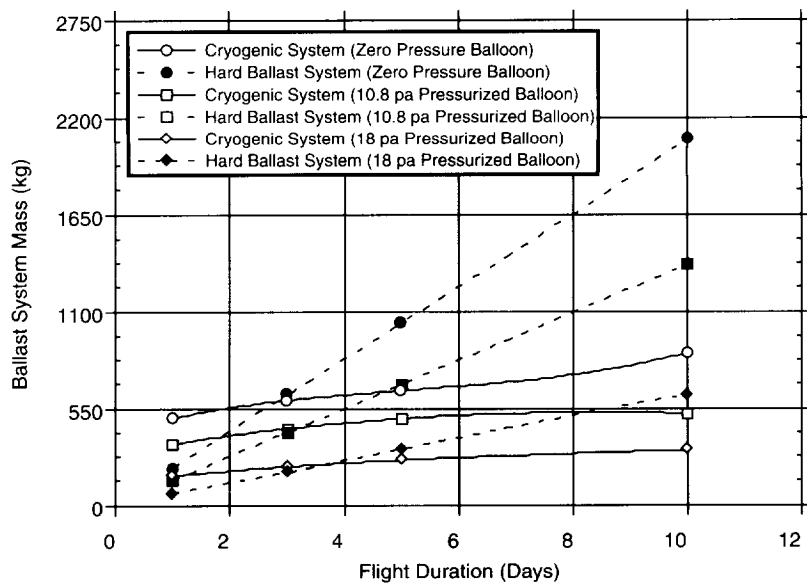
cryogenic systems comes at flight durations of about 3 days. Additionally, the figure shows how quickly the hard-ballast system consumes the entire nominal payload of 1400 kg for this balloon.

With innovative heat exchanger design and balloon-specific hardware considerations, cryogenic helium replenishment shows significant promise for scientific ballooning. With improved altitude stability at a smaller weight penalty, helium balloons will remain a viable scientific platform for some time to come.

Contact: Steven Raqué (Code 842)  
804-824-1675

Sponsor: Office of Space Science

*Mr. Raqué is an aerospace engineer in the Balloon Projects Branch. He earned a degree in aerospace engineering from Virginia Polytechnic Institute and State University and has been at GSFC for 7 years. He was recently one of the recipients of a NASA Group Achievement Award for Long Duration Balloon Vehicle Development.*



Comparison of cryogenic and hard ballast system masses for both zero pressure and pressurized polyethylene balloons.

## NEW TOOLS AND CAPABILITIES

## THE DETECTOR DEVELOPMENT LABORATORY

**G**SFC'S DETECTOR DEVELOPMENT Laboratory (DDL) began operation this year. The DDL is a microelectronics fabrication facility dedicated to the development of advanced detectors for NASA missions. The laboratory is built around a 4400 sq ft clean room, housing an extensive array of semiconductor processing equipment. The facility is capable of designing, fabricating, and testing a wide range of detectors that span the spectrum from high-energy cosmic rays to the far-infrared and submillimeter wavelengths. The projects undertaken by the DDL are varied; several of them are described here.

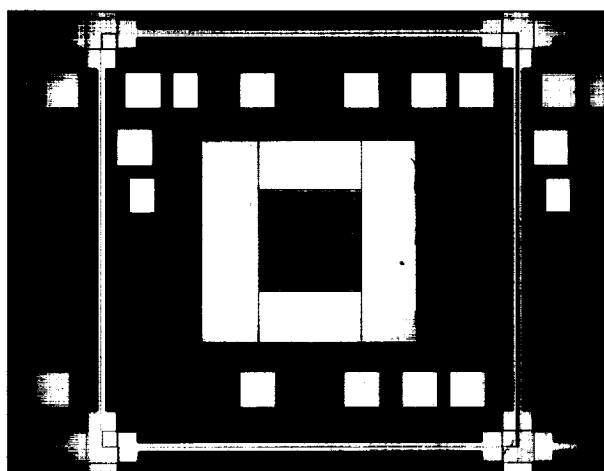
***Ultrathin Bolometer Array***

Advances have been made in bulk silicon micromachining with the development of a new far-infrared detector, known as the ultrathin bolometer array. The ultrathin bolometer (as shown in the first figure), a 1 $\mu$ m thick detector, represents the thinnest, free-standing, micromachined, monolithic silicon bolometer yet fabricated. By enhancing some of the micromachining processes developed for earlier silicon X-ray microcalorimeters and infrared bolometers, and using new processes developed in the DDL, we were able to produce prototype devices. Because of very specific etching patterns in certain chemicals, silicon can be chemically "micromachined" into many desired shapes and three-dimensional structures. Micromachining these devices employs a combination of anisotropic chemical etching and reactive ion etching to produce free-standing, micro-air-bridges of single-crystal silicon, surrounded by

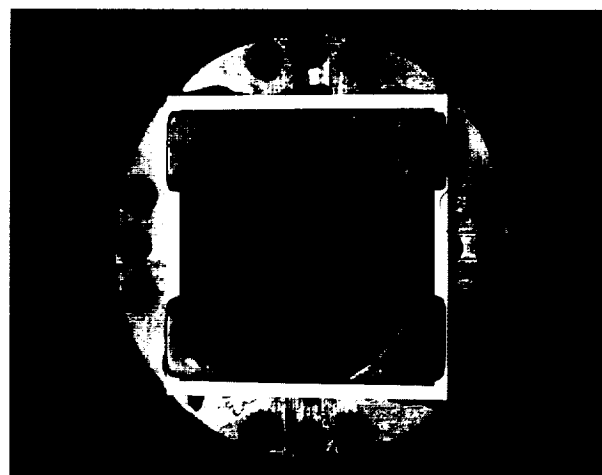
openings that pass completely through the silicon wafer. The prototype bolometer arrays are 1 mm square detectors, suspended on four 500  $\mu$ m long legs ranging from 6 to 20  $\mu$ m in width, and are a mere 1  $\mu$ m thick. Single-crystal silicon, which is the starting material for these detectors, becomes transparent in the visible spectrum at this extreme thinness, so these detectors are "see-through" when viewed under an optical microscope.

***Frequency-Sensitive Bolometer Resonance Mesh***

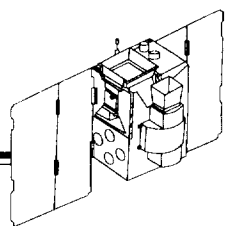
A singular application for bulk silicon micromachining has been to produce resonance meshes for the proposed frequency-sensitive bolometer. The resonance meshes are designed to act as low-loss capacitive filters, tuned to resonantly reflect in-band radiation back toward another mesh containing a resistive bolometer. The resonance mesh (as shown in the second figure) is unique for its large overall area and open, web-like design. The air-bridges that make up the resonance meshes are silicon beams 10  $\mu$ m wide by 10  $\mu$ m thick, forming a 1 cm, open-square grid with a grid spacing of 1 mm. These gossamer webs are suspended on a frame of silicon 300  $\mu$ m thick, the starting thickness of a silicon wafer. Such meshes are also unique because they are the first micromachined devices to contain patterned metal features located on the air-bridge. These thermally evaporated gold features are suspended on an open-square grid made of micromachined silicon; the gold resonance features are located at each grid intersection point. The



*Ultra-thin bolometer array.*



*Frequency-sensitive bolometer resonant mesh.*

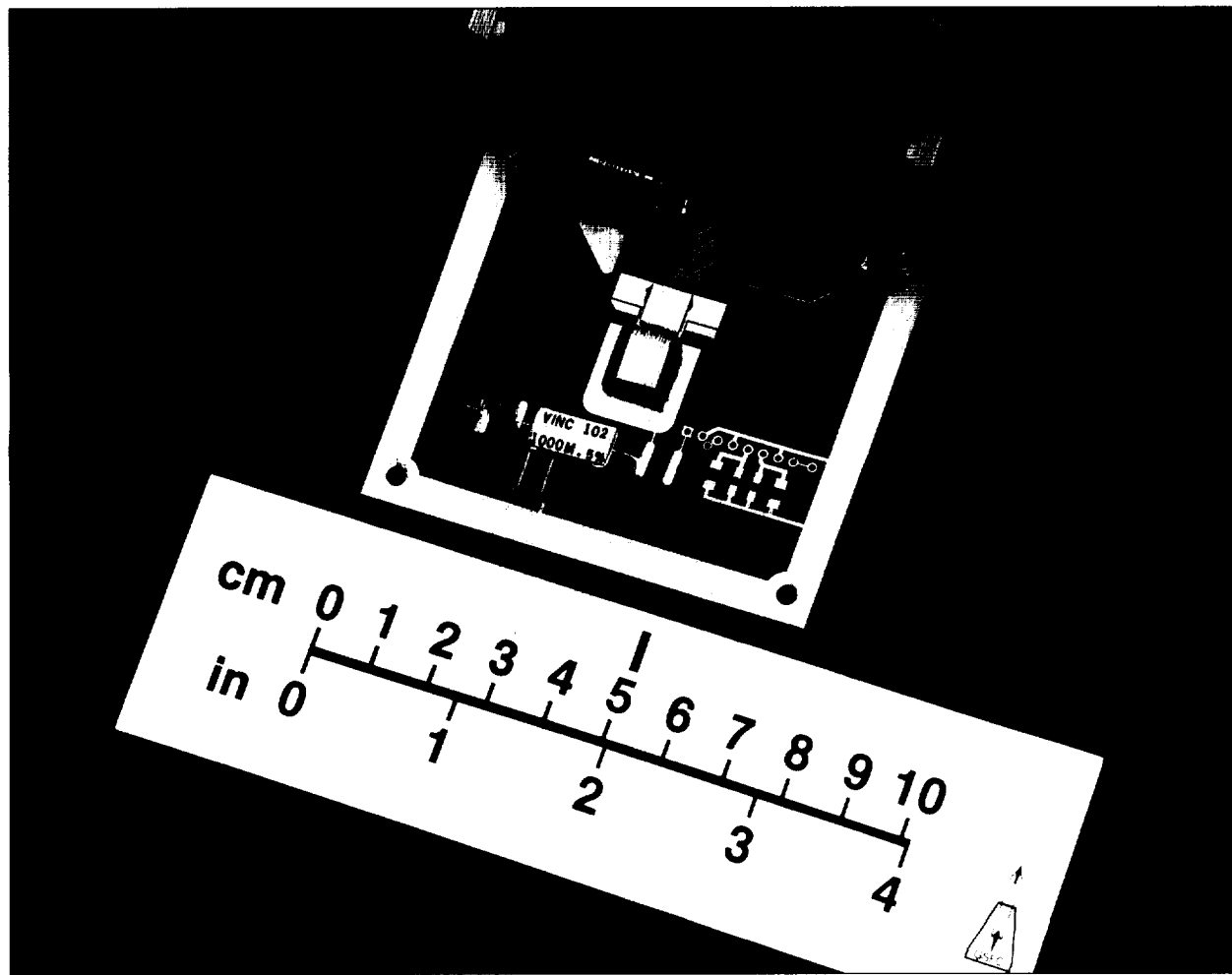


fabrication of the resonance meshes employs silicon micromachining techniques identical to those used to produce the ultrathin bolometer array; however, the tenfold increase in final device thickness allows us to increase the device's area to the required 1 cm<sup>2</sup>. The concept realized during the development of the resonance mesh will be expanded to include an ion-implanted resistive thermometer, located on the grid, which will act as the sensing element of the frequency-sensitive bolometer.

### ***CdZnTe Detectors***

A CdZnTe detector array is being developed for the proposed gamma-ray Burst ArcSecond Imaging and Spectroscopy spaceflight mission, to accurately locate

gamma-ray bursts, determine their distance scale, and measure the physical characteristics of the emission region, as discussed elsewhere in this volume. We have fabricated the finest-pitch strip detector on CdZnTe to date (as shown in the third figure). Two-dimensional strip detectors with 100  $\mu$ m pitch have been fabricated and wire-bonded to readout electronics to demonstrate the ability of the strip detector to localize low-energy gamma-rays to less than 100  $\mu$ m. We have obtained the first radiation damage results on CdZnTe. A CdZnTe detector exposed to MeV neutrons showed a small amount of activation but no detector performance degradation for fluences up to  $10^{10}$  neutrons/cm<sup>2</sup>. A CdZnTe detector has also been flown on a balloon payload for the first time to measure intrinsic CdZnTe background rates.



*CdZnTe detectors.*

### ***Solar Blind Ultraviolet Detectors***

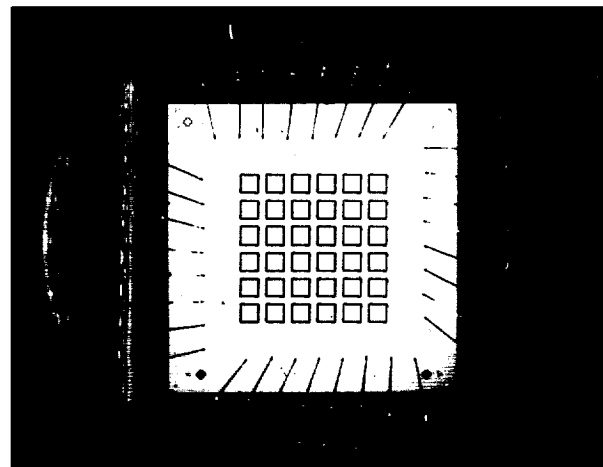
The wide bandgap (3.5 eV) of gallium nitride (GaN) allows efficient detection of ultraviolet (UV) radiation, with insignificant response to visible- and longer-wavelength radiation. Photons with energy above the bandgap are absorbed and detected, while photons with energies less than the bandgap pass through the detector. This allows instruments utilizing GaN UV detector arrays to operate in an environment with significant visible radiation without expensive visible blocking filters and extensive stray light baffling. The GaN arrays can achieve order-of-magnitude savings in weight, volume, and power, compared to the photomultiplier tubes and microchannel plates currently in use. GaN detectors have been fabricated and tested that achieve greater sensitivity in the UV than any GaN detector reported by other investigators, while showing unmeasurably small response to visible radiation.

### ***Low-Noise Cryogenic Transistors***

In collaboration with Stanford University, we have designed, fabricated, tested, and screened low-noise cryogenic junction field-effect transistors (JFETs) for the Gravity Probe-B Project. The JFETs will be integrated by Stanford into their sensor assembly. We have delivered sample JFETs and two hybrid detector modules for evaluation. The JFETs are custom-designed and processed for ultra-low-noise performance at low temperatures (77 K), and exhibit the lowest noise performance of any field-effect transistor tested by Stanford.

### ***X-Ray Microcalorimeter Arrays***

Microcalorimeters determine the energy of an X-ray by measuring the temperature rise in a thermally isolated mass when an X-ray is absorbed. This allows fast, high-resolution X-ray spectrometers to be built without the loss in efficiency found with dispersive elements. Previous X-ray microcalorimeter arrays have been either one-dimensional linear arrays or two-dimensional arrays made by interleaving two linear arrays. We have designed and fabricated 36-element silicon X-ray microcalorimeters in a 6 x 6 array (as shown in the fourth figure), in support of the X-ray Spectrometer (XRS) instrument. This architecture allows more efficient use of the X-ray image produced by the instrument's telescope than single or double linear arrays.



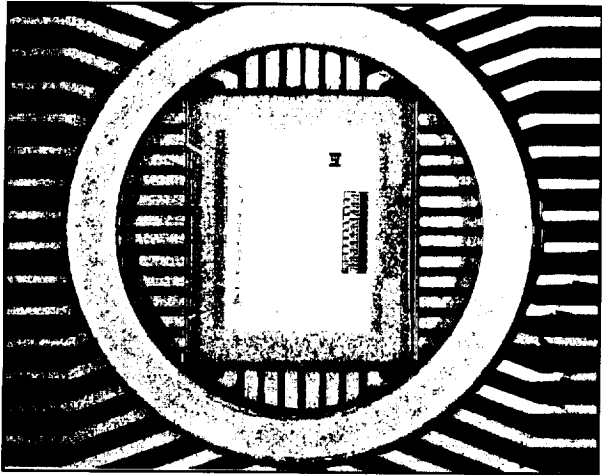
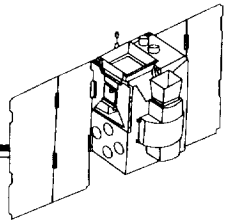
*X-ray microcalorimeter arrays.*

### ***Anticoincidence Silicon Detectors***

Anticoincidence silicon (Si) detectors have been successfully fabricated and tested for use in the XRS instrument. Anticoincidence detectors are used to tag unwanted cosmic ray events so they can be removed from data obtained by the instrument's calorimeter array. The detectors have been integrated with the calorimeters in a breadboard model, and test results have demonstrated that the concept of using a solid-state Si detector in the backplane of the calorimeters for the anticoincident detector is an elegant solution. Si detectors have been fabricated to areas of  $0.5 \text{ cm}^2$ , and in thicknesses from 50 to 300 mm. In the near future, these detectors will be fabricated to  $1 \text{ cm}^2$  area, and 500 mm thick. We have developed a simple fabrication process that enables the detectors to be made quickly.

### ***Infrared Arrays for Cassini***

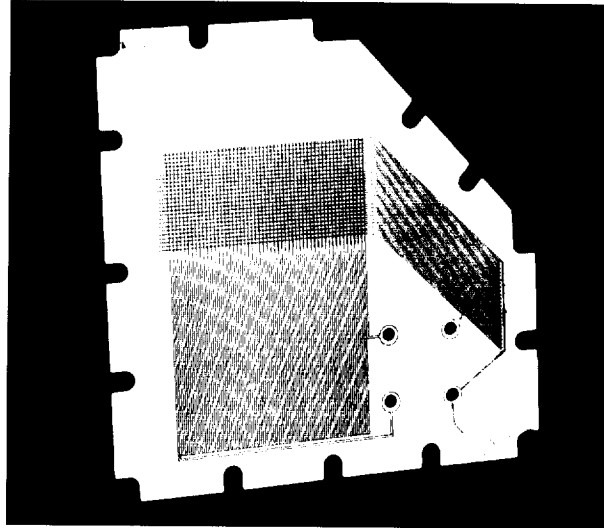
Long-wavelength mercury-cadmium-telluride (MCT) infrared arrays have been delivered for integration into the Composite Infrared Spectrometer instrument on the Cassini mission to Saturn. Each array is a 10-element linear array of square photoconductive MCT infrared detectors, measuring  $200 \mu\text{m}$  on a side. This array is one of three focal planes comprising the instrument's interferometer (as shown in the fifth figure). The arrays exhibit high sensitivity in the infrared, from  $2 \mu\text{m}$  to longer than  $18 \mu\text{m}$ .



*Infrared arrays for Cassini.*

### ***Cross Delay Line Detectors***

An innovative anode array was developed in collaboration with the University of California at Berkeley for use in two instruments (Ultraviolet Coronagraph Spectrometer and Solar Ultraviolet Measurements of Emitted Radiation) on the Solar and Heliospheric Observatory. The cross delay line anode arrays were designed at Berkeley and fabricated at GSFC (see the sixth figure). The anode arrays have been delivered and integrated into the instruments.



*Cross delay line detectors.*

Contact: Brent Mott (Code 718.1)  
301-286-7708

Sponsor: Office of Space Science  
GSFC Director's Discretionary Fund

*Mr. Mott is currently Head of the Electron Device Development Section. He has a B.S. in Physics and an M.S. in Electrical Engineering from the University of Maryland.*

### AN IMPROVED LIGHTNING DETECTION AND RANGING SYSTEM

THE LIGHTNING DETECTION and Ranging (LDAR) system developed at Kennedy Space Center (KSC) detects and locates lightning by measuring the time taken by the radio frequency (RF) noise generated by a lightning discharge to reach each of several antennas. This "time-of-arrival" technique works because the time difference between any two antennas uniquely defines a hyperbolic surface in space, on which the source of the RF must lie. A second pair of antennas defines another hyperbolic surface; the intersection with the first hyperbolic surface defines a line on which the source must lie. The time difference from a third pair of antennas determines a third hyperbolic surface, which intersects the first two at a unique point in space. This point is the location of the RF source and, hence, the location of the lightning discharge.

One of the antenna sites is used as a reference site. An RF signal threshold level is set at the reference site to filter out ambient RF noise. Signals above the threshold are assumed to come from lightning discharges, and the peak signal detected by each of the antennas is assumed to result from the same lightning discharge source. That peak is the identifiable feature in the RF noise from which the various differences in time of arrivals can be measured. Clearly, spurious noise spikes from any antenna can invalidate the data. The original LDAR system was transferred to NASA GSFC's Wallops Flight Facility from KSC in late 1980. The system hardware included two Hewlett-Packard minicomputers, a NASA-designed preprocessor, and four Biomation 8100 high-speed digitizers.

Recently, GSFC contractors working for NYMA, Inc., completely redesigned and rebuilt the LDAR electronics. They replaced the preprocessor and digitizers with a data acquisition board they designed, and replaced the two minicomputers with personal computers. The cost of the new system is a small fraction of the > \$100,000 hardware cost of the original system. In addition, the performance has been greatly enhanced. System sensitivity has been improved, and the attenuators at each of the antenna sites were optimized to overcome signal saturation problems that plagued the old system.

The throughput rate of good data has been increased by greater than a factor of 100. The higher data rate has allowed the development of techniques to eliminate

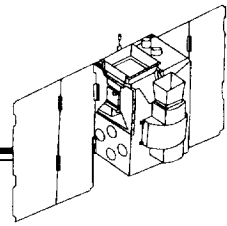
noise-contaminated data. The NYMA employees accomplished this upgrade by working on a noninterfering basis with their regular duties, and by spending less than a thousand dollars for parts.

KSC has recently developed a new and expensive version of LDAR. Their new system eliminates noise-contaminated data by using a second set of LDAR antennas, and by requiring that the lightning discharge locations determined by each set of antennas agree. Wallops Flight Facility does not have suitable sites to install another set of LDAR antennas, so we were forced to consider other methods.

Our technique to eliminate bad data uses the high-data-collection rate that records multiple points from the same lightning discharge. Our criterion for good data is that each point must be confirmed by the existence of other points from the same discharge. We judge points to be from the same discharge if they are received during times and at locations that are consistent with our understanding of the physics of the lightning process. Additional confirmation comes from analyzing the amplitude of the signal strength of the RF signal received at each antenna. We have also made significant improvements to the real-time display system.

These improvements have enhanced the value of LDAR data as a tool for making decisions during range operations. The data are plotted on a map overlay of the local region. Pan and zoom of the display are fully supported. Data are color-coded, based on when strikes occurred; color is automatically changed as the data age. Discharges that occurred within the past 5 minutes are displayed in red, from 5 to 15 minutes in yellow, 15 to 30 in green, and so on. The operator can change both colors and time intervals. The operator can also choose to display only data from the previous 5 minutes. The left mouse button enables a moveable box of interest. When enabled, the altitudes of the discharges within the box are displayed in a separate window. The right mouse button enables an arrow on the map overlay that can be moved with the mouse; the azimuth and range of the point at the tip of the arrow is then displayed.

Time and location of the last discharge are always displayed. Statistics on the number of events recorded and the number plotted in each time interval are similarly



displayed. The operator can also dynamically change all the filtering criteria used to determine valid data. In addition to data filtering based on the time between data points and the distances between their locations, the operator can filter the databased on the amplitude of the signal strength at each antenna as a function of range. In addition to the real-time mode, we have written software to playback all of the raw data recorded. All of the real-time display functions work during playback, along with new functions that allow the operator to easily move around within the data file and display the raw data. Color prints of the display can be made, as well as printouts listing the raw data recorded.

This new LDAR system has been in operation since the summer of 1995, and has been providing high-quality data

that are consistent with data from the National Lightning Data Network (which locates cloud-to-ground lightning strikes), and with direct radar measurements of the location of lightning channels within clouds.

This work could not have been done without the dedicated efforts of Charles Etheridge and Dennis Swartz (both with NYMA, Inc., a subcontractor to Allied Signal, Inc.).

Contact: John Gerlach (Code 822.3)  
804-824-1188

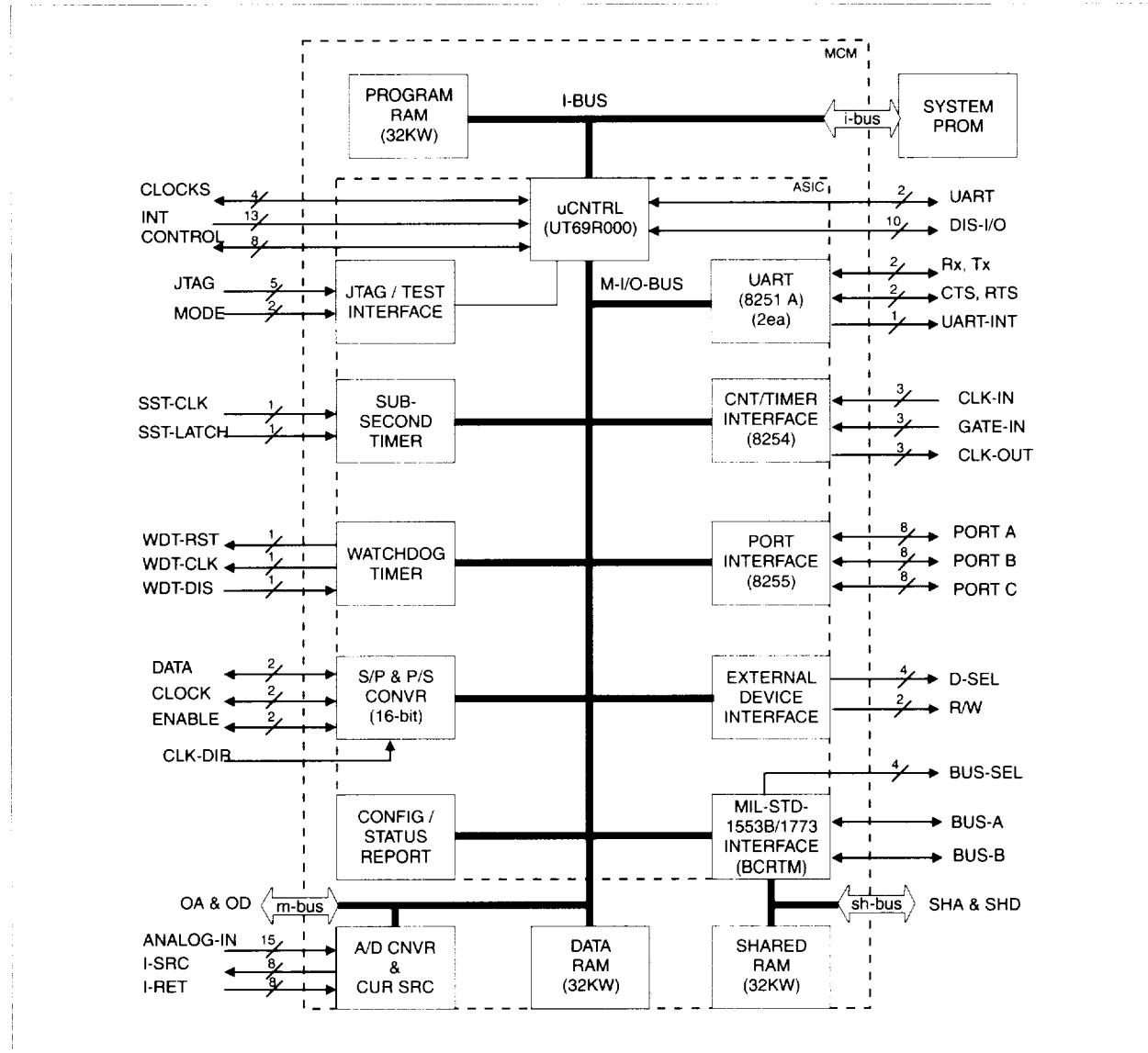
Sponsor: Office of Mission to Planet Earth

*Dr. Gerlach is a physical scientist at the NASA/GFSC's Wallops Flight Facility. He is the scientific coordinator for the Atmospheric Sciences Research Facility.*

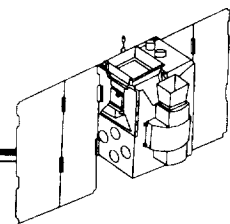
## THE ESSENTIAL SERVICES NODE: A LOW-POWER DATA SYSTEM ON A CHIP

THE ESSENTIAL SERVICES Node (ESN) is a multichip module (MCM) under development by GSFC's Flight Data Systems Branch. The ESN is a solution to many of the common problems faced by spacecraft system designers. It is a low-power (< 1 W), low-cost (< \$20,000), small and lightweight (2.5" x 2.5" x 0.2"), radiation-hardened (> 100 Krad) spacecraft data system on a single chip. An architectural block diagram is shown in the figure.

The ESN solves a number of other spacecraft problems: it eliminates custom interfaces by standardizing to common interfaces; it reduces system development cost and time by providing system designers with a "tool box" of common devices; it supports a standard bus architecture in the MIL-STD-1553B/1773 bus; it eliminates the need for "orphan" telemetry by incorporating their functions; and its powerful microprocessor provides for autonomous operations.



An architectural block diagram of the essential services node.



The ESN interfaces instruments and subsystems to a spacecraft's MIL-STD-1553B or 1773 bus. It can read commands or data from instruments or subsystems, process the information, and send it to a spacecraft's command and data-handling (C&DH) system. The ESN can also receive commands from a spacecraft's C&DH system, process the information, and send it to an instrument or subsystem.

The ESN is a multipurpose, multifunctional device. It can transmit or receive parallel, serial, MIL-STD-1553B/1773, and processor-independent commands. It can transmit or receive parallel, serial, and MIL-STD-1553B/1773 telemetry. It also has the ability to easily interface to multiple devices.

The ESN's MCM contains a digital application-specific integrated circuit (ASIC), memory chips, analog logic, and power-strobing circuitry. The digital ASIC is a UTMC 50k gate-array. It contains the UT69R000 reduced instruction set (RISC) microprocessor, a UTBCRTM bus interface, a standard counter/timer interface (8254), a standard port interface (8255), two standard UART interfaces (8251), a watch-dog timer interface, a subsecond timer interface, an external device interface, a synchronous serial-to-parallel interface, a synchronous parallel-to-serial interface, a programmable wait-state generator, and an analog control interface.

The ESN's MCM memory consists of six 32 K x 8 random access memory (RAM) chips: two for program RAM, two for data RAM, and two for shared RAM. The analog logic consists of an 8-channel, 1 mA current source and a 16-channel, 12-bit analog-to-digital converter. The power-strobing circuitry consists of transistors that switch the analog power off and on to reduce the overall ESN power requirement.

The ESN's MCM does not contain application-specific circuits (e.g., oscillator, programmable read-only memory, differential drivers/receivers, opto-isolators, buffers, etc.).

These devices are outside the MCM module, but on the same printed circuit board as the MCM.

The standard ESN software is table-driven, but the ESN will support unique application software. However, by using the ESN's table-driven software, most applications will not require application software.

In the ESN's table-driven system, the ESN would initialize in a predefined state. The bus controller would send commands over the MIL-STD-1553B/1773 bus that would define and activate ESN's tables. The software tables will contain fields for source address, destination address, data/command format, data/command frequency, and others. Simple command and data transfers are possible without unique application software.

For detailed specifications of the ESN's interfaces, timing diagrams and sample interface circuits, readers are referred to the ESN Interface Control Document. Because the ESN uses many industry-standard devices and interfaces, readers are referred to appropriate Harris, UTMC, or Intel documentation.

Contact: Robert Caffrey (Code 735.2)  
301-286-4766  
Internet:  
[robert\\_caffrey@ccmail.gsfc.nasa.gov](mailto:robert_caffrey@ccmail.gsfc.nasa.gov)

Sponsor: Office of Space Communications

*Mr. Caffrey is an electrical engineer in the Flight Data Systems Branch. Mr. Caffrey earned two degrees from the University of Maryland, a co-op B.S. in Electrical Engineering, and a B.S. in Computer Science. Mr. Caffrey has been at GSFC for over 10 years. He spent the first 8 years developing both hardware and software for the Laboratory for Atmospheres Shuttle Solar Backscatter Ultraviolet instrument; he has spent the last 2 years developing the ESN for the Flight Data Systems Branch.*



# ACRONYMS

---

<b>ACE</b>	Advanced Composition Explorer	<b>BASIS</b>	Burst ArcSecond Imaging and Spectroscopy
<b>A/D</b>	analog-to-digital	<b>BB</b>	bit blocks
<b>ADEAS</b>	Attitude Determination Error Analysis System	<b>BER</b>	bit error rate
<b>AGNS</b>	Automated Ground Network System	<b>BOREAS</b>	Boreal Ecosystem Atmosphere Study
<b>AIM</b>	Arctic Ice Mapping	<b>BPSK</b>	binary phase shift keying
<b>AIRS</b>	Atmospheric Infrared Sounder	<b>BRTS</b>	Bilateration Ranging Transponder System
<b>AL</b>	electrojet index		
<b>AMASE</b>	Astrophysics Multispectral Archive Search Engine	<b>C&amp;DH</b>	Command and Data Handling
<b>ANSI</b>	American National Standards Institute	<b>CADU</b>	Channel Access Data Unit
<b>AOL</b>	Airborne Oceanographic Lidar	<b>CAP</b>	Communications Address Processor
<b>ARC</b>	NASA/Ames Research Center	<b>CAPL</b>	Capillary Pumped Loop
<b>arcsec</b>	arcsecond	<b>CARA</b>	Center for Astrophysical Research in Antarctica
<b>ASC</b>	ACE Science Center	<b>CCD</b>	charge-coupled device
<b>ASC</b>	Altimeter Support Center	<b>CCRS</b>	Canada Center for Remote Sensing
<b>ASCA</b>	Advanced Satellite for Cosmology and Astrophysics	<b>CCSDS</b>	Consultative Committee for Space Data Systems
<b>ASCII</b>	American Standard Code for Information Interchange	<b>CDC</b>	cooperating data center
<b>ASIC</b>	Application-Specific Integrated Circuit	<b>CDF</b>	Common Data Format
<b>ASSET</b>	Advanced System Synthesis and Evaluation Tool	<b>CDP</b>	Crustal Dynamics Project
<b>ASTER</b>	Advanced Spaceborne Thermal Emission Reflection Radiometer	<b>CDR</b>	Critical Design Review
<b>ATM</b>	Airborne Topographic Mapper	<b>CD-ROM</b>	compact disk-read only memory
<b>AU</b>	astronomical unit	<b>CERES</b>	Clouds and Earth's Radiant Energy System
<b>AVHRR</b>	Advanced Very High Resolution Radiometer	<b>CESDIS</b>	Center of Excellence in Space Data and Information Systems

# ACRONYMS

---

<b>CGRO</b>	Compton Gamma Ray Observatory	<b>DCT</b>	Discrete Cosine Transform
<b>CIPS</b>	Constraint-Based Intelligent Planners and Schedulers	<b>DDF</b>	Director's Discretionary Fund
<b>CLASS</b>	Communications Link Analysis Simulation Systems	<b>DDL</b>	Detector Development Laboratory
<b>CLIPS</b>	C Language Integrated Production System	<b>DDS</b>	Direct Digital Synthesizer
<b>CLP</b>	Command Load Processor	<b>DIMES</b>	Diffuse Microwave Emission Survey
<b>CMBR</b>	Cosmic Microwave Background Radiation	<b>DIRBEE</b>	Diffuse Infrared Background Experiment
<b>CMOS</b>	complementary metal-oxide semiconductor	<b>DMSP</b>	Defense Meteorological Satellite Program
<b>CMMA</b>	custom metallized multigate array	<b>DORIS</b>	Doppler Orbitography and Radiopositioning Integrated by Satellite
<b>COARE</b>	Coupled Ocean Atmosphere Response Experiment	<b>DSP</b>	digital signal processor
<b>COBE</b>	Cosmic Background Explorer	<b>EBnet</b>	EOS Data Information System Backbone Network
<b>COHO</b>	Coordinated Heliospheric Observations	<b>eV</b>	electron volt
<b>COTS</b>	commercial-off-the-shelf	<b>ECOM</b>	EOS Communication
<b>CPHTS</b>	Capillary Pumped Heat Transport System	<b>EDC</b>	Earth Resources Observation System Data Center
<b>CPU</b>	central processing unit	<b>EDM</b>	Engineering Development Modules
<b>CRC</b>	cyclic redundancy check	<b>EDOS</b>	EOS Data and Operations Systems
<b>CSC</b>	Computer Sciences Corporation	<b>EOL</b>	end of life
<b>CVD</b>	chemical-vapor-deposited	<b>EOS</b>	Earth Observing System
<b>DAAC</b>	Distributed Active Archive Center	<b>EOSDIS</b>	EOS Data and Information System
<b>DAO</b>	Data Assimilation Office	<b>ENSO</b>	El Nino/Southern Oscillation
<b>DAS</b>	data assimilation systems	<b>EPROM</b>	Extended Programmable Read-Only Memory
<b>dB</b>	decibels	<b>ERBE</b>	Earth Radiation Budget Experiment
<b>dBm</b>	decibel milliwatt	<b>ERBS</b>	Earth Radiation Budget Satellite

# ACRONYMS

---



---

<b>ESN</b>	Essential Services Node	<b>GADFLY</b>	GPS Attitude Determination Flyer
<b>ESS</b>	Earth and Space Sciences	<b>GARP</b>	Ground Network Advanced Receiver
<b>ETM</b>	Engineering Test Modules	<b>GB</b>	gigabytes
<b>EUV</b>	extreme ultraviolet	<b>Gbps</b>	gigabytes per second
<b>EUVE</b>	Extreme Ultraviolet Explorer	<b>GCM</b>	general circulation model
<b>FAO</b>	United Nations Food and Agriculture Organization	<b>GenSAA</b>	Generic Spacecraft Analyst Assistant
<b>FAST</b>	Fast Auroral Snapshot Explorer	<b>GEODE</b>	GPS Enhanced Orbit Determination Experiment
<b>FDD</b>	Flight Dynamics Division	<b>GHz</b>	gigahertz
<b>FDDS</b>	Flight Dynamics Distributed System	<b>GIF</b>	Graphics Interchange Format
<b>FDF</b>	Flight Dynamics Facility	<b>GLOBE</b>	Global Learning and Observation to Benefit the Environment
<b>FDDI</b>	fiber data distributed interface	<b>GN</b>	ground network
<b>FDPC</b>	Flight Dynamics Product Center	<b>GOPS</b>	giga (billion) operations per second
<b>FITS</b>	Flexible Image Transport System	<b>GPCP</b>	Global Precipitation Climatological Project
<b>F/L</b>	forward link	<b>GPS</b>	Global Positioning System
<b>FO</b>	fiber optic	<b>GRIS</b>	Gamma-Ray Imaging Spectrometer
<b>FOT</b>	flight operations team	<b>GRTS</b>	CGRO remote terminal system
<b>FOT</b>	fiber optical transceiver	<b>GSFC</b>	NASA/Goddard Space Flight Center
<b>FOV</b>	field of view	<b>GSOC</b>	Guide Star Occultation Prediction Utility
<b>FPGA</b>	field programmable gate array	<b>GSS</b>	Generalized Support Software
<b>FS</b>	frame synchronizer	<b>GTDS</b>	Goddard Trajectory Determination System
<b>FSSR</b>	Flight Software Systems Requirements	<b>GUI</b>	Graphical User Interface
<b>ftp</b>	file transfer protocol	<b>GW</b>	gravity wave

# ACRONYMS

---

<b>HDF</b>	hierarchical data format	<b>IMACCS</b>	Integrated Monitoring, Analysis, and Control COTS System
<b>HDPP</b>	heat-driven pulse pump	<b>IMF</b>	interplanetary magnetic field
<b>HES</b>	Heuristic Evolutionary Search	<b>IMOC</b>	Integrated Mission Operations Center
<b>HIRS</b>	High Resolution Infrared Radiation Sounder	<b>IMS</b>	Information Management System
<b>HP</b>	Hewlett-Packard	<b>IOP</b>	input/output processor
<b>HPCC</b>	High Performance Computing and Communications	<b>IP</b>	Internet Protocol
<b>HQ</b>	headquarters	<b>IRAS</b>	Infrared Astronomical Satellite
<b>hr</b>	hour	<b>IRHS</b>	Infrared Heterodyne Spectrometer
<b>HRG</b>	Hemispherical Resonator Gyroscope	<b>ISCCP</b>	International Satellite Cloud Climatology Project
<b>HSI</b>	Hyperspectral Imager	<b>ISLSCP</b>	International Satellite Land-Surface Climatology Project
<b>HST</b>	Hubble Space Telescope	<b>ISTP</b>	International Solar and Terrestrial Physics
<b>HTML</b>	Hypertext Markup Language	<b>ITOCC</b>	Integration and Test Operations Control Center
<b>HTRS</b>	Honeywell Task and Resource Scheduler		
<b>HTS</b>	high-temperature superconductor		
<b>HVS</b>	Human Visual System		
<b>Hz</b>	Hertz		
<b>I/O</b>	input/output	<b>JFET</b>	junction field effect transistors
<b>IDL</b>	Interactive Data Language	<b>JPEG</b>	Joint Photographic Experts Group
<b>IF</b>	intermediate frequency	<b>JPL</b>	Jet Propulsion Laboratory
<b>IGSE</b>	Instrument Ground Support Equipment		
<b>IIFS</b>	Intelligent Information Fusion System	<b>K</b>	Kelvin
<b>IIRV</b>	Improved Inter-Range Vectors	<b>kbps</b>	kilobits per second
		<b>Kbps</b>	kilobytes per second
		<b>keV</b>	kilo-electron volts

# ACRONYMS

---



---

<b>kg</b>	kilogram	<b>MISR</b>	Multiangle Imaging Spectroradiometer
<b>kHz</b>	kiloHertz	<b>mm</b>	millimeter
<b>KSC</b>	Kennedy Space Center	<b>μm</b>	micrometer
<b>ksp</b>	kilo symbols per second	<b>msec</b>	microsecond
		<b>MOC</b>	Mission Operations Center
		<b>MODIS</b>	Moderate Resolution Imaging Spectroradiometer
<b>LAC</b>	Laser Altimeter Canister	<b>MOPITT</b>	Measurements of Pollution in the Troposphere
<b>LAN</b>	local area network	<b>MRVQ</b>	mean removed vector quantization
<b>LDAR</b>	Lightning Detection and Ranging	<b>MSU</b>	Microwave Sounding Unit
<b>LH</b>	latent heat	<b>MTPE</b>	Mission to Planet Earth
<b>LLIS</b>	Lessons-Learned Information System	<b>MTTF</b>	mean time to failure
<b>LoTTS</b>	Long-Term Trending System	<b>MUMICAT</b>	Multiuser, Multi-Interference Communication Analysis Tool
<b>LTIS</b>	Loral Test and Information System	<b>MVQ</b>	model-based vector quantization
<b>MA</b>	multiple access	<b>NASA</b>	National Aeronautics and Space Administration
<b>mA</b>	milli-amp	<b>NASCOM</b>	NASA Communications
<b>MacTAC</b>	Macintosh Telemetry and Command System	<b>NCO</b>	numerically controlled oscillator
<b>MB</b>	megabyte	<b>NDVI</b>	normalized difference vegetation index
<b>mb</b>	millibar	<b>NIST</b>	National Institute of Standards and Technology
<b>MCM</b>	Multichip Module	<b>nm</b>	nanometer
<b>MCS</b>	Mission Control System	<b>NMC</b>	National Meteorological Center
<b>MDA</b>	McDonnell Douglas Aerospace	<b>NOAA</b>	National Oceanic and Atmospheric Administration
<b>MeV</b>	million electron volts		
<b>MHz</b>	megahertz		
<b>MidEx</b>	Mid-Sized Explorer Satellite		

# ACRONYMS

---

<b>NODIS</b>	NSSDC On-line Data and Information Service	<b>PMP</b>	pass management program
<b>NRC</b>	National Research Council	<b>PN</b>	pseudorandom noise
<b>NRZ</b>	non-return-to-zero	<b>PNMF</b>	pseudorandom noise matched filter
<b>nsec</b>	nanosecond	<b>PODS</b>	Precision Orbit Determination System
<b>NSF</b>	National Science Foundation	<b>POR</b>	point of resolution
<b>NSIDC</b>	National Snow and Ice Data Center	<b>PORTCOM</b>	Portable Tracking and Data Relay Satellite System Communicator
<b>NSSC-1</b>	NASA Standard Spacecraft Computer-1	<b>PoRTIA</b>	Piggyback Room Temperature Instrument for Astronomy
<b>NSSDC</b>	National Space Science Data Center	<b>psia</b>	pounds per square inch absolute
<b>OBC</b>	onboard computer	<b>psid</b>	pounds per square inch difference
<b>OLR</b>	outgoing longwave radiation	<b>PSP</b>	prototype parallel service processor
<b>OLS</b>	Operational Linescan System	<b>QBO</b>	Quasi-Biennial Oscillator
<b>ONS</b>	Onboard Navigation System	<b>QPSK</b>	quadrature phase shift key
<b>OODB</b>	object-oriented database	<b>QTN</b>	quasi-thermal noise
<b>OTDR</b>	Optical Time Domain Reflectometer	<b>RADARSAT</b>	Radar Satellite
<b>PACOR</b>	Packet Processor	<b>RAID</b>	redundant array of inexpensive devices
<b>Pa-s</b>	Pascal-second	<b>RAM</b>	random access memory
<b>PC</b>	personal computers	<b>RD</b>	rotational discontinuity
<b>PCI</b>	peripheral components interface	<b>RDBMS</b>	relational database management system
<b>PDF</b>	probability density functions	<b>RF</b>	radio frequency
<b>PERL</b>	Practical Extraction and Report Language	<b>RFDU</b>	RF distribution unit
<b>PI</b>	Principal Investigator	<b>RISC</b>	reduced instruction set
<b>PIFS</b>	parallel integrated frame synchronizer chip	<b>RIU</b>	remote interface unit

# ACRONYMS

---

<b>R/L</b>	return link	<b>SSA</b>	S-band single access
<b>RMS</b>	remote manipulator system	<b>SSM/I</b>	Special Sensor Microwave/Imager
<b>rms</b>	root mean square	<b>SST</b>	sea-surface temperature
<b>ROSAT</b>	Roentgen Satellite	<b>SSTI</b>	Small Satellite Technology Initiative
<b>RSEC</b>	Reed and Solomon Error Correction Chip	<b>STARLink</b>	Satellite Telemetry Data and Return Link
		<b>STATMUX</b>	statistical multiplier
<hr/>		<b>STI</b>	Superconductor Technologies, Inc.
<b>s</b>	second	<b>STINT</b>	Standard Interface
<b>SAO</b>	Semi-Annual Oscillation	<b>STOL</b>	Spacecraft Test Operations Language
<b>SAMPEX</b>	Solar, Anomalous, and Magnetospheric Particle Experiment	<b>STOL</b>	Systems Test and Operations Language
<b>SAR</b>	Synthetic Aperture Radar	<b>STS</b>	space transport system
<hr/>		<b>3-D</b>	three-dimensional
<b>SDC</b>	snow-depth climatology	<b>TCP/IP</b>	Transmission Control Protocol/Internet Protocol
<b>SH</b>	sensible heat	<b>TDRSS</b>	Tracking and Data Relay Satellite System
<b>SIS</b>	Spacecraft Interface Simulator	<b>TDS</b>	Tracking Data System
<b>SLA</b>	Shuttle Laser Altimeter	<b>Tg</b>	teragram
<b>SLR</b>	Satellite Laser Ranging	<b>TM</b>	Thematic Mapper
<b>SMEX</b>	Small Explorer	<b>TOGA</b>	Tropical Ocean Global Atmosphere
<b>SMMR</b>	Scanning Multichannel Microwave Radiometer	<b>TONS</b>	TDRSS Onboard Navigation System
<b>SMP</b>	symmetric multiprocessing	<b>TOPEX</b>	Ocean Topography Experiment
<b>SN</b>	space network	<b>TOVS</b>	TIROS Operational Vertical Sounder
<b>SNMP</b>	simple network management protocol	<b>T/P</b>	TOPEX/Poseidon
<b>SPOT</b>	Satellite pour L'Observation de la Terre	<b>TPOCC</b>	Transportable Payload Operational Control Center
<b>SPU</b>	signal processing unit	<b>TRACE</b>	Transistion Region and Coronal Explorer
<b>SPW</b>	signal processing workstation		
<b>SRAM</b>	static random access memory		
<b>SRL</b>	Shuttle Radar Laboratory		

# ACRONYMS

---

<b>TRMM</b>	Tropical Rainfall Measuring Mission	<b>VBS</b>	variable-bit synchronization
<b>TTL</b>	transistor-transistor logic	<b>VHDL</b>	very-high-speed integrated circuit hardware description language
<b>TURFTS</b>	TDRSS User RF Test Set	<b>VLBI</b>	Very Long Baseline Interferometry
<hr/>		<b>VLSI</b>	very large-scale integration
<b>UDP</b>	User Datagram Protocol	<b>VQ</b>	vector quantization
<b>UIX</b>	User Interface and Executive	<hr/>	
<b>URAP</b>	Unified Radio and Plasma Wave Investigation	<b>W</b>	Watt
<b>URL</b>	Universal Resource Locator	<b>WSC</b>	White Sands Complex
<b>UT</b>	Universal Time	<b>WWW</b>	World Wide Web
<b>UTC</b>	Universal Time Coordinate	<hr/>	
<b>UV</b>	ultraviolet	<b>XRS</b>	X-Ray Spectrometer
<hr/>		<b>XTE</b>	X-Ray Timing Explorer
<b>V0</b>	Version 0		

## **AUTHOR INDEX**

<i>Author</i>	<i>Page</i>	<i>Author</i>	<i>Page</i>
<b>Ambrose, Rich</b> .....	50	<b>Coronado, Patrick</b> .....	75
<b>Anselm, Bill</b> .....	96	<b>Cromp, Robert</b> .....	73
<b>Anyamba, Ebby</b> .....	156		
<b>Badger, John</b> .....	21	<b>Davis, Don</b> .....	42, 46
<b>Becker, Donald</b> .....	78	<b>Dent, Carolyn</b> .....	9
<b>Benn, Ricardo</b> .....	5	<b>Doll, Clarence</b> .....	14
<b>Benner, Steve</b> .....	207	<b>Dorband, John</b> .....	78
<b>Blaney, Greg</b> .....	44	<b>Dougherty, Andrew</b> .....	104
<b>Blumenstock, Gerry</b> .....	209	<b>Duran, Steve</b> .....	68, 70, 71
<b>Bony, Sandrine</b> .....	160, 200	<b>Dwek, Eli</b> .....	147
<b>Bordi, Francesco</b> .....	110		
<b>Bracken, Michael</b> .....	64	<b>Fast, Kelly</b> .....	135
<b>Brambora, Clifford</b> .....	83	<b>Foster, James</b> .....	163
<b>Bufton, Jack</b> .....	189	<b>Fung, Inez</b> .....	179
<b>Caffrey, Robert</b> .....	224	<b>Gaddy, Edward</b> .....	206
<b>Campbell, William</b> .....	73	<b>Garrick, Joseph</b> .....	26
<b>Caroglanian, Armen</b> .....	81	<b>Garvin, James</b> .....	183
<b>Casper, Paul</b> .....	48	<b>Gehrels, Neil</b> .....	145
<b>Castles, Stephen</b> .....	214	<b>Gerlach, John</b> .....	222
<b>Chang, Alfred T. C.</b> .....	165	<b>Ghuman, Parminder</b> .....	46
<b>Cheung, Cynthia</b> .....	150	<b>Goldstein, Melvyn</b> .....	129
		<b>Gramling, Cheryl</b> .....	17

# AUTHOR INDEX

---

<i>Author</i>	<i>Page</i>	<i>Author</i>	<i>Page</i>
<b>Grubb, Thomas</b> .....	68, 71	<b>Koschmeder, Lou</b> .....	19
<b>Hall, Forrest</b> .....	173	<b>Kostiuk, Theodor</b> .....	135
<b>Harrel, Linda</b> .....	81	<b>Krabill, William</b> .....	168
<b>Harris, Jonathan</b> .....	42	<b>Krimchansky, Alexander</b> .....	40
<b>Hart, Roger</b> .....	24	<b>Kyle, H. Lee</b> .....	198
<b>Hartley, Jonathan</b> .....	57	<b>Land, Thomas</b> .....	35
<b>Hei, Don</b> .....	11	<b>Lau, William K.-M.</b> .....	158, 160, 200
<b>Henegar, Joy</b> .....	83	<b>Lauriente, Michael</b> .....	112, 114
<b>Hines, Colin</b> .....	195	<b>Le, Chi</b> .....	48
<b>Horne, William</b> .....	32	<b>Leake, Stephen</b> .....	24
<b>Imhoff, Marc</b> .....	176	<b>Lemoine, Frank</b> .....	170
<b>Israel, David</b> .....	21	<b>Lemon, Michael</b> .....	40
<b>Jackson, Arthur</b> .....	19	<b>Leung, Ronald</b> .....	116
<b>Jaster, Mark</b> .....	120	<b>Leventhal, Ed</b> .....	50
<b>Keski-Kuha, Ritva</b> .....	209	<b>Li, Xiaofan</b> .....	158
<b>Kessel, Ramona</b> .....	126	<b>Livengood, Timothy</b> .....	135
<b>Kirichok, Matthew</b> .....	29	<b>Marshall, Andrew</b> .....	170
<b>Klimas, Alex</b> .....	131	<b>Mather, John</b> .....	138
<b>Kolasinski, John</b> .....	211	<b>Mathews, G. Jason</b> .....	101
		<b>Matthews, Elaine</b> .....	179
		<b>Matusow, David</b> .....	98
		<b>Mayr, Hans</b> .....	195

# AUTHOR INDEX

<i>Author</i>	<i>Page</i>	<i>Author</i>	<i>Page</i>
<b>McCarron, Steve</b> .....	50	<b>Scolese, Christopher</b> .....	110
<b>Mendelsohn, Chad</b> .....	7	<b>Schweiss, Robert</b> .....	83
<b>Mengel, John</b> .....	195	<b>Segal, Jeffrey</b> .....	59
<b>Mica, Joe</b> .....	118	<b>Sellers, Piers</b> .....	173
<b>Militch, Peter</b> .....	62	<b>Serlemitos, Peter</b> .....	143
<b>Moore, Mike</b> .....	93	<b>Shaller Hornstein, Rhoda</b> .....	11
<b>Moseley, Harvey</b> .....	141	<b>Shaughnessy, Jim</b> .....	48
<b>Mott, Brent</b> .....	218	<b>Shirah, Gregory</b> .....	60
 		<b>Short, Jr., Nicholas</b> .....	73, 75
<b>Neeck, Steven</b> .....	110	<b>Smith, Miles</b> .....	62
 		<b>Solomon, Jeff</b> .....	46
<b>Oberright, John</b> .....	116	<b>Stark, Michael</b> .....	55
 		<b>Sterling, Thomas</b> .....	78
<b>Parsons, Ann</b> .....	145	<b>Stone, Robert</b> .....	133
<b>Pfister, Robin</b> .....	85	<b>Sud, Yogesh C.</b> .....	160, 200
 		<b>Sui, Chung-Hsiung</b> .....	158
<b>Raqu�, Steven</b> .....	216	<b>Susskind, Joel</b> .....	156
<b>Rash, James</b> .....	2	<b>Tilton, James</b> .....	91
<b>Roberts, D. Aaron</b> .....	129	<b>Towheed, Syed</b> .....	101
<b>Rubincam, David</b> .....	192	<b>Tueller, Jack</b> .....	145
<b>Ryan, James</b> .....	186		

# **AUTHOR INDEX**

---

<i>Author</i>	<i>Page</i>	<i>Author</i>	<i>Page</i>
<b>Weidow, David</b> .....	53	<b>Younes, Badri</b> .....	5, 81
<b>White, Richard</b> .....	88		
<b>Woodard, Mark</b> .....	98	<b>Zillig, David</b> .....	32, 35, 38





**ON THE COVER:**

*The figure on the front and back covers of this report depicts the Mission Operations and Data Systems Directorate end-to-end system. At one end is the near-Earth unmanned scientific satellite. At the other is the vast diverse community of users who rely on space-related data for a myriad of scientific and other pursuits. The infrastructure in between these two end-points is comprised of the Tracking and Data Relay Satellite System (TDRSS), the ground station, and the mission operations hub. This hub is not only responsible for spacecraft command, control and monitoring activities but also maintains a full spectrum of research and technology development programs that are needed to take mission operations into the future.*

**Executive Editor:**

Gerald Soffen

**Editors:**

Walter Truszkowski  
Howard Ottenstein  
Kenneth Frost  
Stephen Maran  
Lou Walter  
Mitch Brown

**With Special Thanks To:**

Sue Hart  
Carol Ladd  
Terri Randall  
Britt Griswold  
Chris DeGrazia

**Technical and Scientific Editing, Artwork and Production:**

Brenda Vallette, Carol Smouse, Mitchell Hobish, and Kathy Pedelty

